THERMOPHYSICAL PROPERTIES

FROM THE SPEED OF SOUND

A thesis submitted to

the University of London

for the degree of

Doctor of Philosophy

by

ANTHONY ROBERT HOLMES GOODWIN

Department of Chemistry
University College London
20 Gordon Street
LONDON
WC1H 0AJ

February 1988

ACKNOWLEDGEMENTS

I would like to thank Dr M.B. Ewing for his advice, patience, and encouragement throughout this work, especially during the time spent in writing this thesis. I also acknowledge the co-operation and help received from other members of the thermodynamics research group, in particular Dr J.P.M. Trusler.

I gratefully acknowledge the award of a Research Scholarship by British Gas plc, and the interest shown by Dr G. O'Hair of their London Research Station was much appreciated.

The resonator and pressure vessel were machined by Mr D.J. Morfett, whom along with his colleagues in the mechanical workshop I thank for their advice and assistance.

I am also grateful for the unfailing support and encouragement I have received from my parents and sister who in addition typed the tables, and last but not least my wife Vanessa who also faithfully reproduced the figures included in this thesis.

Finally, I acknowledge the efforts of Veronica Jackson who typed the majority of this thesis.

ABSTRACT

The speed of sound in various gases between 250 and 350 K has been obtained from measurements of the frequencies of the radial modes of spherical acoustic resonators; two resonators were used and both apparatus are described. The radius of each resonator was obtained from the speed of sound in argon. Measurements with the 60 mm radius resonator were made below 115 kPa on the six substances: *n*-butane; methylpropane; *n*-pentane; methylbutane; dimethylpropane; and, methanol. Perfect gas heat capacities and second and third acoustic virial coefficients for these substances have been calculated from the results, and estimates are given for the second and third (p,V_m,T) virial coefficients. A sealed resonator of radius 40 mm was used to obtain acoustic results below 7 MPa on argon and the industrially important gases methane, a natural gas, and air. Measurements with argon provided an opportunity to study the model used to account for acoustic energy losses in the resonator. The speed of sound, for the industrially important gases, was compared with estimates obtained from several equations of state.

TABLE OF CONTENTS

LIST OF TABLES

Page

LIST OF FIGURES

CHAPTER ONE

INTRODUCTION

Accurate measurements of the speed of sound u can be used to study the equation of state of a gas. Conventionally, equation-of-state information is obtained from (p, V_m, T) measurements[1-7] which suffer from a number of significant systematic errors, some but not all of which may be reduced by recourse to more sophisticated experimental techniques. The effect of adsorption becomes a significant source of error when the experimental pressure is a large fraction of the vapour pressure;[8] this is necessarily the case at low reduced temperature $T_r \approx 0.7$.[9] The speed of sound suffers from quite different systematic errors which are usually more easily identified and reduced. In particular, since u is formally independent of the amount of substance, it is in principle immune from the effects of adsorption.

In the zero-pressure limit the speed of sound in a gas is given by

$$u^2 = RT\gamma^{pg}/M \stackrel{def}{=} A_0 \qquad (1.1)$$

where T is the thermodynamic temperature, R the universal gas constant, M the molar mass, and

$$\gamma^{pg} = C_{p,m}^{pg}/C_{V,m}^{pg} = 1/(1 - R/C_{p,m}^{pg}) \qquad (1.2)$$

is the ratio of the perfect-gas heat capacities at constant pressure and at constant volume. Thus, if γ^{pg} is known (for example in a monatomic gas $\gamma^{pg} = 5/3$ exactly) then

measurements of $A_0(T)$ at different temperatures form the basis of primary thermometry[10-14] and A_0(273.16 K) serves to determine R if M is also known.[15-17] Alternatively, $A_0(T)$ for a pure gas may be used to obtain $C^{pg}_{p,m}(T)$[18-21] if R, T, and M are known; while for a binary gaseous mixture, the mole fraction x may be obtained provided that $C^{pg}_{p,m}$ is known for each component.[22-24] Composition changes can be accurately monitored for a binary gaseous mixture by u measurements, without removing any substance; this offers advantages in measurements of the thermal diffusion factor[25] and in binary diffusion measurements.

(u, T, p) information may be utilized to evaluate any proposed form of the equation of state $V_m = V_m(p, T)$[26,27] or assist in the optimization of an existing (p, V_m, T) surface for a particular application.[28-30] An important industrial application of equations of state lies in calculation of mass flow rates through sonic nozzle flow meters;[31,32] these have been proposed for use with natural gas at ambient temperatures and pressures of up to 7 MPa[33] for the calibration of high-pressure custody transfer meters.[34]

Several different techniques for measurement of u in the gas phase have evolved. Interferometric methods exploit standing waves in an acoustic cavity. In this work a spherical interferometer has been employed to determine u; the precision obtainable with a sphere was noted by Bancroft,[35] has more recently been advocated by Rudnick and collaborators[36] and notably by Moldover *et al.*[37]

The theoretical description of the acoustic properties of a spherical envelope for the measurement of u have been developed by Moldover, Mehl and Greenspan,[38] and are discussed in Chapter Three. The detailed theoretical model has been facilitated by the simple geometry of a sphere. The most important corrections to the measured resonance frequencies f obtained in a perfectly spherical isotropic resonator account for: (1), the thermal boundary layer, with allowance for incomplete thermal accommodation of the gas with the shell; (2), the viscous boundary layer; (3), the finite compliance of the shell; and (4), openings in the wall of the resonator such as may be required to admit gas or to couple sound to remote transducers. The corrections to f, contribute to the resonance half width g, which including bulk dissipation provides a theoretical g. Comparison of measured and calculated resonance half widths allows evaluation of the thermal conductivity of the fluid and, where applicable, of the bulk viscosity. The radial resonances of a spherical cavity are especially useful for accurate speed of sound measurements.

The radially symmetric modes are non-degenerate, have high quality factors Q $\left(= f/(2g)\right)$ and the gas motion is normal to the resonator's inner surface. A consequence of the latter is that there is no viscous damping at the gas-wall interface for radial modes. The high quality factors permit the use of small inefficient transducers in the resonator's wall, thus minimizing the perturbation to the resonator-gas boundary. Measurements of the resonant

frequency for a particular mode yields the quantity (u/a), where a is the internal radius. To make absolute measurements of u a knowledge of a as a function of p and T is required. $\{(u/a), T, p\}$ measurements suffice to determine gaseous imperfections in the form of an equation of state. However, a knowledge of $a(T, p=0)$ allows the evaluation from equation (1) of R, T, or $C^{pg}_{p,m}(T)$. Combination of $C^{pg}_{p,m}(T)$ with an equation of state provides sufficient information to calculate any thermodynamic quantity for a pure substance or gaseous mixture. The radial resonances have been shown to be determined mainly by the resonator's volume;[39,40] the first non-vanishing correction to the resonance frequency resulting from geometric imperfections is of the second order. Thus, only the volume is required for accurate absolute measurements utilizing the radial modes, and a resonator constructed to usual machine-shop tolerances, without recourse to special machining methods is sufficient.

The values of $a(T, p)$ can be obtained from: (1), volume determination by weighing with a fluid of known density;[41] (2), dimensional microwave methods;[42-45] and (3), by calibrating with a gas of known A_0 (for example, Ar) combined with the pressure dependence determined by additional auxiliary methods.

The measurements presented here have been obtained with two spherical resonators operated in the temperature range 250 to 350 K, and at sufficiently high pressures and sufficiently low frequencies that linear hydrodynamics

applies.[46] A spherical resonator of nominal radius 60 mm was used for (u, T, p) measurements on pure non-cyclic isomers of C_4 and C_5 alkanes and methanol in the reduced temperature range $0.53 \leqslant T_r \leqslant 0.78$, at sufficiently low pressures to avoid the known effects of precondensation.[47] The measurements have served to determine $C_{p,m}^{pg}$ and acoustic virial coefficients which, when known over a temperature range, may be used to estimate (p, V_m, T) virial coefficients. Second acoustic virial coefficients at low reduced temperatures are particularly useful in the determination of intermolecular pair potential-energy functions.[48]

The vapour pressure of methylbutane was determined by comparative ebulliometry, extended to cover the temperature range 255 to 323 K. This provides particularly useful information for evaluating adjustable parameters in empirical equations of state.

A sealed spherical resonator of nominal radius 40 mm was constructed specifically for operation to 7 MPa† with the industrially important fluids methane, air, and natural gas. This information is required for evaluating equations of state applicable to such fluids, especially where these are used for calculations of mass flow rates through nozzles.

Methane undergoes vibrational relaxation. For the 40 mm resonator the first five radial modes occur in the f range 7 to 32 kHz, and at $p < 300$ kPa u measurements on methane showed significant speed dispersion.

---

†Although able to operate to 21 MPa no measurements were performed above 7 MPa.

The high-pressure apparatus has provided an opportunity to study the model used to describe acoustic energy losses in the spherical resonator at pressures at least a factor of seven greater than previously achieved.

REFERENCES

1. Saville, G. *Experimental Thermodynamics, Volume II, Experimental Thermodynamics of Non-Reacting Fluids.* Le Neindre, B.; Vodar, B.: Editors. For IUPAC. Butterworths: London, 1975. Chapter 6.

2. Cox, J.D.; Lawrenson, I.J. *Specialist Periodical Reports, Chemical Thermodynamics, Volume 1.* McGlashan, M.L.: Senior Reporter. Chemical Society: London. 1973, Chapter 3.

3. Brielles, J.; Dédit, A.; Lallemand, M.; Le Neindre, B.; Leroux, Y.; Vermesse, J.; Vidal, D. *Experimental Thermodynamics, Volume II, Experimental Thermodynamics of Non-Reacting Fluids.* Le Neindre, B.; Vodar, B.: Editors. For IUPAC. Butterworths: London. 1975, Chapter 7.

4. Malbrunot, P. *Experimental Thermodynamics, Volume II, Experimental Thermodynamics of Non-Reacting Fluids.* Le Neindre, B.; Vodar, B.: Editors. For IUPAC. Butterworths: London. 1975, Chapter 8.

5. Knobler, C.M. *Specialist Periodical Reports, Chemical Thermodynamics, Volume 2.* McGlashan, M.L.: Senior Reporter. Chemical Society: London. 1978, Chapter 7.

6. Mason, E.A.; Spurling, T.H. *The Virial Equation of State.* Pergamon: Oxford. 1969, Chapter 3.

7. Knobler, C.M. *Pure and Appl. Chem.* 1983, 55, 455.

8. Reference 1, pp.341-342.

9. $T_r = T/T^c$ where T^c is the critical temperature.

10. Plumb, H.; Cataland, G. *Metrologia* 1966, 2, 127.

11. Grimsrud, D.T.; Werntz, J.H. *Phys. Rev.* 1967, 15, 181.

12. Quinn, T.J. *Temperature. Monographs in Physical Measurement.* Editor: Cook, A.H. Academic Press: London. 1983, pp.84-98.

13. Colclough, A.R. *Proc. R. Soc. London* 1979, A365, 349.

14. Moldover, M.R.; Mehl, J.B. *Precision Measurements and Fundamental Constants II.* Taylor, B.N.; Phillips, W.D.(eds) Nat. Bur. Stand. (U.S.), Spec. Publ. 1984, 617, 281.

15. Gammon, B.E. *J. Chem. Phys.* 1976, 64, 2556.

16. Colclough, A.R.; Quinn, T.J; Chandler, T.R.D. *Proc. R. Soc. London A* 1979, 368, 125.

17. Moldover, M.R.; Trusler, J.P.M.; Edwards, T.J.; Mehl, J.B.; Davis, R. *J. Res. Natl. Bur. Std. (U.S.).* To be published.

18. Bancroft, D. *Am. J. Phys.* 1956, 24, 355.

19. Mehl, J.B.; Moldover, M.R. *J. Chem. Phys.* 1981, 74, 4062.

20. Mehl, J.B.; Moldover, M.R. *Proc. Eighth Symp. Thermophysical Properties.* Sengers, J.: Editor. *Am. Soc. Mech. Eng.:* New York. 1982. pp.134-141.

21. Ewing, M.B.; McGlashan, M.L.; Trusler, J.P.M. *J. Chem. Thermodynamics* 1986, 18, 511.

22. Keolian, R.; Garrett, S.; Maynard, J.; Rudnick, I. *J. Acoust. Soc. Am. Suppl.1,* 1973, 64, S561.

23. Keolian, R.; Garrett, S.; Maynard, J.; Rudnick, I. *Bull. Am. Phys. Soc.* 1979, 24, 623.

24. Brooks, J.S.; Hallock, R.B. *Rev. Sci. Instrum.* 1983, 54, 1199.

25. van Itterbeck, A.; Nihoul, J. *Acustica* 1955, 5, 142.

26. Reference 15.

27. Gammon, B.E.; Douslin, D.R. *J. Chem. Phys.* 1976, 64, 203.

28. Younglove, B.A.; McCarty, R.D. *Thermodynamic Properties of Nitrogen Gas Derived from Measurements of Sound Speed.* NASA Ref. Publication 1051 and NBSIR 79-1611. 1979.

29. Younglove, B.A.; McCarty, R.D. *J. Chem. Thermodynamics* 1980, 12, 1121.

30. McCarty, R.D. *Experimental Thermodynamics Volume II, Experimental Thermodynamics of Non-Reacting Fluids.* Le Neindre, B.; Vodar, B.: Editors. For IUPAC. Butterworths: London. 1975, Chapter 10.

31. Johnson, R.C. *J. Basic Eng. Trans. A.S.M.E.* series *D.* 1970, 92, 580.

32. Johnson, R.C. *Tables of Critical-Flow Functions and Thermodynamic Properties for Methane and Computational Procedures for both Methane and Natural Gas.* NASA. Spec. Pub. 3074, 1972.

33. Current maximum operating pressure of the British natural gas grid transmission system.

34. Peigne, M.G. *Measurement and Control* 1972, 5, T148.

35. Reference 18.

36. References 23 and 24.

37. Moldover, M.R.; Waxman, M.; Greenspan, M. *High Temp. High Press.* 1979, 11, 75.

38. Moldover, M.R.; Mehl. J.B.; Greenspan, M. *J. Acoust. Soc. Am.* 1986, 79, 253.

39. Campbell, I.D. *Acustica* 1955, 5, 145.

40. Mehl, J.B. *J. Acoust. Soc. Am.* 1982, 71, 1109.

41. Reference 17.

42. Reference 37.

43. Gallop, J.C.; Radcliffe, W.J. *J. Phys. E.* 1981, 14, 461.

44. Dominique, J.; Gallop, J.C.; Radcliffe, W.J. *J. Phys. E.* 1983, 16, 1200.

45. Gallop, J.C.; Radcliffe, W.J. *J. Phys. E.* 1986, 19, 413.

46. Greenspan, M. *Physical Acoustics. Volume IIA.* Mason, W.P.: Editor. Academic Press: London. 1965, pp. 1-43.

47. Mehl, J.B.; Moldover, M.R. *J. Chem. Phys.* 1982, 77, 455.

48. Ewing, M.B.; McGlashan, M.L.; Trusler, J.P.M. *Mol. Phys.* 1987, 60, 681.

49. Ambrose, D. *J. Phys. E.* 1968, 1, 41.

50. Ambrose, D. *Specialist Periodical Reports, Chemical Thermodynamics, Volume 1.* McGlashan, M.L.: Senior Reporter. Chemical Society: London. 1973, Chapter 7, pp. 240-246.

51. Ambrose, D. *Experimental Thermodynamics, Volume II, Experimental Thermodynamics of Non-Reacting Fluids.* Le Neindre, B.; Vodar, B.: Editors. For IUPAC. Butterworths: London. 1975, Chapter 13, pp. 626-634.

CHAPTER TWO

EQUATION OF STATE

2.1 INTRODUCTION

According to the phase rule, a phase of fixed composition has two degrees of freedom. Therefore, a chosen third intensive property, say X_3, can be written in terms of two independent intensive properties X_1 and X_2 by an equation of state

$$X_3 = X_3(X_1, X_2), \tag{2.1.1}$$

from which any intensive property can be expressed using the appropriate thermodynamic relations in terms of X_1 and X_2.

2.2 EQUATIONS OF STATE

Equations of state for a gaseous phase of fixed composition are classically expressed in terms of the intensive variables pressure p, molar volume V_m, and temperature T, in one of the following forms: (1), an infinite power series expansion in one intensive property p or V_m; and (2), closed empirical equations. The second category may be divided further into simple cubic equations in V_m which closely resemble van der Waals equation of state and more complicated expressions which have a variety of functional forms.

Virial expansion

The virial equation of state

$$Z = pV_m/RT = 1 + B(T)/V_m + C(T)/V_m^2 + \ldots \qquad (2.2.1)$$

may be derived[1] rigorously from statistical mechanics. In equation (1), R is the gas constant and B, C, ..., the second, third, ..., virial coefficients. The molar volume is often an inconvenient experimental variable for a gas and consequently the pressure-explicit expansion

$$Z = pV_m/RT = 1 + B'(T)p/(RT) + C'(T)p^2/(RT) + \ldots \qquad (2.2.2)$$

if often preferred. The coefficients B', C', ..., are related to the virial coefficients of equation (1) by

$$B' = B, \quad C' = (C - B^2)/(RT), \ldots, \qquad (2.2.3)$$

where both series of coefficients are, for a given substance, functions of T only.[2] A statistical mechanical derivation of equation (1) relates B, C, ..., to the intermolecular potential energies of clusters of two, three, ..., molecules at a time. In particular, the second virial coefficient is given by

$$B(T) = -2\pi L\int_0^\infty [\exp\{-U(r)\}/(kT)]r^2 dr, \qquad (2.2.4)$$

where $U(r)$ is the pair-wise intermolecular potential energy function and r is the intermolecular separation.[3] Expressions for the higher virial coefficients are complicated by the non-pairwise additivity of intermolecular potential energies. For example, C is given by

$$C(T) = -8\pi^2 L/3 \int_0^\infty \int_0^\infty \int_0^\infty [\exp\{-U(r_{12})/(kT)\} - 1]$$

$$\times[\exp\{-U(r_{13})/(kT)\} - 1].[\exp\{-U(r_{23})/(kT)\} - 1]$$

$$\times r_{12} r_{13} r_{23} dr_{12} dr_{13} dr_{23}$$

$$- 8\pi^2 L/3 \int_0^\infty \int_0^\infty \int_0^\infty [\exp\{-\Delta U_3(r_{12},r_{13},r_{23})\}/(kT) - 1]$$

$$\times\exp[-\{U_{12}(r_{12}) + U_{13}(r_{13}) + U_{23}(r_{23})\}/(kT)] \quad (2.2.5)$$

$$\times r_{12} r_{13} r_{23} dr_{12} dr_{13} dr_{23} , \ldots,$$

in which the function $\Delta U_3(r_{12},r_{13},r_{23})$ expresses the difference between the potential energy of a cluster containing three molecules and the sum of their pairwise energies.[3]

For a multicomponent gaseous mixture, virial coefficients are given by

$$B(T,x_A,x_B,\ldots) = \sum_i \sum_j x_i x_j B(T)_{ij}, \quad (2.2.6)$$

$$C(T,x_A,x_B,\ldots) = \sum_i \sum_j \sum_k x_i x_j x_k C(T)_{ijk}, \ \ldots, \quad (2.2.7)$$

$$(i,j,k,\ldots = A,B,C,\ldots),$$

and analogous relations for the coefficients of equation (2) apply. In particular, for a binary gaseous mixture $\{(1-x)A + xB\}$ equation (6) is written

$$B(T,x) = (1-x)^2 B_{AA} + 2(1-x)x B_{AB} + x^2 B_{BB}, \quad (2.2.8)$$

where B_{AA} and B_{BB} are the second virial coefficients of pure A and B respectively, and B_{AB} arises from interactions between molecules A and B.

Both equations (1) and (2) have the disadvantage that they are infinite series which must be truncated to represent a given set of measurements; criteria for determining the number of coefficients that can be justified for a set of (p, V_m, T) results have been discussed.[4-6] However, the problem of finding "true" values for the individual coefficients is more subtle. To obtain reliable values of B, measurements must be extended to pressures sufficiently low that the definition

$$B = \lim_{p\to 0}\{pV_m/(RT) - 1\}V_m \qquad (2.2.9)$$

is realised.[7,8] Similar conditions must be applied to avoid large systematic errors in experimentally determined higher coefficients in either expansion.

The quasi-chemical approach formulates the equation of state in terms of the formation of molecular clusters B_N in the gas phase by reversible polymerisation of N molecules of gas B. The standard equilibrium constant $K_N^{\ominus}$ for the polymerisation

$$N\mathrm{B} = \mathrm{B}_N \qquad (2.2.10)$$

is given by

$$K_N^{\ominus}(g,T) = f(\mathrm{B}_N)/\{f(\mathrm{B})\}^N . \quad (p^{\ominus})^{N-1} . \qquad (2.2.11)$$

where

$$f_A = \{x_A p\}\exp[\int_0^p \{V_m/(RT) - 1/p\}dp] \qquad (2.2.12)$$

is the fugacity for species A = B_i with i = 1,2,...,N of reaction (10), and $p^{\ominus}$ is the standard pressure. At sufficiently low pressures, the fugacity reduces to the

partial pressure

$$p_A = x_A p = \lim_{p \to 0} f_A. \qquad (2.2.13)$$

Consequently, equation (11) can be written in the form

$$K_{p,N}(g,T) = \lim_{p \to 0} \{x_A p/(x_B p)\}^N \qquad (2.2.14)$$

where $K_{p,N}$ is no longer a standard equilibrium constant, and the total pressure p and the molar volume V_m are given by

$$p = \sum_i x_A p, \text{ and} \qquad (2.2.15)$$

$$V_m = RT/\{\sum_i i x_A p\}, \text{ with} \qquad (2.2.16)$$

$$A = B_i;\ i = 1,2, \ldots, N. \qquad (2.2.17)$$

Whooley[9] showed that a knowledge of virial coefficients B, C, ..., is sufficient for evaluation of K_2, K_3, ..., from the relations

$$B = -K_2 RT, \qquad (2.2.18)$$

$$C = (4K_2^2 - 2K_3)(RT)^2, \ldots . \qquad (2.2.19)$$

An obvious inconsistency in this approach is that perfect gas behaviour has been assumed in the derivation of equations (13) to (17).

Simple cubic equations

The empirical equations of state discussed here are elaborations of van der Waals[10] equation of state (VDW)

$$p = RT/(V_m - b) - a/V_m^2 \qquad (2.2.20)$$

$$= (RT/V_m)/(1 - 4y) - a/V_m^2 \qquad (2.2.21)$$

with

$$y = b/(4V_m), \qquad (2.2.22)$$

where b is the volume excluded by the molecules. The first

term of equation (20) and (21) is an approximation to the pressure of a hard-sphere gas, while the second term represents the effect of attractive interactions between molecules.

Although equations (20) and (21) often give no more than qualitative agreement with experiment they never lead to physical nonsense, except perhaps at the critical point where, in common with all analytic equations of state, it lacks an appropriate singularity.

Use of two conditions at the critical point

$$(\partial p/\partial V_m)_T = 0, \quad (\partial^2 p/\partial V_m^2)_T = 0; \quad (T = T^c,\ p = p^c,\ V_m = V_m^c) \tag{2.2.23}$$

where T^c, p^c, and V_m^c are the critical temperature, pressure, and molar volume respectively allows the VDW equation to be written in reduced form

$$(p/p^c) = 8(T/T^c)/(3V_m/V_m^c - 1) - 3(V_m^c/V_m)^2, \tag{2.2.24}$$

with the critical compression factor

$$Z^c = p^c V_m^c/(RT^c) = 3/8. \tag{2.2.25}$$

Equation (24) is a statement of the principle of corresponding states. A pure fluid is said to follow the principle of corresponding states when Z can be written in the form:

$$Z = pV_m/(RT) = \phi(p/p^c,\ T/T^c), \tag{2.2.26}$$

where for each fluid ϕ is the same function. Thus, substances such as Ar, Kr, and Xe which obey equation (26) have the same compression factors at the same reduced temperatures and pressures. Simple substances which deviate slightly from the

principle are CH_4, CO, O_2, and N_2. Extending equation (26) to three independent variables, to include for example electric dipole moment, allows the formulation of a more general expression so that substances which do not obey equation (26) can be included in the treatment. An important example is Pitzer's equation[11]

$$Z = \phi_\omega(p/p^c,\ T/T^c,\ \omega), \qquad (2.2.27)$$

where ω the acentric factor is defined by

$$\omega = \log_{10}\{p^c/p^{1+g}(T/T^c = 0.7)\} - 1, \qquad (2.2.28)$$

and was chosen so that $\omega = 0$ for Ar, Kr, and Xe. Further important examples extend corresponding states with molecular shape factors.[12-14] Numerous equations of state have been proposed as improvements to equation (26); usually they are useful only in the limited (p, V_m, T) ranges where the additional parameter has been optimised.

The simple cubic equations of state for a pure substance may be represented by the generalized expression

$$p = RT/(V_m - b) - a(T)/\{V_m^2 + V_m cb - (c - 1)b^2\}, \qquad (2.2.29)$$

where $a(T)$ and b are parameters that have been adjusted using T^c, p^c, and ω. The choice of c has usually been more empirical.

When $c = 1$ equation (29) becomes the Redlich-Kwong equation of state (RK),[15] where $a(T)$ is given by

$$a(T) = a(T^c)/T^{\frac{1}{2}}, \qquad (2.2.30)$$

and $Z^c = 1/3$. (Critical compression factors for the cubic equations of state are compared in table 2.1.)

Table 2.1 Critical compression factors $Z^c = p^c V_m^c/(RT^c)$ for simple cubic equations of state with fixed values of parameter c in (29). Initials for the equations are defined in the text. For comparison $Z^c = 0.290$ within experimental error for seven substances: Ar, Kr, Xe, CH_4, N_2, O_2, and CO.

Equation	c	Z^c	Reference
VDW	1	3/8	10
RK	1	1/3	15
RKS	1	1/3	16
GL	1	1/3	17
PR	2	0.307401	21
H	3	0.286186	22

Several further modifications have been proposed to equation (30). Soave,[16] extended the temperature dependence by writing

$$a(T) = a(T^c).\alpha(T/T^c,\omega) = a(T^c)[1 + m(\omega)\{1 - (T/T^c)^{\frac{1}{2}}\}]^2, \quad (2.2.31)$$

where m is an additional parameter that has been correlated by

$$m = e + f\omega + g\omega^2. \quad (2.2.32)$$

Soave's values for e, f, and g are given in table 2.2. Combination of equations (29), (31), and (32) lead to the Redlich-Kwong-Soave equation of state (RKS).

Table 2.2 Values of adjustable parameters e, f, and g of equation (32) for cubic equations of state obtained by the original authors. Initials of equations of state are defined in the text.

Equation	e	f	g	Reference
RKS	0.480	1.574	-0.176	15
PR	0.37464	1.54226	-2.6992	21

Soave[16] and Gibbons and Laughton[17] have reported that the RKS equation of state is able to predict vapour pressures at $T/T^c > 0.7$ to within 2 per cent of experimental results for C_1–C_8 hydrocarbons and to within 4 per cent for polar substances such as CH_3OH and H_2O. For $T/T^c < 0.7$ the equation is less successful; for example the vapour pressures for polar substances may deviate by 30 per cent. By comparison the vapour pressures predicted by the RK equation, which does not contain ω, may be in error by as much as 300 per cent for C_1-C_8 hydrocarbons.[16]

Gibbons and Laughton[17] modified $\alpha(T/T^c)$ so that the calculation of vapour pressures was reliable to better than 2 per cent over the whole liquid range for a wide range of substances including H_2, CH_4, H_2O, CH_3OH, HCl, CS_2, CO_2, aromatic compounds, and hydrocarbons. The expression obtained by Gibbons and Laughton is given by

$$a(T) = a(T^c)\alpha(T/T^c) = a(T^c)[1 + X(T/T^c - 1) + Y\{(T/T^c)^{\frac{1}{2}} - 1\}] \quad (2.2.33)$$

in which X and Y are substance dependent constants; values for some substances are given in reference (17). Gibbons and Laughton found that their equations of state (GL) {equation (33) and the generalized cubic equation (29) with $c = 1$} predicted gaseous Z's to within a few per cent for hydrocarbons and polar substances even at $T/T^c < 0.7$. The uncertainty for polar substances of predicted gaseous densities was about 1 per cent which is similar to other cubic equations of state for non-polar substances.[17,18-20]

The Peng-Robinson equation of state (PR) results when $c = 2$ in the generalized equation (29) with $a(T)$ given by equations (31) and (32).[21] In equation (32) the adjustable parameters e, f, and g were selected so that the calculated vapour pressures were in error by no more than 3 per cent for the C_1-C_8 hydrocarbons, N_2, CO_2, and H_2S. Peng and Robinson's values for e, f, and g are given in table 2.2.

Harmens and co-workers have developed equations of state from equation (29) with $c = 3$[22] and with c as an adjustable parameter.[23]

The empirical equations discussed above retain the VDW approximation for a hard sphere fluid but elaborate the attractive term. An alternative approach is to modify the repulsive contribution. The virial expansion for a hard sphere fluid to seventh order is[24]

$$Z_H = pV_m/(RT) = 1 + 4y + 10y^2 + 18.365y^3 + 28.26y^4 + 39.5y^5 + 57y^6 + \ldots , \quad (2.2.34)$$

where y is given by equation (22). By comparison, the VDW expansion for hard spheres,

$$Z_H = 1 + 4y + 16y^2 + 64y^3 + 256y^4 + \ldots , \qquad (2.2.35)$$

is correct only to the second virial coefficient. Perhaps the best representation in closed form for the hard sphere compression factor Z_H is that due to Carnahan and Starling:[25]

$$Z_H = (1 + y + y^2 - y^3)/(1 - y)^3 \qquad (2.2.36)$$

$$= 1 + 4y + 10y^2 + 18y^3 + 28y^4 + 40y^5 + 54y^6 + \ldots . \qquad (2.2.37)$$

Non-cubic empirical equations

Extensive alterations to the repulsive and attractive terms of van der Waals equation have been proposed which lead to expressions that are no longer cubic in V_m. The equation of state developed by Beattie and Bridgeman,[26] which is probably the best known example, can be written

$$p = RT/V_m + (B_0RT - A_0 - Rc/T^2)/V_m^2 + (aA_0 - B_0bRT - RB_0c/T^2)/V_m^3 + RB_0bc/(V_m^4T^2), \qquad (2.2.38)$$

where a, b, c, A_0 and B_0 are adjustable constants. Although equation (38) retains a degree of mathematical simplicity, it can only provide representations of fluid (p, V_m, T) surfaces at densities ρ less than the critical density ρ^c.

Benedict, Webb and Rubin[27] (BWR) sought to modify equation (38) to obtain an equation that could describe for simple hydrocarbons the fluid (p, V_m, T) properties below $2\rho^c$, critical compression factors and, vapour pressure. Their

functional form, which was obtained from detailed examination of gaseous (p, V_m, T) results, is

$$p = RT/V_m + (B_0RT - A_0 - C_0/T^2)/V_m^2 + (bRT - a)/V_m^3 + a\alpha/V_m^6 + \{c(1 + \gamma/V_m^2)\exp(-\gamma/V_m^2)\}/(V_m^3T^2), \quad (2.2.39)$$

where a, b, c, A_0, B_0, C_0, α, and γ are adjustable parameters and values are available for a large number of simple organic and inorganic gases.[28]

Further modifications of equation (39) to provide more precise representations of (p, V_m, T) results and more recently other properties,[29,30] have given a variety of functional forms all of which contain exponential terms. The earliest example is due to Strobridge,[31] and his expression for N_2 has 16 parameters and two exponential terms.

Before the equations of state discussed above for pure fluids can be applied to mixtures, recipes must be adopted for the generalization of the adjustable parameters to mixtures. In the van der Waals one fluid approximation the molecular parameters of equation (20) for a multicomponent mixture are defined by[32]

$$b(x_A,x_B, \ldots) = \sum_{ij}\sum x_i x_j b_{ij}, \text{ and} \quad (2.2.40)$$

$$a(x_A,x_B, \ldots) = \sum_{ij}\sum x_i x_j a_{ij}; \qquad (i,j = A,B, \ldots) \quad (2.2.41)$$

where

$$b_{AB}^{1/3} = \tfrac{1}{2}(b_{AA}^{1/3} + b_{BB}^{1/3}), \quad (2.2.42)$$

which is exact for hard spheres, and

$$a_{AB} = \zeta\{a_{AA}a_{BB}/(b_{AA}b_{BB})\}^{\frac{1}{2}}b_{AB}, \qquad (2.2.43)$$

are the modified Lorentz-Berthelot combining rules. For the RKS, PR, and GL equations of state, the adjustable parameters for mixtures are given by

$$b(x_A,x_B,\ldots) = \sum_i x_i b_i, \quad (i = A,B,\ldots), \qquad (2.2.44)$$

with no cross terms, while $a(x_A,x_B,\ldots)$ is obtained from equation (41) with

$$a_{ij} = (1 - \xi_{ij})(a_{ii}a_{jj})^{\frac{1}{2}}, \quad (i,j = A,B,\ldots;\ i \neq j). \qquad (2.2.45)$$

In equation (45), ξ serves the same purpose as ζ in equation (43), and is a constant close to unity.

The generalization to mixtures of the eight parameters in the BWR equation of state are given in references (33) and (34).

As experimental results have accumulated for pure and multicomponent systems, both the functional form of the equation of state and the dependence of the adjustable parameters on composition have evolved to provide better representations of experiment. In particular two recent equations of state have been reported for the prediction of natural gas compression factors. Schouten *et al.*[35-39] developed {for the Thermodynamic Research Committee of Groupe European de Recherches Gazieres (GERG)} an equation of state based on equation (1) truncated after the third virial coefficients, valid for the components and composition ranges given in table 2.3. The virial coefficients $B(T,x_A,x_B,\ldots)$ were obtained from equation (6),

with the interaction virial coefficients determined experimentally from studies of binary mixtures of natural gas constituents, and $C(T,x_A,x_B,...)$ obtained from equation (7) with the approximation

$$C_{ijk} = \xi(C_{iii}C_{jjj}C_{kkk})^{1/3}, \qquad (2.2.46)$$

for species i, j, and k. In equation (46) ξ is a temperature independent adjustable parameter close to unity. In the

Table 2.3 Mole fractions x_B of allowed components B in the GERG equation of state for the calculation of Z for natural gas.

Component B	x_B
CH_4	$\geqslant 0.5$
N_2	$\leqslant 0.5$
CO_2	$\leqslant 0.3$
C_2H_6	$\leqslant 0.2$
C_3H_8	$\leqslant 0.05$
C_4H_{10} [a]	$\leqslant 0.015$
C_4H_{12} [a]	$\leqslant 0.005$
H_2	$\leqslant 0.1$
CO	$\leqslant 0.03$
He	$\leqslant 0.005$

[a] Includes all isomers.

temperature range 273 to 303 K and for pressures up to 8 MPa (which is the range of applicability claimed by Schouten) Melvin[40] found that Z was predicted to 0.1 per cent for natural gas. Starling *et al.*[41] followed the approach of Strobridge and developed {for the Gas Research Institute (GRI)} two modified BWR equations of state based primarily on experimental compression factors, vapour pressures, second virial coefficients, and molar excess enthalpies; one equation for CH_4 and the other for the substances given in table 2.4. The equations have been extended to permit the calculation of Z for natural gas to within 0.1 per cent in the temperature range 225 to 355 K at pressures up to 10 MPa. Both the GERG and GRI equations have been validated against the same set of experimental compression factors for real and synthetic natural gas mixtures.

Table 2.4 Components allowed with the GRI equation of state for the calculation of natural gas Z.

Component				
N_2	CH_4	nC_4H_{10}	nC_6H_{14}	O_2
CO_2	C_2H_6	iC_4H_{10}	nC_7H_{16}	CO
H_2S	C_3H_8	nC_5H_{12}	nC_8H_{18}	H_2
He		iC_5H_{12}	nC_9H_{20}	
			$nC_{10}H_{22}$	

2.3 EXPERIMENTAL METHODS

Equations of state are frequently studied by (p, V_m, T) methods. Unfortunately, molar volume $V_m = V/n$ (an intensive quantity) cannot be measured directly and must be inferred from vessel volume V and amount of substance n (both extensive quantities). However, standard thermodynamic relations allow the equation of state to be written in terms of other, directly measurable, intensive quantities such as the speed of sound. Thus, it is possible to study the equation of state without recourse to measurement of either volume or amount of substance.

Boyle's tube, shown in figure 2.1 is a simple apparatus for direct study of the equation of state, and allows measurement of the pressure p of a fixed amount of substance n confined within a variable volume V at a constant temperature T. The amount of substance present in the apparatus may be inferred from the $\lim_{p\to 0}\{pV/(RT)\}$ where R is the gas constant. The precision of the volume measurements can be increased in more sophisticated versions using a series of vessels joined by capillary tubing; the position of the mercury meniscus may be determined either visually or by means of electrical contact measurements. The experimental volumes may be calibrated by determining the mass of mercury required to exactly fill each one at the temperature of the experiment. Alternatively, the apparatus can be calibrated using a reference gas having a known equation of state. The method then becomes a relative one. The sample pressure needs to be accurately known; in

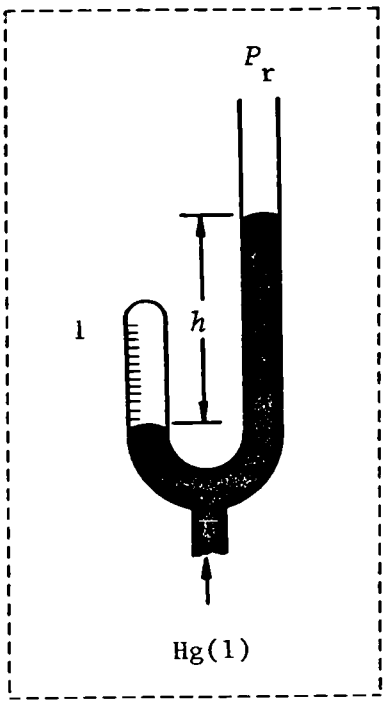

Figure 2.1. A Boyle's-tube for $(p,V)_{n,T}$ measurements. The Hg(l) serves to: (1) confine a constant amount of substance n of a gas in the previously calibrated left hand volume V ; and (2) to determine the sample pressure p_s relative to the reference pressure p_r in limb 1. The sample pressure is given by $p_s = p_r + \rho(\mathrm{Hg})gh$, where g is the local acceleration of free fall. The thermostat is indicated by the dotted line.

---

more complex experiments this is achieved by measuring the pressure of a reference gas that is required to null a differential pressure transducer, using a piston gauge or manometer.

In the methods discussed above, the temperature range is limited to that in which mercury is a liquid with an acceptably low vapour pressure. Alternatively, Hg can be avoided in gas expansion methods by use of values between the experimental volumes. The expansion method devised by Burnett[42] is shown in figure 2.2. Initially the

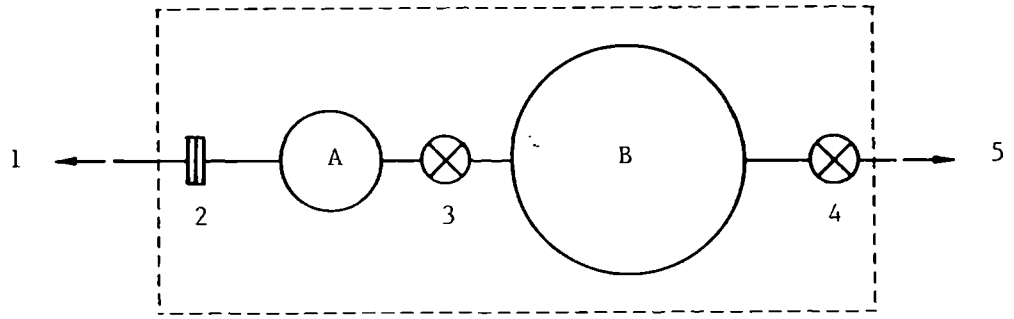

Figure 2.2. A schematic diagram of Burnett's apparatus. Two vessels A of volume V_A and B of volume V_B are connected *via* valve 3. The pressure in A is measured using the external pressure gauge 1 and null-detecting pressure transducer 2. The apparatus is connected to a vacuum system and sample supply 5 *via* valve 4. The dashed line is the thermostat.

apparatus is evacuated and then filled with sample to a suitable pressure; valve 3 is closed and vessel B evacuated.

Once equilibrium has been reached the pressure $p_0 = p_0(n_0, V_A)$ before the first expansion is measured. Valve 4 is then closed and valve 3 opened, so that the amount of substance n_0 occupies the volume (V_A+V_B). Again, when equilibrium has been attained, valve 3 is closed, and the new pressure $p_1 = p_1(n_0, V_A+V_B) = p_1(n_1, V_A)$ is measured before vessel B is again evacuated. An amount of substance n_1 remains in the apparatus. Further expansions are performed until the pressure can no longer be measured with sufficient accuracy or until the lowest pressure required is reached. Before the qth expansion from volume V_A the pressure p_{q-1} is given by

$$p_{q-1} = RTZ_{q-1}n_{q-1}/V_A. \qquad (2.3.1)$$

After the qth expansion to V_B the pressure p_q is

$$p_q = RTZ_q n_{q-1}/(V_A + V_B). \qquad (2.3.2)$$

Comination of equations (1) and (2) gives the pressure ratio

$$p_{q-1}/p_q = NZ_{q-1}/Z_q, \qquad (2.3.3)$$

where

$$N = (V_A + V_B)/V_A \qquad (2.3.4)$$

is the apparatus constant. It has been assumed that the pressure dependence of the vessel volumes, if significant, has been obtained in other experiments. Equation (3) is non-linear in the pressures. However, Burnett[42] described an elegent graphical analysis in which N is obtained from the pressure measurements using

$$N = \lim_{p\to 0}(p_{q-1}/p_q), \qquad (2.3.5)$$

and the compression factor Z_q at pressures p_q is given by

$$Z_q(p_q) = p_q N^q (Z_0/p_0). \qquad (2.3.6)$$

Rearrangement of equation (6) allows (Z_0/p_0) to be determined from a second extrapolation:

$$(Z_0/p_0) = Z_q/p_q N^q = \lim_{p\to 0}(p_q N^q)^{-1} \qquad (2.3.7)$$

In contrast with other (p, V_m, T) methods discussed here, the Burnett method gives Z directly at the experimental pressure. Consequently, the technique has often been used at high pressures, where with other approaches truncation of the virial expansion at the appropriate order may be a problem. In addition the Burnett method does not require the measurement of n or V. Although significantly greater demands than usual are placed on the pressure measurements, these are especially difficult to satisfy at low pressures. However, if two Burnett apparatus are connected by a differential pressure transducer then the pressure difference between a sample gas in one apparatus can be measured relative to that of a reference gas in the second apparatus.[43] This approach has been used successfully for sub-atmospheric measurements; a variation including 3 rather than 4 vessels has also been described.[44] This method requires only the measurement of one pressure.

The (p, V_m, T) methods described above may also be used for the study of gaseous mixtures. In particular measurements of $B(T,x)$ for a binary mixture, of B_{AA}, and of B_{BB} have been used with (2.2.8) to determine B_{AB}. More direct methods for binary mixtures are based on measurement

of the interaction virial coefficients:

$$\delta_{AB}(T) = B_{AB}(T) - \tfrac{1}{2}\{B_{AA}(T) + B_{BB}(T)\}. \qquad (2.3.8)$$

The interaction virial coefficient can be obtained directly from either the pressure change on mixing at constant volume[45] or the volume change on mixing at constant pressure.[46] The latter method has been little used.

In the above discussion of (p, V_m, T) methods the effect of adsorption has been ignored. Adsorption may be significant even at quite modest fractions of the vapour pressure p^{l+g}. Consequently, below the normal boiling temperature, where pressures are necessarily a large fraction of p^{l+g}, the accuracy of measurements is severely limited. The severity of adsorption of a substance at a particular pressure will depend on the surface-area-to-volume ratio and varies from one experimental method to another. For example, in a method with a moving mercury surface, compression measurements suffer from loss of material trapped by the advancing liquid, while in expansion experiments a retreating meniscus exposes degassed surfaces. For expansion methods which do not involve mercury, the effects of adsorption can be reduced by careful choice of the surface-area-to-volume ratios; if $V_A/V_B \approx S_A/S_B$, where S denotes surface area then the increase in surface area available for adsorption following an expansion is balanced approximately by the reduction in the total pressure and the effect is small provided that adsorption is linear in the pressure. However, this is not

so in measurements of the pressure change on mixing where the effects of adsorption can be large.[47] Adsorption models have been used to calculate corrections.[48]

Full accounts of (p, V_m, T) methods and results can be found in the literature for pure substances[49-53] and for mixtures.[54,55]

If an equation of state is to be studied under conditions where adsorption is significant then alternatives to (p, V_m, T) measurements must be sought. In particular, methods which are independent of the amount of substance are preferred. Also, if empirical equations of state are to be used for predicting a particular thermodynamic property then it is desirable that some measurements of that property be used in the correlation on which the equation of state is based.

The equation of state in the form

$$H_m = H_m(p,T) \qquad (2.3.9)$$

can be studied using an adiabatic flow calorimeter such as that shown schematically in figure 2.3. If the calorimeter is adiabatic and the changes in the potential and kinetic energies of the gas are negligible then the molar enthalpy change is

$$H_m(T_2,p_2) - H_m(T_1,p_1) = P/\dot{n}. \qquad (2.3.10)$$

In equation (10) P is the constant power dissipated in the heater C and $\dot{n}(= dn/dt)$ is the flow rate of the gas through the calorimeter.

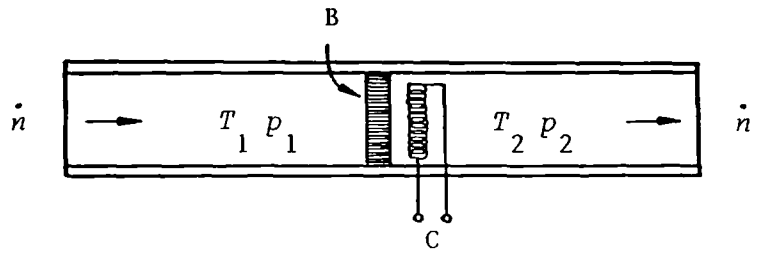

Figure 2.3. Schematic representation of an adiabatic flow calorimeter constructed from a thermally insulated tube A fitted with a throttle B and heater C. The temperatures T_1 and T_2 and pressures p_1 and p_2 as well as $\dot{n}$ are measured.

In the isothermal Joule-Thomson experiment the electrical power is adjusted so that $T_2 = T_1$, and equation (10) then becomes

$$H_m(T,p_2) = H_m(T,p_1) = P/\dot{n}. \qquad (2.3.11)$$

The isothermal Joule-Thomson coefficient ϕ_{JT}, defined by

$$\phi_{JT} = (\partial H/\partial p)_T = \{V_m - T(\partial V_m/\partial T)_p\} = -(RT^2/p)(\partial Z/\partial T)_p \qquad (2.3.12)$$

$$= \lim_{p_1 \to p_2} [\{H(T,p_2) - H(T,p_1)\}/(p_2 - p_1)],$$

and can provide equation of state information in a regime where adsorption would be a severe problem in (p, V_m, T) methods.[56] The main experimental difficulties arise from

heat leaks near the throttle and despite the attractions, the ϕ_{JT} experiment has proved difficult.

When no power is supplied to the heater the experiment is isenthalpic and provides the isenthalpic Joule-Thomson coefficient

$$\mu_{JT} = (\partial T/\partial p)_H = -\{V_m - T(\partial V_m/\partial T)_p\}/C_{p,m} \qquad (2.3.13)$$

from which equation of state information can also be obtained, provided that $C_{p,m}$ is known.

If the throttle B is removed from the calorimeter so that $p_2 = p_1$ and an electrical power P is dissipated in the heater, then the calorimeter becomes a heat capacity apparatus and $C_{p,m}$ may be obtained from the relation

$$C_{p,m} = (\partial H_m/\partial T)_p = \lim_{T_2 \to T_1} [\{H_m(T_2,p) - H_m(T_1,p)\}/(T_2 - T_1)]. \qquad (2.3.14)$$

Therefore, an alternative to ϕ_{JT} measurements is provided by μ_{JT} and $C_{p,m}$ measurements obtained from isenthalpic and heat capacity calorimeters in the same flow system. ϕ_{JT} is then obtained from the expression

$$\phi_{JT} = - C_{p,m}\mu_{JT}. \qquad (2.3.15)$$

This method has been applied successfully to obtain equation of state information for pure gases[57] and binary gaseous mixtures.[58]

The molar enthalpy of mixing $\Delta_{mix}H_m$ can be measured in an adiabatic flow calorimeter.[59] Measurements at sufficiently low pressures provide values of $(\delta_{AB} - T d\delta_{AB}/dT)$.

For gaseous flow calorimetric measurements on a condensible pure fluid, the constant flow rate may be obtained by boiling the liquid; $\dot{n}$ is then calculated from the electrical

power supplied to the boiler and the molar enthalpy of evaporation, $\Delta_l^g H_m$. Usually $\Delta_l^g H_m$ is obtained using another calorimeter in the same system.[60] Measurements of $\Delta_l^g H_m$, $p^{l+g}(T)$, and liquid molar volume can provide equation of state information from Clapeyron's equation.

The equation of state may be expressed in the form:

$$u = u(T,p). \tag{2.3.16}$$

The speed of sound u is formally independent of the amount of substance and can be accurately measured by interferometric techniques.

For a non-relaxing gas the measurable mechanical quantity u is related to the thermodynamic properties ρ and κ_S, the isentropic compressibility, by

$$u^2 = 1/(\rho\kappa_S) = V_m/(M\kappa_S) = (\partial p/\partial\rho)_S \tag{2.3.17}$$

$$= (ZRT/M)/[1 - p/Z(\partial Z/\partial p)_T - \{1 + T/Z(\partial Z/\partial T)_p\}^2/(C_{p,m}/R)]. \tag{2.3.18}$$

Equation (17) can be written in the alternative form

$$u^2 = A_0(T) + A_1(T)p + A_2(T)p^2 + \ldots \tag{2.3.19}$$

which is useful for gases studied along an isotherm. In equation (19), $C_{p,m}^{pg}(T)$ can be obtained from

$$A_o(T) = RT\gamma^{pg}(T)/M = RT/\{M(1 - R/C_{p,m}^{pg}(T)\}. \tag{2.3.20}$$

In addition, the second β_a, third γ_a, ..., acoustic virial coefficients may be obtained using the relations

$$\beta_a(T) = \{M/\gamma^{pg}(T)\}A_1(T) = RTA_1(T)/A_0(T), \text{ and} \tag{2.3.21}$$

$$\gamma_a(T) = \{M/\gamma^{pg}(T)\}A_2(T) = RTA_2(T)/A_0(T), \ldots . \tag{2.3.22}$$

The (p, V_m, T) virial coefficients B and C, or the coefficients C', may be calculated from acoustic virial coefficients, known over a temperature range, by solving the differential equations:

$$\beta_a(T) = 2B + 2(\gamma^{pg} - 1)T\mathrm{d}B/\mathrm{d}T + (\gamma^{pg} - 1)^2/\gamma^{pg}T^2\mathrm{d}^2B/\mathrm{d}T^2, \text{ and} \tag{2.3.23}$$

$$\begin{aligned}\gamma_a(T) = &[\{(1 + 2\gamma^{pg})/\gamma^{pg}\}C + \{(\gamma^{pg^2} - 1)/\gamma^{pg}\}T\mathrm{d}C/\mathrm{d}T \\ &+ \{(\gamma^{pg} - 1)^2/2\gamma^{pg}\}T^2\mathrm{d}^2C/\mathrm{d}T^2 - B\beta_a \\ &+ \{(\gamma^{pg} - 1)/\gamma^{pg}\}\{B + (2\gamma^{pg} - 1)T\mathrm{d}B/\mathrm{d}T + (\gamma^{pg} - 1)T^2\mathrm{d}^2B/\mathrm{d}T^2\}^2] \\ &\times \{1/(RT)\}\end{aligned} \tag{2.3.24}$$

$$\begin{aligned}= &(\gamma^{pg} + 2)C' + 2(\gamma^{pg} - 1)T\mathrm{d}C'/\mathrm{d}T \\ &+ \{(\gamma^{pg} - 1)^2/2\gamma^{pg}\}T^2\mathrm{d}^2C'/\mathrm{d}T^2 \\ &+ \Gamma(T).\end{aligned} \tag{2.3.25}$$

In equation (25) $\Gamma(T)$ is given by

$$\begin{aligned}\Gamma(T) = &\{1/(RT)\}[B^2 + \{(\gamma^{pg} - 1) + 4(\gamma^{pg} - 1)^2\}(T\mathrm{d}B/\mathrm{d}T)^2 \\ &+ \{(\gamma^{pg} - 1)^3/\gamma^{pg}\}(T^2\mathrm{d}^2B/\mathrm{d}T^2)^2 + 4(\gamma^{pg} - 1)TB\mathrm{d}B/\mathrm{d}T \\ &+ 2\{(\gamma^{pg} - 1)^2/\gamma^{pg}\}T^2B\mathrm{d}^2B/\mathrm{d}T^2 + 2\{(\gamma^{pg} - 1)^2(2\gamma^{pg} - 1)/\gamma^{pg} \\ &\times T^3\mathrm{d}B/\mathrm{d}T\mathrm{d}^2B/\mathrm{d}T^2]\end{aligned} \tag{2.3.26}$$

and is independent of C' and its derivatives. Explicitly, values of B have been obtained either by direct numerical integration of equation (23) with suitable initial conditions,[61-63] or by resorting to assumptions for example, those based on model intermolecular-potential energy functions.[64] C has been extracted from equation (24) by similar methods.[64]

For gaseous mixtures, γ^{pg} is given by

$$\gamma^{pg}(T,x_A,x_B,\ldots) = \sum_i x_i C^{pg}_{p,m}(i,T) / \sum x_i \{R - C^{pg}_{p,m}(i,T)\};$$

$$(i = A,B,\ldots,). \qquad (2.3.27)$$

However, $\beta_a(T,x_A,x_B,\ldots)$ can only be written in the simple form

$$\beta_a(T,x_A,x_B,\ldots) = \sum_{ij}\sum x_i x_j \beta_a(T)_{ij}, \quad (i,j = A,B,\ldots), \qquad (2.3.28)$$

analogous to equation (2.2.6), when the $\gamma^{pg}(T,i)$ for all species i are equal.[65] In particular for a binary gaseous mixture, $u(p)_T$ measurements provide sufficient information to determine the mole fraction, when $C^{pg}_{p,m}$ and M are known for each component.

In an interferometric experiment with a fixed geometry the experimental quantity is (u/d), where d is a characteristic dimension of the cavity such as path length L for a cylinder or radius a for a sphere. Consequently, the coefficients of an equation analogous to (19) are expressed as (A_i/d^2) and, although the acoustic virial coefficients are given by $(A_i/d^2)/(A_0/d^2)$, d is required before γ^{pg} can be obtained. Methods for determining $d(T,p)$ have been mentioned in Chapter One. By contrast, a constant-frequency variable-path length experiment necessarily gives u directly.

Although u is formally independent of amount of substance, recent experimental work[66,67] at pressures approaching p^{1+g} have shown anomalous results. These have been interpreted by Mehl and Moldover in terms of a precondensation phenomena.[67] They observed that the effect

was both greatest at low frequencies and depended on the surface finish of the resonators. The resulting perturbation is apparent as an increase in the resonance halfwidth and a decrease in the resonance frequency. Consequently, those measurements affected by precondensation can be identified and rejected. Model calculations indicate another, but smaller, anomaly at $p < 0.3\ p^{l+g}$ where the effect on the resonance frequency far exceeds that on the halfwidth. Since this anomaly is predicted to be independent of frequency, its existence could not be demonstrated except by measurements in resonators with different surface-area-to-volume ratios.[67] However, recent values of $C^{pg}_{p,m}$ obtained from $u(p,T)$ measurements at pressures below $0.3\ p^{l+g}$ compare favourably with those determined by flow calorimetry[68] or calculated from spectroscopic data.[69] In any case the uncertainties in equation of state information from (p, V_m, T) or ϕ_{JT} measurements, under similar conditions, are likely to be much greater.

REFERENCES

1. Mayer, J.E.; Mayer, M.G. *Statistical Mechanics.* Wiley: New York. Second Edition. 1977.
2. Mason, E.A.; Spurling, T.H. *Encyclopedia of Physical Chemistry and Chemical Physics. Volume 10.2, The Virial Equation of State.* Rowlinson, J.S.: Editor. Pergamon: Oxford. 1969. Chapter 1.
3. Maitland, G.C.; Rigby, M.; Smith, E.B.; Wakenham, W.A. *Intermolecular Forces. Their Origin and Determination.* Clarendon: Oxford. 1981. Chapter 3.
4. Hall, K.R.; Canfield, F.B. *Physica* 1967, 33, 481.
5. Holleran, E.M. *J. Chem. Thermodynamics* 1970, 2, 779.
6. Ewing, M.B.; Marsh, K.N. *J. Chem. Thermodynamics* 1979, 11, 793.
7. Scott, R.L.; Dunlop, R.D. *J. Phys. Chem.* 1962, 66, 639.
8. Knobler, C.M. *Pure and Appl. Chem.* 1983, 55, 455.
9. Woolley, H.W. *J. Chem. Phys.* 1953, 21, 236.
10. van der Waals, J.D. Thesis: Leydon 1873.
11. Pitzer, K.S.; Lippman, R.F.; Curl, R.F. Jr., Huggins, C.M.; Peterson, D.E. *J. Amer. Chem. Soc.* 1955, 77, 3433.
12. Leland, T.W.; Chappelear, P.S. *Ind. Eng. Chem.* 1968, 60, 15.
13. Leach, J.W., Chappelear, P.S., Leland, T.W. *A.I.Ch.E.J.* 1968, 14, 568.
14. Fisher, G.D.; Leland, T.W. *Ind. Eng. Chem. Fundamentals* 1970, 9, 537.
15. Redlich, O.; Kwong, J.N.S. *Chem. Rev.* 1949, 44, 223.

16. Soave, G. *Chem. Eng. Sci.* 1972, 27, 1197.

17. Gibbons, R.M.; Laughton, A.P. *J. Chem. Soc. Faraday Trans. 2*, 1984, 80, 1019.

18. Martin, J.J. *Ind. Eng. Chem. Fundam.* 1979, 18, 81.

19. Leland, T.W. *Phase Equilibria and Fluid Properties in the Chemical Industry.* Knapp, H.: Editor. DECHEMA; Frankfurt. 1980.

20. Gibbons, R.M. *The Application of Thermodynamics in Industry.* Society of Chemical Industry: Blackwell: London. 1984.

21. Peng, D.Y.; Robinson, D.B. *Ind. Eng. Chem. Fundam.* 1976, 15, 59.

22. Harmens, A. *Cryogenics* 1977, 17, 519.

23. Harmens, A.; Knapp, H. *Ind. Eng. Chem. Fundam.* 1980, 19, 291.

24. Ree, F.H.; Hoover, W.G. *J. Chem. Phys.* 1964, 40, 939.

25. Carnahan, N.F.; Starling, K.E. *J. Chem. Phys.* 1969, 51, 635.

26. Beattie, J.A.; Bridgeman, O.C. *Proc. Amer. Acad. Arts Sci.* 1929, 63, 229.

27. Benedict, M.; Webb, G.B.; Rubin, L.C. *J. Chem. Phys.* 1940, 8, 334.

28. Reid, R.C.; Sherwood, T.K. *The Properties of Gases and Liquids.* McGraw Hill: New York. Second Edition. 1966.

29. McCarty, R.D. *Experimental Thermodynamics, Volume II: Experimental Thermodynamics of Non-reacting Fluids.* Le Neindre, B.; Vodar, B.: Editors. For IUPAC. Butterworths: London. 1975. Chapter 10.

30. Younglove, B.A.; McCarty, R.D. *J. Chem. Thermodynamics* 1980, 12, 1121.

31. Strobridge, T.R. *The Thermodynamic Properties of Nitrogen from 64 to 300 K Between 0.1 and 200 Atmospheres*. Tech. Note. U.S. Nat. Bur. Stand. 129, 1962.

32. Leland, T.W.; Rowlinson, J.S.; Sather, G.A. *Trans. Faraday Soc.* 1968, 64, 1447.

33. Benedict, M.; Webb, B.; Rubin, L.C. *J. Chem. Phys.* 1942, 10, 747.

34. Benedict, M.; Webb, G.B.; Rubin, L.C. *Chem. Eng. Prog.* 1951, 47, 419.

35. Schouten, J.A.; Michels, J.P.J.; Prins, C.; van der Gulik, P.S.; Trappeniers, N.J. (in press) Report No.8410-1. van der Waals Laboratory, Netherlands. 1984.

36. Schouten, J.A.; ten Seldam, G.A.; Biswas, S.N.; Michels, J.P.J.; Trappeniers, N.J. (in press) Report No.8410-2. van der Waals Laboratory, Netherlands, 1984.

37. Schouten, J.A.; Michels, J.P.J.; ten Seldam, C.A.; Trappeniers, N.J. (in press) Report No.8410-3. van der Waals Laboratory, Netherlands. 1984.

38. Schouten, J.A.; Michels, J.P.J. (in press) Report No. 8410-4. van der Waals Laboratory, Netherlands, 1984.

39. Schouten, J.A.; Michels, J.P.J.; ten Seldam, G.A. (in press) Report No.4810-5. van der Waals Laboratory, Netherlands. 1985.

40. Melvin, A. *Proc. Congress Gas Quality - Specification and Measurement of Physical and Chemical Properties of Natural Gas.* van Rossum, G.J.: Editor. Elsevier; Oxford. 1986, p.852.

41. Starling, K.E.; Klein, M.; Little, F.G. *Proc. Congress Gas Quality - Specification and Measurement of Physical and Chemical Properties of Natural Gas.* van Rossum, G.J.: Editor. Elsevier: Oxford. 1986, p.211-237.

42. Burnett, E.S. *J. Appl. Mech.* 1936, 3, A136.

43. Toczylkin, L.S. PhD Thesis, University of London, 1984.

44. Ewing, M.B.; Marsh, K.N. *J. Chem. Thermodynamics* 1979, 11, 793.

45. Knobler, C.M.; Beenakker, J.J.M.; Knapp, H.F.P. *Physica* 1959, 25, 909.

46. Din, F.; Burn, I. *Trans. Faraday Soc.* 1965, 61, 1351.

47. Reference 8.

48. Reference 8.

49. Reference 2. Chapter Three.

50. Cox, J.D.; Lawrenson, I.J. *Specialist Periodical Reports, Chemical Thermodynamics Volume 1.* McGlashan, M.L.: Senior Reporter. Chemical Society: London. 1973. Chapter 5.

51. Saville, G. *Experimental Thermodynamics. Volume 2. Experimental Thermodynamics of Non-Reacting Fluids.* Le Neindre, B.; Vodar, B.: Editors for IUPAC. Butterworths: London. 1975. Chapter 6.

52. Brielles, J.; Dédit, A.; Lallemand, M.; Le Neindre, B.; Leroux, Y.; Vermesse, J.; Vidal, D. *Experimental Thermodynamics, Volume II, Experimental Thermodynamics of Non-Reacting Fluids.* Le Neindre, B.; Vodar, B.: Editors. For IUPAC. Butterworths: London. 1975. Chapter 7.

53. Malbrunot, P. *Experimental Thermodynamics, Volume II, Experimental Thermodynamics of Non-Reacting Fluids.* Le Neindre, B.; Vodar, B.: Editors. For IUPAC. Butterworths: London. 1975. Chapter 7.

54. Reference 2. Chapter Three.

55. Knobler, C.M. *Specialist Periodical Reports, Chemical Thermodynamics, Volume 2.* McGlashan, M.L.: Senior Reporter. Chemical Society: London. 1978. Chapter 7.

56. Francis, P.G.; Phutela, R.C. *J. Chem. Thermodynamics* 1979, 11, 747.

57. Bier, K.; Kunze, J.; Maurer, G. *J. Chem. Thermodynamics* 1976, 8, 857.

58. Bier, J.; Kunze, J.; Maurer, G. *J. Chem. Thermodynamics* 1980, 12, 151.

59, Reference 8.

60. Counsell, J.F. *Specialist Periodical Reports, Chemical Thermodynamics, Volume 1.* McGlashan, M.L.: Senior Reporter. Chemical Society: London. 1973. Chapter 6.

61. Bruch, L.W. *Phys. Rev.* 1969, 178, 303.

62. Bruch, L.W. *Phys. Rev. A* 1970, 2, 2167.

63. Mehl, J.B.; Moldover, M.R. *Proc. Eighth Symp. on Thermophysical Prop.* Sengers, J.V. Editor: Am. Soc. Mech. Eng.: New York. 1982, p.134.

64. Ewing, M.B.; Goodwin, A.R.H.; McGlashan, M.L.; Trusler, J.P.M. *J. Chem. Thermodynamics* (submitted)

64. Van Dael, W. *Experimental Thermodynamics Volume II, Experimental Thermodynamics of Non-Reacting Fluids.* Le Neindre, B.; Vodar, B.; Editors. For IUPAC. Butterworths: London. 1975. Chapter 11.

66. Reference 30.

67. Mehl, J.B.; Moldover, M.R. *J. Chem. Phys.* 1982, 77, 455.

68. Reference 63.

69. Ewing, M.B.; Goodwin, A.R.H.; McGlashan, M.L. Trusler, J.P.M. *J. Chem. Thermodynamics* 1987, 19, 721.

CHAPTER THREE

ACOUSTICS

3.1 INTRODUCTION

In this chapter we briefly discuss the Navier-Stokes equations of hydrodynamics for a pure gas. Under a wide range of conditions the effect of shear viscosity and thermal conductivity are small in the bulk fluid and do not perturb the sound speed. Molecular thermal relaxation is also considered; this phenomena can severely perturb the speed of sound u from the thermodynamics value $\{u^2 = (\partial p/\partial \rho)_S = (\rho \kappa_S)^{-1}\}$ and cause speed dispersion, while also increasing the absorption.

The discussion continues in section three with a closed cavity responding to a source of sound, whose strength is constant for sufficient time to create a steady-state; the wave motion then forms a standing wave when the frequency of the source is close to a natural frequency of the cavity and resonance occurs. The enclosure considered here is spherical, and thus provides a simple geometry for which the wave equation can be solved to satisfy the boundary conditions. Consequently, expressions have been obtained to relate resonance frequencies of the normal modes to the speed and absorption of sound in a gas. For a sphere the

radially symmetric modes are of particular interest, since the tangential fluid velocity is zero everywhere, and there is no viscous damping at the wall. These modes are also insensitive to geometric imperfections and, consequently, the resonator can be constructed without recourse to special machining methods, and a knowledge of the mean radius is sufficient to calculate a speed of sound. Combined with the favourable surface-area-to-volume ratio the radial mode resonances have high quality factors, which implies that small inefficient transducers can be used and that accurate measurements can be made with relative ease. Furthermore, for a sphere the shell motion in response to the acoustic pressure can be exactly modelled when constructed from an isotropic elastic material.

In the following discussion considerable emphasis is placed on the implications of the required formulae rather than a thorough derivation of each.

3.2 NAVIER-STOKES EQUATIONS OF HYDRODYNAMICS

In the presence of sound the pressure, temperature, and density are represented by $p + p_a(\vec{r},t)$, $T + T_a(\vec{r},t)$, and $\rho + \rho_a(\vec{r},t)$, where p_a, T_a, and ρ_a are small acoustic contributions to the equilibrium p, T, and ρ. Provided the acoustic quantities are small then the essential assumptions of linear acoustics are valid; namely the acoustic contributions are sufficiently small that their cross products and higher-order terms can be neglected, and also that the fluid speed is small compared to the sound speed. In practice these criteria can always be satisfied at

sufficiently small amplitudes.

The equations of motion for a gas with thermal conductivity and viscosity can be obtained by considering a small volume element of an unbounded gas. The Navier-Stokes equation for a viscous compressible fluid, which consists of a relationship between stress and spatial derivatives of velocity for a gas and Newton's second law, is given by

$$\rho(\partial\vec{U}/\partial t) = -\vec{\nabla}p_a + (\eta_b + 4\eta/3)\vec{\nabla}(\vec{\nabla}\cdot\vec{U}) - \eta\vec{\nabla}\times(\vec{\nabla}\times\vec{U}),^{(1,2)} \tag{3.2.1}$$

correct to first order in the acoustic variables, where $\vec{U} = \vec{U}(\vec{r},t)$ is the fluid velocity, η is the coefficient of shear viscosity and η_b of the coefficient of bulk viscosity; the origin of η_b will be considered in section two. Equation (1) can be separated into a pair of equations

$$\rho(\partial\vec{U}_l/\partial t) = -\vec{\nabla}p_a + (\eta_b + 4\eta/3)\vec{\nabla}(\vec{\nabla}\cdot\vec{U}_l) \text{ and,} \tag{3.2.2}$$

$$\rho(\partial\vec{U}_r/\partial t) = -\eta\nabla^2\vec{U}_r, \tag{3.2.3}$$

where $\vec{U}_l$ is the longitudinal component and $\vec{U}_r$ the rotational (transverse) component of the fluid velocity.[2]

The heat flow in the gas is described by Fourier's equation

$$\vec{J}_H = -\kappa\vec{\nabla}T_a, \tag{3.2.4}$$

where $\vec{J}_H$ is the heat current density and κ the coefficient of thermal conductivity. The acoustic cycle can also be expressed thermodynamically for a phase of fixed composition

by combination of the first and second laws,(3) with the result

$$TdS = q + W + pdV, \tag{3.2.5}$$

where S and V are the entropy and volume of the closed system respectively, and q is the heat, and W the work done on the system. If the gas viscosity is neglected, $W = -pdV$ and (5) reduces to $dS = q/T$, and if it is assumed that thermodynamic equilibrium is attained instantaneously within any infinitesimally small element dV of volume, then differentiation with respect to time gives

$$(\partial S/\partial t) = T^{-1}(\partial q/\partial t). \tag{3.2.6}$$

Using the equation of heat density continuity

$$(\partial q/\partial t) = -dV\vec{\nabla}\cdot\vec{J}_H, \tag{3.2.7}$$

and equation (4), (6) can be recast in the form:

$$(\partial S_a/\partial t) = (\kappa V_m/T)\nabla^2 T_a, \tag{3.2.8}$$

where S_a is the acoustic contribution to S_m the molar entropy, and V_m is the molar volume. Equation (8) provides a means of calculating the energy transfer as heat from thermal conduction.

The thermodynamic equation of state, for a phase of fixed composition is required to interelate ρ_a, p_a, and T_a through

$$\rho_a = (\partial\rho/\partial p)_T p_a + (\partial\rho/\partial T)_p T_a = \rho(\gamma\kappa_S\rho_a - \alpha_p T_a), \tag{3.2.9}$$

in which κ_S is the isentropic compressibilities respectively,

$\gamma = C_p/C_V$ is the ratio of the heat capacity at constant pressure to the heat capacity at constant volume, and $\alpha_p = V^{-1}(\partial V/\partial T)_p$ is the isobaric expansivity. S_a can also be related to T_a and p_a thermodynamically by:

$$S_a = (\partial S_m/\partial T)_p T_a + (\partial S_m/\partial p)_T p_a = C_{p,m} T_a/T - \alpha V_m p_a. \quad (3.2.10)$$

The longitudinal velocity $\vec{U}_l$ can be eliminated from equation (2) with the equation for mass-density continuity

$$(\partial \rho_a/\partial t) + \rho \nabla \cdot \vec{U}_l = 0, \quad (3.2.11)$$

and ρ_a subsequently eliminated using equation (9) to give

$$\nabla^2 p_a = \gamma/u^2\{(\partial^2/\partial t^2) - l_v u(\partial/\partial t)\nabla^2\}(p_a - \beta T_a), \quad (3.2.12)$$

where $\beta = (\partial p/\partial T)_V = \alpha/(\gamma \kappa_S)$ is the thermal pressure coefficient and l_v the characteristic viscous length given by

$$l_v = (\eta_b + 4\eta/3)/(\rho u). \quad (3.2.13)$$

Combination of equations (8) and (10) to eliminate S_a results in

$$\nabla^2 T_a = 1/(l_h u)(\partial/\partial t)\, T_a - \{(\gamma - 1)/(\gamma\beta)\} p_a , \quad (3.2.14)$$

where l_h, the characteristic thermal length, is given by

$$l_h = \kappa V_m/(u C_{p,m}). \quad (3.2.15)$$

Finally elimination of ρ_a from equation (2) using equations (9) and (11) gives the expression for the longitudinal fluid velocity:

$$\rho(\partial \vec{U}_l/\partial t) = - \vec{\nabla} T_a\{ + u l_v \gamma(\partial/\partial t)(p_a - \beta T_a). \quad (3.2.16)$$

Equations (12) and (14) can always be solved exactly for T_a and p_a. However, since the effects of viscosity and thermal conduction are small, it is sufficient to consider solutions correct to first order in η, η_b, and κ. Although equation (3) is not related to p_a and can be neglected in the bulk fluid, it is important when boundary conditions are to be satisfied.

For simple-harmonic wave motion with angular frequency ω, the longitudinal wave equations (12) and (14) can be solved simultaneously for T_a and p_a to give two positive roots which define the propagational and thermal modes.[6] A third solution for simple-harmonic motion arises from the rotational terms in the hydrodynamic equation (3) and defines the shear mode.[7] The propagational mode is sound-like and involves only longitudinal gas flow. The associated acoustic pressure p_p and temperature T_p generated by the propagating wave are both given by eigenfunctions of ∇ that have eigenvalues $-k^2$, where

$$k = (\omega/u) + i\alpha \qquad (3.2.17)$$

is the propagation constant for angular frequency ω. The coefficient of absorption α is given to first order in L_v and L_h by

$$\alpha = \omega/(2u)\{L_v + (\gamma - 1)L_h\}, \qquad (3.2.18)$$

which is appropriate when L_v and L_h are $<<1$ and ω is small. The dimensionless quantities L_v and L_h are related to l_v and l_h through

$$L_v = \omega l_v/u, \text{ and} \tag{3.2.19}$$

$$L_h = \omega l_h/u. \tag{3.2.20}$$

Equations (17) and (18) show that $u = (\rho\kappa_S)^{-\frac{1}{2}}$ is independent of frequency and the attenuation is small. However, if ω is large or l_v and l_h are not much less than unity, then second-order terms in L_v and L_h should be included, and the phase speed is not equivalent to $u = (\rho\kappa_S)^{-\frac{1}{2}}$. For Ar at 100 kPa and 300 K when the frequency is 100 kHz, L_v and L_h are both approximately 1×10^{-4}, and the phase speed and $u = (\rho\kappa_S)^{-\frac{1}{2}}$ are fractionally equivalent to a few parts in 10^8;[8] at 1 kPa and 20 kHz in Ar the phase speed differs from u fractionally by a few parts in 10^5.

The contribution of the propagational mode to T_a and $\vec{U}_1$ are given in terms of p_p through

$$T_p = \{(\gamma - 1)/(\gamma\beta)\}(1 - iL_h)p_p, \text{ and} \tag{3.2.21}$$

$$\vec{U}_{1,p} = 1/(i\omega\rho)(1 - iL_v)\vec{\nabla}p_p. \tag{3.2.22}$$

The thermal mode also contributes to T_a in the form of T_h, which again is an eigenfunction of ∇^2 with eigenvalue $-k_h^2$ and propagation constant

$$k_h = (1 + i)/\delta_h, \tag{3.2.23}$$

where δ_h, the thermal penetration length, is given by

$$\delta_h = (u/\omega)(2L_h)^{\frac{1}{2}} = \{\kappa M/(\pi\rho C_{p,m} f)\}^{\frac{1}{2}}. \tag{3.2.24}$$

Equation (23) describes thermal waves which are rapidly attenuated in the bulk fluid. The contribution of the

thermal mode to T_a and $\vec{U}_l$ are obtained by substitution of k_h from (23) into equations (12) and (14) to give

$$p_h = i\gamma\beta(L_h - L_v)T_h, \tag{3.2.25}$$

and hence by substitution of p_h in equation (16):

$$\vec{U}_{l,h} = \{\gamma\beta L_h/(\omega\rho)\}\vec{\nabla}T_h. \tag{3.2.26}$$

Finally, the shear mode is also rapidly attenuated with a propagation constant

$$k = (1 + i)/\delta_S, \tag{3.2.27}$$

where δ_S, the shear-wave penetration length, is given by

$$\delta_S = (u/\omega)(2L_S)^{\frac{1}{2}} = (2l_S u/\omega)^{\frac{1}{2}} = \{2\eta/(\rho\omega)\}^{\frac{1}{2}}, \tag{3.2.28}$$

where l_S, the characteristic shear length, does not include the bulk viscosity. The shear mode makes no contribution to T_a and p_a, and for gases δ_S is of the same order as δ_h.

By contrast in a closed cavity, where boundary conditions must be satisfied, thermal and shear modes become important. If the movement of any element of a non-rigid enclosure is assumed to depend only on the acoustic pressure acting there, then the boundary is one of local reaction.[9] Consequently, the boundary condition can be conveniently written in the form:

$$U_n(\vec{r}_S) = p_a(\vec{r}_S)y(\vec{r}_S,\omega)/(\rho u), \tag{3.2.29}$$

where U_n is the normal component of the total fluid velocity, at each position $\vec{r}_S$ on the surface S, and y_S is the specific acoustic admittance. Additional boundary conditions are

that the temperature must be continuous at the gas-wall interface, and that the tangential component U_t of $\vec{U}$ must vanish at the surface. These three boundary conditions cannot be satisfied by the propagational mode alone and generally three modes are required.[10] Consequently, at the gas-wall interface additional energy is withdrawn from the propagational mode, and the amplitudes of the thermal and shear modes are increased so that the temperature fluctuations and tangential velocity due to the propagational mode cancel. The amplitudes of the thermal and shear modes are a maximum at the boundary and decay according to their respective characteristic lengths δ_h and δ_S given by equations (24) and (28) respectively; the decay lengths are proportional to $(\omega\rho)^{-\frac{1}{2}}$ and consequently, are of increasing importance at low densities and frequencies. The region near the surface for which these modes are important are known as the boundary layers and are typically much less than the sound wave length in depth. Therefore, the contribution of the thermal and shear modes to the normal fluid flow must be included when the boundary condition for normal fluid flow is considered. Finally, the boundary condition (29) is satisfied by combination of the specific acoustic admittance, which arises from the thermal and shear boundary layers, and the mechanical admittance of the wall. Equation (29) can also be used to specify the boundary condition for standing waves in a cavity.[11] Consequently, we can now consider standing waves in a spherical acoustic cavity and the contributions to y_S which are important. However, the origin of η_b will be discussed first in the next section.

Complete discussions of linear acoustics,[12] the Navier-Stokes equations of hydrodynamics for a pure fluid,[12,13] and equation of continuity can be found in the literature.[14,15]

3.3 MOLECULAR THERMAL RELAXATION

In the presence of sound the density is continuously fluctuating at a frequency $\{\omega/(2\pi)\}$. The pressure of a gas depends on the translational modes of motion and, since few molecular collisions are required for equilibration of translational energy, the translational modes will adjust almost instantaneously to a change in the density of the gas. Consequently, for a monatomic gas at moderate temperature where only translational modes are accessible, thermodynamic equilibrium is achieved rapidly. However, for a polyatomic gas part of the energy change in the translational modes must be distributed between the available rotational and vibrational modes. These processes, of translation-rotation (T-R) and translation-vibration (T-V) transfer require finite times, and the pressure will decay with a time constant governed by the slowest process to the value which would be determined from thermodynamic arguments. The T-R and T-V exchanges, which are termed thermal relaxation, require molecular collision and obviously depend on the total gas density.[16] If the time constant for attainment of local thermodynamic equilibrium in a gas following a density change is much greater than $1/\omega$, where ω is the angular frequency, then heat and momentum transfer in the bulk gas are the only energy loss mechanisms and

absorption is classical. However, the propagational mode will no longer have a phase speed identical with $u = (\rho\kappa_S)^{-\frac{1}{2}}$, and is said to be dispersed. In addition, very high angular frequencies or low pressures are required to relax the rotational modes completely and under these conditions classical absorption will be severe as may classical dispersion.[17] When $1/\omega$ is much greater than the time constant for attainment of local equilibrium, so that T-R and T-V transfers can take place, then again sound attenuation and dispersion from these sources are not problems. Consequently, thermal-relaxation processes are important when the time constants and $1/\omega$ are comparable, in which case bulk viscosity needs to be included and classical effects may be only a small contribution to absorption. In summary, equilibrium will be achieved at each point in the acoustic cycle. If ω is large then some or all of the internal degress of freedom may cease to participate in the acoustic cycle. Each degree of freedom will have its own characteristic time of response known as its relaxation time.

The rate of approach of the j-th degree of freedom with energy E_j to its equilibrium value E_j^E is proportional to the difference $\Delta E = E_j - E_j^E$ through the first-order equation:

$$(\partial E_j/\partial t) = -\Delta E_j/t_j. \qquad (3.3.1)$$

This equation defines the relaxation time t_j of the j-th degree of freedom. When the sound is harmonic with angular frequency ω, the amplitude of actual energy fluctuations in the j-th degree of freedom is reduced from ε_j to $\varepsilon_j/(1 - i\omega t_j)$, where ε_j is the energy fluctuations which

would have occurred had equilibrium been attained simultaneously. Consequently it follows that, for the periodic temperature change associated with the acoustic wave, the j-th degree of freedom's contribution to either $C_{V,m}$ or $C_{p,m}$ will also be modified by a factor $(1 - i\omega t_j)^{-1}$.[18]

The relaxation times for T-R transfer are usually only a factor of ten greater than those for translational motion and, except for simple diatomics such as H_2, in polyatomic molecules the T-R transfer occurs almost every collision.[19] Consequently at ambient temperatures, where a large number of closely spaced rotational levels are populated, at worst only one rotational relaxation time is required, and the process can usually be ignored at audio frequencies.[20]

In contrast, the spacing between vibrational levels is comparatively large and only a small number of levels are populated. For a simple harmonic oscillator the transition probability $P_{0\to1}$ (activation), per molecular collision for the transfer between ground state (v=0) and the first excited state (v=1), is related to $P_{1\to0}$ (deactivation) probability through

$$P_{0\to1} = P_{1\to0} \exp\left[-\{h\nu/(kT)\}\right]. \qquad (3.3.2)$$

In equation (2) h is Planck's constant, T the thermodynamic temperature, k Boltzman's constant and ν the vibrational frequency. The vibrational relaxation time t_{vib} is related to $P_{1\to0}$ and $P_{0\to1}$ through

$$t_{vib} = \{(P_{1\to0} - P_{0\to1})Z\}^{-1}, \qquad (3.3.3)$$

where Z is the number of collisions which one molecule encounters per second. Combination of (2) and (3) gives

$$P_{1\rightarrow 0} = Zt_{vib}\{1 - \exp(-h\nu/kT)\} = Z_{1\rightarrow 0}^{-1}, \qquad (3.3.4)$$

where Z_{10} is the average number of collisions required for a molecule in the $V = 1$ state to deactivate the $V = 0$ state, is a more useful quantity since it is a measure of the difficulty of energy exchange. Consequently, a Z_{10} of unity corresponds to a transfer every collision.

Using Ehrenfest's Adiabatic Principle,†(21) and assuming that only repulsive intermolecular forces influence energy transfer, Landau and Teller developed a simple theory of vibrational relaxation which predicts P_{10} is proportional to $\exp(-T^{1/3})$;(22,23) many non-polar molecules show this behaviour over a wide temperature range.(24) For CH_4, since $Z_{10} \approx 10^4$, vibrational-relaxation speed dispersion cannot be ignored for the acoustic measurements reported in Chapter Six but, for C_4 and C_5 hydrocarbons $Z_{10} \approx 2$ and speed dispersion is not a problem for the acoustic measurements reported in Chapter Five;(25) Z_{10} refers to the fundamental vibrational transition with lowest wavenumber.

The effective molar heat capacity at constant volume at an angular frequency ω is given by

$$C_{V,m}^{eff}(T,p,\omega) = \{C_{V,m}(T,p) - \Sigma_j C_{vib,j,m}(T)\} + \Sigma_j C_{vib,j,m}(T)/(1 - i\omega t_j), \qquad (3.3.5)$$

---

†The principle states that if a changing force acts on a quantized periodic motion, the process is adiabatic if the force change is small during a period of motion, and non-adiabatic if the change is large during this time.

where $C_{V,m}(T,p)$ is the equilibrium value, and $C_{vib,j,m}$ is the contribution of the j-th vibrational mode of motion. For a molecule with m atoms there are $(3m - 5)$ vibrational modes when the molecule is linear, and $(3m - 6)$ when non-linear. Equation (5) assumes that the molecular degrees of freedom are independent, but in reality coupling between vibrational modes may be strong. The molar heat capacity at constant pressure can be written in the same form as (5) to give

$$C^{eff}_{p,m}(T,p,\omega) = \{C_{p,m}(T,p) - \Sigma_j C_{vib,j,m}(T)\} + \Sigma_j C_{vib,j,m}(T)/(1 - i\omega t_j). \quad (3.3.6)$$

Combination of equations (5) and (6) yields

$$\gamma(\omega,T,p) = [\gamma + \Sigma_j\{i\omega t_j/(1 - i\omega t_j)\}C_{vib,j,m}(T)/C_{V,m}(T,p)] /[1 + \Sigma_j\{i\omega t_j/(1 - i\omega t_j)\}C_{vib,j,m}(T)/C_{V,m}(T,p)], \quad (3.3.7)$$

where $\gamma(\omega,T,p)$ is the effective heat capacity ratio. If it is assumed that there is a single relaxation time t arising from one vibrational state or from a number of states coupling in series[26] then equation (8) can be written

$$\gamma(\omega)/\gamma = [1 + \{i\omega t/(1 - i\omega t)\}\Delta]/[1 + \{i\omega t/(1 - i\omega t)\gamma\Delta] , \quad (3.3.8)$$

where $\Delta = C_{vib,m}/C_{p,m}$. The series mechanism of vibrational relaxation can be understood by considering a molecule with two active vibrational modes with wavenumbers ν_1 and ν_2. Translational energy is first transferred into the $0 \rightarrow 1$

excitation of the ν_1 mode, this process constitutes the rate controlling step with relaxation line t_1; the mode ν_1 usually has the lowest vibrational wavenumber. Following this transfer a rapid process occurs where the one quantum of vibrational energy from mode ν_1 plus any required increment of translational energy is used to excite the $0 \rightarrow 1$ transition of mode ν_2, in a time t_{12}. The overall observed relaxation time t is related to t_1 by

$$t_1 = \{C_{\text{vib},1,\text{m}}(T)/\Sigma\ C_{\text{vib},j,\text{m}}(T)\}t. \qquad (3.3.9)$$

Most polyatomic molecules show this kind of behaviour.[27] Equation (8) can be expanded, when $\omega t << 1$, in a series to give

$$\gamma(\omega)/\gamma = 1 + (\gamma - 1)\Delta(1 - \gamma\Delta)(\omega t)^2 - (\gamma - 1)\Delta(\omega t) + O(\omega^3 t^3). \qquad (3.3.10)$$

The phase speed for simple harmonic motion is then given by

$$u(\omega) = u[1 + \tfrac{1}{2}(\gamma - 1)\Delta(\omega t)^2\{1 - 1/4\Delta(1 - 3\gamma)\}] + O(\omega^3 t^3), \qquad (3.3.11)$$

and the bulk viscosity is

$$\eta_b = (\gamma - 1)\rho u^2 \Delta t,^{(28)} \qquad (3.3.12)$$

where $u = (\rho\kappa_S)^{-\frac{1}{2}}$; for monatomic gases $\eta_b = 0$.

The phase speed $u(\omega)_{T,p}$ at low ω is equivalent to $u_{T,p}$ where $C^{\text{eff}}_{p,\text{m}} = C_{p,\text{m}}$, although as ω increases $u(\omega)_{T,p}$ asymtotically approaches a large value where $C^{\text{eff}}_{p,\text{m}}(\omega \rightarrow \infty) = C_{p,\text{m}} - \Sigma_j C_{\text{vib},j,\text{m}}$, passing through a point of inflection at an ω related to $1/t$,

and $u(\omega)_{T,p}$ is dispersed from $u_{T,p}$. However, $t\rho$ is constant and so t is larger at lower densities. Consequently, the frequency at which dispersion may be significant is lower at lower densities for a particular system.

The vibrational relaxation behaviour of gaseous mixtures can be qualitatively understood by considering the binary mixture $\{(1 - x)A + xB\}$. When only A can relax and A-A intermolecular energy exchange is inefficient but A-B very efficient, then small quantities of B will activate the relaxation process decreasing the relaxation time. It is known from theory and experiment that H_2O is a good catalyst for energy transfer particularly for CO_2.[29] If A-A exchange is efficient and A-B is not, then addition of B can have an anti-catalytic effect. However, when $x << 1$ the relaxation time is not appreciably affected and the mixture will relax like pure A.[30] When B can also undergo vibrational relaxation and, if pure A and B each have one vibrational relaxation time, then in the mixture one or two relaxation times will exist. Between A and B there are 4 allowed T-V transfers and one possible V-V transfer in which vibrational energy for a mode of A with frequency ν_i is transferred to a mode with frequency ν_j of B with a relaxation time t_{V-V}).[31] If V-V transfer does not occur then two characteristic relaxation times $t(A,x)$ and $t(B,x)$ may be observed. For simplicity, assume pure A relaxes slowly with t_A and pure B rapidly with t_B: if V-V intermolecular transfer is fast ($\nu_i \simeq \nu_j$) compared to the other processes, then only one relaxation time characteristic

of B will be observed. This process is analogous to the rapid intramolecular vibrational energy exchange which occurs in series coupling. However, if V-V transfer is slow so that $t_{(A,x)} > t_{V-V} > t_{(B,x)}$ then two relaxation times are again possible; one for the vibrational heat capacity of A, relaxing *via* the rate determining V-V transfer, and another for that of B relaxing independently. This situation is analogous to an intramolecular V-V transfer, which is slow compared to T-V transfer for the lowest wavenumber vibrational mode, where more than one vibrational relaxation time might be observed.

In gaseous mixtures diffusion also causes additional sound absorption and contributes to η_b. Alternating temperature gradients (which cause thermal diffusion) and alternating density gradients (which result in preferential flow of the lighter component) both create a periodic separation of the components. However, if binary diffusion is absent then the separation is reversible, but concentration gradients are damped by irreversible diffusion and energy is lost from the acoustic cycle. For a binary has mixture $\{xA + (1-x)B\}$ the additional contribution to η_b is given by

$$\eta_{b,diff} = \{\gamma^2 x(1 - x)pD_{12}/u^2\}[\{(M_A - M_B)/M\} + \{(\gamma - 1)D_T/\{\gamma D_{12}x(1 - x)\}\}]^2, \qquad (3.3.13)$$

where M is the mean molar mass of the mixture, M_A and M_B are the molar masses of components A and B, D_{12} is the binary

diffusion coefficient, and D_T the thermal diffusion factor.[32] Kohler has commented on the magnitude of $\eta_{b,diff}$ for particular gas mixtures. When one component is H_2 or He and the other a heavier species then the effect is large, although with air (0.8 N_2 + 0.2 O_2) the increase in absorption over the classical effect is only by a factor 1.003.[33] Furthermore, in disparate $\{M_A << M_B\}$ binary gas mixtures double sound propagation has been predicted with a fast and slow propagational mode.[34]

Finally in chemically reacting gaseous mixtures, or pure substances undergoing dimerization, it is known that further contributions to absorption and dispersion occur.[35-37]

Complete coverage of vibrational and rotational relaxation in gases, and gaseous mixtures, experimental methods, surveys of t_j measurements, and descriptions of chemically reacting systems can be found in the literature.[38,39,40]

3.4. ACOUSTIC MODEL

We begin the discussion of the acoustic model with the time dependent wave equation

$$\{\nabla^2 + (k/\omega)(\partial^2/\partial t^2)\}\Psi(\vec{r},t) = 0, \qquad (3.4.1)$$

where $\Psi(\vec{r},t)$ is the velocity potential for a region of the cavity. The acoustic pressure p_a and acoustic particle velocity U are related to $\Psi(\vec{r},t)$ through

$$p_a(\vec{r},t) = i\omega\rho\Psi(\vec{r},t) \text{ and} \qquad (3.4.2)$$

$$U(\vec{r},t) = \nabla\Psi(\vec{r},t). \qquad (3.4.3)$$

Assuming a simple-harmonic time dependence, the velocity potential may be written

$$\Psi(\vec{r},t) = \Phi(\vec{r})\exp(-i\omega t), \qquad (3.4.4)$$

where the spatial function $\Phi(\vec{r})$ is a solution of the Helmholtz equation:

$$(\nabla^2 + k^2)\Phi(\vec{r}) = 0. \qquad (3.4.5)$$

The propagation constant k in equation (5) is given by

$$k = (\omega/u) + i\alpha, \qquad (3.4.6)$$

where α is the coefficient of absorption. The solutions of the Helmholtz equation that are allowed within a cavity must satisfy the boundary condition

$$U_n(\vec{r}_S) = p_a(\vec{r}_S)y(\vec{r}_S,\omega)/(\rho u) \qquad (3.4.7)$$

for all positions $\vec{r}_S$ on the surface of the enclosure. In equation (7), U_n is the normal component of the fluid velocity, y is the specific acoustic admittance and ρ is the fluid density.

In spherical coordinates, the solutions of (5) that are finite at the origin are given by

$$\Phi_N(\vec{r}) = j_l(kr)Y_{nm}(\theta\zeta), \quad (N = l,n,m) \qquad (3.4.8)$$

where j_l is the l-th order spherical bessel function and the Y_{nm} are spherical harmonics. In a rigid sphere of radius a, centred at the origin, containing a fluid free from dissipative effects then $y = 0$, $k = \omega/u$, and equation (7) reduces to

$$\{dj_l(k_{ln}r)/dr\}_{r=a} = 0. \qquad (3.4.9)$$

The eigenvalues $\nu_{ln} = k_{ln}a$ are then the n-th turning points of the spherical bessel functions of order l and are labelled l = 0,1,2 ... and n = 1,2,... . Extensive tables of ν_{ln} can be found in the literature;[41,42] an abbreviated list sufficient for the present work is given in table 3.1. In this zeroth-order approximation, derived first by Rayleigh,[43] the natural frequencies are given by

$$f_{ln}^{(0)} = u\nu_{ln}/(2\pi a). \qquad (3.4.10)$$

Consequently, measurement of $f_{ln}^{(0)}$ and the sphere radius give a value for the speed of sound. The modes are $(2l+1)$ fold degenerate and have l longitudinal nodal surfaces with $m = -l,\ldots,0,\ldots l$ axial nodes and $(n+1)$ spherical nodes, except for l = 0 where there are n spherical nodes.

Table 3.1 Values of ν_{ln} for l = 1,2,3,...9 and n = 1,2,3...9 taken from reference (41). The usual convertion for the labelling of ν_{ln} is adopted here with ν_{01} = 0.

ν_{ln}	l=0	1	2	3
n=1	0.0	2.08157598	3.34209366	4.51409965
2	4.49340946	5.94036999	7.28993230	8.58375496
3	7.72525184	9.20584014	10.61385504	11.97273003
4	10.90412166	12.40444502	13.84611188	15.24453182
5	14.06619391	15.57923641	17.04290219	18.46814778
6	17.22075527	18.74264558	20.22185656	21.66660692
7	20.37130296	21.89969648	23.39049019	24.85008531
8	23.51945250	25.05282528	26.55258922	28.02387443
9	26.66605426	28.20336100	29.71027992	31.19101609

ν_{ln}	l=4	5	6	7
n=1	5.64670362	6.75645633	7.85107768	8.93483888
2	9.84044604	11.07020687	12.27933398	13.47203035
3	13.29556386	14.59055216	15.86322182	17.11750573
4	16.60934590	17.94717953	19.26270994	20.55942813
5	19.86242396	21.23106830	22.57805807	23.90644997
6	23.08279562	24.47482532	25.84608427	27.19924537
7	26.28326537	27.69371570	29.08434633	30.45750216
8	29.47063674	30.89600220	32.30249156	33.69217225
9	32.64889472	34.08659873	35.50632973	36.90992061

Table 3.1 Continued

ν_{ln}	l=8	9
n=1	10.01037075	11.07941839
2	14.65126281	15.81921549
3	18.35631834	19.58188902
4	21.84001208	23.10656842
5	25.21865244	26.51660256
6	28.53646066	29.85949274
7	31.81510523	33.15875397
8	35.06676462	36.42771813
9	38.29891634	39.67463338

For a real practical resonator containing a real gas, the admittance of the boundary $y_S(\vec{r}_S,\omega)$ is a function of the gas thermophysical properties and the mechanical compliance of the wall. Also, the cavity will have a slightly imperfect geometry and will contain small surface imperfections, for example from the presence of acoustic transducers. In order to determine the speed of sound from the study of the eigenfrequencies F_N, the normal modes and corresponding eigenvalues of a real cavity containing a real fluid must be related to those of the ideal enclosure

containing a gas free from dissipative effects. The required expressions have been obtained for a resonator, containing a source point, using a Green's function for the cavity which is expressed in terms of the eigen functions of the ideal cavity $\phi_N(\vec{r})$.[44,45] Consequently, the eigenfunction $\Phi_N(\vec{r},\omega)$ which defines the normal modes and their corresponding eigenvalues $K_N(\omega)$ can then be found for a real cavity and gas combination, where $y_S(\vec{r}_S,\omega) \neq 0$. Provided the surface admittance is uniform over all the surface S of the resonator (or uniform over defined portions of S) and S is close to S_I of the geometrically perfect cavity, then it has been shown that $\Phi_N(\vec{r},\omega)$ has the same form as $\phi(\vec{r})$;[44,45] for a carefully manufactured resonator $S \approx S_I$. Therefore a first order solution for $K_N(\omega)$ is appropriate, which can be obtained with $\Phi_N = \phi$ and $S = S_I$ with the result

$$\{K_N(\omega)/k_N\} = 1 - \{i/(2k_N V \Lambda_N^0)\iint_S y_S(\vec{r}_S,\omega)\phi_N^2(\vec{r}_S)dS\} \qquad (3.4.11)$$

correct to first order in y_S, where the integration is performed over all S. In equation (11) V is the volume of the cavity and Λ_N^0 the N-th normalisation constant for the idealized cavity given by

$$\Lambda_N^0 = 1/V\iiint\phi_N^2(\vec{r})dV, \qquad (3.4.12)$$

and $K_N(\omega)$ is related to:

$$K_N(\omega) = \omega_N(\omega)/u = 2\pi F_N(f)/u. \qquad (3.4.13)$$

The frequency appropriate to the experiment must be employed, for free oscillations of the N-th standing wave

the real part of $\omega = \omega_N = 2\pi(f_N - ig_N)$ must be used, and for driven motion in steady state measurements $\omega = 2\pi f$ where f is the source frequency; $\omega = 2\pi f_{0n}$ when the cavity is driven at its n-th radial resonance frequency.

In a spherical cavity the modes for which $l=0$ are radially symmetric, non-degenerate, and usually have high quality factors Q. These modes are especially useful in determining (u/a) since the acoustic particle velocity is normal to the wall and, consequently, there is no contribution to $y_S(\vec{r}_S,\omega)$ from viscous damping at the gas-wall interface;[46-48] the $l=0$ modes have been used extensively in this work.

For the $l=0$ case a particular form of equation (12) has been obtained,[46] and since $\phi_{0n} = j_0(\nu_{0n})$ and $\Lambda^0_{0n} = 3/2 j_0^2(\nu_{0n})$, the complex natural frequency of n-th radial mode can be recast in the form:

$$F_{0n}(f) = (f_{0n} - ig_{0n}) = \nu_{0n}u/(2\pi a) - iu/(2\pi a)\alpha(f) - iu/(2\pi a)\iint y_S(\vec{r}_S,f)dS/\iint dS. \qquad (3.4.14)$$

The neglect of terms to second order in y_S, which are uniform over S result in an uncertainty $-\frac{1}{2}(y_S/\nu_{0n})^2$.[45] The imaginary term represents the losses and is observed as the resonance half width g defined as $\frac{1}{2}$ the resonance line width at $1/\sqrt{2}$ of the maximum amplitude (excluding any background), or the decay constant in free vibrations. The observed complex resonance frequency of the radial mode is usually written in the form

$$F_{0n} = f_{0n} - ig_{0n} = \nu_{0n}u/(2\pi a) + \Sigma_j(\Delta f - ig)_j, \qquad (3.4.15)$$

where $(\Delta f - ig)_j$ is the j-th perturbation term and includes the bulk attenuation and surface contributions. This first-order perturbation model, for the radial modes, was first discussed by Mehl and Moldover.[45] They considered the contributions to y_S from: (1) the thermal boundary layer y_n; (2) the non-zero mechanical compliance of the wall y_w; and (3) y_0 that arises from the presence of openings in the enclosure. Elsewhere, Mehl has considered the perturbations due to imperfect geometry on the radial,[49] and non-radial modes;[50] Mehl has also considered the compilance of an isotropic elastic sphere.[51] More recently Moldover, Mehl and Greenspan[47] have presented the exact theory for the viscous and thermal boundary layers of a sphere and have also included in their model, using perturbation theory, the effects of surface roughness and joins between the two hemispheres. However, the boundary condition imposed for the temperature at the gas-wall interface by Moldover *et al.* has been extended to include the temperature-jump effect, required for low pressure measurements, by Ewing, McGlashan and Trusler.[48]

The first-order perturbation model has been extensively tested by measurements below 1 MPa using a variety of radial and non-radial modes.[46,47,48,52]

In the remainder of this chapter the important contributions to the total specific acoustic admittance of the boundary, which have been reported previously,[46-51]

are briefly discussed for the radial modes. However, some interesting points concerning non-radial modes are mentioned. The effects of geometric imperfections are also mentioned, as is the steady-state response.

Thermal boundary layer

For radial modes the fluid flow is irrotational and the boundary condition for the temperature requires the temperature to be continuous at the gas-wall interface. For a gas enclosed by a metal surface this reduces to a requirement for constant temperature at the wall. Therefore the boundary condition can be written $T_a(r=a) = 0$, where T_a is the total acoustic temperature. The thermal boundary layer for a pure fluid that obeys the Navier-Stokes equations has been discussed in detail elsewhere,[46-48] and provides an accurate description of the behaviour of real gases provided the molecular mean free path is much less than the acoustic wavelength λ. However, this approach assumes that the thermal conductivity of the gas close to the wall is equal to the bulk gas thermal conductivity and thus neglects the temperature jump effect. Ewing, McGlashan and Trusler[48] have applied a more fundamental boundary condition; that is the heat current density in the gas and wall must be equal at the interface. This condition is fulfilled by assuming an apparent temperature discontinuity ΔT between the temperature of the gas (assumed equal to the bulk gas temperature T) and the wall temperature at the gas-wall interface. Assuming that simple kinetic theory is applicable ΔT is given by[53-55]

$$\Delta T = J_h l_a/\kappa, \qquad (3.4.16)$$

where κ is the gas thermal conductivity, J_h is the magnitude of the heat current density into the wall at the surface, and the thermal accommodation length l_a is

$$l_a = (\kappa/p)\{\pi MT/(2R)\}^{\frac{1}{2}}\{C_{V,m}/R + \tfrac{1}{2}\}^{-1}\{(2 - h)/h\} \qquad (3.4.17)$$

In this equation, M is the molar mass of a gas with molar heat capacity at constant volume $C_{V,m}$ and h is the thermal accommodation coefficient; h is defined as the ratio of actual energy transported across the interface to that which would have been transported had all the molecules come to thermal equilibrium with the wall before re-emission. The value of h depends on the surface finish of the wall material and absorbed layer of molecules; for He on a vacuum-flasked smooth tungsten surface $h = 0.017$,[55] while for Ar on a machined and mechanically polished aluminium alloy surface $h = 0.84$.[48] Values are closer to unity for heavier gases and surfaces which are not vacuum flashed.[56,57]

The thermal boundary condition for the temperature assuming classical heat flow with a small temperature discontinuity across the gas-wall interface is given by[48]

$$T_a(r=a) = -J_h l_a/\kappa = -l_a(dTa/dr)_{r=a}. \qquad (3.4.18)$$

Ewing, McGlashan and Trusler have subsequently obtained an expression for the specific acoustic admittance of the thermal boundary layer:

$$y_h = (\gamma - 1)\omega/(2a)\delta_h\{(1 - i) - (\delta_h/a) + 2i(l_a/\delta_h)\}, \qquad (3.4.19)$$

correct to first order in (δ_h/a) and (l_a/δ_h), and second order in (δ_h/λ), where δ_h is given by equation (3.2.24). Assuming y_h is uniform over the surface then combination of surface admittance term in equations (14) and (19) gives the shift in resonance frequency and contribution to the resonance half width from the thermal boundary layer as:

$$(\Delta f_h - ig_h) = -(1 + i)\{(\gamma - 1)/(2a)\}f\delta_h + \{(\gamma - 1)/(2a^2)\}f\delta_h^2 + (\gamma - 1)\,(l_a/a), \quad (3.4.20)$$

correct to first order in y_s. In equation (20), the first term describes the loss at a plane surface, the second term accounting for the curvature of the surface only contributes to the resonance half width, and the third term, which contributes only to $\Delta f_h/f$, takes account of the temperature jump effect, and contributes only to $\Delta f_h/f$. Since l_a, from equation (17), is proportional to p^{-1} the temperature-jump effect is of increasing importance as the pressure is reduced; for Ar at 10 kPa and 273.16 K with h = 0.84 the term $(\gamma-1)(l_a/a) = 17 \times 10^{-6}$ in a resonator with a = 60 mm.

The thermal penetration length, given by equation (3.2.24), is proportional to $\rho^{-\frac{1}{2}}$ and consequently the values obtained from equation (19) for $(\Delta f - ig)_h/f$ are largest at the lowest density on an isotherm. For a plane surface neglecting the temperature jump effect, $(\Delta f - ig)_h a/f$ is shown in figure 3.1 as a function of density for Ar and CH_4.

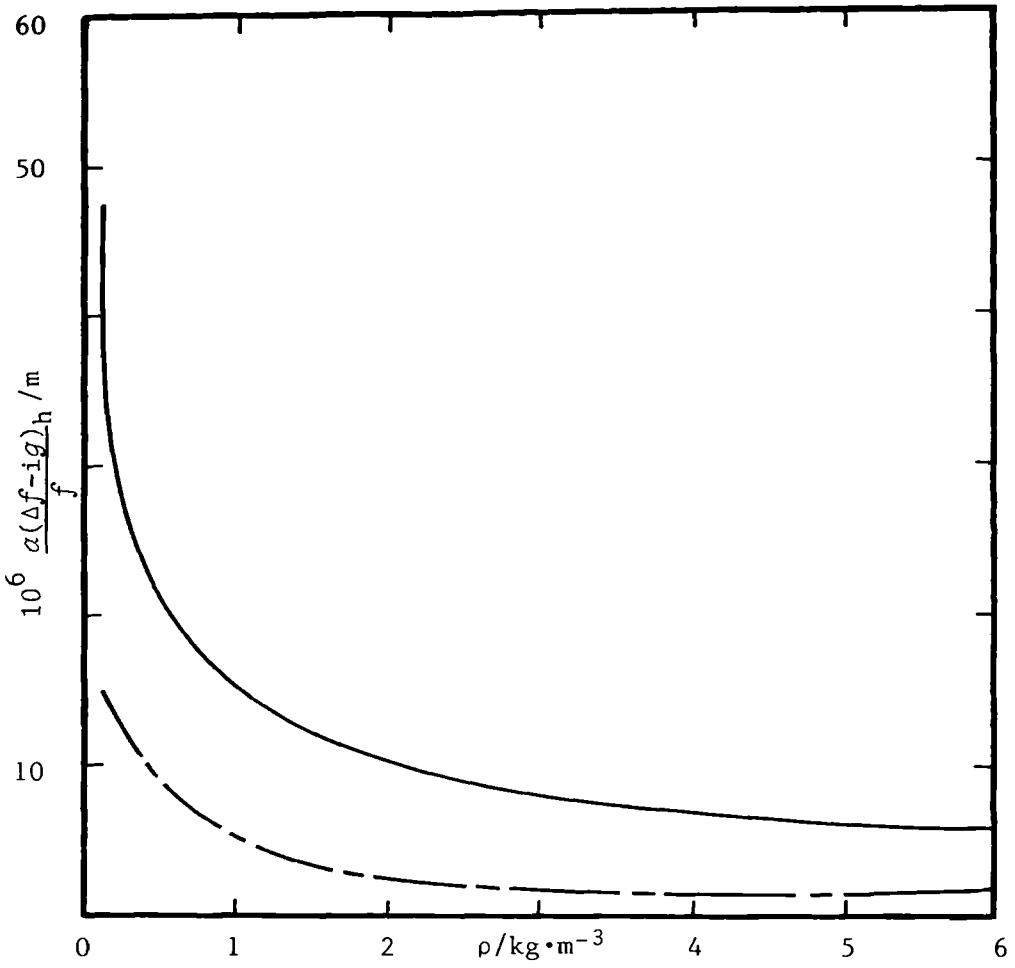

Figure 3.1. The thermal boundary layer correction for a plane surface $(\Delta f - ig)_h/f$ multiplied by the spherical resonators radius a, as a function of mass density ρ for; ——— Ar, —·—·— CH_4 at 5kHz and 300 K. Calculated with $C^{pg}_{p,m}(CH_4)/R = 4.1943$,[58] and $C^{pg}_{p,m}(Ar)/R = 5/2$ with the density and gas imperfections calculated from equation (2.2.1) truncated after the second virial coefficient; the required second virial coefficients were taken from a corresponding state square-well expression.[59] The thermal conductivities and there density dependence were taken from reference (60).

The contribution to the thermal boundary layer from thermal wave propagation in the shell wall material w has been considered by Trusler.[61] He concluded that $(\Delta f_h - ig_h)/f$ would be modified by an additional factor $(1+i)(\gamma-1)\{\delta_w/(2a)\}(\kappa/\kappa_w)$, where δ_w is the thermal penetration length in the wall, and κ_w the thermal conductivity of the wall material. For a metal wall, for example an Al alloy, $\{\kappa_w(273.2\ K) = 170\ W\cdot m^{-1}\cdot K^{-1}\}$[61] containing Ar $\{\kappa(Ar, 273.2\ K) = 16.3\ mW\cdot m^{-1}\cdot K^{-1}\}$,[62] $\kappa/\kappa_w \simeq 7 \times 10^{-5}$ and since $\delta_w f^{\frac{1}{2}} \simeq 5 \times 10^{-3}\ m\cdot s^{-\frac{1}{2}}$ for the same alloy, then at 5 kHz $(\delta_w/2)(\kappa/\kappa_w) \simeq 5 \times 10^{-10}$ which would be negligible.

Shell motion

The experimental results given in Chapter Six were obtained at pressures up to 7 MPa and suggest that the effect of shell motion are especially important at these pressures. The theory for the perturbation arising from the elastic response of a spherical shell will now be reviewed in some detail.

The response of a spherical isotropic shell to an internal acoustic mode has been calculated from the exact theory of classical elasticity. This was first performed by Greenspan for the coupling between radial (l=0) acoustic modes and the radial shell motion.[63] Mehl has subsequently treated the general non-radial case.[51] Moldover, Mehl and Greenspan have presented a treatment specific to radial modes.[47] They included the effect of radiation from the external surface at r=b. Two boundary conditions were

required, At $r=a$ the radial component of the shell and gas velocities must match {as required by equation (7)}, where the radial component of the shell velocity is equal to the radial force per unit area (equivalent to the acoustic pressure [47]) exerted on the shell by the gas multiplied by the specific acoustic admittance of the shell. At $r=b$ the effect of radiation into the fluid surrounding the resonator was accounted for with a radiation boundary condition,[47] assuming this fluid was infinite, and that there were no reflections from surrounding components; no account was taken of the resonator's mechanical supports.

The specific acoustic admittance of the shell at $r=a$ is given by[47,51]

$$y_w = -i\rho\omega u a/(\rho_w u_{w,l}^2) S_0(k_w a), \tag{3.4.21}$$

where the subscript 0 refers to the radial shell motion. In equation (21) $k_w = \omega/u_{w,l}$, where $u_{w,l}$ is the longitudinal wave speed in the shell material. The dimensionless function S_0 in equation (21) is given by

$$S_0 = -q\{(G_1 + qRG_2)/(G_3 + qRG_4)\}, \tag{3.4.22}$$

where

$$q = 1/2(1 - \sigma)/(1 - 2\sigma), \text{ and} \tag{3.4.23}$$

$$R = \rho(g, r\geq b)\{u(g, r\geq b)\}^2/(\rho_w u_{w,l}^2) \times [\{k(g, r\geq b)\}^2/\{1 + ik(g, r\geq b)b\}], \tag{3.4.24}$$

accounts for the radiation from the surface at $r=b$ into the

surrounding gas ($r \geqslant b$), with $k(g, r \geqslant b) = \omega / u(g, r \geqslant b)$. In equation (23) σ is Poisson's ratio. The parameters G_i ($i = 1,2,3,4$) in equation (22) are given by

$$G_1 = (1 + AB - qB^2)\tan(B - A) - (B - A) - qAB^2, \qquad (3.4.25)$$

$$G_2 = (1 + AB)\tan(B - A) - (B - A), \qquad (3.4.26)$$

$$G_3 = \{(qA^2 - 1)(qB^2 - 1) + AB\}\tan(B - A) - (1 + qAB)(B - A) \qquad (3.4.27)$$

and

$$G_4 = (1 + AB - qA^2)\tan(B - A) - (B - A) + qA^2B, \qquad (3.4.28)$$

where $A = k_w a$ and $B = k_w b$.

The radial (l=0) resonance of the shell are given by the frequencies at which the denominator of equation (22) vanishes.[47,51] The lowest radial shell resonance is the breathing mode, whose frquency is designated f_{br}. Usually the other radial resonances occur at much higher frequencies, and correspond to the longitudinal resonances of flat plates.[47,51] At low acoustic frequencies, less than f_{br}, the acoustic pressure wave stretches the shell and the response of the shell is determined by the elasticity of its material.

At radial acoustic frequencies sufficiently removed from the radial resonances of the shell the function S_0 is of order unity. For an Al shell ($\rho_w u_{w,l}^2 \simeq 1.1 \times 10^{11}$ Pa) which contains Ar(g) at a density of 100 kg·m^{-3} ($\rho_g u_g^2 \simeq 1 \times 10^7$ Pa), the factor $\rho_w u_{w,l}^2 / (\rho_g u_g^2) \simeq 10^{-4}$. Consequently $y_w << 1$ provided the radial shell and acoustic frequencies are

adequately separated. Therefore, the shift Δf_w in resonance frequency and contribution to g from the shell motion can be obtained from the third term of equation (14) assuming y_w is uniform over all S, with the result:

$$(\Delta f_w - i g_w) = -\rho_g u_g^2 f/(\rho_w u_{w,1}^2) S_0(k_w a), \qquad (3.2.29)$$

which can be evaluated for any wall material using (22) to (27).

The required properties of some useful wall materials are given in table 3.2. The fractional frequency shift $\Delta f_w/f$

Table 3.2 Speed of longitudinal waves $U_{w,1}$, density ρ_w and Poisson's ratio σ for possible wall materials Al, Cu, and a stainless steel similar to grade 316 (BS 316S16),[64] at all $T/K \approx 293$ taken from reference (62)

Material	$U_{w,1}/m \cdot s^{-1}$	$\rho/kg \cdot m^{-3}$	σ
Al	6398	2700	0.355
Cu	4759	8933	0.343
316516	5980	7800	0.283

and fractional contribution g/f to the half width from the wall motion calculated from equations (22-28), and (29), for an Al resonator with a = 40 mm, b = 50 mm, containing Ar and surrounded at $r = b$ by N_2 both at 300 K are shown in figures 3.2 and 3.3 as a function of pressure for the first seven

radial modes; the frequency of mode (0.8) is close to f_{br} at approximately 31.2 kHz. Figure 3.2 indicates that for radial modes with $n \leqslant 6$, at a pressure of 7 MPa, $10^6\ \Delta f_w/f < 700$. However, for the first four radial modes g_w/f is insignificant at all pressures up to 7 MPa; the remaining modes up to the seventh radial have increased contributions to g as f approaches f_{br}.

The quantity $\Delta f/(fp)$ calculated from equation (29) with the admittance function for an elastic sphere radiating into free space is shown, as a function of frequency for an Al resonator, in figure 3.4. Although the calculations were carried out for a resonator containing CH_4 and surrounded by N_2 at 300 K, the qualitative features are similar if argon replaces methane and nitrogen; obviously f_{br} is unaffected. Furthermore, a change in temperature of 50 K would not produce changes distinguishable on the scale of figure 3.4.

Moldover, Mehl and Greenspan[47] have obtained an approximate form for S_0, when radiation is neglected, in the zero frequency limit; for acoustic resonance frequencies below f_{br} this limit of S_0 has been divided by a resonance term $\{1 - (f/f_{br})^2\}$. Their approximation for $S_0(f)$ can be written

$$\begin{aligned} S_0(f) &= -q\{3i\ (b - a)(a - qp) - 3qab^2 + (b - a)^3\} \\ &\quad /\{-3q(b - a)(a^2 + ab + b^2) + 3ab(b - a) + (b - a)^3\} \\ &\quad \times \{1 - (f/f_{br})^2\}^{-1} \\ &= S_0(0)\{1 - (f/f_{br})^2\}^{-1}, \end{aligned} \tag{3.4.30}$$

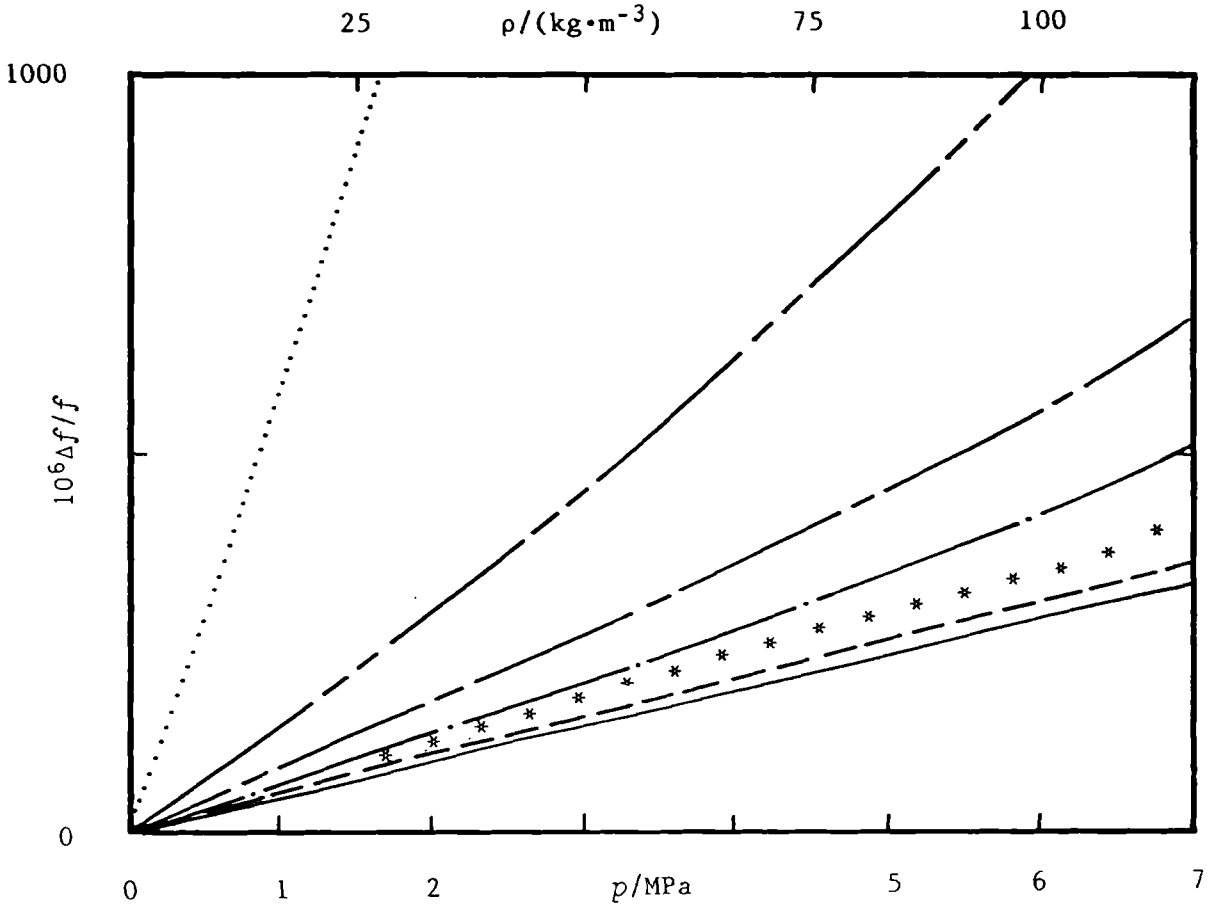

Figure 3.2. Fractional resonance frequency shift $\Delta f/f$ arising from the shell motion calculated from equation (29) combined with equations (22 - 28), including radiation from the external surface into N_2 for the following radial acoustic modes in Ar at 300 K as a function of pressure and density: ———, (0,2); – – – (0,3); * * *, (0,4); ——·—— (0,5); —— – ——, (0,6); —— – – ——, (0,7); ·····,(0,8). The resonator formed from Al, with a = 40 mm and b = 50 mm, for which the required mechanical properties are given in table 3.2. The densities of N_2 and Ar were calculated from equation (2.2.1) truncated after the second virial coefficient; B's were obtained reference (59). $u(N_2, 300\ K, p)$ was calculated from a cubic equation of state,[65,66] which compared favourably with experiment,[67] and for Ar $u(p)$ was taken from this work.

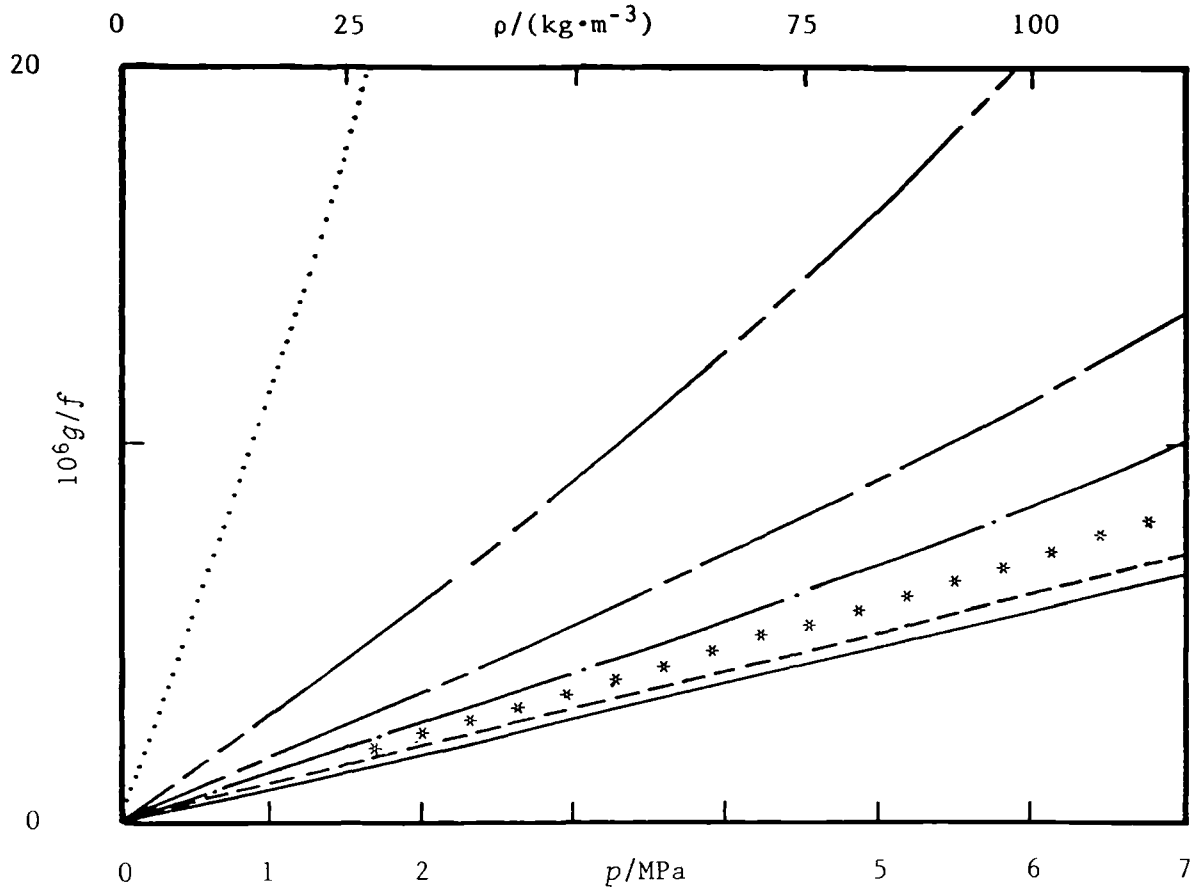

Figure 3.3. Contributions to the resonance half width divided by resonance frequency g/f for shell motion arising from radiation, for Ar contained in an Al resonator (a = 40 mm, b = 50 mm) surrounded by N_2 at 300 K for the following modes: ———, (0,2); — — — , (0,3); * * *, (0,4); —— · ——, (0,5); —— — ——, (0,6); —— — — ——, (0,7); and, ·····, (0,8). The required mass densities and speeds of sound were calculated as for figure 3.2. The mechanical properties of the shell are given in table 3.2.

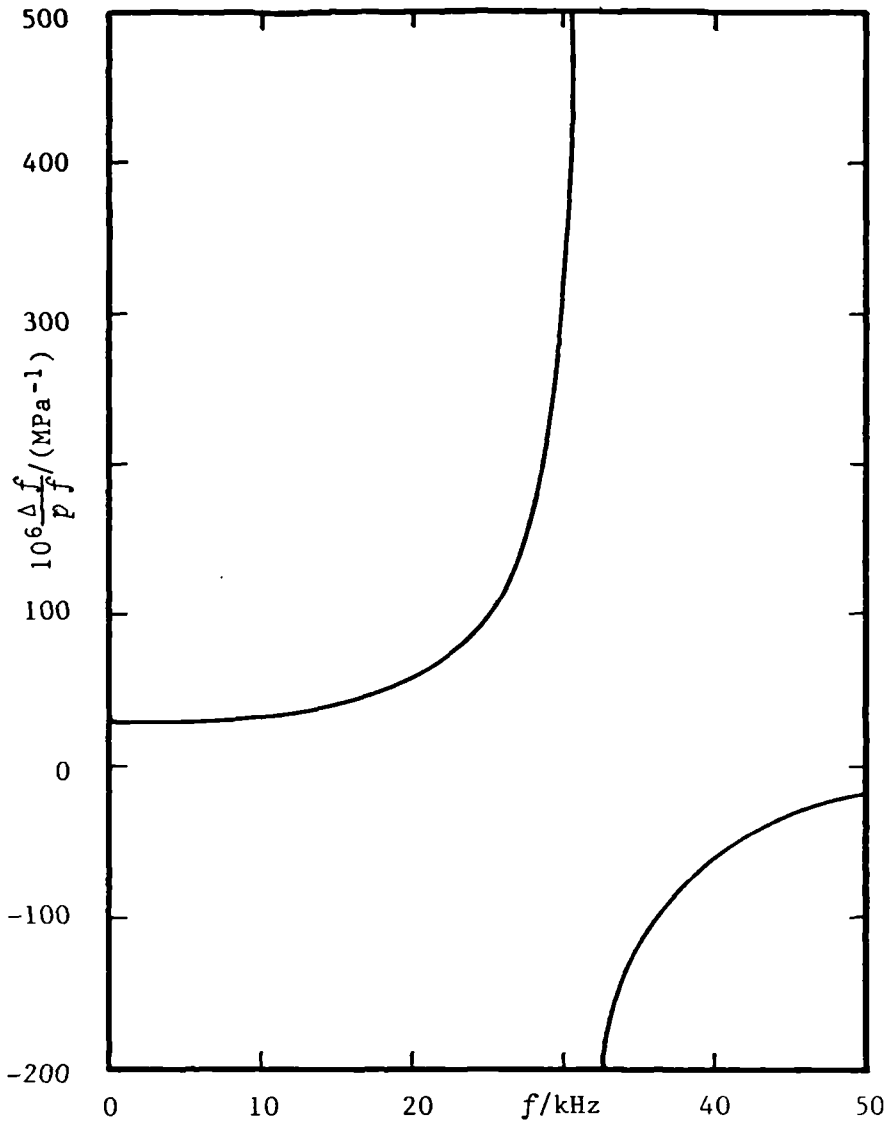

Figure 3.4. The function $\Delta f/(pf)$, where $\Delta f/f$ is the fractional frequency shift and p is the pressure , for a perfectly spherical isotropic elastic shell as a function of frequency. Calculations were performed for an Al resonator with a = 40 mm,b = 50 mm, and wall properties given in table 3.2. The resonator contained CH_4, surrounded by N_2, both at 300 K. The densities ρ of CH_4 were calculated from equation (2.2.1) with second virial coefficients given in reference (59); ρ_{N_2} was calculated as prescribed for figures 3.3 and 3.2. $u(CH_4, 300\ K, p)$ was taken from this work and, $u(N_2, 300\ K, p)$ from a cubic equation of state.[65,66]

where a and b are the inner and outer radius of a resonator, and q is given by equation (23). However, $\Delta f_w/f$ obtained from the approximation (39) when used in equation (29) to replace $S_0(k_w a)$ agrees with the exact result given by equations (22 - 29) neglecting radiation $\{S_0(k_2 a) = -qG_1/G_2\}$ to within 5 per cent for $f \leqslant 3/4\ f_{br}$ at densities below 100 kg·m^{-3}; the comparison was based on calculations for an Al resonator with mechanical properties given in table 3.2, a = 40 mm and b = 50 mm, containing Ar.

A further simplied form of equation (22) when radiation is neglected and $q = 1$ ($\sigma = 1/3$) has been derived by Greenspan,[63] which is also an isolated mode approximation; equation (30) is also an isolated mode approximation. The specific acoustic admittance is then given by

$$y_w = -i2\pi a f \rho u S_0' / \{1 - (f/f_{br})^2\} \qquad (3.4.31)$$

in which

$$S_0' = (1 + 2t^3) / \{2(t^3 - 1)\rho_w u_{w,1}^2\}, \text{ and} \qquad (3.4.32)$$

$$f_{br} = [(t^3 - 1)/\{2\pi^2(t - 1)(1 + 2t^3)\}]^{\frac{1}{2}}(u_{w,1}/a), \qquad (3.4.33)$$

where $t = b/a$. The fractional frequency shift is then given by

$$\Delta f_w/f = S_0' \rho_g u_g^2 / \{1 - (f/f_{br})^2\}. \qquad (3.4.34)$$

Calculations of $\Delta f_w/f$ from this equation differ insignificantly at $f \leqslant 3/4\ f_{br}$ and $\rho_g < 5$ kg·m^{-3} from the result obtained from equation (29) with $S_0(f)$ from equation (30), and $\sigma = 0.355$ as is appropriate for Al. However, at

ρ_{Ar} = 100 kg m^{-3}, which is equivalent to $p \approx 5.5$ MPa at T = 300 K, the same comparison indicates a discrepancy of up to 10 per cent at $f \leqslant 314\ f_{br}$ in $\Delta f_w/f$. Consequently, since $S_0(f)$ {or $S_0(k_w a)$} is only weakly dependent on Poisson's ratio σ, in the zero-frequency limit equations (32) and (33) provide a simple qualitative means of comparing possible wall materials. The magnitude of $\Delta f_w/f$ is proportional to S_0' of (32) for a particular wall material. Values of S_0' are shown in figure 3.5 as a function of t for Al, Cu, and a stainless steel with $u_{w,l}$ and ρ_w from table 3.2. S_0' decreases rapidly as the shell thickness increases from t = 1, and for stainless steel S_0' is approximately half the value for Al for any $t > 1$. For a shell with $b \approx 1.3a$, the magnitude of S_0' has reached half the value for an infinitely thick shell. As equation (33) shows, the radial breathing resonance frequency f_{br} is a function of a, t, and $u_{w,l}$ so the quantity $f_{br}a$, shown in figure 3.6, provides a further comparison for different wall materials. For aluminium and stainless steel, f_{br} differs by less than 10 per cent, but for copper, which might be desirable to reduce temperature gradients, $f_{br}(Cu) \approx 2/3\ f_{br}(Al)$. In previous experimental work the shift in resonance frquency due to shell motion has been accounted for with equation (34).[42,46,48,52,68-79]

Moldover, Mehl and Greenspan[47] have also considered damping of the radial breathing resonance in the shell wall in terms of the shell resonance quality factor W_w at f_{br}.

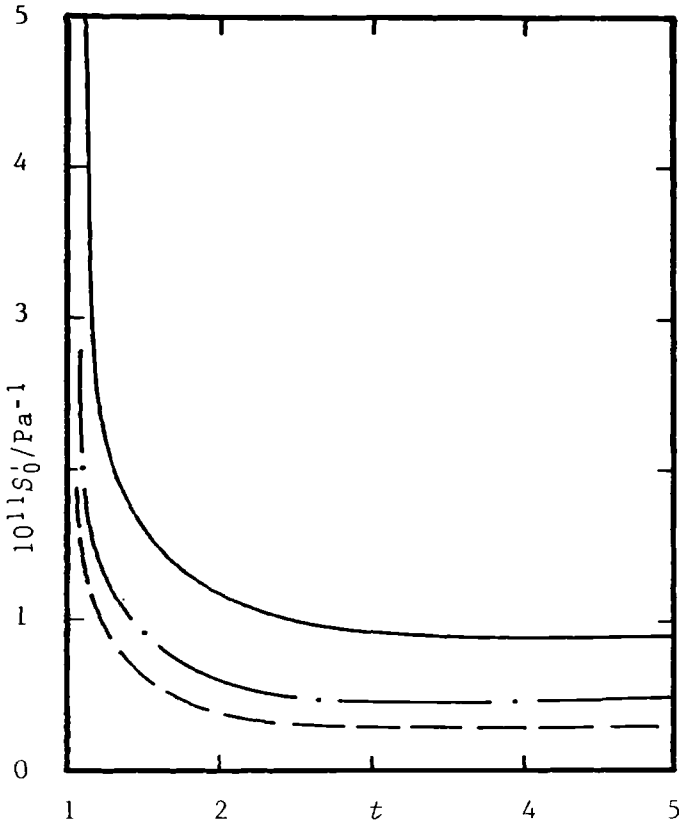

Figure 3.5. S_0' from equation (32) as a function of $t = b/a$ for: ——— Al; —— · ——, Cu; and, – – – stainless steel similar to grade 316. The required properties $u_{w,1}$ and ρ_w for these three materials are given in table 3.2.

In the isolated mode approximation $S_0(f)$ of equation (30) {radiative losses are neglected} has been modified to give

$$S_0''(f) = S_0(0)\{1 - (f/f_{br})^2 + i(f/f_{br})/Q_w\}. \qquad (3.4.35)$$

Substitution of $S_0''(f)$ for $S_0(k_w a)$ in equation (35), then gives the shift in frequency and contribution to the resonance half width as

$$(\Delta f - i\gamma)_w = -f_0 \rho_g u_g^2/(\rho_w u_{w,1}^2) S_0''(f). \qquad (3.4.36)$$

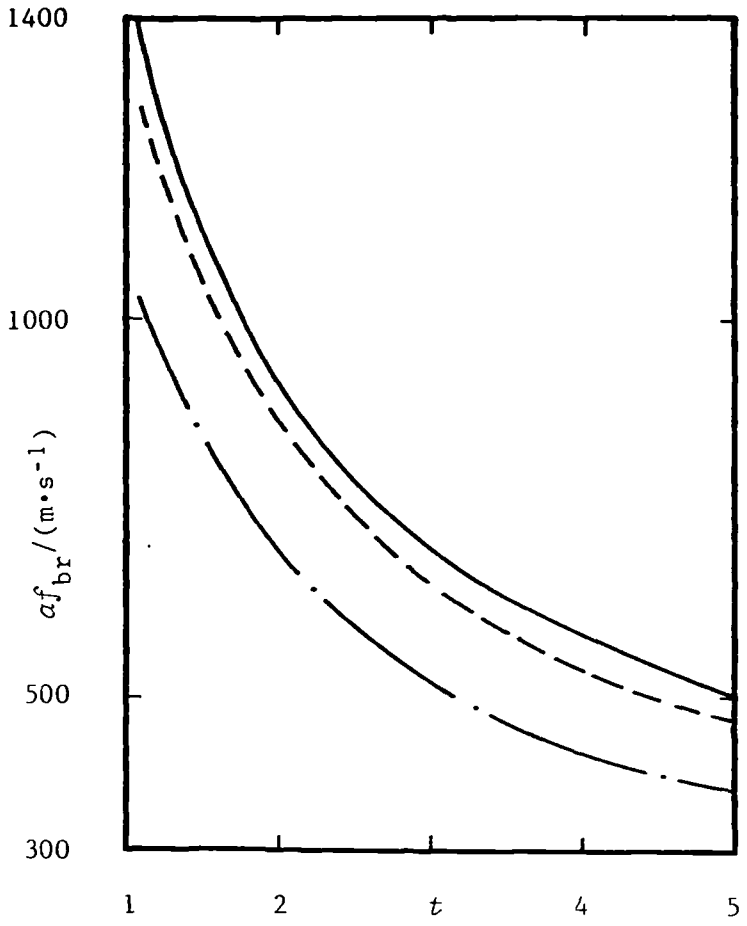

Figure 3.6. The quantity af_{br} calculated from equation (34) as a function the ratio $t = b/a$ for the wall materials: ——— Al; – – –, stainless steel similar to grade 316;[64] and,——·——— Cu. $u_{w,1}$ for each metal is given in table 3.2.

Equation (36) has been used to calculate the contributions to g/f for a resonator constructed from Al containing Ar at a density of 50 $kg \cdot m^{-3}$ and 300 K, for four values at Q_w in the range $10 \leqslant Q_w \leqslant 10\ 000$; the results are shown in figure 3.7 and clearly indicate that this loss is significant only for small values of Q_w and frequencies close to f_{br}.

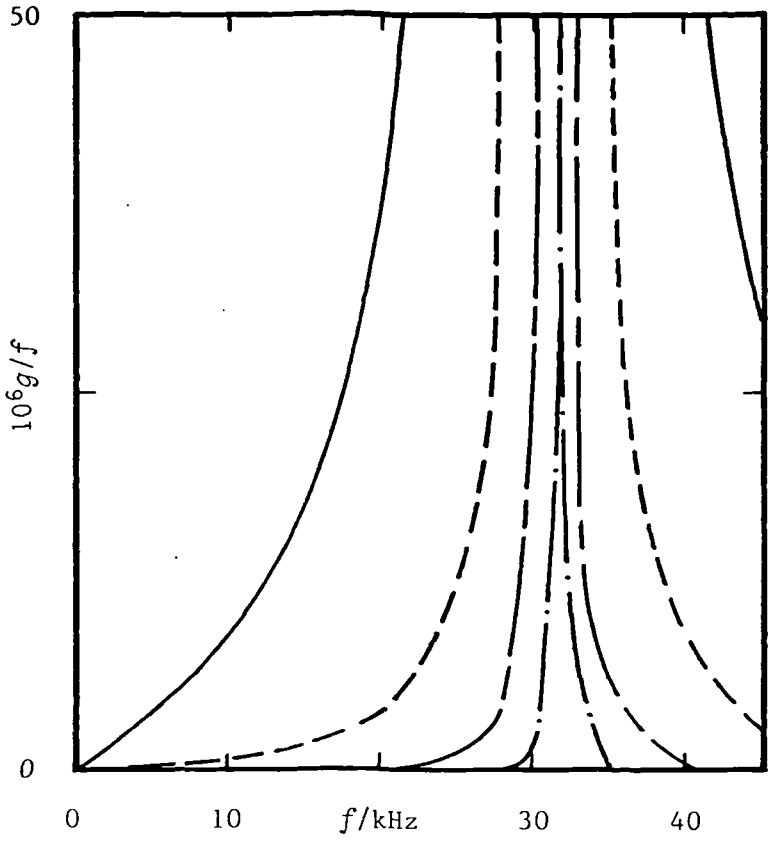

Figure 3.7. Contributions to g_w/f from a damped radial breathing resonance of an Al resonator with a = 40 mm , b = 50 mm , f_{br} = 31.6 kHz and mechanical properties in table 3.2, containing Ar at 50 kg·m^{-3} at 300 K as a function of frequency for the following valves of Q_w : ——, 10; – – – , 100; —— – – —— , 1000; and, —— · ——,10000.

The eigenvalues Λ_{ln} of the shell resonances for a perfectly spherical isotropic shell have been calculated from the exact theory of elasticity.[51] Mehl has calculated the lowest non-zero eigenvalues for l=0,1,2,..,6

as a function of $(b/a)=t$ for an Al resonator with a = 50 mm. Values of Λ_{ln} are given in table 3.3 for t=1.2 and t=1.25, taken from reference (51); the $(2l+1)$ fold degeneracy of each shell resonance is also given and the type of shell resonance indicated.[51] Each value of Λ_{ln}, for a given t, can be related to a particular shell resonance frequency f^{w}_{ln} for a resonator, with internal radius a, through

$$f^{w}_{ln}/\mathrm{kJz} = \Lambda_{ln}\, 20.4\ z/a, \qquad (3.2.37)$$

where z = 0.05 m.

Although direct coupling between the gas and shell resonances should occur only when the modes have the same l (Moldover, Mehl and Greenspan[47] have given experimental evidence at p < 1 MPa to support the importance of mode symmetry in determining coupling), higher-order coupling between, for example, l=0 acoustic modes in the gas and the l=1,2,3 .... shell modes might occur when the resonance frequencies are similar[51] and at high gas densities where the effect is largest.

There are also other shell resonances for an isotropic elastic sphere which do not couple to any acoustic mode except through weak viscous effects.[51] These modes are purely torsional, have no radial displacement, and are for motion at constant volume.[73] However, the shell vibrations which couple to acoustic modes have radial and transverse components which are not volume preserving.

Mehl[51] has also considered the l=1 coupling of acoustic and shell motion in the zero-frequency limit. In

Table 3.3 Eigenvalues $\Lambda_{\ell n}$ for the resonance frequencies of an Al (σ = 0.355) isotropic spherical shell with t=1.2 and t=1.25 taken from reference (51), for n=1 and ℓ=0,1,2...6; with ℓ=1, Λ_{12} is the first non-zero eigenvalue. Each shell resonance is $(2\ell+1)$ fold degenerate, and can be classified as either bending B† or extentional E modes. $\Lambda_{\ell n}$ is the n-th value of $k_1 a = a\omega/u_{w,1}$ for shell resonances with radial displacement proportional to $Y_{\ell n}(\theta,\zeta)$ {which can be excited by internal acoustic modes with pressure proportional to $Y_{\ell n}(\theta,\zeta)$} for which the resonance condition is fulfilled.[47,51]

$\Lambda_{\ell n}$					
ℓ	n	t-1.2	t=1.25	$(2\ell+1)$	Mode type
0	1	1.250	1.225	1	E[a]
1	1	0.0	0.0	3	E[b]
1	2	1.513	1.468	3	E
2	1	0.523	0.527	5	B
3	1	0.695	0.713	7	B
4	1	0.883	0.937	9	B
5	1	1.133	1.232	11	B
6	1	1.435	1.565	13	B

[a] Radial breathing mode. [b] Uniform free translational motion.

† Bending motion in a perfect isotropic sphere involves stretching.[72]

this case, the acoustic pressure exerts a force which excites translational shell motion. For a shell which does not undergo deformations the fractional shift in resonance frequency for the acoustic resonances is given by

$$\Delta f_w(1,n)/f(1,n) = (m_g/m_w)/(\nu_{1,n}^2 - 2), \qquad (3.4.38)$$

where m_g is the mass of gas within the resonator of mass m_w.[51] Equation (38) strictly only applies to acoustic modes $(1,n)$ with frequency below the first non-zero shell resonance with eigenvalue Λ_{12} for which deformations are important; the inertial response of the shell {equation (38)}, is largest for the (1,1) mode with $\nu_{1,1} = 2.081$. Furthermore the (1,1) mode has the largest shell correction for any mode for a particular gas at a density, except when the shell and acoustic resonances overlap. Mehl has used this simple model to estimate the contribution to the frequency shift of the $(1,n)$ acoustic modes from the stiffness of mechanical supports;[51] provided the $(1,n)$ acoustic resonances are sufficiently removed from the translational resonance of the support, the effect is small compared to the inertial effect of equation (38). However, resonators are often only mounted in one position, for example a pole, and the effect of support stiffness will be different for horizontal shell motion to that of vertical shell motion. Such differences may be sufficient to remove the degeneracy of the (l,n) acoustic modes since the average gas motion of the $(2l+1)$ components may have different orientations with respect to the support. Mehl[51] and Moldover *et al.*[47] have reported $(1,n)$ mode splitting.

For the (1,1) mode this was sufficient to remove the degeneracy and might be attributed to the asymmetric mechanical supports, since it increased with increasing density.

Real practical spherical resonators are constructed from two hemispheres joined at the equator, the poles often have bosses remaining from the machining process, which may be used to provide mechanical supports. The equatorial joint may result in extra frictional losses in the shell which might be observed in the half-widths.[47] The presence of holes in the walls allows bending motion without stretching which results in deformations from sphericity and, consequently, a further small perturbation may arise from the shell. However, the pure bending energy is small compared with stretching energy and bending without stretching would imply non-uniform forces acting on the shell.[72] Such a situation should not arise from radial acoustic modes in the gas. The present theory of shell motion is not strictly applicable to real resonators and the inadequacy of the theory will be most pronounced at large values of $\rho_g u_g^2$.

Openings in the resonator wall

The openings in the wall that are relevant for the spherical resonators described in Chapters Five and Six are (1), a gas inlet tube with circular cross-section; (2), cylindrical tubes which couple sound to remote transducers; and (3), annular slots formed between the wall and the plugs carrying the acoustic transducers.

The perturbation to radial modes from each opening in the resonator wall is given by

$$(\Delta f_t - i g_t) = -i\{u/(2\pi a)\} S_0/(4\pi a^2) y_0(\vec{r}_S, f), \qquad (3.4.39)$$

where it has been assumed that y_0 is uniform over the surface area S_0 occupied by the opening. In order to calculate $(\Delta f - ig)_0$, y_0 of the opening must be known.

For a tube of radius c extending a distance $z = L$ from its opening into the cavity ($r=a$) at $z = 0$, the specific acoustic impedance at $z = L$ is

$$Z(z=L) = i\rho u \tanh(\delta_L - i\gamma_L),^{(74)} \qquad (3.4.40)$$

where the ratio of reflected to incident wave amplitudes is $\exp(-2\gamma_L)$ and the phase shift is $(2\delta_L + \pi)$. It is assumed that the frequency is below $\chi_{10} u/(2\pi c)$, where $\chi_{10} = 1.841$ is the first radial resonance eigenvalue for an ideal cylinder, so that only plane waves propagate and bulk adsorption is ignored. The corresponding specific acoustic admittance at $z=0$ on the cavity's inner surface is

$$y_{0,t} = \rho u / Z_{(z=0)} = i \cot(\delta_L + i\gamma_L + k_{KH} L), \qquad (3.4.41)$$

where

$$k_{KH} = k + (1 + i)\alpha_{KH},^{(75)} \qquad (3.4.42)$$

is the tube propagation constant with

$$k = 2\pi f/u \quad \text{and} \qquad (3.4.43)$$

$$\alpha_{KH} = \{\pi f/(uc)\}\{\delta_S + (\gamma - 1)\delta_h\}, \qquad (3.4.44)$$

is the Kirchoff-Helmholtz tube attenuation constant.[76] The thermal δ_h and shear δ_S penetration lengths are given by equations (3.2.24) and (3.2.28) respectively. Strictly equation (44) is valid only for a plane surface but, provided δ_S and $\delta_h << c$ it gives an accurate representation of the viscous and thermal boundary-layer of a cylinder.[77] The parameters δ_L and δ_L, which both depend on the conditions at $z=L$, need to be considered in more detail.

If the tube is open at $z=L$ and free to radiate into free space then

$$\gamma_L = (1/4)(kc)^2,^{(78)} \tag{3.4.45}$$

$$\delta_L = (3/5)(kc),^{(78)} \tag{3.4.46}$$

but if the open tube is fitted with a flange that has dimensions which are large compared to the acoustic wavelength λ then

$$\delta_L = 8kc/(3\pi), \tag{3.4.47}$$

$$\gamma_L = (kc)^2/2, \tag{3.4.48}$$

provided $(kc)^2/2 << 8kc/(3\pi) << 1$. By contrast if there is no radiation,

$$\delta_L = 0, \text{ and} \tag{3.4.49}$$

$$\gamma_L = 0. \tag{3.4.50}$$

However, if the tube terminates in a closed chamber of volume V which has dimensions much less than λ then

$$\delta_L = -\arctan\{\pi c^2/(kV)\}, \tag{3.4.51}$$

provided there are no losses in the chamber, and

$$\gamma_L = 0 \tag{3.4.52}$$

for rigid chamber walls.[79] The chamber and tube form a Helmholtz resonator,[79,80] which has a resonance frequency of

$$f_{HR} \approx (uc/2)\{\pi/(LV)\}^{\frac{1}{2}}, \tag{3.4.53}$$

with a quality factor

$$Q_{HR} \approx 2/(\pi c)\{VL^3/(\pi c)\}^{\frac{1}{2}}. \tag{3.4.54}$$

If the chamber is not sealed, so that $V \to \infty$ then the terminal admittance can be enhanced by leakage conductance so

$$\delta_L \approx 0 \quad \text{and} \quad \gamma_L = 0, \tag{3.4.55}$$

which is the same result as for an open tube with no radiative losses.

Alternatively, the tube may be closed at $z=L$ by a rigid wall so $\gamma_L=0$, and δ_L can be estimated from equation (51) with $V=0$ which gives $\delta_L=-\pi/2$; the phase shift is then zero.

The tube has resonances when y_0 is a maximum which for an open tube gives

$$f_m = \{u/(2\pi L)\}(m\pi + \alpha_{KH}L - \delta_L);$$

$$m = 0,1,2 \ldots \tag{3.4.56}$$

The perturbation to the spherical resonator arising from the tube is given by equations (39) and (41) with the δ_L and γ_L appropriate for the tube's termination. However, for design

purposes it is sufficient to note that cot ($kL + \delta_L$), with δ_L=0 for an open tube and δ_L=-π/2 for a closed tube, should be small at the required resonances $k = \nu_{ln}/a$ in the spherical cavity. The function cot ($\nu_{0n}L/a$) for the radial spherical modes perturbed by an open tube is shown in figure 3.8. Since for the radial modes $\nu_{0n} \simeq (2n-1)\pi/2$, figure 3.8 shows that $L=a$ is the "best" length (cot ν_{0n} < 0.3 for all radial modes) but such a long tube may not be practical. Consequently a short tube with L/a=0.1 has been compared with L/a=1 for a real resonator of radius a=40 mm containing argon at 300 K. The real and imaginary parts of the function cot ($kL+\alpha_{KH}L+i\alpha_{KH}L$), which neglects radiation from the end of an open tube, are plotted for L/a=0.1 and 1 in figures 3.9 and 3.10 for Ar at densities ρ of 1 and 100 kg$\cdot$m^{-3} over the frequency range up to 40 kHz for the former and 15 kHz for the latter. For both values of (L/a) the resonances are sharp and strong at high ρ, but are weaker and considerably broadened at low ρ; the resonance frequencies are lowered as ρ decreases. For (L/a)=0.1 $f_1 > f_{(0,8)}$, and for (L/a)=1.0 the radial acoustic resonances lie between the resonances of the tube.

Annular slots between the resonator's wall and plugs carrying the acoustic transducers are the third type of opening which needs to be considered. An annular slot may be modelled by the parallel semi-infinite plates separated by a distance d and extending to a depth $x=L$, where it is closed by a rigid wall. The specific acoustic admittance of the resonators surface at z=0 ($r=a$) is given by

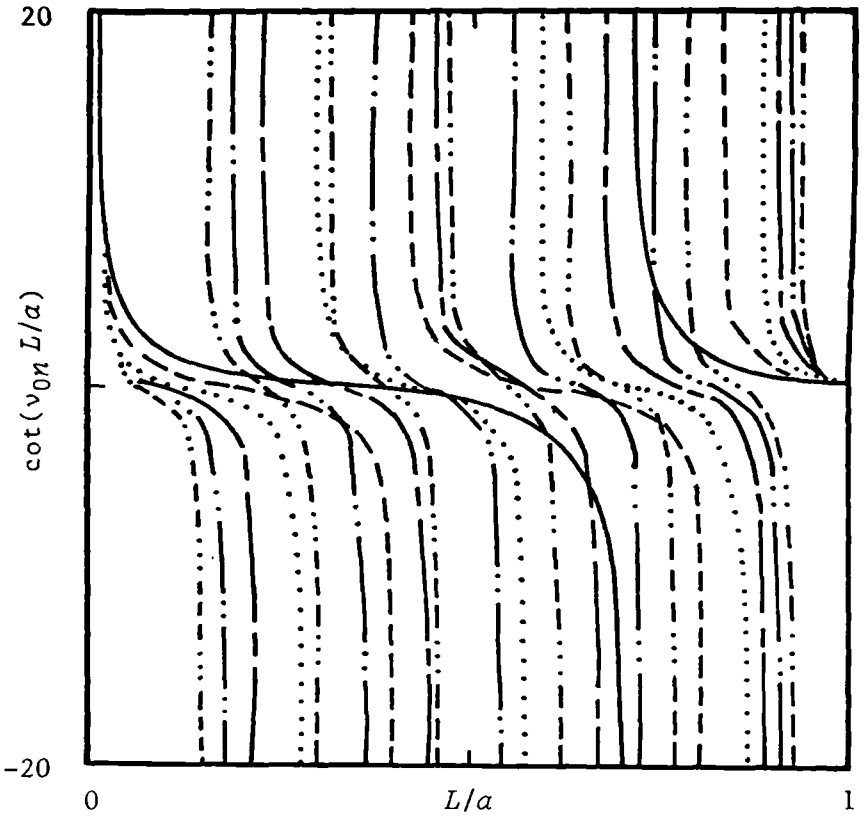

Figure 3.8. Cot($\nu_{on}L/a$) for a rigid lossless system as a function of L/a for the first five radial modes: —— (0,2); – – – –,(0,3); ····· (0,4); —— – —— (0,5); — · · —— (0,6); and, – – – ··· – – – (0,7).

$$y_{0S} = (k_x/k)\ \tanh\ (-\ ik_xL)[1 - (1 + i)(\delta_S/d)$$

$$\tanh\ \{(1 - i)d/(2\delta_S)\}],^{(81)} \qquad (3.4.57)$$

where δ_S and δ_h are the thermal and shear penetration lenghs respectively. In (57) k_x is the propagation constant for plane waves travelling along the crack, which provided $\lambda >> d$, is

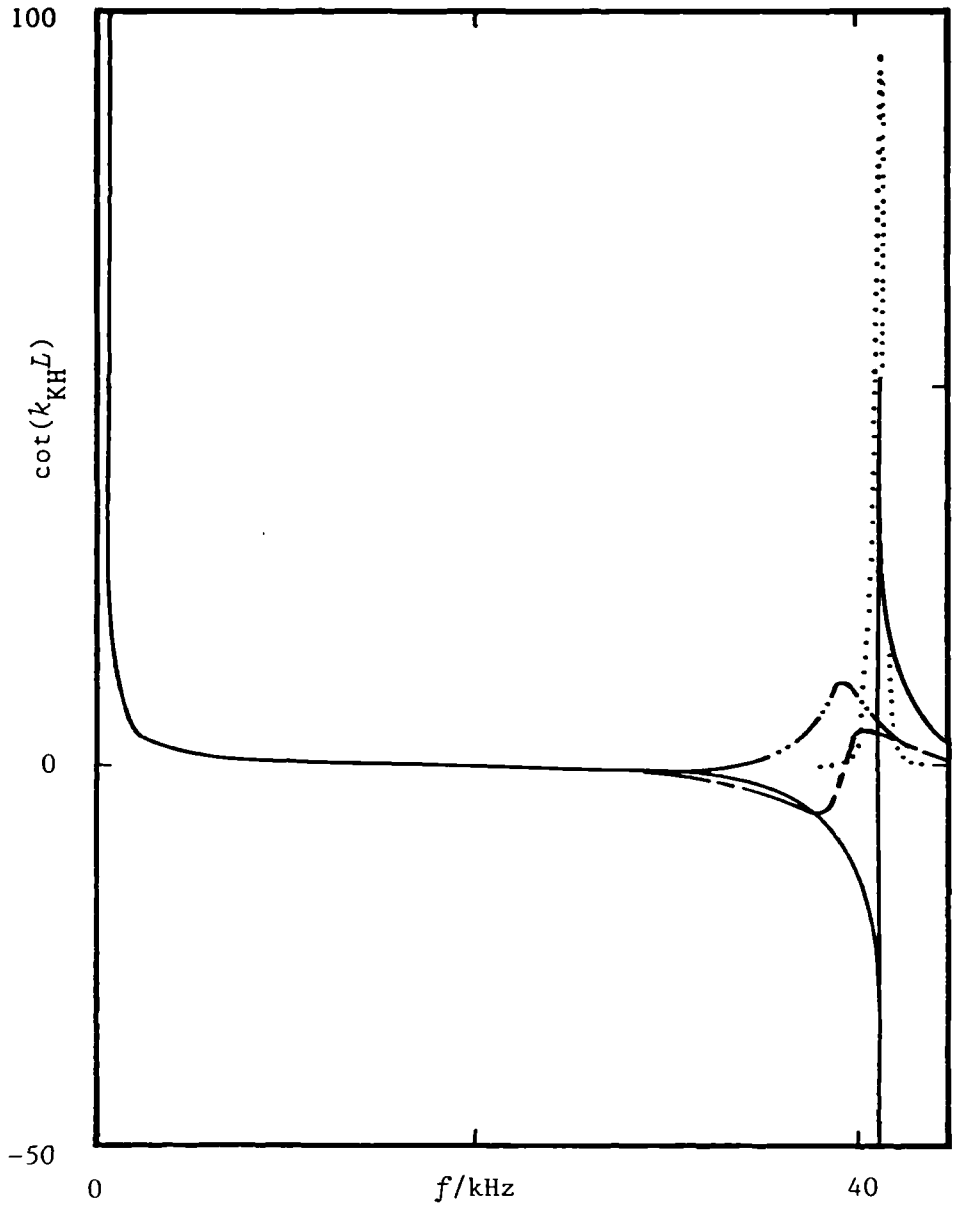

Figure 3.9. Rm{cot($k_{KH}L$)} and - Im{cot($k_{KH}L$)} as a function of f for a tube with L = 4 mm protruding from a resonator with a = 40 mm, containing Ar at 300 K for the following densities: ——, Rm{cot($k_{KH}L$)} at 100 kg·m^{-3}; ·····, - Im{cot($k_{KH}L$)} at 100 kg·m^{-3}; —— – ——, Rm{cot($k_{KH}L$)} at 1 kg·m^{-3}; and, —— · · ——, -Im{cot($k_{KH}L$)} at 1 kg·m^{-3}.

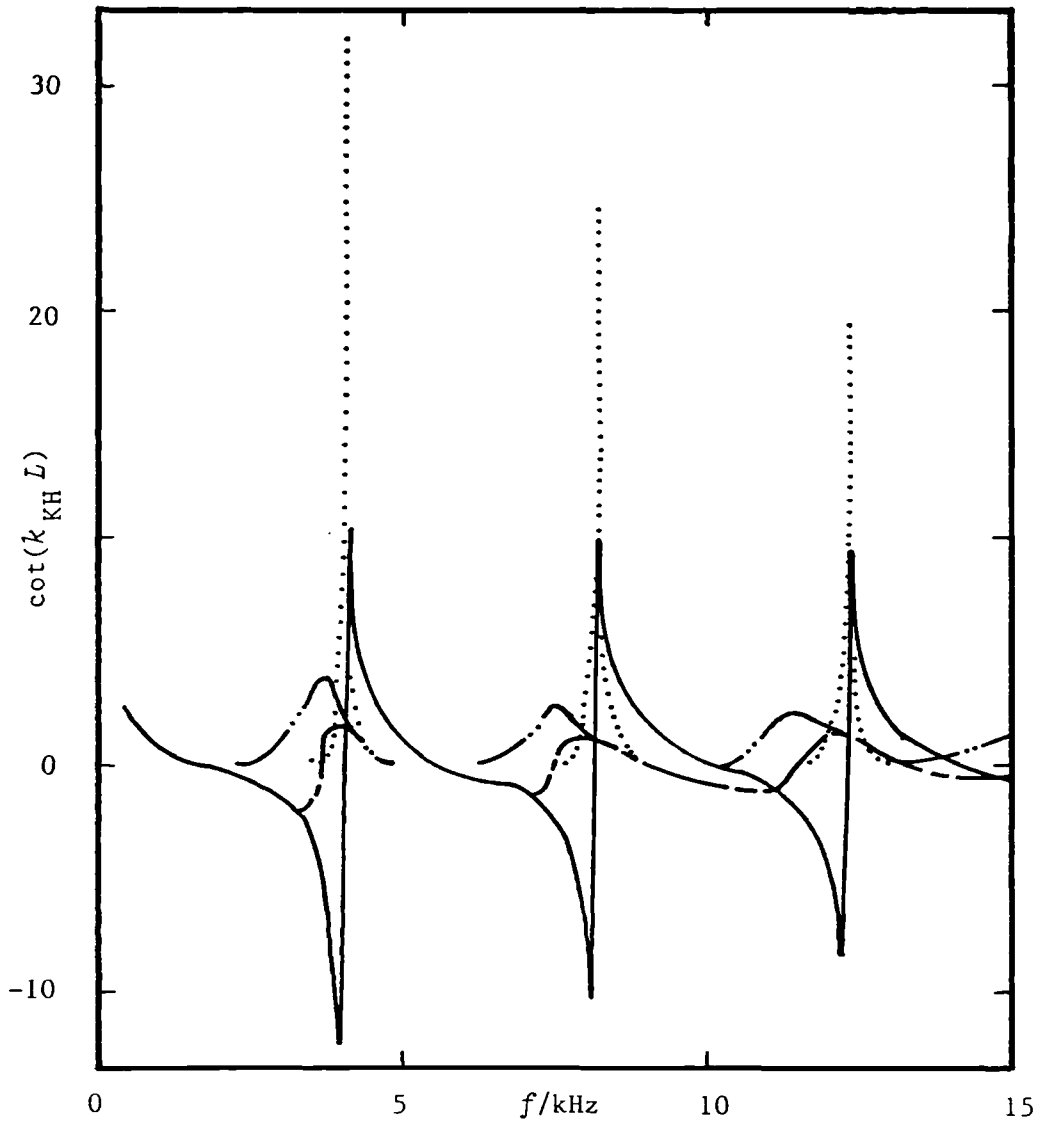

Figure 3.10. Rm{cot($k_{KH}L$)} and - Im{cot($k_{KH}L$)} as a function of f for a tube with L = 40 mm protruding from a resonator with a = 40 mm containing Ar at 300 K for densities of 100 kg•m^{-3} [——,Rm{cot($k_{KH}L$)} and •••••,- Im{cot($k_{KH}L$)}] and 1 kg•m^{-3} [—— – ——,Rm{cot($k_{KH}L$)} and —— • • ——, -Im{cot($k_{KH}L$)}]. -Im{cot($k_{KH}L$)} is proportional to g, while Rm{cot($k_{KH}L$)} is proportional to Δf.

given by

$$k_x = \left\{k^2[\{1 + (\gamma - 1)F_3(\delta_h/d)\}/\{1 - F_3(\delta_S/d)\}]\right\}^{\frac{1}{2}} \qquad (3.4.58)$$

where

$$F_3(\xi) = (1 + i)\xi \ \tanh\ \{(1 - i)/(2\xi)\}, \qquad (3.4.59)$$

in which ξ represents either (δ_h/d) or (δ_S/d). For a wide slot (δ_S/d) and (δ_h/d) both tend to zero and equation (57) reduces to (41) of a circular tube of length L. In contrast with the sharp resonances of a tube, the resonances in a narrow slot are highly damped and y_{0S} varies slowly with frequency. Trusler[81] has also considered the case of a slot open at $x=L$, and provides a further expression for y_{0S}. For a narrow slot, the frequency dependence of the two expressions are very similar, although in the zero-freuqncy limit, y_{0S} for a closed slot has a finite value while y_{0S} tend to zero for an open slot. The perturbation to the radial modes from an annular slot closed at L, which perturbs the cavities' surface area by an amount S_{0A} is obtained by the combination of equations (57) and (39), correct to first order in y_{0S}.

Imperfect spherical geometry

Practical resonators are machined in two halves which approximate hemispheres such that, to within the limit of the mechanical measurements, the equatorial and polar radii are equal. Each "hemisphere" is likely to be highly axisymmetric and to be cut off, at the equator, by a plane

perpendicular to the axis of symmetry. However, to eliminate most of the surface roughness left by machining, the hemispheres are polished, which may remove the axial symmetry. Polishing is usually performed before final machining of the equatorial plane so that the polar and equatorial radii for a hemisphere are equal. Although the axes of symmetry are likely to be parallel, they may not be coincident. Consequently a shoulder or step may occur at the join.

Mehl has considered the perturbation to the ideal resonators eigenvalues ν_{ln} arising from imperfect geometry, for the radial (l=0) modes due to axisymmetric imperfections,[49] {this was considered earlier by Campbell[82]} and more recently from arbitrary shape changes for both radial and non-radial ($l \geqslant 1$) acoustic modes.[50] In both cases the perturbations which are of interest arise from shape changes which leave the resonator's volume unchanged from that of ideal geometry. He considered the shape changes to a resonator which differs, by a small deformation parameter ε, from the perfect shape, where the surface is described through

$$r/a = 1 - \varepsilon F(\theta,\zeta), \tag{3.4.60}$$

in which $F(\theta,\zeta)$ is a smoothly varying function of order unity. The resulting perturbation to the resonance frequencies for the radial modes is given by

$$\Delta f = f_{0n}\varepsilon^2 C_{0n}, \tag{3.4.61}$$

to lowest order in ε; values of C_{0n} for some simple shape

functions $F(\theta,\zeta)$ have been calculated and reported elsewhere.[40]

The $(2l+1)$-fold degeneracy of a non-radial mode is broken by a shape imperfection and the perturbation to each component is proportional to ε with the C_{ln} depending on the relative orientation of the shape imperfections and the non-radial component. However, the average shift in frequency of the $(2l+1)$ components is still of order ε^2 as for the radial modes. If non-radial modes are to be used to estimate ε so that the perturbations to the radial modes can be calculated, then the various components must be sufficiently resolved to allow each frequency to be determined. Furthermore, for axisymmetric shape imperfections the degeneracy is usually only reduced to $(l+1)$ and the problem of identifying the "singlet" remains.

All microwave resonances of a sphere have $l > 0$ and like the non-radial acoustic modes are $(2l+1)$-fold degenerate with perfect geometry. Measurements of such resonances are important since they provide a non-acoustic means of estimating geometric deformations, the radius a, and the variation of a with temperature and pressure. As for non-radial acoustic modes, the appropriately weighted mean of the $(2l+1)$ components must be used when calculating a. However, microwave resonances in a metal sphere can have very high Q's and it is more likely that the components will be resolved. For example, the quality factor Q of the lowest magnetic mode TM 11 (with $\nu_{11}^{TM} = 2.744$) of an aluminium resonator of radius 40 mm is about 20000 compared

with 360 for the corresponding acoustic mode {$\nu(1,1) = 2.082$} in Ar at 300 K and 100 kPa; the lowest electric mode TE 11 {$\nu_{11}^{TE} = 4.493407$} has a Q of approximately 34800, in the same resonator, and the acoustic modes (0,2) and (3,1) with similar eigenvalues {$\nu(0,2) = 4.493409$ and $\nu(3,1) = 4.514100$} have Q's of about 1750 and 420 respectively in Ar at 300 K and 100 kPa.

Finally we shall briefly review two important cases. Firstly, for a resonator constructed from two perfect hemispheres whose radii differ; one with $a' = a(1 - \varepsilon)$ resulting in a step of width $a\varepsilon$ at the equator. The resulting perturbation to the resonance frequencies of the radial modes from those of a perfect sphere having the same volume are given by equation (61), with C_{0n} from reference (49). For a typical value of $\varepsilon = 3 \times 10^{-4}$, obtained in a resonator used by Mehl and Moldover,[46,52,68,69,83] the fractional shift in resonance frequency (l=0) for n in the range $3 \leqslant n \leqslant 8$ (with C_{0n} between -2.9 and 0.1) $\Delta f/f < \pm 1 \times 10^{-6}$. However, for the (0.2) mode $C_{02} = -14.6$ and $10^6 \Delta f/f = -1.3$; the comparatively large perturbation results from the near overlap with the (3,1) mode.[49] For this geometric imperfection non-radial modes are perturbed to order ε^2.

Secondly, for a resonator with one hemisphere turned so as to have insufficient depth, a minor spherical segment is created and the resulting perturbation $\Delta f/f$ (again with $\varepsilon = 3 \times 10^{-4}$) is considerably less than 1×10^{-6} for the first seven radial modes. Further examples can be found in the literature.[47,49,50]

Steady-state response of an acoustic cavity

For a simple-harmonic source {in our case with time dependence $\exp(-i\omega t)$} operating at a real frequency $f = \omega/(2\pi)$, acting from a small surface S_S on the resonator's inner surface which has radial surface velocity $U_S(r_S)$ relative to the rest of the shell, with strength constant over sufficient time for a steady-state to be achieved then the response of the cavity has been calculated using a Green's function.[47,84,85] The resulting steady-state acoustic pressure at a frequency for any point $\vec{r}$ in the resonator is given by

$$p_f(\vec{r},\vec{r}_S) = -if\rho u^2/(2\pi V)\sum_N \Phi_N(\vec{r})/[\Lambda_N\{F_N^2(f) - f^2\}] \times \int_{S_S} \Phi_N(\vec{r}_S)U_S(\vec{r}_S)dS, \qquad (3.4.62)$$

for the eigenfunctions Φ_N of the normal modes, with corresponding complex natural mode frequencies $F_N(f) = \omega_N(\omega)/(2\pi)$, of the N-th normal mode. In equation (60), Λ_N is the average value of Φ_N over the resonators volume V, and N again represents the three required indices (l,n,m). However, the frequency dependence of the normal modes is small, and F_N is effectively constant for source f close to $\mathrm{Re}(F_N)$. $\mathrm{Re}\{p_f(\vec{r},\vec{r}_S)\}$ describes the acoustic pressure component in phase with the driving source and $\mathrm{Im}\{p_f(\vec{r},\vec{r}_S)\}$ the component in quadrature with the source.

The resonator's response to a steady-state excitation is usually determined at a point $\vec{r}$ with a separate detector, which is typically a pressure transducer

(microphone) whose complex output voltage $(u - iv)$ is proportional to $p_f(\vec{r},\vec{r}_S)$.

Consequently, if $f_N - ig_N = F_N$ is to be determined by observing the resonant behaviour of the cavity then the contributions from the other modes must be small for f near f_N. In the usual experimental situation one or only a small number of modes are stimulated by the source at a given driving frequency. Therefore, only one or a small number of terms need be included in the summation of equation (62), and the remaining background terms may be represented by a Taylor series expansion in frequency about $f = f_N$, for f near f_N. In the case that only one mode is excited the detector output can be written in terms of a simplified form of equation (62), with only one term in the summation, to give

$$u - iv = -iA_N f/(F_N^2 - f^2) + B + C(f - f_N) + \ldots, \qquad (3.4.63)$$

where A_N, B, C, ..., are complex constants, and B, C, ..., represent the background. In equation (61) A_N is dominant, and the complex natural frequency $F_N = f_N - ig_N$ and the remaining required constants are determined from measurements of $(u - iv)$ over a range of f near f_N.

If the measurement point $\vec{r}$ (or $\vec{r}_S$ since the Green's function is symmetric to interchange of $\vec{r}_S$ and $\vec{r}$) is coincident with a node of a standing wave then the resonance will not be observed; real sources often resemble and so approximate point sources.

For non-radial modes in a practical resonator the $(2l+1)$-fold degeneracy may be partially or fully resolved, in which case further terms in the summation of (62) are required; Moldover *et al.*[47] required 2 extra terms to adequately describe measurements on the (1,2) mode. However, for radial modes ($l=0$) equation (62) is usually sufficient. Although even at low frequency when bulk attenuation is severe overlap of adjacent modes may be significant, and further terms in (63) may be required; measurements of $u - iv$ over the coupled modes is desirable. It is envisaged that such a case may arise from vibrational relaxation attenuation.

If background terms are negligible then the Lorentzian formula

$$u - iv = [a/\{g_N - i(f - f_N)\}], \qquad (3.4.64)$$

is applicable provided $g_N << f_N$, where a is constant.

REFERENCES

1. Herzfeld, K.F.; Litovitz, T.A. *Pure and Applied Physics Vol.7. Absorption and Dispersion of Ultrasonic Waves.* Massey, H.S.W.: Editor. Academic Press: London. 1959, p.25-48.
2. Morse, P.M.; Ingard, K.U. *Theoretical Acoustics.* McGraw-Hill: New York. 1968, p.278-279.
3. McGlashan, M.L. *Chemical Thermodynamics.* Academic Press: London. 1979, p.16, p.72-76.
4. Reference 2, p.280.
5. Reference 2, p.239-241, 279.
6. Reference 2, p.281-284.
7. Reference 2, p.285.
8. McCottrell, T.L.; McCoubrey, J.C. *Molecular Energy Transfer in Gases.* Butterworths: London. 1961, p.12.
9. Reference 2, p.260
10. Reference 2, p.285-291.
11. Reference 2, p.554-561.
12. Reference 2, p.227.300.
13. References 1 and 2
14. Reference 5.
15. Kinsler, L.E.; Frey, A.R.; Coppens, A.B.; Saunders, J.V. *Fundamentals of Acoustics.* Wiley: New York. 1982, p.101-102.
16. Reference 1, p.203.
17. Greenspan, M. *Physical Acoustics. Vol.IIA.* Mason, W.P.: Editor. Academic Press: London. 1965. p.1-43.
18. Reference 2, p.297.

19. Relaxation times for viscous and thermal conduction processes are short $t \approx 10^{-10}$ s.

20. Lambert, J.D. *Vibrational and rotational relaxation in gases.* Clarendon Press: Oxford. 1977, p.20, and chapter 5.

21. Ehrenfest, P. *Koninkl. Ned. Akad. Wetenschap. Proc.* 1914, 16, 591.

22. Landau, L.; Teller, E. *Phys. Z. Sawj. Un.* 1936, 10, 34.

23. Reference 1, p.86-90.

24. Reference 20, p.8, 53-58, 61-62.

25. Reference 20, p.64-65.

26. Reference 20, p.84-85 and Reference 1, p.105-130.

27. Reference 20, p.85-93.

28. Reference 2, p.298-300.

29. Reference 20, p.76 and Reference 1, p.207-215; 328-331.

30. Reference 1, p.136-138, 206-215.

31. Reference 20, p.93-100.

32. Kohler, M. *Z. Physik* 1949, 127, 40.

33. Reference 1, p.216.

34. Huck, R.J.; Johnson, E.A. *Phys. Rev. Lett.* 1980, 44, 142.

35. Reference 1, p.138-143.

36. Mazo, R.M. *J. Chem. Phys.* 1958, 28, 1223.

37. Garcia-Colin, L.S.; de la Selva, S.M.T. *Proc. Eighth Symp. on Thermophysical Prop.* Sengers, J.V. Editor: Am. Soc. Mech. Eng.: New York. 1982, p.178.

38. Reference 1.

39. Reference 8.

40. Reference 20

41. *Royal Society Mathematical Tables, Vo.7. Bessel Functions Part III Zeros and Associated Values.* Olver, F.W.J.: Editor. Cambridge University Press: Cambridge. 1960.

42. Trusler, J.P.M. PhD. Thesis, University of London. 1984.

43. Rayleigh, J.W.S. *The Theory of Sound, Vol.2.* Dover: New York. 1945. pp.264-271.

44. Reference 42, p.47-51.

45. Reference 2, p.559-564.

46. Mehl, J.B.; Moldover, M.R. *J. Chem. Phys.* 1981, 74, 4062.

47. Moldover, M.R.; Mehl, J.B., Greenspan, M. *J. Acoust. Soc. Am.* 1986, 79, 253.

48. Ewing, M.B.,; McGlashan, M.L.; Trusler, J.P.M. *Metrologia* 1986, 22, 93.

49. Mehl, J.B. *J. Acoust. Soc. Am.* 1982, 71, 1109.

50. Mehl, J.B. *J. Acoust. Soc. Am.* 1986, 79, 278.

51. Mehl, J.B. *J. Acoust. Soc. Am.* 1985, 78, 782.

52. Moldover, M.R.; Mehl, J.B. *Precision Measurements and Fundamental Constants II.* Taylor, B.N.- Phillips, W.D.: Editors. Nat. Bur. Stand. Spec. Pub. 617, 1984. p.281-286.

53. Kennard, E.H. *Kinetic Theory of Gases* McGraw-Hill: New York. 1938, p.311-316.

54. Thomas, L.B.; Golike, R.C. *J. Chem. Phys.* 1954, 22, 300.

55. Harris, R.E. *J. Chem. Phys.* 1967, 46, 3217.

56. Shields, F.D.; Faugh, J. *J. Acoust. Soc. Am.* 1969, 46, 158.

57. Shields, F.D. *J. Chem. Phys.* 1975, 62, 1248.

58. McDowell, R.S.; Kruse, F.H. *J. Chem. Eng. Data* 1963, 8, 547.

59. Reference 3, p.201-203.

60. Maitland, G.C.; Rigby, M.; Smith, E.B.; Wakenham, W.A. *Intermolecular Forces. Their Origin and Determination.* Clarendon: Oxford. 1981. p.571.

61. Reference 42, p.74-77.

62. Kaye, G.W.C.; Laby, T.H. *Table of Physical and Chemical Constants and some Mathematical Functions.* Fourteenth Edition. Longman: London. 1973.

63. Greenspan, M. Unpublished work quoted in Reference 45.

64. British Standard 970: part 4. 1970, p.18.

65. Gibbons, R.M.; Laughton, A.P. *J. Chem. Soc. Faraday Trans. 2*, 1984, 80, 1019.

66. Reference 65 with T^c = 126.2 K, p^c = 3.394 MPa, and ω = 0.04.

67. Younglove, B.A.; McCarty, R.D. *J. Chem. Thermodynamics* 1980, 12, 1121.

68. Mehl, J.B.; Moldover, M.R. *Proc. Eighth Symp. on Thermophysical Prop.* Sengers, J.V. Editor: Am. Soc. Mech. Eng.: New York. 1982, p.134.

69. Mehl, J.B.; Moldover, M.R. *J. Chem. Phys.* 1982, 77, 455.

70. Ewing, M.B.,; Goodwin, A.R.H.; McGlashan, M.L.; Trusler, J.P.M. *J. Chem. Thermodynamics* 1987, 19, 721.

71. Ewing, M.B.; Goodwin, A.R.H.; McGlashan, M.L.; Trusler, J.P.M. *J. Chem. Thermodynamics*, 1988, 20, 000.

72. Landau, L.D.; Lifshitz, E.M. *Course of Theoretical Physics Vol.7. Theory of Elasticity.* Pergamon: Oxford. 1973, p.54.

73. Shah, A.H.; Ramkrishran, G.V.; Datta, S.K.
J. Appl. Mech. 1969, 36, 431.

74. Reference 2, p.469.

75. Kirchoff, G. *Ann. Physik* 1868, 134, 177;
Annalesde Chemie 1868, 15, 491.

76. Reference 43, p.319-328.

77. Shields, F.D.; Lee, K.P.; Wiley, W.J. *J. Acoust. Soc. Am.* 1965, 37, 724.

78. Reference 15; p.202.

79. Reference 15, Chapter 10, p.225-228, 323, 232.

80. Reference 2, p.489-490.

81. Trusler, J.P.M. Unpublished work.

82. Campbell, J.D. *Acustica* 1955, 5, 145.

83. Moldover, M.R.; Waxman, M.; Greenspan, M.
High-Temp. High-Press. 1979, 11, 75.

74. Reference 2, p.559-561.

85. Reference 42, p.41-46.

CHAPTER FOUR

EXPERIMENTAL TECHNIQUES

4.1 INTRODUCTION

The resonance frequencies and half widths have been calculated from comparative measurements, performed with a network analyser, of the amplitude and phase of the received signal relative to the transmitted signal.

The temperature of the gas within the spherical resonator and the $T^{g+1}(p)$ required for vapour pressure determination by comparative ebulliometry were measured using long-stem platinum resistance thermometers calibrated on IPTS-68.

The pressure measurements required for the $u(p,T)$ results were determined using differential pressure transducers with a quartz-spiral gauge, an oil lubricated pressure balance, or a metallic spiral gauge; atmospheric pressure was determined with a Fortin barometer. The differential pressure transducers, used with the high-pressure appatatus, were calibrated against an air-lubricated pressure balance; these calibrations are given in section 4.

The samples used in this work and their chemical purities are reported in section 5, together with their purification and analysis.

4.2 MEASUREMENT OF F_{0n}

The sine-wave signals used for acoustic measurements were synthesized by a network analyser. (Hewlett-Packard HP 4192A impedance analyser) which was controlled by a microcomputer (Hewlett-Packard HP 87A) over an HP-IB interface, and was phase locked to the 10 MHz time base of a counter (Hewlett-Packard HP 5315B option 004 with thermostatted quartz crystal); the fractional accuracy of the frequencies was better than 10^{-7}. The HP 4192A output, which was variable between 0.005 and 1.1 V r.m.s. and 5 to 13×10^6 Hz in increments of 0.001 V r.m.s. and 0.001 to 1 Hz, was amplified to 70 V r.m.s. and mixed with a 200 V dc bias before passing to the source transducer. A 1 V r.m.s. reference signal was supplied to the HP 4192A from a resistive-potential divider placed in parallel with the output of the power-amplifier.

The detectors[†] output typically between 10 - 100 V r.m.s. close to an acoustic resonance was fed into a low noise amplifer (ZN459CP) which had a potential difference

---

[†]Commercially available electret capacitance microphones were used as detectors in both apparatuses, which had built in field-effect transistors to act as preamplifers (and also impedance matches). These devices were powered by an external 1.5 V dc battery and dissipated less than 1 mW and should have not caused significant temperature gradients in the sphere wall.

gain of 10^4; for measurements with the high-pressure apparatus a differential amplifer based on three operational-amplifers was used.(1) The output signal was further amplified with a potential difference gain variable between 10 and 30 in steps of 10 (but usually operated at 10), filtered to remove low and high frequency noise with a 1 to 100 kHz band pass amplifer, and then fed to the measurement channel of the network analyser. At the network analyser, the input signal was typically between 0.1 and 1 V r.m.s. near an acoustic resonance. However, when the input was greater than 1 V r.m.s. it was often useful to reduce the network analyser output to prevent overflow of the HP 4192A. The amplitude $\bar{a}$ and phase angle ϕ were measured, with a time constant of 1 s by the network analyser, relative to the reference signal with a resolution of 0.01 per cent and 0.0002 respectively. The band-pass amplifer shifted ϕ negligibly, and since the reference signal was taken after the power amplifier this device gave no relevant phase shift.

The measurement procedure employed to obtain $F_{0n} = f_{0n} - ig_{0n}$ from equation (3.4.63), where f_{0n} is the resonance frequency and g_{0n} the half-width, is similar to that described by Mehl and Moldover,(2) and Moldover *et al.*(3) Once thermal and hydrostatic equilibrium had been reached, estimates of f_{0n} and g_{0n} were obtained from manual scans of the appropriate frequency ranges. The network analyser was then stepped from a frequency near $f_{0n} - g_{0n}$ to $f_{0n} + g_{0n}$ in eleven discrete equally spaced frequencies. At each frequency, a time t was allowed for the acoustic pressure to

stabilize such that the fractional systematic error, given approximately by $(g/f)\exp(-2\pi tg)$, in the resonance frequency was less than 10^{-7} before $\bar{a}$ and ϕ were recorded. Often the measurement procedure was repeated from $f_{0n} + g_{0n}$ to $f_{0n} - g_{0n}$, to remove any significant uncertainty due to temperature drifts. Also, when the signal to noise ratio was particularly poor, $\bar{a}$ and ϕ were measured repeatedly at each frequency and their averages used. Measurements of $\bar{a}$ and ϕ at each frequency were then expressed in terms of the real and imaginary parts of the complex potential difference ratio w of the received and reference signals,

$$w = \bar{a}\cos(\phi) - i\bar{a}\sin(\phi) = u - iv. \qquad (4.2.1)$$

The 11 frequencies and 11 (or in some instances 22) complex potential differences were used to evaluate F_{0n}, A_{0n}, B and if necessary, C in the theoretical form of the resonance {equation (3.4.63)}

$$w = A_{0n}f/(F_{0n}^2 - f^2) + B + Cf, \qquad (4.2.2)$$

using a non-linear regression analysis similar to the one described by Mehl.[4] In equation (2) A_{0n} is a complex amplitude proportional to the source strength (and any phase shifts between source and detector), and B and C are the first two complex terms in a Taylor's series that accounts for the background, such as may arise from the influence of other resonances apart from that under study. In this work no terms higher than C in the Taylor's series

were required to adequately represent the measurements, and in most cases only B was significant. With a precision of about 0.1 per cent in w, and with resonance quality factors of several thousand a fractional resolution in f_{0n} of 10^{-7} or better is possible, or rather 0.1 per cent in g_{0n}. In figure 4.1 it is shown for measurements of $w(f)$ near $f(0,4)$ in methylpropane at 320 K and 113 kPa, that the resonances do indeed follow the theoretical form (2) to the accuracy required to determine f_{0n} to a fractional precision better than 1×10^{-6}.

4.3 TEMPERATURE MEASUREMENTS

The temperatures were measured using a long-stem platinum resistance thermometer calibrated on the International Practical Temperature Scale of 1968 (IPTS-68).[5,6] In the temperature range 273.15 to 903.89 K the T_{68} are calculated using

$$T_{68} = 273.15\ \text{K} + t + 0.045(t/100\ ^{\circ}\text{C})\{(t/100\ ^{\circ}\text{C}) - 1\} \times \{(t/419.58\ ^{\circ}\text{C}) - 1\}\{(t/630.74\ ^{\circ}\text{C}) - 1\}^{\circ}\text{C} \quad (4.2.1)$$

where t is a Celcius temperature obtained by iteration from

$$t = \{(W - 1)/\alpha\} + \delta(t/100\ ^{\circ}\text{C})\{(t/100\ ^{\circ}\text{C}) - 1\}, \quad (4.3.2)$$

with the resistance ratio

$$W = \{R(T_{68})/R(273.15\ \text{K})\} = R(T_{68})/R_0. \quad (4.3.3)$$

Between 13.81 and 273.15 K the T_{68} is given by

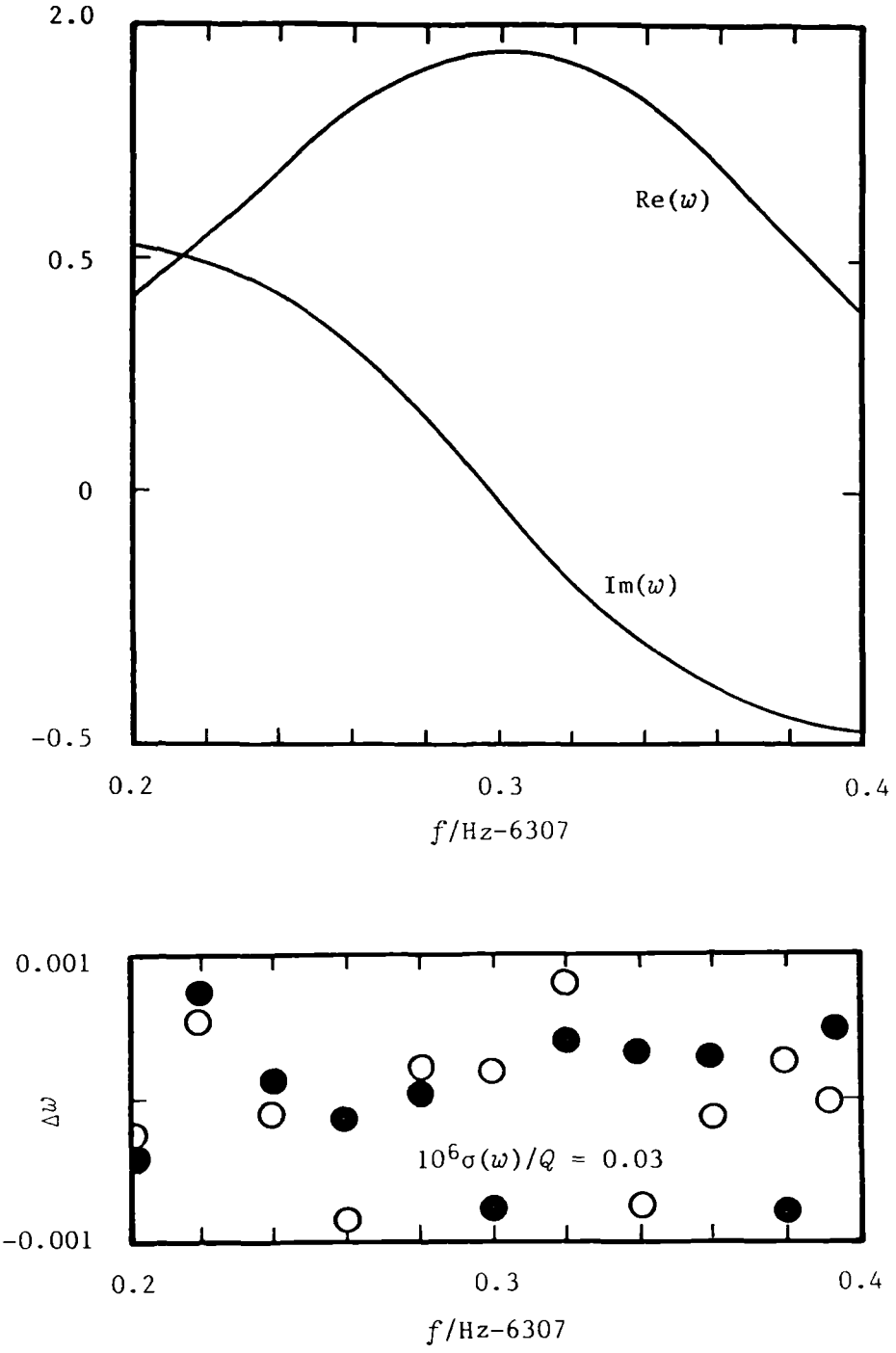

Figure 4.1. Top: In phase and quadrature components of w as a function of f near $f_{(0,4)}$ in methylpropane at 320 K and 113 kPa.
Bottom: Measured w as deviation from equation (2) truncated after the constant background term with the fitted parameters based on the measurements.

$$T_{68} = \sum_{j=0}^{20} a_j \{(\ln W_{CCT-68}/3.28 + 1\}^j \text{ K}, \qquad (4.3.4)$$

where the a_j are defined constants,[6] and

$$W_{CCT-68} = W - \Delta W(T_{68}) \qquad (4.3.5)$$

in which ΔW is a deviation function for a particular thermometer. For the range between 90.188 K and 273.15 K ΔW has the form

$$\Delta W_4(T_{68}) = b_4(T_{68} - 273.15 \text{ K}) + e_4(T_{68} - 273.15 \text{ K})^3 \times (T_{68} - 373.15 \text{ K}).^{(6)} \qquad (4.3.6)$$

The constants R_0, α, δ, b_4, and e_4 of equations (2) and (6) were determined for each thermometer from resistance measurements at the triple points of water and mercury and the nominal melting temperatures of tin and zinc.

The temperature of the spherical resonators and consequently of the gas contained within the cavity were measured using a Leeds and Northrup (serial number 780308) long-stem platinum resistance thermometer (PRT) calibrated on IPTS-68; the required constants for the temperature range 90.188 to 903.89 K for this PRT are given in table 4.1. The resistances were measured to 10 μΩ using an ac bridge (Tinsley type 5840), operating at 375 Hz and a current of 1 mA. The bridge was checked frequently against a standard resistor (Tinsley model, nominally 10 Ω) housed in a thermostatted container, of resistance $R_S(T_S)$ given by

$$R_S(T_S)/\Omega = 9.9999_7 - 1.53 \times 10^{-5} (T/\text{K} - 296.15) - 7.23 \times 10^{-7} (T/\text{K} - 296.15)^2, \qquad (4.3.7)$$

where T_S is the resistor's temperature as measured by a mercury in glass thermometer with an accuracy of 0.2 K. The PRT resistance was measured frequently in a triple point of water cell,[7] and over the 4 a period of the measurements reported here increased by 40 μΩ.

Table 4.1 Constants required to calculate T_{68} in the temperature range 90.188 to 903.89 K from measurement of the resistance of a platinum element, for the three long stem Leeds and Northrup (LN) platinum resistance thermometers (PRT) used in this work.

	PRT Model and Serial Number		
	LN:780308	LN:1046978	LN:1046982
I/mA	1[a]	2[b]	2[b]
R_0/Ω	25.56007	25.53700	25.56085
$10^3\alpha/^oC^{-1}$	3.93579	3.92530	3.92548
$\delta/^oC$	1.49579	1.49692	1.49680
$10^6 e_4/K$	-21.2	40	0
$10^6 b_4/K$	-18.1	-67	-60

[a] Tinsley 5840 ac bridge operating at 375 Hz.

[b] Leeds and Northrup dc bridge.

The temperature $T^{g+1}(H_2O,p)$ and $T^{g+1}(\text{sample},p)$ required for the comparative ebulliometric determination of p^{1+g} (to be discussed in Chapter Five) were calculated from measurements

of the resistances of two Leeds and Northrup long-stem PRT's (serial numbers LN:1046982 and LN:1046978) calibrated on IPTS-68, for which the required calibration constants are given in table 4.1 The resistance measurements were performed with a Leeds and Northrup dc bridge (serial number 1053275) operating at 2 mA, with a resolution of 0.1 mΩ (1 mK); this bridge had been calibrated against the same 10 Ω standard as the ac bridge.

4.4 PRESSURE MEASUREMENTS

Low-pressure

The gaseous sample in the spherical resonator was isolated from the pressure gauge using a differential capacitance manometer (Baratron, mode 221AH-A-10) which was operated as an approximately null-reading instrument; the pressure differences Δp were always less than 0.2 kPa and usually less than 0.02 kPa. The span of the manometer was 1.73 kPa and the manufacturer's calibration showed no deviations greater than 0.1 per cent of reading from linearity.

Absolute pressures p below 115 kPa were measured with a precision of 1 Pa using a quartz-spiral gauge (Ruska DDR 6000) fitted with an optical null detector. For the range $115 < p/\text{kPa} < 250$, a bronze-spiral dial gauge (Bundenberg Ltd) gave a precision of 0.1 kPa in the gauge pressure; atmospheric pressure p_a was obtained to better than 13 Pa from the height h of the mercury column using

$$p_a/\text{kPa} = 101.325(h/\text{mm})\{(1 + \alpha(T/\text{K}) - 273.15)/$$

$$(1 + \beta(T/\text{K} - 273.15)\}g/(760\ g'),^{(8)} \qquad (4.4.1)$$

where α is the linear thermal expansion coefficient of the brass scale ($\alpha = 1.84 \times 10^{-5}\ \text{K}^{-1}$), and β the relative expansivity of mercury in glass ($\beta = 1.818 \times 10^{-4}\ \text{K}^{-1}$). In equation (1) g is the local acceleration of free fall (for our laboratory[9] $g = 9.811856\ \text{m}\cdot\text{s}^{-2}$) and $g' = 9.80665\ \text{m}\cdot\text{s}^{-2}$ is the standard acceleration of free fall. For $u(p)_T$ measurements with Ar, where $A_1/A_0 \simeq 4.7 \times 10^{-6}\ \text{kPa}^{-1}$ at 300 K, the 0.5 kPa accuracy of the bronze-spiral gauge was just adquate; but for similar measurements with hydrocarbons and methanol, where for example $A_1/A_0 \simeq 1.1 \times 10^{-3}\ \text{kPa}^{-1}$ for n-C_5H_{12} at 270 K, this pressure gauge was totally inadequate. Consequently for the hydrocarbons and methanol studies, at low reduced temperatures, the pressure was restricted to a maximum of 115 kPa. The zero pressure reading of the gauges were set using a high vacuum system that combined a 38.1 mm diameter oil (Santovac) vapour diffusion pump, with an ultimate low pressure of 0.1 mPa, and a single stage rotary backing pump. During acoustic measurements the pressure of the Ar in the line between the pressure gauges and the Baratron was adjusted using a separate rough vacuum system.

The quartz-spiral gauge was calibrated by the manufacturers to an accuracy of 1 Pa; this calibration was accepted for the bulk of the low-pressure acoustic measurements. However, before commencing measurements on

n-pentane the thermostat of the quartz-spiral gauge malfunctioned, and the gauge overheated. Subsequently, the gauge calibration was checked at five pressures every 20 kPa from approximately 20 kPa upward with a precise mercury manometer, which has a precision and accuracy of 1 Pa, with the result

$$p/\mathrm{kPa} = 9.988526_5(\phi_R/\mathrm{V}), \qquad (4.4.2)$$

where p is the pressure measured by the manometer and quartz spiral gauge and ϕ_R is the corresponding dc potential difference from the spiral gauge. Equation (2) was obtained from a constrained (p = 0 when ϕ_R = 0) linear regression which gave $\sigma(p)$ = 1 Pa; an unconstrained fit gave $p = -1.7\times10^{-4}$ kPa at ϕ_R = 0, again with $\sigma(p) \simeq$ 1 Pa.

The mercury manometer has been described in detail elsewhere.[10] No attempt was made to control the mercury temperature. However, the temperature was estimated from the mean of two temperatures obtained from two small glass jars containing mercury, fitted with mercury-in-glass thermometers which had a precision of 0.01 K, placed adjacent to the manometer one at approximately the height of each meniscus. Finally from the knowledge of the height difference Δh between two menisci, the local acceleration of free fall, and the density ρ of mercury as a function of T,[11-14] p can be calculated; $p = g\rho\Delta h$.

High-pressure

The pressure of the sample, contained in a sealed spherical resonator, was compared to the N_2 pressure in the

pressure vessel containing the sphere with a differential strain-gauge pressure transducer (DPT) D, shown in figure 4.2, at a height h_S above the resonator's equator. The pressure transducer A also served to isolate the sample from the pressure measurement system and was operated approximately as a null-reading device; the details of each pressure transducer employed will be given later. Nitrogen reference pressures between 0.5 and 7 MPa were measured at a height ($h_{N_2} + h_0$) above the pressure transducer A with an oil lubricated pressure balance D (Bundenberg Ltd, model 280L: serial number 7967/280L) *via* an oil/N_2 interface E, while below 250 kPa the bronze-spiral gauge, described previously, was used; both measurements required the Fortin barometer for measurements of atmospheric pressure p_a.

Typically when performing acoustic measurements with either differential pressure transducer (DPT), valve 2 shown in figure 4.2 was closed to prevent any temperature fluctuations, arising from variations in pressure at the piston gauge and, consequently, pressure disturbances in the pressure vessel; usually the sample pressure was measured before and after acoustic measurements.

The total sample pressure at the spherical resonator's equator, when measured by the pressure balance, is given by

$$p = p_g + p_a + h_0\rho_0 g + h_{N_2}\rho_{N_2} g + h_S\rho_S g, \qquad (4.4.3)$$

where p_g is the pressure exerted by the oil lubricated piston gauge, and each term $h\rho g$ represents the pressure due to the

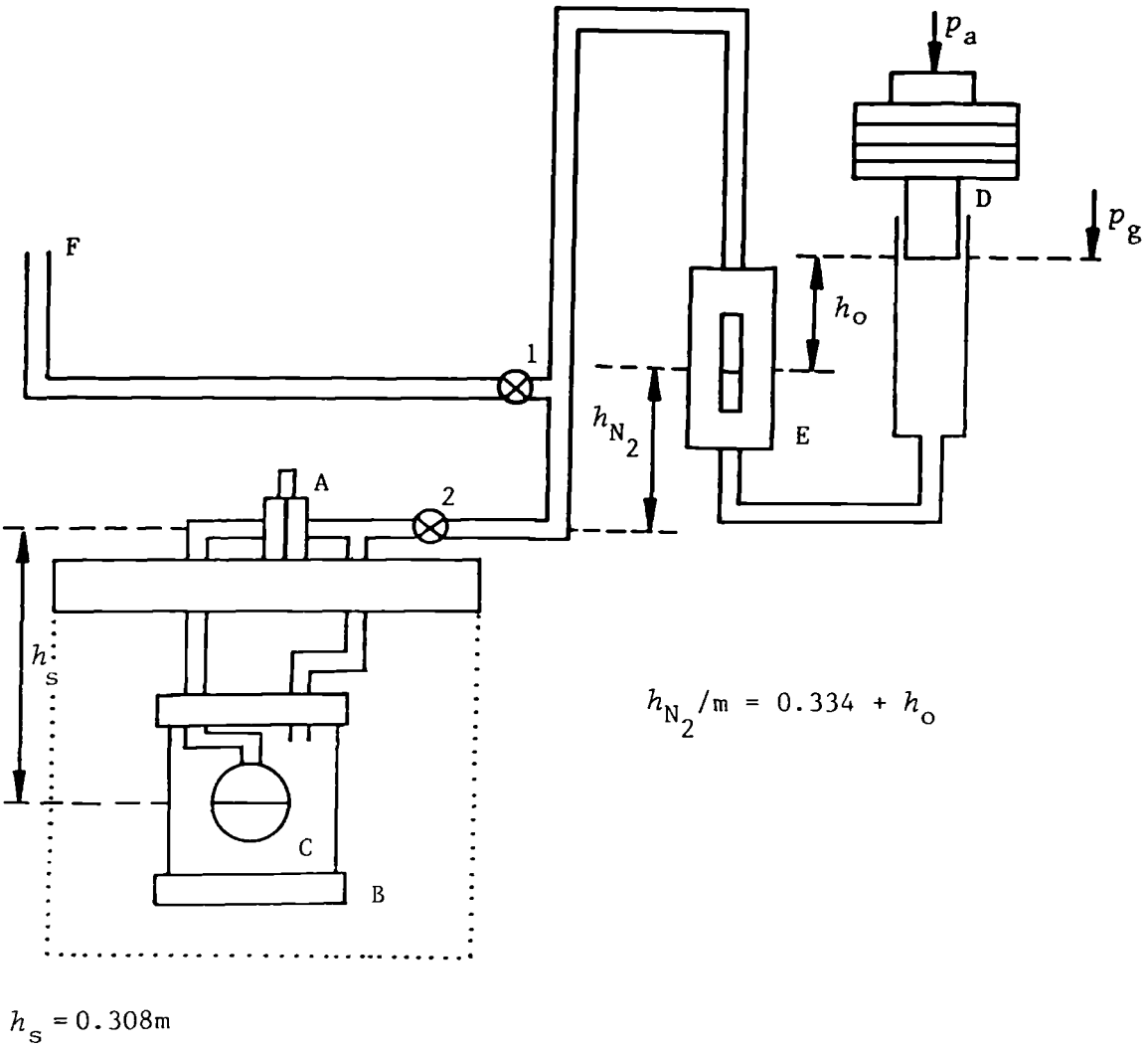

Figure 4.2. Schematic representation of sample pressure measurement system, for high-pressure sealed spherical resonator C contained within a pressure vessel B, using a differential pressure transducer A and an oil lubricated pressure balance D with N_2 connecting A and E, the oil N_2 interface. The dotted line is the thermostat. F leads to a rotary vacuum pump , the bronze-spiral gauge for $p < 260$ kPa, and if required the quartz-spiral gauge.

fluid column of height h and mean density ρ; g is the local acceleration of free fall and h_S, h_0, and h_{N_2} are defined in figure 4.2. The densities ρ required in equation (3) for N_2 and the sample S were calculated from equation (2.2.1) truncated after the second virial coefficient,[15] while for oil (Shell: Tellus 27) ρ_0 = 878 kg·m^{-3}; the term $g\sum_j \rho_j h_j$ never amounted to more than 1 kPa, and could be estimated with a precision better than 0.01 kPa. Nevertheless, the height h_0 of oil, as measured by means of a scale placed on the sight-gauge E, was kept within 10 mm of the zero-point by injecting oil from a screw-press and reservoir and, consequently, contributed no more than 0.1 kPa to $g\sum_j \rho_j h_j$.

Although equation (3) should strictly contain a term representing the interfacial pressure difference between two fluid phases (N_2 + oil), this term has been neglected since it was never greater than 5 Pa.

The pressure p_g is given by

$$p_g = p_g'(g/g')\{1 - (\rho_a - \rho_a')/\rho_w\} / [(1 + \alpha_1 p_g)\{1 + \alpha_2(T - T')\}], \qquad (4.4.4)$$

where p_g' is the nominal gauge pressure determined from the calibrated masses constructed from steel with ρ_w = 8000 kg·m^{-3} and the remaining terms account for the local acceleration of free fall, the buoyancy correction for an air density ρ_a, and the effects of temperature and pressure.[16,17] The piston area was determined by the manufacturers to be within 4 × 10^{-4} of the nominal value,

and was the major source of uncertainty in the pressure measurements. In equation (4), ρ_a was obtained from a knowledge of the air temperature and pressure assuming a relative humidity of 50 per cent;[18] the uncertainty arising from this assumption is negligible.

The temperature T of the piston gauge was measured with a mercury-in-glass thermometer, placed in an oil filled well drilled into a cylindrical steel bar situated near and of similar size to the piston-cylinder assembly. ρ_a' is the reference density of air taken to be 1.2 $kg \cdot m^{-3}$, to which the masses were referred when calibrated, and T_a' the temperature at which the manufacturer's calibrated the piston gauge. The constants a_1 and a_2 were supplied by Bundenberg Ltd: a_1 = 2.9 10^{-9} kPa^{-1}; and, a_2 = 2.7 10^{-5} K^{-1}. The gauge was adequately levelled with a standard engineer's level, so that the resulting uncertainty $\delta p/p < 2$ 10^{-6}. Over the required operational pressure range the piston gauge was found to have a fractional precision in pressure of better than 5 10^{-5}.

The masses of the dead-weights provided by the piston gauge manufacturer, have been determined previously,[19] to provide a proportionality constant n = (4.112244 ± 0.000050) $g \cdot kPa^{-1}$ between mass and nominal pressure. This procedure provides a means of evaluating contributions to p_g' from any additional mass added, and also to obtain the "true" pressure value for each dead-weight; subsequently no combination of the supplied masses would result in an uncertainty in pressure greater than 0.08 kPa. The

(piston + table) unit which was equivalent to a pressure of 100 kPa according to Bundenberg, was rotated using a turbine of mass 373.40 g and, consequently, added 90.80 kPa to p'_g.

Two strain-gauge DPT's have been used; both required a constant external dc excitation voltage and gave a dc output, which was proportional to the pressure difference and the supply voltage. The excitation voltage was supplied from a zenor reference voltage IC,[20] (Type LH0070-1) with a nominal output of 10.000 V dc accurate to 0.01 per cent; the maximum current was 5 mA and the temperature coefficient was typically 4 ppm·K^{-1}. The adjustments for zero-pressure differential were made when both sides of the transducer were evacuated with a vacuum system similar to the one described previously.

Each span was calibrated at, and relative to, atmospheric pressure using a N_2(g) lubricated pressure balance (Ruska: type 2465-751-00, serial number 18510) which, when with the low pressure piston cylinder assembly (L-257), could operate from 1.4 to 100 kPa. The piston had an area a_0(296 K) = 335.579 mm^2 as determined by Ruska; this value of a_0 was assigned a fractional systematic error of 94 × 10^{-6} and a fractional random error of 4.3 × 10^{-6}. The effect of pressure on a_0 was negligible. The calibration performed by the manufacturer was made by comparison of this gauge with another piston gauge whose calibration was traceable to the National Bureau of Standards. The masses of the dead-weights have been verified using an

Oertling 2 kg oil-damped double-pan swing balance (serial number 34863) and Stanton 39M (NPL calibrated) masses.[21] No attempt was made to perform span calibration at other line pressures.[22] Since the DPT's were used as null-reading instruments, the zero-shift as a function of line pressure was determined with a steel-spiral gauge (Bundenberg Ltd); this steel-spiral gauge had a precision of 20 kPa and required the Fortin barometer to measure atmospheric pressure.

The first DPT instrument (Druck: PDCR 10/75L, serial number 135784) could withstand a line pressure of 7.5 MPa and had a positive and negative span of 17.5 kPa; each span could withstand an overload of a factor of 2 before recalibration was required but only a factor of 10 before diaphragm failure occurred; unfortunately, this was verified experimentally. The device was temperature compensated in the range 273 to 373 K and a simple resistive potential divider was used to set zero voltage at zero pressure differential. Before use both spans were calibrated at 293 K with the $N_2(g)$ lubricated pressure-balance, with 26 observations the positive span was represented by

$$\Delta p_+^D/\text{kPa} = 0.7040_6(\phi/\text{mV}), \qquad (4.4.5)$$

with a standard deviation of 3.6 Pa up to a pressure of 17.5 kPa (ϕ = 24.86 mV), where

$$\Delta p_+ \stackrel{\text{def}}{=} p_{TOT}(\text{positive span}) - p_{TOT}(\text{negative span}) > 0 \qquad (4.4.6)$$

in which p_{TOT} is the total line pressure at either port, and ϕ is the dc voltage output from the DPT. Similarly the negative span, based on 20 intercomparisons, was given by

$$\Delta p_{-}^{D}/\text{kPa} = 0.70409(\phi/\text{mV}), \tag{4.4.7}$$

with a standard deviation of 13 Pa where

$$\Delta p_{-} \stackrel{\text{def}}{=} p_{TOT}(\text{negative span}) - p_{TOT}(\text{positive span}) > 0; \tag{4.4.8}$$

equation (7) was found applicable up to 17.5 kPa.

Finally the zero-shift as a function of line pressure Φ_2^D was observed, as described above, at 27 equally spaced pressures from 0.1 to 7 MPa and the results could be adequately represented by

$$\Phi_2^D/\text{mV} = -1.78 \times 10^{-4}(p_{TOT}/\text{kPa}) + 3.0 \times 10^{-9}(p_{TOT}/\text{kPa})^2, \tag{4.4.9}$$

with a standard deviation of 0.006 mV; Φ_2^D should be subtracted from measured dc voltages to obtain the ϕ required in equations (5) and (7). This device was more than adequate for the determination of pressure differences for our purposes. Unfortunately, after satisfactory completion of measurement at 273.16 K with Ar only, the diaphragm in the Druck DPT failed.

The replacement DPT instrument (Schaevitz: P642-0001, serial number 83911) was considerably more robust, this device could operate at line pressures up to 20 MPa with

pressure differentials of 20 MPa without diaphragm failure, and was temperature compensated between 263 and 298 K. Since this device required a 30 mA into 10 Ω supply, the output of the zener reference IC was passed to a unity voltage gain power amplifier (μA 759UIC) to supply 9.9993 V dc. The DPT output was fed into a unity gain differential amplifer (μA 741CP) where, if required, the zero-pressure differential reading could be eliminated by an offset dc voltage which was also fed to the input of the differential amplifer. This offset voltage was generated from a simple resistive potential divider which fed a non-inverting and an inverting unity gain operational amplifer (TL073CP) to provide the correct sign and magnitude of the dc voltage.

Schaevitz calibrated the positive span at 298 K only and claimed that at Δp_+^S = 100 kPa the DPT output was 5.007 V dc with a 10.0 V dc excitation, and that lower pressure differentials have an output linear to 0.2 per cent of full scale output. They also checked the zero-shift at three pressures from 5 to 20 MPa; a maximum deviation of -0.2 per cent of full scale reading was observed at 15 MPa.

Comparison of the positive span against the pressure exerted by the N_2(g) lubricated pressure balance at 17 pressures from 7 to 93 kPa could be adequately represented by

$$\Delta p_+^S/\text{kPa} = 19.699(\phi/\text{V}) + 6.27 \times 10^{-3}(\phi/\text{V})^3, \qquad (4.4.10)$$

with a standard deviation of 9 Pa, where Δp_+ is defined in

equation (6). At Δp_+^S > 100 kPa the output ϕ was invarient and could be overloaded up to 500 kPa before the zero-pressure differential voltage setting was disturbed. Figure 4.3 shows the calibration results as deviations from equation (10). Although the negative span was expected to operate to Δp_-^S = 100 kPa, it functioned to only $\Delta p_-^S \approx 31$ kPa, and any pressure Δp_-^S > 50 kPa resulted in a significant change in the zero-pressure differential reading. However, the negative span was calibrated up to 25 kPa at five pressures starting at 6 kPa. These

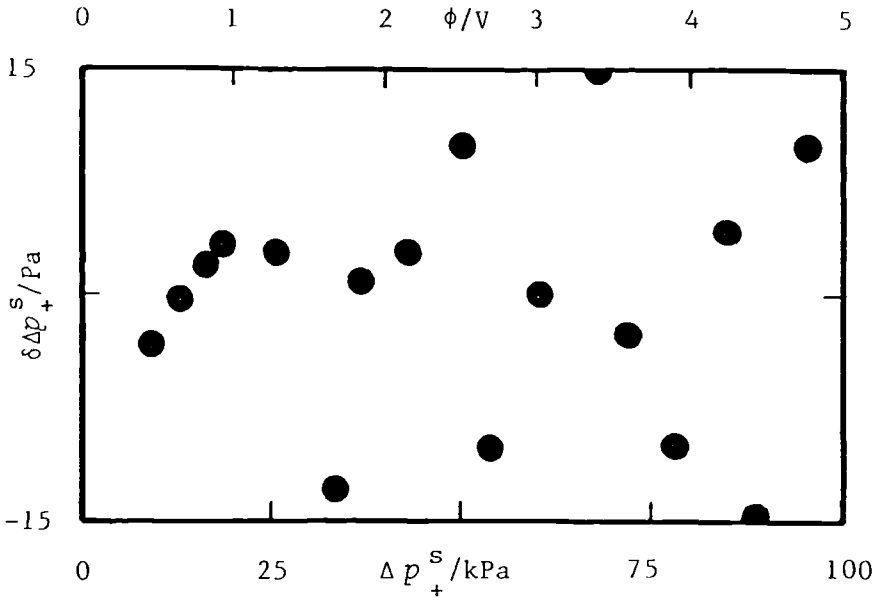

Figure 4.3. Deviations $\delta\Delta p_+^S = \Delta p_+^S - \Delta p_+^S$ (calc) of experimental Δp_+^S from equation (10) (obtained from an unweighted regression analysis), as a function of DPT output voltage ϕ and pressure difference Δp_+^S defined by equation (6).

comparisons can be represented by

$$\Delta p^{S}_{-}/\mathrm{kPa} = 19.69_{6}(\phi/\mathrm{V}), \qquad (4.4.11)$$

with a standard deviation of 4 Pa, where as in equation (10) ϕ is the DPT dc voltage output. In figure 4.3 the comparisons Δp^{S}_{-} versus ϕ are shown as deviations from equation (11). The shift in zero pressure differential reading Φ_{Z} as a function of line pressure was obtained from 0.6 to 7 MPa and could be described with a standard deviation of 0.2 mV by

$$\Phi_{Z}/\mathrm{V} = -7.89 \times 10^{-6}(p_{TOT}/\mathrm{kPa}); \qquad (4.4.12)$$

the calibration results are shown in figure 4.5 as deviations from this equation.

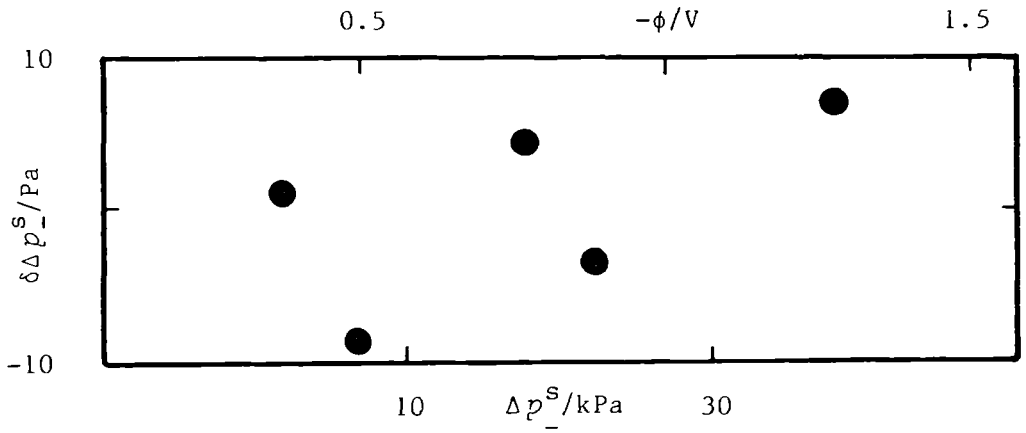

Figure 4.4. Deviations $\delta\Delta p^{S}_{-} = \Delta p^{S}_{-} - \Delta p^{S}_{-}$ (calc) of Δp^{S}_{-}, defined by (8) and determined by calibration, from equation (11) (obtained from an unweighted analysis) as a function of ϕ and Δp^{S}_{-}.

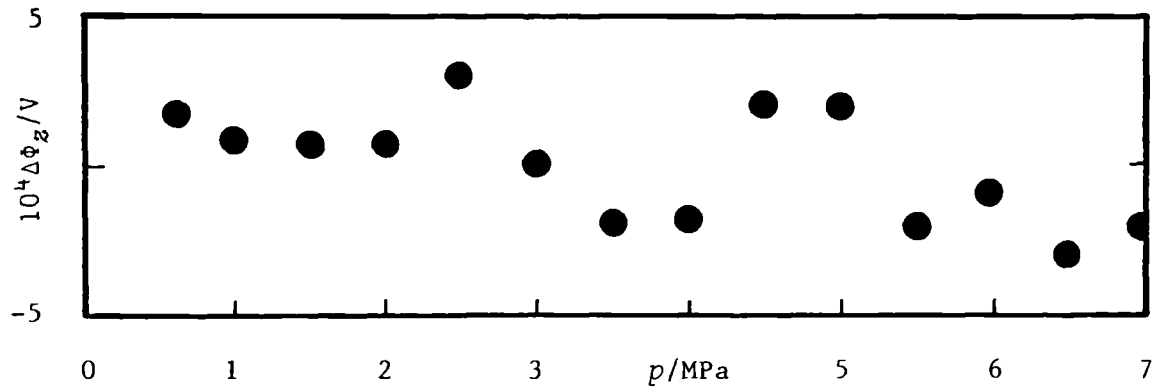

Figure 4.5. Deviations $\Delta\Phi_z = \Phi_z - \Phi_z$ (calc) of observed zero-shift as a function of line pressure (when $\Delta p_-^s = \Delta p_+^s = 0$) from equation (12).

All the calibration equations for the DPT's were obtained using an adaptive regression algorithm,[23] which selected terms from an array of positive and negative powers varying between p_{TOT}^{-3} and p_{TOT}^{3} for Φ_z and ϕ^{-3} and ϕ^3 for Δp. All coefficients entered the regression at a probability greater than 0.99, and no further significant terms remained unselected on termination of the analysis; the constraints $\Delta p = 0$ when $\phi = 0$ and $\Phi_z = 0$ when $p_{TOT} = 0$ were not required, since p_{TOT}^{0} or ϕ^0 were always insignificant.

The high pressure spherical resonator was constructed primarily for operation to 7 MPa with CH_4. Since for methane $10^6 A_1/A_0$ is in the range -30 kPa^{-1} at 255 K to -6 kPa^{-1} at 350 K, a fractional imprecision in u^2 of 10^{-6} implies a precision of between 33 and 167 Pa in the pressure measurements. However, the oil lubricated pressure balance has a fractional imprecision in p of 5×10^{-5} which at 7 MPa implies an error of 350 Pa. Clearly at 250 K a fractional

imprecision in u^2 of only 10^{-5} is possible according to this simple estimate; the piston gauge has a fractional accuracy in p of 4 x 10^{-4} which implies $\delta u^2/u^2 \simeq 8 \times 10^{-5}$.

4.5 GAS SAMPLES

The pure gases used in this work are given in table 4.2, with their normal melting T^{s+l}, and boiling temperatures T^{g+l}, critical temperature T^c, and critical pressure p^c.

Table 4.2 Gaseous substances B with respective T^{s+l}, $T^{g+l}(p^\ominus)$, T^c, and p^c. The T^{s+l} were taken from reference (24).

B	T^{s+l}/K	T^{l+g}/K	T/K	p^c/MPa	Ref
Ar	83.75	87.28	150.8	4.87	25
CH_4	90.65	111.63	190.58	4.604	26
CH_3OH	179.65	337.65	512.64	8.092	27
n-C_4H_{10}	135.75	272.65	425.18	3.797	26
$CH_3CHCH_3CH_3$	113.55	261.42	408.15	3.648	26
n-C_5H_{12}	143.45	309.21	469.7	3.369	26
$CH_3CHCH_3CH_2CH_3$	113.15	301.03	460.43	3.381	26
$CH_3C(CH_3)_2CH_3$	-	282.63	433.78	3.199	26

In table 4.3 the suppliers and their quoted purities are given. No attempt was made to analyse or to purify further the samples or argon and methane. However the remaining materials were analysed by g.l.c. and p.t.g.c., with flame ionization detectors;[29] in table 4.4 the analysis results, injector

Table 4.3 Substance B, supplier, and quoted mole fraction purity x_B

B	Supplier	Supplier's quoted purity, x_B	Remarks
Ar	B.O.C. PLC	0.99998[a]	Manufacturer certified: $10^6 x_{O_2} < 5$
CH_4	Cambrian Gases Ltd	0.99995	$10^6 x_{N_2} < 10$ Ultra high purity
CH_3OH	B.D.H. Chemicals PLC	0.999	Hygroscopic
n-C_4H_{10}	Cambrian Gases Ltd	0.999	-
$CH_3CHCH_3CH_3$	Cambrian Gases Ltd	0.9996	-
n-C_5H_{12}	Aldrich Chemicals PLC	0.96	-
$CH_3CHCH_3CH_2CH_3$	Fluka Chemicals (UK) Ltd	0.999	-
$CH_3C(CH_3)_2CH_3$	Cambrian Gases Ltd	0.999	-

[a] Reference (28)

temperatures, and column type are given. G.l.c. is performed at one injector temperature, p.t.g.c. is performed at several injector temperatures over a range stepping upward in small increments at regular time intervals (for example, every 120 s a 5 K temperature change was imposed); the latter method provides sharper, more uniform, detector response curves and is preferred for quantitative analysis.[30] For n-butane, methylpropane, dimethylpropane, and methylbutane the samples were distilled from the suppliers' cylinders into glass sample ampoules, from which the liquid could be degassed

by vacuum sublimation using liquid-nitrogen cooled cold finger; no attempt was made to repeat the sublimation process with a CO_2(s) and acetone mixture. Finally, the liquid samples were dried over grade 4A molecular sieves, previously baked at 550 K at 1 mPa for 24 h, where they remained for 12 h before transfer to the resonator. Periodic analysis of samples recovered from the resonator showed that there was no appreciable contamination and, consequently, it was possible to use the same fluid, after repeated degassing and drying, for many isotherms; to avoid delays three ampoules, each containing sufficient fluid for an isotherm, were in use during a series of measurements. However, the *n*-pentane and methylbutane were considered suitable for further purification by distillation. These samples were distilled on a 0.96 m × 19 mm Podielniak heligrid column, insulated with aluminium foil surrounded by foam-rubber pipe insulation, operating between 90 and 100 theoretical plates; the maximum volume in the boiler was 1000 cm^3. A refrigerated fluid was recirculated through a total reflux condenser which could deliver 40 cm^3 aliquots to an ampoule attached to the take off head. An electrical heater was used to ensure thorough convective stirring of the liquid held in the take of head from which distilled samples were withdrawn at time intervals which gave an overall reflux ratio much greater than 100. Further analysis of the central third of the distilled material was performed and the results are given in table 4.5. Again the sample was degassed by vacuum sublimation with N_2(l) and dried over 4A molecular sieves before use in the resonator.

Table 4.4 Analysis of substance B by g.l.c. with injector temperature T_I and p.t.g.c. with start injector temperature T_{IS} and stop T_{IST}, and column type given below

Substance	G.l.c.		p.t.g.c.			Remarks
B	x_B	T_I/K	x_B	T_{IS}	T_{IST}	
CH_3OH	-	-	-	353	423	No impurities detected 2 m × 3 mm stainless steel column with Porapak Q as the stationary phase.
n-C_4H_{10}	0.0005	393	0.9995	323	473	Two impurities of $x_C=1\times10^{-4}$ and $x_B=4\times10^{-4}$ occurring before and after main response peak respectively. Porapak Q 2 m × 3 mm column.
$CH_3CHCH_3CH_3$	-	-	0.9990	323	473	2 m × 3 mm Porapak Q column. 3 impurities 10^4x_c=2,1, and 7, the latter occurs after, but close to, main response curve, the other two occur before.
n-C_5H_{12}	0.98	298	-	-	-	4 m × 2 mm Si oil column. 1 impurity.
$CH_3CH(CH_3)CH_2CH_3$	0.9995	393	0.9995	323	473	2 m × 3 mm Porapak Q column. Two impurities 10^4x_C=1, and 10^4x_B=4, the latter occurred after and the former before the main response curve both only just resolved.
$CH_3C(CH_3)_2CH_3$	0.9995[a]	-	-	-	-	Single impurity $10^4x_C \approx 5$ 46 m × 0.5 mm S.C.O.T. Carbowax column.

[a]Reference (31)

Table 4.5 Final analysis of retained central third of distilled material of *n*-pentane and methylbutane. The distillation procedure and analysis method have been described in the text.

Substance B	G.l.c. x_B	G.l.c. T/K	Remarks
n-C_5H_{12}	0.9999_0	293	Si oil 4 m × 3 mm column. One impurity 10^4x_c=1, close to main detector response curve.
$CH_3CH(CH_3)CH_2CH_3$	0.9999	373	Porapak Q 2 m × 3 mm column. G.c.m.s. detected $10^4x_{H_2O}$=14 prior to drying.

For methanol our analysis detected no impurity. However, it is known from the manufacturers and Vogel[32] that similar grade material typically has $10^4x(CH_3CHOCH_3) = 2$ and $10^4x(H_2O) = 1$. Therefore, the sample was distilled with a vacuum jacketed Podielniak series 3500 1.5 m x 25 mm heligrid column operating at between 150 and 200 theoretical plates with an intermittent take-off head maintaining a reflux ratio of 200. Again the central third of the distilled material was retained. This distillation was performed under air and so as to remove any remaining H_2O the sample was dried by the Lund and Bjerrum method:[33]

$$Mg(s) + 2C_2H_5OH(l) \xrightarrow[293\ K,\ I_2]{Ar(p>p^{\ominus})} H_2(g) + Mg(OC_2H_5)_2$$

$$\downarrow + 2H_2O$$

$$Mg(OH)_2(s) + 2C_2H_5OH(l) \qquad (4.5.1)$$

This method is only successful if an inert gas atmosphere, in this case argon, is used and $x(H_2O) < 0.01$ before the reaction commences. On completion of the reaction, as indicated by the cessation of effervescence, the CH_3OH was transferred by distillation to an argon filled boiler (that was fitted with four bubble caps) in which it was degassed by boiling. Finally it was transferred to a vacuum chamber, further degassed by vacuum sublimation, before small aliquots of the CH_3OH were distilled to previously baked (500 K for 5 h) and evacuated pyrex ampoules which were then sealed with a small flame. So that the H_2O content in each of the three ampoule batches could be evaluated, a sample was taken from each batch for Karl Fisher titrations,[34] which indicated that each batch contained a mole fraction of H_2O in the range $4.2 \leqslant 10^4 x(H_2O) \leqslant 5.1$. Further evidence for the presence of H_2O was obtained from 1 200 MHz ^1H n.m.r. spectrum, in which the methyl protons appeared as a broad decoupled peak rather than the doublet (and quartet for OH proton) expected if no H^+ were present. However, no evidence for the ^1H chemical shift of the OH proton of water was observed; at 200 MHz ^1H n.m.r. δ of 132 ppm when referenced to TMS is expected for the OH proton.[35] Consequently the CH_3OH

would, even after extensive dehydration, appear to have a mole fraction $x_{H_2O} \approx 5 \times 10^{-4}$.

REFERENCES

1. Horowitz, P.; Winfield, H. *The Art of Electronics.* Cambridge University Press: Cambridge. 1980, p.279-286. Section 7.09.
2. Mehl, J.B.; Moldover, M.R. *J. Chem. Phys.* 1981, 74, 4062.
3. Moldover, M.R.; Mehl, J.B.; Greenspan, M. *J. Acoust. Soc. Am.* 1986, 79, 253.
4. Mehl, J.B. *J. Acoust. Soc. Am.* 1978, 64, 1523.
5. Preston-Thomas, H.; Quinn, T.J.; Hudson, R.P. *Metrologia* 1985, 21, 75.
6. The International Practical Temperature Scale of 1968 Amended Edition. *Metrologia* 1976, 12, 7.
7. Quinn, T.J. *Temperature. Monographs in Physical Measurement.* Editor: Cook, A.H. Academic Press: London. 1983, p.160-162.
8. Kaye, G.W.C.; Laby, T.H. *Tables of Physical and Chemical Constants.* Longman: London. Fourteenth Edition. 1973, p.23.
9. Dabek, Z.K. Applied Geophysics Unit, Institute of Geological Sciences. Value of g has standard deviation of 3×10^{-7} $m \cdot s^{-2}$. Values at other heights can be obtained from $\partial g/\partial h = -3.086 \times 10^{-6}$ s^{-2}. However, this has been ignored in this work.
10. Toczylkin, L.S. PhD Thesis, University of London. 1984.
11. Beattie, J.A.; Blaindell, B.E.; Kaye, J.; Gerry, H.T.; Johnson, C.A. *Proc. Amer. Acad. Arts Sci.* 1941, 71, 371.

12. Cook, A.H. *Brit. J. Appl. Phys.* 1956, 7, 285.

13. Cook, A.H. *Phil. Trans. A* 1961, 254, 125.

14. Reference 8, p.29.

15. McGlashan, M.L. *Chemical Thermodynamics.* Academic Press: London. 1979, p.209.

16. Cross, J.L. *Reduction of Data for Piston Gauge Pressure Measurements.* Nat. Bur. Stand. Monograph 65, 1963.

17. Lewis, S.; Peggs, G.N. *The Pressure Balance. A Practical Guide to its use.* National Physical Laboratory. 1979.

18. Reference 8, p.18-19.

19. Hugill, J.A. PhD Thesis, University of Exeter, 1978.

20. Reference 1, p.194-198.

21. Ewing, M.B. Unpublished work.

22. Akeley, L.T. *J. Basic Eng.* series *D* 1972, 94, 893.

23. Ewing, M.B. Unpublished work.

24. Reference 8, p.167-172.

25. Matthews, J.F. *Chem. Rev.* 1972, 72, 71.

26. Kudchadker, A.P.; Alani, G.H.; Zwolinski, B.J. *Chem. Rev.* 1968, 68, 659.

27. Ambrose, D. *Vapour-Liquid Critical Properties.* National Physical Laboratory. Report 107. 1980.

28. Cockett, A.H.; Smith, K.C. *Comprehensive Inorganic Chemistry, Vol.1.* Bailor, J.C.; Emeléus, H.J.; Nyholm, R.S.; Trotman-Dickenson, A.F.: Editors. Pergamon Press: Oxford. 1973. Chapter 5, p.181-185.

29. Vogel, A.I. *Textbook of Quantitative Inorganic Analysis* Fourth Edition. Bassett, J.; Denney, R.C.; Jeffery, G.H.; Mendham, J.: Editors. Longman: London. 1981. p.212.

30. Reference 29, p.214.

31. Ewing, M,B.; McGlashan, M.L.; Trusler, J.P.M. *J. Chem. Thermodynamics* 1986, 18, 511.

32. Vogel, A.I. *Textbook of Practical Organic Chemistry.* Fourth Edition. Furniss, B.S.; Hannaford, A.J.; Rogers, V.; Smith, P.W.G.; Tatchell, A.R.: Editors. Longman: London. 1978, p.268.

33. Reference 32, p.269-270.

34. Reference 29, p.687-688.

35. Chauvel, J.P.,Jr.; True, N.S. *Chemical Physics* 1985, 95, 435.

CHAPTER FIVE

LOW PRESSURE MEASUREMENTS

5.1 INTRODUCTION

This chapter reports results of acoustic measurements in the temperature range 260 to 330 K (which corresponds to reduced temperatures $0.53 \leqslant T/T^{c} \leqslant 0.78$) and at pressures below 115 kPa (or about 0.71 of the vapour pressure) for the six substances: *n*-butane; methylpropane; *n*-pentane; methylbutane; dimethylpropane; and, methanol. For each of the 47 isotherms speeds of sound were calculated from the resonance frequencies of up to seven radial modes of a spherical acoustic resonator, the radius of which was determined in separate measurements with argon. Perfect-gas heat capacities, and second and third acoustic

virial coefficients were obtained for each isotherm. Except for methanol, the acoustic virial coefficients were analysed to provide estimates of the (p,V_m,T) virial coefficients. Analysis of resonance half-widths provided estimates of the bulk viscosities and hence of vibrational relaxation times.

The vapour pressures, obtained by comparative ebulliometry, for methylbutane over the temperature range 255 to 323 K are also reported.

5.2 APPARATUS

Acoustic

The spherical resonator and associated apparatus used for the low-pressure determination of the speed of sound is shown in figure 5.1. Since the apparatus has been described in detail elsewhere,[1,2] only the important features are given here. Two hemispheres turned from aluminium alloy AlSiMgMn† were bolted together at an interlocking step to form a resonator with nominal internal radius 60 mm and wall thickness 12 mm. Mechanical measurements performed on the hemispheres prior to their assembly indicated that perturbations to the lowest seven radial resonance frequencies arising from geometric imperfections were fractionally less than 1×10^{-6}. To avoid interference between (0,2) and (3,1) modes, the transducers were located $\pi/2$ apart. The source, shown in figure 5.2, was flush with

---

† I.S.O. equivalent of BS 1474 Al 6082 formally denoted HE30 condition TF.

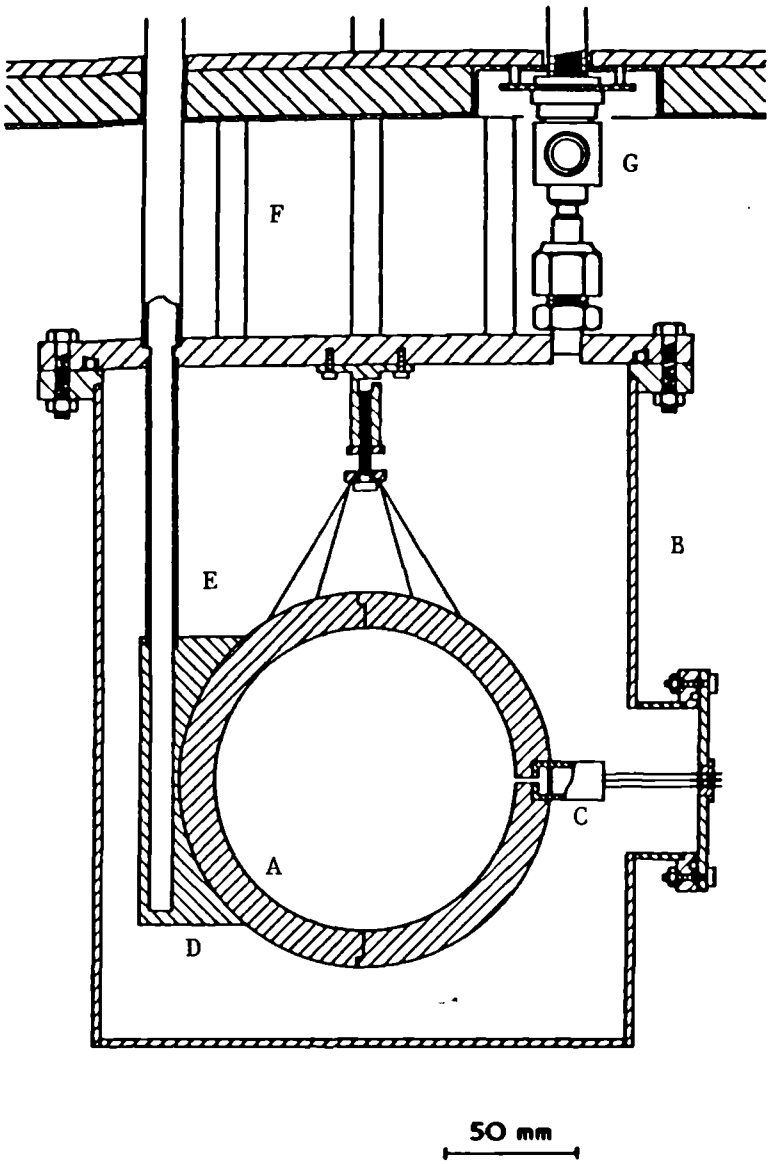

Figure 5.1. The resonator A suspended in the brass vessel B. The microphone C, a commercial electret device, was mounted in a chamber whose volume was estimated to be about 28 mm^3 and coupled to the resonator by a 1mm × 6mm wave guide. The Cu block D and stainless steel tube E held the long-stem platinum resistance thermometer LN780308 which had been calibrated on IPTS-68. The sample entered B through valve G, the pressure was sensed by the baratron *via* tube F.

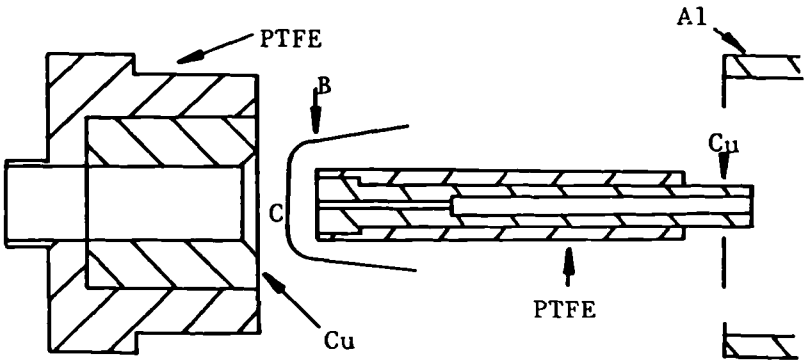

Figure 5.2. Electrostatic capacitance source transducer with active element of diameter 3.5 mm, formed from a 12 μm thick Melinex (Polyethylene terephthalate ICI plc) film B metalized on one side C with about 50 nm of Al. This device was operated with 200 V dc bias and up to 60 V r.m.s driving signal.

---

the inner surface while the microphone was fixed (but not sealed) in a small volume in the wall and coupled to the interior by a short cylindrical wave guide. The sphere was suspended in a cylindrical vessel which was placed in a stirred fluid [approximately $\{0.5\ C_2H_5(OH)_2 + 0.5\ H_2O\}$] thermostat controlled to 1 mK; the resulting temperature fluctuations, as measured with the long-stem platinum resistance thermometer (LN 7080308) located in the copper block bolted to the resonator, were not greater than 0.1 mK. Measurements of a resonance frequency and of the resistance of the thermometer indicated that the gas and resonator reached thermal equilibrium essentially simultaneously. The gas under study passed freely between the resonator and the containing vessel through a 1 mm diameter hole drilled in the wall of the sphere.

Before a series of measurements, the apparatus was baked at 340 K under vacuum until the pressure indicated by an ionization gauge in the pumping line had been less than 0.5 mPa for 24 h.

Vapour Pressure

The vapour pressure of methylbutane was determined by comparative ebulliometry,[3] in which $T^{g+1}(p)$ of the sample is compared to that of water, the vapour pressure of which is known very precisely. In the ebulliometric method a liquid is boiled at a constant pressure and its vapour condensed and returned to the boiler. The temperatures of the condensing sample and reference fluid are measured when a steady state has been reached.

The ebulliometer used for boiling the sample is illustrated in figure 5.3 and was similar to that described by Ambrose *et al.*[4] The boiler was of the same design as that used for the water standard, but a Davies type condenser cooled to about 250 K was used. The reference ebulliometer was housed in a vermiculate-insulated vessel and joined through 6 mm diameter plastic tubing, *via* two traps cooled with liquid nitrogen, to the sample ebulliometer and pressure controller (Texas Instruments). The pressure was maintained constant by the controller using helium ballast gas and the sample and reference fluids did not migrate significantly to the cooled trap. The condensation temperatures of sample and reference were measured with two long-stem platinum resistance thermometers which were both calibrated on IPTS-68.

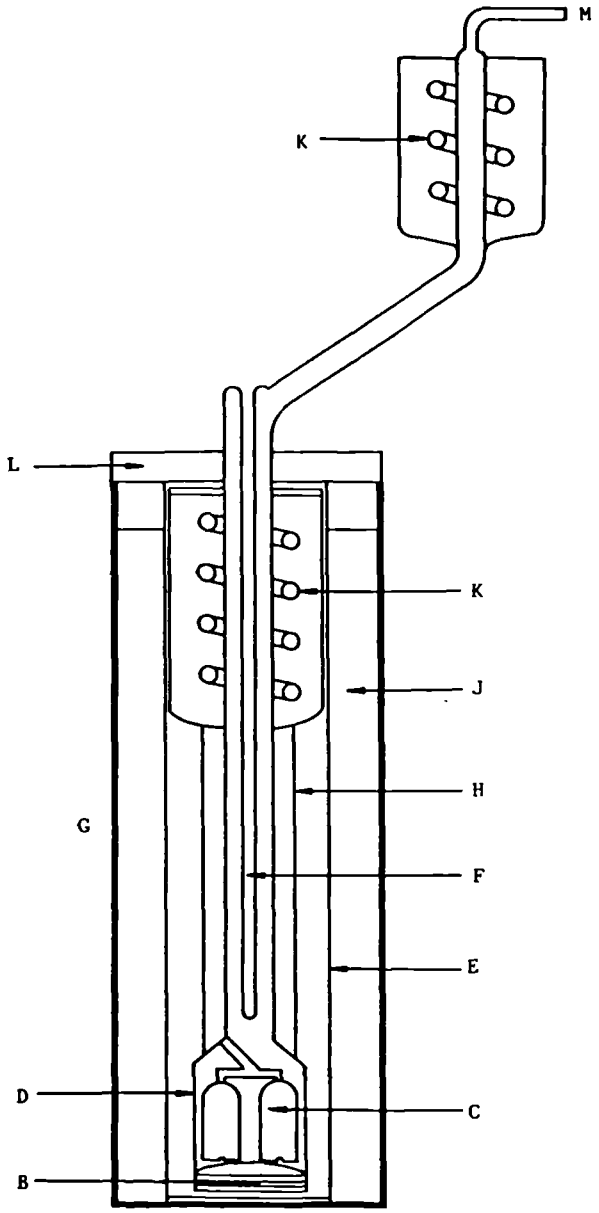

Figure 5.3. The pyrex glass Ebulliometer used for methylbutane. B, heater consisting of element from coffee percolator sandwiched between Al and sandanyo discs; C, bubble caps; D, boiler; E, liquid-tight pyrex container; F, thermometer well; G, Dewar; H, Al radiation shield in between two layers of Kayowool blanket insulation; J, {0.5 $C_2H_5(OH)_2$ + 0.5 H_2O} fluid; K, part of recirculating coolant system tubing; L, foamed polystyrene; M, line to Davies condenser, $N_2(l)$ cooled traps, pressure controller, standard ebulliometer and vacuum system.

Before commencing measurements, the previously degassed and dried sample (stored in an ampoule) was connected to a side arm (not shown in figure 5.3) and the ebulliometer evacuated at a temperature of 300 K. After 12 h the 50 cm^3 liquid sample was distilled in to the boiler. The measurements were made over the pressure range $15 < p/kPa < 220$ over which ebulliometry performs well.[5,6] The methods of determining vapour pressure, including comparative ebulliometry, have been discussed extensively in the literature.[6,7]

5.3 LOW PRESSURE RESULTS

5.3.1 Analysis of Acoustic Measurements

The resonance frequencies f and half-widths g were measured for the lowest five or seven radial modes of the cavity. The thermal boundary layer correction was calculated using the transport and equilibrium properties discussed below; the accommodation coefficient was taken as unity. Since the perturbation arising from shell motion was always small, this correction was calculated using the simple isolated mode approximation for a shell with Poisson's ratio 1/3. The constants S_0' and f_{br} in equation (3.4.34) were taken as 26.9 TPa^{-1} and 21.2 kHz respectively. The parameters δ_L and γ_L in equation (3.4.41) for the coupling tube were taken as zero while for the filling tube δ_L and γ_L were given by equations (3.4.47) and 3.4.48) for a flanged tube radiating into free space. The heat capacity $C_{p,m}$ and density ρ were estimated from virial coefficients {and equation (2.2.1) truncated after the second virial

coefficient} determined in a preliminary analysis of the results. The thermal boundary layer gives rise to the most important correction at low densities and is proportional to $(\gamma - 1)$ and $\kappa^{\frac{1}{2}}$. For measurements reported in this chapter, an error of less than 3 per cent in the thermal conductivity would contribute fractionally less than 10^{-6} to u. Even less demand is placed on the accuracy of the virial coefficients. In the analysis the resonance frequencies were weighted by the lesser of

$$(2 \times 10^{-6} f/\delta f)^2 \tag{5.3.1}$$

and unity, where δf is the estimated standard deviation of f. If the acoustic model were complete and the thermodynamic and transport properties exact then the excess half width

$$\Delta g = g_{\text{expt}} - g_{\text{h}} - g_0 - g_{\text{b}} \tag{5.3.2}$$

would be zero. In equation (2), g_{b} is the bulk loss contribution to the resonance half width given by

$$g_{\text{b}} = u/(2\pi)\alpha \tag{5.3.3}$$

$$= \pi(f/u)^2\{4\eta/(3\rho) + \eta_{\text{b}}/\rho + (\gamma - 1)\kappa M/(\rho C_{p,\text{m}})\}, \tag{5.3.4}$$

where α is the coefficient of absorption. In general, the bulk viscosity is not known for polyatomic gases, but the different dependence of the various terms in equation (5.3.2) may be used to estimate η_{b} and to isolate unknown

loss mechanisms by analysis of Δg using the equation

$$\Delta g = b_h(f/\rho)^{\frac{1}{2}} + \{(b_b/\rho) + b_b'\}(f/u^2) + b_r f + \sum b_n f_{0n}. \qquad (5.3.5)$$

In this equation, b_h^2 is proportional to any error in the thermal conductivity, $b_b = \pi\eta_b$ with b_b' representing any density dependence in η_b, and b_r denotes a constant $\Delta g/f$ for the resonator; b_n are constants, similar to b_r, for a particular mode that might arise, for example, from inadequate modelling of the openings in the resonator's wall. In general the excess half widths, after allowance for η_b, are more complex than a simple term b_r, but for the higher frequencies $\Delta g/f$ is approximately independent of frequency and pressure. Also if the model were complete the speeds of sound determined from each radial resonance frequency, at a given temperature and pressure, would agree. In polyatomic molecules, molecular thermal relaxation may cause sound speed dispersion. However, a further source of sound dispersion arises when measurements are performed at pressures close to the vapour pressure. In this regime, the acoustic admittance at the gas-wall interface increases. This precondensation phenomenon[8] is observed experimentally as an increased loss and a decrease in resonance frequency; the effect is greatest at low frequencies.

The experimental quantity is (u/a), so the results were fitted by

$$(u/a)^2 = A_0/a^2 + (A_1/a^2)p + (A_2/a^2)p^2 + \ldots, \qquad (5.3.6)$$

and the coefficients so determined were (A_1/a^2). At lower temperatures, the results for the hydrocarbons could be unambiguously accommodated within experimental error by equation (6) truncated after the term in p^2. However, at higher temperatures, where a wider pressure range was available, further terms were required in the series. Since significant differences will occur between estimates of A_2 and to a lesser, and decreasing, extent between estimates of A_1 and A_0, given by three- and four-term analyses, the pressure range was progressively truncated so as to yield the "best" three-term equation. The differences in $C_{p,m}^{pg}$ and the second acoustic virial coefficient between three- and four-term analyses are taken as a bound on the likely systematic errors arising from truncating of the infinite series. The second β_a and third γ_a acoustic virial coefficients are determined from the (A_1/a^2) using equations (2.3.21) and (2.3.22) respectively. The mean radius a, which is required to obtain $C_{p,m}^{pg}/R$ {from (A_0/a^2) using equation (2.3.20)} and speeds of sound, has been determined from auxiliary experiments with argon for which A_0 is known with sufficiently high accuracy. Twelve isotherms with argon between 250 and 320 K were analysed using the transport properties given by Maitland *et al.*[9] and an accommodation coefficient of 0.84 as previously determined.[2] The leading three terms in equation (6) were sufficient to describe the results within the experimental uncertainty. The values of a so determined can be represented by

$$10^6[\{a(T)/60.1446\ \text{mm})\} - 1] = 22.2\{(T/\text{K}) - 273.16\} + 0.011\{(T/\text{K}) - 273.16\}^2, \qquad (5.3.7)$$

with a standard deviation of 0.2 μm. The linear thermal expansivity obtained from these results agrees to 1 per cent with the precise measurements reported by Kroeger and Swenson[10] for pure aluminium. The second acoustic virial coefficient for argon can be represented by the smoothing equation

$$\beta_a/(\text{cm}^3\cdot\text{mol}^{-1}) = 108.02 - 0.05494(T/\text{K}) - (23970\ \text{K}/T). \qquad (5.3.8)$$

Deviations $\Delta\beta_a$ from this equation are shown in figure 5.4[§] for the experimental results and for β_a curves representing the deviations from integrations of the HFD-C,[11] BBMS,[12] and HFD-B2[13] pair-potential energy functions including the first quantum correction.[14] The β_a (273.16 K, Ar) determined by Moldover *et al.*[15] in their recent acoustic determination of R is also shown. The HFD-B2, with quantum corrections, lies within 0.5 $\text{cm}^3\cdot\text{mol}^{-1}$ over the experimental temperature range and is roughly within the scatter of the experimental β_a. However, the HFD-C and BBMS functions (again with quantum corrections) differ by 1 $\text{cm}^3\cdot\text{mol}^{-1}$ and lie either side of equation (8). At 273.16 K four

---

[§] The figure reported in reference 93 (figure 3), which is given in Appendix A-1, is incorrect since the quantum corrections to β_a were neglected.

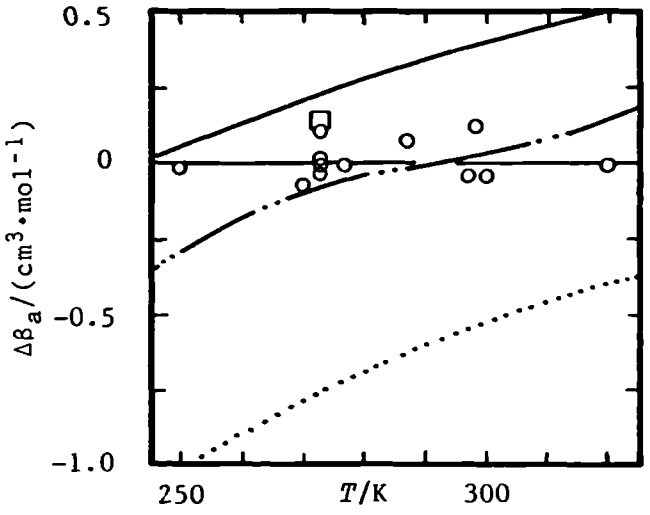

Figure 5.4. Deviations $\Delta\beta_a = \beta_a - \beta_a$ (calc.) from the equation (8) for the second acoustic virial coefficient of Ar. ○, This work; □, reference;[15] ——, HFD-C function [11] including first quantum correction;[14] – – –, BBMS function [12] including first quantum correction; [14] —·—, HFD-B2 [13] function including the first quantum correction.[14]

---

measurements determined over a two year period {three of which were combined in reference (2)} give values of β_a that span only 0.13 $cm^3 \cdot mol^{-1}$, and of a which span only 0.3 μm; clearly, the resonator is dimensionally stable to about 5×10^{-6}. Finally, measurements with argon in this resonator have been found to give b_r, in equation (5), of about 3×10^{-6}.

The accuracy of the acoustic virial coefficients are determined primarily by errors in u^2 and p. Although the uncertainty in $C_{p,m}^{pg}/R$ (is magnified by the factor

$C^{pg}_{V,m}/R$ and) includes contributions from T and a in addition to those from (A_0/a^2), these contribute only about 0.001 which may be small compared with those arising from the presence of impurities. For example, with measurements with a C_4 or C_5 hydrocarbon an impurity $x(H_2O) = 10^{-4}$ would contribute about 0.02 to $C^{pg}_{p,m}/R$ while $x(air) = 10^{-4}$ would contribute about 0.01.

The perfect-gas heat capacities $C^{pg}_{p,m}(T)$ determined for each substance were used to obtain smoothing equations constructed from some combination of negative or positive powers in T. Using an adaptive regression algorithm,[16] the most significant terms in the range T^{-3} to T^3 were selected. Each term selected, and retained, had a statistical significance greater than 0.99 and no significant terms remained at the end of the analysis.

In order to determine the second virial coefficient B from the experimental information it is necessary to solve the differential equation (2.3.23). Numerical integration of this equation with specified boundary conditions has been demonstrated by Bruch[17,18] for ^4He, and by Mehl and Moldover using their precise experimental β_a for ethene; in the latter case the accuracy of the results was confirmed by comparison with precise (p,V_m,T) results. However, this method favours the use of at least one initial condition near the lowest temperature.[20] At low reduced temperatures direct (p,V_m,T) methods are least reliable, consequently, this method is impracticable in the present case. If β_a were known over a wide temperature range then

an algorithm could be applied to yield both B and a spherically symmetric intermolecular pair potential energy U,[20] without recourse to (p,V_m,T) measurements. In the absence of reliable initial conditions semi-empirical methods of solving equation (2.3.23) based on explicit assumptions about the functional form of B have been used in this work. In this approach no explicit account is taken of the integration constants required for the general solution to the differential equation although Boyd and Mountain argued that the method does in fact take implicit account of the homogeneous solution.[21]

The first semi-empirical method used here assumes that B is represented by

$$B(T) = (2\pi L\sigma^3/3)\{g^3 - (g^3 - 1)\exp(\varepsilon/kT)\} \qquad (5.3.9)$$

$$= a + b\ \exp(c/T), \qquad (5.3.10)$$

where L and k are the Avogadro and Boltzmann constants, which may be derived from the square-well potential

$$\left.\begin{aligned} U(r) &= \infty, \quad (r < \sigma), \\ U(r) &= \varepsilon, \quad (\sigma \leqslant r \leqslant g\sigma), \text{ and} \\ U(r) &= 0, \quad (r > g\sigma); \end{aligned}\right] \qquad (5.3.11)$$

figure 5.5 indicates the parameters ε, σ, and g. In equation (11) $U(r)$ is the intermolecular pair potential energy at separation r. Combination of equations (5.3.10) and (2.3.23) yields

$$\beta_a = 2a + 2b[1 - (c/T)(\gamma^{pg} - 1) + \{(\gamma^{pg} - 1)^2/2\gamma^{pg}\}(c/T)\{2 + (c/T)\}]\exp(c/T), \qquad (5.3.12)$$

and the parameters a, b, and c can be determined by non-linear regression analysis with experimental $\beta_a(T)$ and $C^{pg}_{p,m}(T)$. It is known that B is relatively insensitive to the detailed shape of the potential-energy function. Consequently, simple models which may be only crude approximations to the true function are sufficient to represent accurately B and its derivatives.

The second semi-empirical method assumes that B can be represented by some combination of negative and positive powers in T:

$$B(T) = \sum_{j=3}^{3} a_j (T/\mathrm{K})^j . \qquad (5.3.13)$$

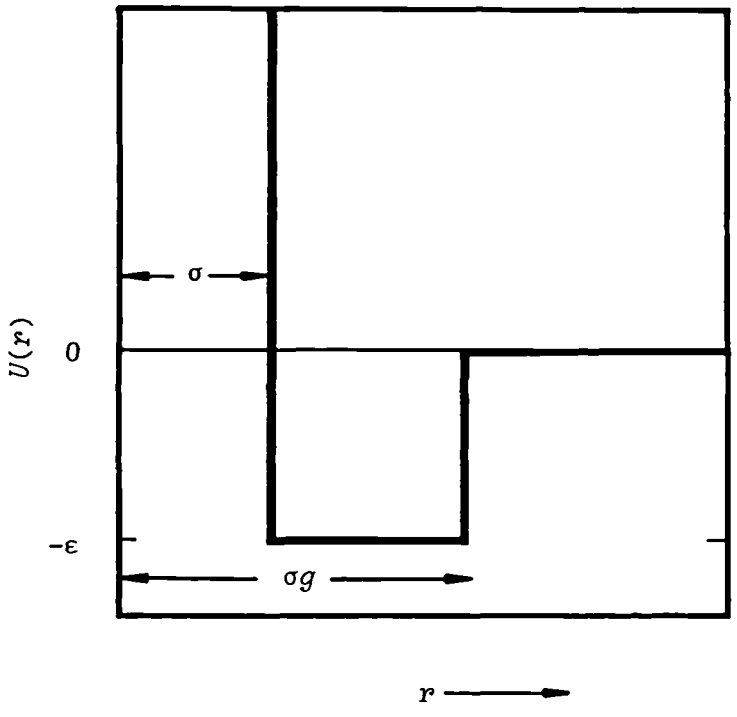

Figure 5.5. The square-well potential.

When substituted into equation (2.3.23) this expression gives

$$\beta_a = 2\sum_j a_j[1 + j(\gamma^{pg} - 1) + j(j - 1)\{(\gamma^{pg} - 1)^2/2\gamma^{pg}\}] \times (T/K)^j, \quad (5.3.14)$$

and using the adaptive regression algorithm,[16] the terms with a significance greater than 0.99 were selected from the assembly j = -3, -2, -1, 0, 1, 2, 3. This approach allows a_j to be determined by multiple linear regression. As with the analysis based on equation (11) the experimental γ^{pg} were used.

Although the errors introduced by imposing a functional form on B when solving the differential equation (2.3.23) are difficult to assess, the differences between the values of B obtained from equations (10) and (13) may be taken as some indication of the uncertainties inherent in the semi-empirical solution. In this work the equation based on the square-well potential has been taken as a basis for comparison with other results.

A similar approach has been adopted for the estimation of third virial coefficients C. Since γ_a was obtained from three term fits to $u^2(p)_T$ with equation (6) this implies that only apparent third virial coefficients are obtained. The quantity T_a, obtained from equation (2.3.24), is given by

$$T_a = RT\gamma_a + B\beta_a - \{(\gamma^{pg} - 1)/\gamma^{pg}\}$$

$$\times \{B + (2\gamma^{pg} - 1)T dB/dT + (\gamma^{pg} - 1)T^2 d^2B/dT^2\}^2 \quad (5.3.15)$$

$$= \{(1 + 2\gamma^{pg})/\gamma^{pg}\}C + \{(\gamma^{pg^2} - 1)/\gamma^{pg}\}T dC/dT$$

$$+ \{(\gamma^{pg} - 1)^2/2\gamma^{pg}\}T^2 d^2C/dT^2, \quad (5.3.16)$$

and depends only on C and its first two derivatives. The square model gives an analytic expression for C when $g \leqslant 2$:[23]

$$C(T) = (b_0^2/8)\{5 - (g^6 - 18g^4 + 32g^3 - 15)x$$

$$- (2g^6 - 36g^4 + 32g^3 + 18g^2 - 16)x^2$$

$$- (6g^6 - 18g^4 + 18g^2 - 6)x^3\}, \quad (5.3.17)$$

where x is given by

$$x = \{\exp(\varepsilon/kT) - 1\} \quad (5.3.18)$$

and b_0 by

$$b_0 = 2\pi L\sigma^3/3. \quad (5.3.19)$$

An expression for C derived from the square-well potential with $g \geqslant 2$ is also known,[23,24] but has not been used here. T_a was obtained from the experimental γ^{pg} and γ_a using equation (15) with all terms associated with B and its first two derivatives, including β_a, were evaluated using the square-well expression (9) determined for B. T_a was then used with the experimental $C_{p,m}^{pg}$ to determine the three adjustable parameters in equation (17) using a non-linear regression analysis.

All of the regression analyses performed to obtain smoothing equations for $C^{pg}_{p,m}$, B, and C were weighted by the normalized inverse variance of the experimental quantity.

In the remainder of this chapter the measurements performed at low pressures are reported under sub-headings for each compound and analysed by the method described above. The analysis of the vapour pressure determinations for methylbutane are reported with the acoustic results.

5.3.2 *n*-butane

The thermal-boundary-layer correction was calculated using thermal conductivities estimated from the measurements of Parkinson and Gray[25] at 323.15 K and 373.15 K. These can be represented by the simple empirical equation advocated by Owen and Thodos:

$$\kappa(T_2) = \kappa(T_1)(T_2/T_1)^n \qquad (5.3.20)$$

with $\kappa(T_1 = 323.15\ \text{K}) = 18.79\ \text{mW}\cdot\text{m}^{-1}\cdot\text{K}^{-1}$ and $n = 1.898$. The thermal conductivities given by equation (20) agree to within 2 per cent with the results of Carmichael and Sage across the entire range 277.6 to 444.3 K covered by their work.[27]† Therefore in the absence of direct measurements at lower temperatures, equation (20) was used to calculate κ at the required temperatures. $\Delta f_h/f$ ranged from 8×10^{-6} for (0,8) at 110 kPa to 79×10^{-6} for (0,2) at 5 kPa. Thus an error of 3 per cent in κ would lead to a fractional error in u of only 10^{-6} in the worst case.

---

†The pressure dependence of κ is negligible in our (p,T) regime.

Shear viscosities between 250 and 320 K were calculated from the extended law of corresponding states, using the scaling equation given by Maitland *et al.* (extrapolated below 285 K);[28] the results may be represented with negligible uncertainty by the simple equation:

$$\eta/(\mu Pa \cdot s) = -0.26 + 0.02593\ (T/K). \qquad (5.3.21)$$

Equation (21) predicts η to within 1 per cent as compared with results reported in the literature.[29-31]

The residual experimental half-widths Δg were analysed according to equation (5), in which the classical bulk absorption was calculated using the transport coefficient discussed above. As expected the term corresponding to η_b was always significant (at a probability > 0.99). If it is assumed that the vibrational states of *n*-butane are strongly coupled then the bulk viscosities, which are shown as a function of temperature in figure 5.6, give a relaxation time t = 1.3 ns at 300 K and 101.3 kPa. This is in close agreement with literature values, and its small magnitude reflects the ease of conformational inversion during collisions. At 300 K there is also some suggestion of a maximum in η_b. However, the result at 320 K is less reliable due to an instability in the source transducer. This is believed to have been caused by charging effects in the polyester-film membrane of the transducer biased with 200 V d.c. At lower temperatures, once charged, the transducer could be operated efficiently for extended periods without bias, while at higher temperatures

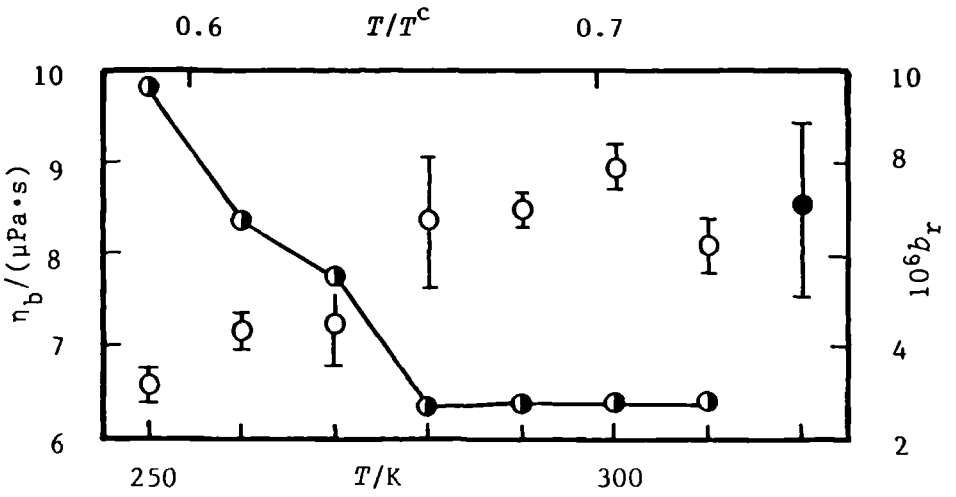

Figure 5.6. Bulk viscosities η_b (left-hand axis) and average fractional excess half widths b_r (right-hand axis) for butane. ○, η_b from analysis including b_r; ●, η_b with $b_r = 0$; ◑——◑, b_r. The error bars represent one standard deviation; T^c is given in table 4.2.

---

continuous bias is required. Near 320 K, neither arrangement was competely satisfactory and the fluctuations in efficiency were evident on the time scale of the measurements.

In the analysis of Δg it was necessary to allow for a small additional unexplained loss mechanism by inclusion in the analysis of the term b_r, at each temperature except 320 K. As shown in figure 5.6, this term was approximately 3×10^{-6} above 280 K, or roughly equal to the value estimated from a typical isotherm in argon, but at lower temperatures b_r increased, reaching 10×10^{-6} at 250 K.

The strong temperature dependence of b_r {the average $(\Delta g/f)$} below the normal boiling temperature (T^{l+g}/K = 272.65), but the absence of any apparent dispersion in the frequency range of the measurements, is indicative of a precondensation phenomenon that has measurable consequences for the line widths but not for the resonance frequencies. The worst-case excess losses after allowance for η_b, but not for the empirical b_r, are illustrated in figure 5.7 for the isotherms at 250 K. Although the behaviour of the unexplained loss is clearly more complicated than a simple constant term, the $\Delta g/f$ for the higher frequency modes used are approximately independent of both frequency and pressure.

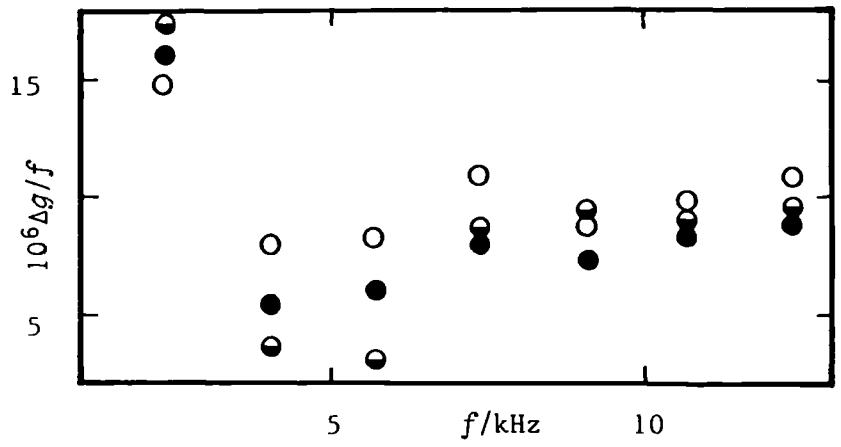

Figure 5.7. Fractional excess half widths $\Delta g/f$ for the lowest seven radial modes in butane at 250 K. ○ , 19.9 kPa; ● , 10.0 kPa; ◒ , 5.0 kPa.

Table 5.1. Mean values of u with standard deviations s determined from N radial modes, and deviations δ from equation (6) at temperatures T and pressure p. The coefficients of equation (6) may be obtained from table 5.2 and equations (2.3.20) to (2.3.22).

T / K	p / kPa	u / m•s^{-1}	$10^6 s(u)/u$	N	$10^6 \delta(u^2)/u^2$
250.000	19.879	197.3665	2.4	7	-0.0
	17.330	197.5803	1.7	7	-1.5
	14.830	197.7896	1.6	7	2.6
	12.418	197.9899	1.5	7	0.6
	10.049	198.1857	1.5	7	-2.0
	2.413	198.4028	1.5	7	-0.4
	4.982	198.5517	1.9	7	0.9
260.000	34.785	200.0949	2.9	7	-2.3
	29.312	200.4751	2.4	7	2.5
	24.695	200.8627	2.3	7	1.9
	19.547	201.2493	2.1	7	-0.2
	14.835	201.6005	1.9	7	-2.0
	9.964	201.9610	1.8	7	-1.8
	4.886	202.3343	2.3	7	1.9
270.000	65.389	201.8076	3.0	5	-3.0
	57.619	202.3593	1.8	5	-1.4
	49.895	202.9030	1.4	5	8.8
	41.618	203.4778	1.1	5	1.4
	32.237	204.1219	0.6	5	-5.1
	24.158	204.6712	0.9	5	-1.8
	16.476	205.1877	1.8	5	-3.1

T / K	p / kPa	u / m·s^{-1}	$10^6 s(u)/u$	N	$10^6 \delta(u^2)/u^2$
270.000	10.571	205.5817	2.0	5	2.1
	8.282	205.7335	2.8	5	2.5
280.000	77.862	204.9608	1.8	5	-0.7
	70.162	205.4564	2.2	5	-2.3
	63.153	205.9045	3.2	5	2.0
	47.902	206.8674	1.9	5	4.8
	39.735	207.3760	2.0	5	-0.2
	31.821	207.8650	2.0	5	-1.0
	22.051	208.4629	2.5	5	-2.3
	15.655	208.8506	2.3	5	-6.0
	8.997	209.2529	3.3	5	4.6
	4.994	209.4956	1.8	5	4.4
290.000	93.286	207.6284	2.0	5	-1.5
	89.871	208.1254	1.3	5	-0.2
	79.395	208.7393	1.2	5	4.1
	69.937	209.2879	1.0	5	3.3
	60.612	210.2527	0.5	5	1.8
	49.209	210.4713	0.4	5	-24.5
	39.782	211.0074	0.7	5	14.2
	29.858	211.5616	1.0	5	3.3
	20.136	212.1011	1.6	5	7.7
	15.024	212.3812	2.0	5	-6.0
	10.496	212.6299	2.3	5	-1.9
	4.947	212.9329	1.6	5	-0.2

T / K	p / kPa	u / m·s^{-1}	$10^6 s(u)/u$	N	$10^6 \delta(u^2)/u^2$
300.000	103.797	211.2367	1.0	5	-0.7
	91.742	211.8820	1.2	5	-0.3
	82.544	212.3705	1.2	5	1.1
	70.909	212.9832	1.1	5	0.9
	59.799	213.5632	1.3	5	0.5
	49.717	214.0851	1.4	5	-0.5
	39.862	214.5915	1.7	5	-0.6
	29.850	215.1020	2.0	5	-1.1
	19.849	215.6081	2.7	5	-0.5
	9.852	216.1102	2.9	5	1.2
310.000	101.709	215.1510	1.2	7	(a)
	91.951	215.6257	1.9	7	(a)
	82.632	216.0762	1.1	7	-1.1
	71.477	216.6112	0.7	7	0.6
	61.992	217.0630	1.0	7	1.3
	51.700	217.5499	0.6	7	0.1
	41.300	218.0389	0.4	7	0.4
	32.047	218.4710	0.6	7	-1.2
	23.838	218.8524	1.0	7	-1.1
	16.143	219.2081	1.4	7	-0.6
	9.109	219.5320	2.8	6	2.0
320.000	109.990	218.4617	4.8	5	1.0
	99.392	218.9346	2.3	5	0.1
	90.263	219.3395	0.6	5	-2.4

T / K	p / kPa	u / m•s^{-1}	$10^6 s(u)/u$	N	$10^6 \delta(u^2)/u^2$
320.000	80.135	219.7868	9.4	4	-1.2
	80.138	219.7862	8.8	4	-5.9
	70.090	220.2291	2.4	5	9.7
	58.480	220.7350	12.1	5	1.8
	49.595	221.1199	5.0	5	-4.4
	38.903	221.5824	4.8	5	3.7
	30.153	221.9571	2.2	5	-5.7
	19.651	222.4069	6.1	5	4.9
	9.915	222.8202	16.0	5	2.1

(a), pressure omitted from final analysis.

Table 5.1 lists mean values of u obtained from the first five or seven radial modes at each pressure along the eight isotherms between 250 and 320 K; the maximum pressure on an isotherm was never greater than 71 per cent of the vapour pressure. The standard deviations of the means, which are also given in table 5.1, are dominated in most cases by the systematic discrepancies between modes rather than random errors. However, random errors arising from the transducer instability discussed above are significant at 320 K. Small corrections have been applied to (u/a) to reduce all values to the stated temperature on the assumption that

$$u(T_2)/u(T_1) = (T_2/T_1)^{\frac{1}{2}}. \qquad (5.3.22)$$

The quality factors $\{Q = f/(2g)\}$ of the resonances used are in the range 4000 to over 30000.

The quantities (u/a) from the full complement of observations were used in the regression analysis with equation (6), each weighted as described above, to determine $C_{p,m}^{pg}$ and the acoustic virial coefficients. Except perhaps at 310 K, only the leading three terms of the infinite series (6) were unambigously required to accommodate the measurements within experimental error. Although the pressure range is small at the lowest temperature (250 K), the third acoustic virial coefficient is correspondingly large and systematic deviations from a two-term fit exceed discrepancies at any one pressure by more than a factor of five. By contrast, the deviations shown in figure 5.8 from the three-term equation are comparable with the distribution of results obtained from the seven modes studied at each pressure. The distribution and its range (fractionally about 5×10^{-6}) is very similar to that obtained for argon. For the isotherm at 310 K, a fourth term was statistically significant but, although A_3 is probably changing very rapidly with temperature, it seems unreasonable for an additional coefficient to be physically significant along this but not along adjacent isotherms. A more likely explanation is that small errors in the measurements (perhaps of T or p) conspired to give this effect. As indicated in table 5.1, this led to the rejection of the two highest pressures from the final analysis but the effect of this is to change the estimates of $C_{p,m}^{pg}$ and β_a by only

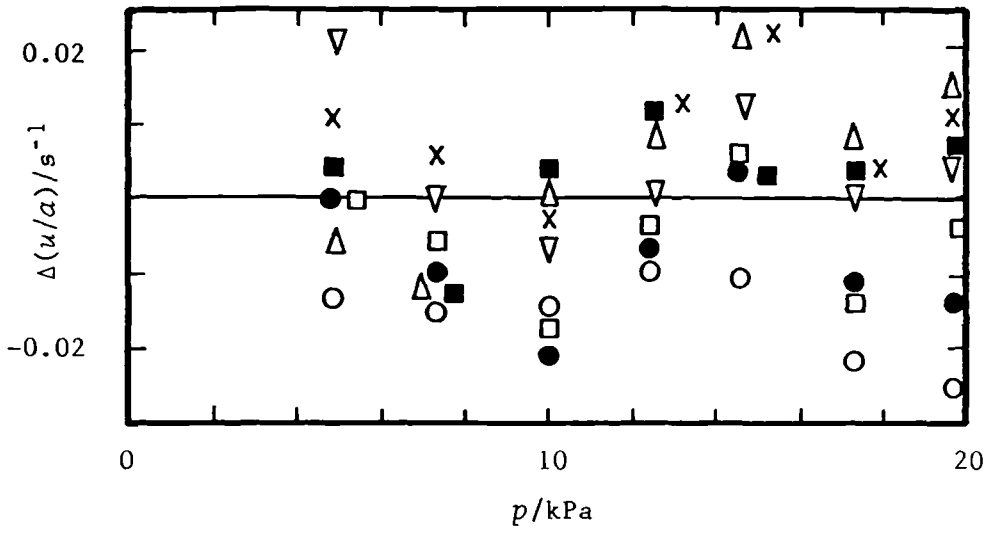

Figure 5.8. Deviations $\Delta(u/a) = [(u/a) - \{u(\text{calc.})/a\}]$, for individual modes in *n*-butane at 250 K from equation (6) with coefficients from table 5.2 and equations (2.3.20) to (2.3.22). ○, (0,2); ●, (0,3); □, (0,4); ■, (0,5); Δ, (0,6); ∇, (0,7); ×, (0,8). At 250 K p^{l+g} = 39.16 kPa for *n*-butane.[33]

0.0003 R and 0.5 $cm^3 \cdot mol^{-1}$ respectively.

The perfect-gas heat capacity $C^{pg}_{p,m}$ is shown in figure 5.9 and, as deviations from

$$C^{pg}_{p,m}/R = 0.03414(T/K) + 440(K/T), \qquad (5.3.23)$$

on the expanded scale of figure 5.10. It is clear that there are inconsistencies in the results which, although small, far exceed the imprecision of any one value and it is suspected that these discrepancies arise from variations in sample purity. The measurements of Sage *et al.*[34] are 0.19 R and 0.34 R below (23) in the overlapping temperature range and

Table 5.2 Perfect-gas heat capacities, second and third acoustic virial coefficients, and standard deviations s obtained by analysis of N modes for n-butane. The resonator radius $a(T)$ required to determine $C_{p,m}^{pg}(T)$ was given by equation (7). The quoted uncertainties are one standard deviation.

T/K	N	$C_{p,m}^{pg}/R$	$\beta_a/(cm^3 \cdot mol^{-1})$	$\gamma_a/(cm^3 \cdot mol^{-1} \cdot kPa^{-1})$	$10^6 s(u^2)/u^2$
250.000	49	10.3091 ± 0.0007	-1689.7 ± 1.3	-1.365 ± 0.050	3.6
260.000	49	10.5596 ± 0.0006	-1548.0 ± 0.7	-0.950 ± 0.017	4.7
270.000	45	10.8336 ± 0.0006	-1424.8 ± 0.4	-0.721 ± 0.006	5.2
280.000	50	11.1191 ± 0.0006	-1319.6 ± 0.3	-0.528 ± 0.004	5.4
290.000	60	11.4471 ± 0.0008	-1225.8 ± 0.4	-0.407 ± 0.004	9.2
300.000	50	11.7248 ± 0.0004	-1143.2 ± 0.2	-0.311 ± 0.002	3.2
310.000	62	11.9973 ± 0.0003	-1069.5 ± 0.2	-0.232 ± 0.002	2.4
320.000	58	12.2746 ± 0.0023	-1004.4 ± 0.7	-0.180 ± 0.006	13.1

diverge further at higher temperatures, while those of Dailey and Felsing[35] at 344.9 K lie 0.25 R above the extrapolation of these results with equation (23). The correlation of Haynes and Goodwin,[37] which covers the fluid region up to 700 K and 70 MPa, and is a fit to the calculations of Chen *et al.*[38] which are based on a combination of spectroscopic and thermodynamic information. Although such calculations can give reliable results, there are two serious complications for a substance such as butane. Firstly, the gas contains both *trans* and *gauche* conformational isomers in equilibrium and, since these exhibit different vibrational heat capacities, knowledge of the equilibrium constant is required. Estimates of the energy difference between *trans* and *gauche*

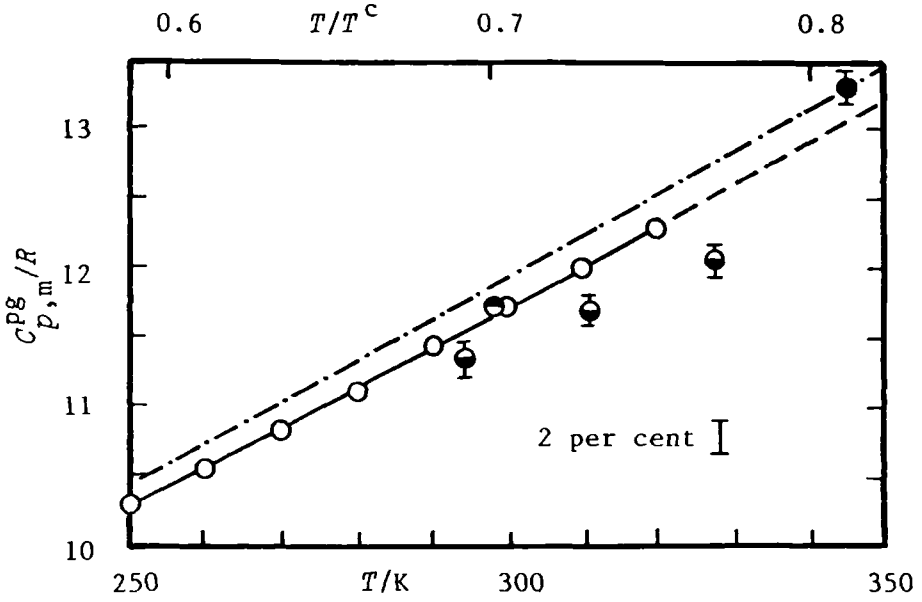

Figure 5.9. Perfect-gas heat capacities $C^{pg}_{p,m}$ for *n*-butane as a function of temperature. ○ , table 5.2; ◒ , reference 34; ● , reference 35; ◓ , reference 36; ——, equation (23); ----, equation (23) extrapolated above 320 K; —·—, reference 37. The error bars represent quoted uncertainties.

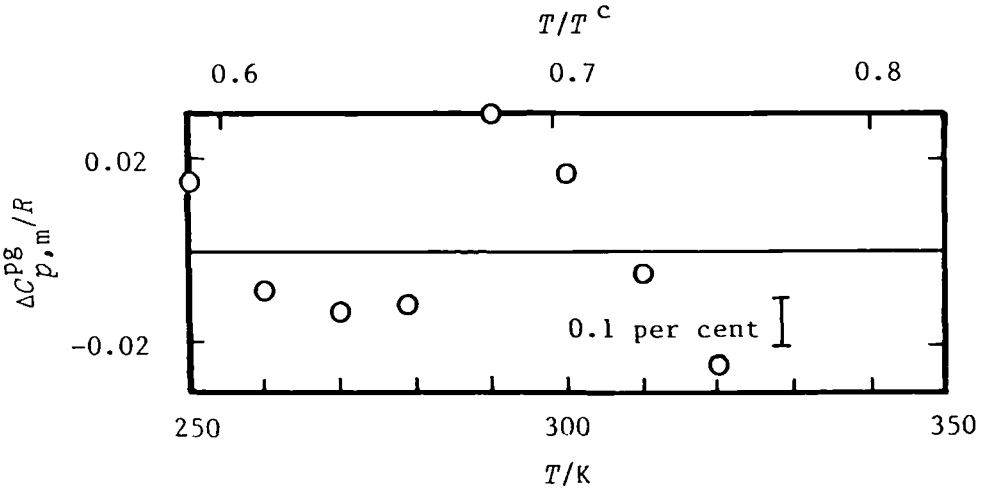

Figure 5.10. Deviations $\Delta C^{pg}_{p,m} = \{C^{pg}_{p,m} - C^{pg}_{p,m}(\text{calc.})\}$ of experimental heat capacities at constant pressure from equation (23).

isomers from different sources vary by up to a factor of two.[38] Secondly, although the normal vibrational frequencies of both isomers are quite well known, the torsional modes corresponding to rotations of the methyl and ethyl groups have not been observed spectroscopically, and estimates of the potential-energy barriers to internal rotation vary considerably.[38] In their calculations, Chen *et al.*[38] adopted those estimates that afforded the best fit to thermodynamic properties, principally the heat capacities reported by Dailey and Felsing.[35] A comprehensive correlation of the thermodynamic properties of C_3 to C_{10} hydrocarbons, due to Scott,[36] gives a value of $C^{pg}_{p,m}$ just 0.07 R above the smoothing equation (23) at 298.15 K. In conclusion the heat capacities presented above are believed to be reliable and the best estimates available, despite variations in sample purity, and the correlation of Haynes and Goodwin is in error by 0.2_2 R at 320 K and 0.1_6 R at 250 K.

Assuming that B can be represented by equation (10), weighted non-linear regression using the experimental β_a and γ^{pg} gave

$$B(T)/(\mathrm{cm}^3\cdot\mathrm{mol}^{-1}) = 165.4 - 135.42 \exp(555\ \mathrm{K}/T), \quad (5.3.24)$$

with a standard deviation of 0.48 $\mathrm{cm}^3\cdot\mathrm{mol}^{-1}$ (about 0.04 per cent) in β_a. Figure 5.11 shows deviations of β_a from equation (24) and (2.3.23) and the experimental γ^{pg}. This quantity is expected to be much less sensitive to impurities than $C^{pg}_{p,m}$ and the small scatter is not attributed to

impurities in the sample. An important feature of the success of this method of calculating B from β_a is the small magnitude of the coefficients of $T\mathrm{d}B/\mathrm{d}T$ and $T^2\mathrm{d}^2B/\mathrm{d}T^2$ in (2.3.23) for a substance with a relatively large molar heat capacity. For example, at 300 K $2(\gamma^{pg} - 1) = 0.187$ and $(\gamma^{pg} - 1)^2/\gamma^{pg} = 0.008$, compared with 0.667 and 0.267 for a monatomic gas, and the three terms in equation (2.3.23) contribute -1392, 297, and -49 $cm^3 \cdot mol^{-1}$ respectively to β_a. However, the excellent fit is not evidence that an accurate solution of B has been obtained. In order to test the sensitivity of the method to the functional form assumed for B, a second approach, using a power series representation of B, was

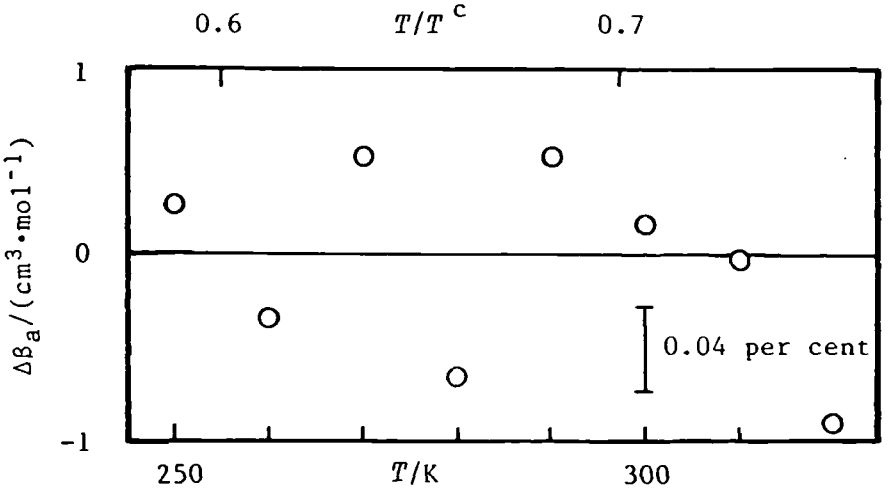

Figure 5.11. Deviations $\Delta\beta_a = \{\beta_a - \beta_a(\mathrm{calc.})\}$ of the β_a given in table 5.2 from equation (23), and (2.3.23) with $C_{p,m}^{pg}/R$ from table 5.2.

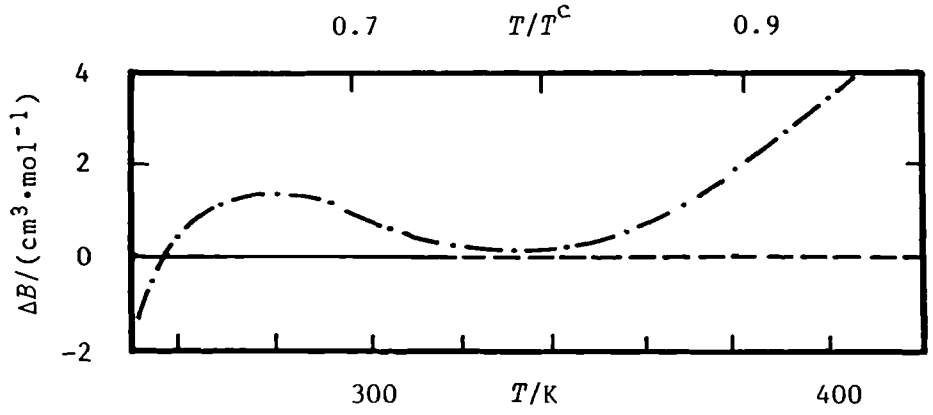

Figure 5.12. Deviations ΔB = [B\{ equation (25)\} - B\{ equation (24)\}] as a function of T for n-butane, —·—.

---

applied. The experimental β_a and γ^{pg} from table 5.2 were used with equation (14) to obtain

$$B(T)/(cm^3 \cdot mol^{-1}) = -177.0 - 1.2143 \times 10^7 \, (K/T)^2 - 1.2009 \times 10^{10} \, (K/T)^3, \qquad (5.3.25)$$

with a standard deviation of 0.44 $cm^3 \, mol^{-1}$ in β_a. The estimates of B from (25) are shown as deviations from (24) in figure 5.12 up to 420 K. In the experimental temperature range the agreement is better than 2 $cm^3 \cdot mol^{-1}$ (0.2 per cent); even with an extrapolation to 400 K the deviation is only 3.6 $cm^3 \cdot mol^{-1}$. It is also known that a Lennard-Jones (28-6) function, with ε/k = 770 K and σ = 0.4001 nm, fits β_a with excellent precision and second virial coefficients which agree to within about 0.08 per cent with equation (24) below 320 K.

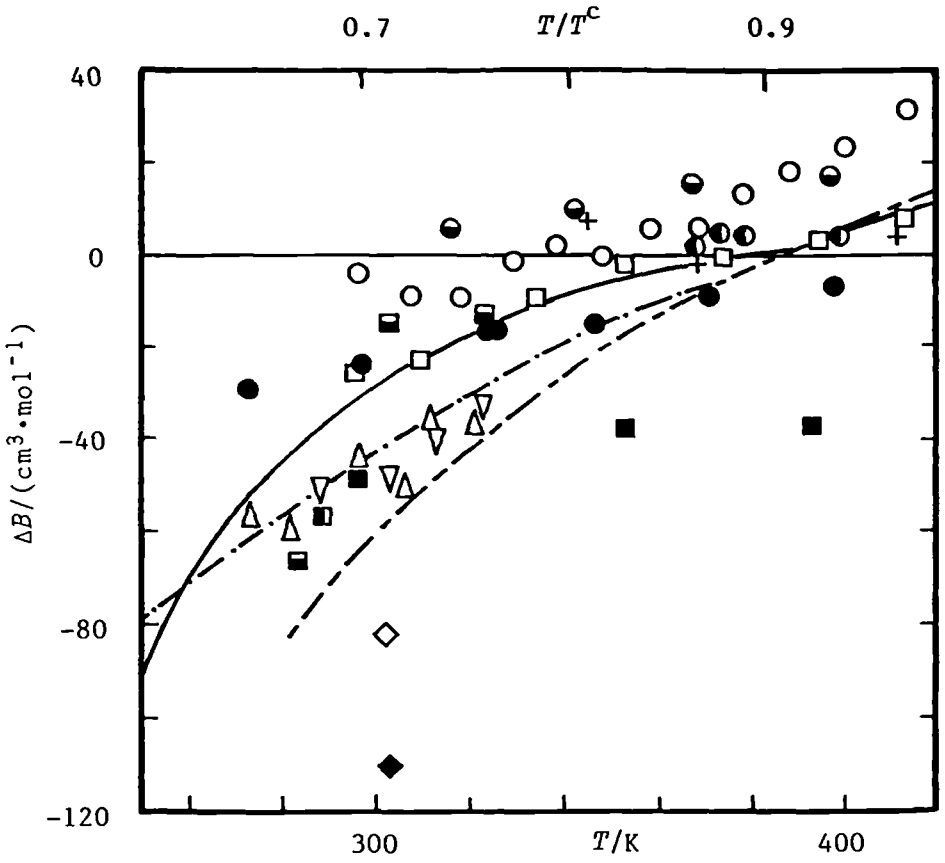

Figure 5.13. Deviations $\Delta B = \{B - B(\text{calc.})\}$ of literature second virial coefficients from equation (24). ◇ , Reference 40; ◆ , reference 41; + , reference 42; ◧ , reference 43; ○ , reference 44; ⬓ , reference 45; △ , reference 46; ● , reference 47; ◐ , reference 48; ▽ , reference 49; □ , reference 50; ■ , reference 51; ◒ , reference 52; —·—, reference 37; — – —, reference 53; ———, reference 54.

Even at 400 K, the agreement is within 0.3 per cent.[39] The second virial coefficients reported by other workers[37,40-54] are plotted as deviations from the square-well equation (10), in figure 5.13 where the ordinate scale has been compressed by a factor of 10 compared with 5.12. Below 320 K, the results of McGlashan and Potter[44] and those of Bottomley and Spurling[47] are in good agreement with ours, but those of Schäfer and co-workers[46,49,51] show deviations of between -30 and -60 $cm^3\ mol^{-1}$. At higher temperatures, equation (24) extrapolates to agree with the bulk of reported values near 400 K, especially those of Gunn,[42] Jones and Kay,[48] and Strein *et al.*[50] All three correlations[37,53,54] shown in the figure are much too negative at the lower temperatures, although the recommendations of Dymond and Smith[54] agree within their stated bounds above 315 K. At higher temperatures, the correlations increase to fit the results of Beattie and Stockmayer[55] which lie above equation (24) by 8.6 $cm^3 \cdot mol^{-1}$ at 423.15 K.

To obtain the third virial coefficient C the method described in the analysis section was followed. The experimental quantity $RT\gamma_a$ is shown in figure 5.14 together with the derived quantity T_a. The analysis of T_a to determine the three adjustable parameters in equation (17), the square-well model expression for C, gave

$$C/b_0^2 = 0.625 - 1.3986x + 2.0188x^2 - 0.6636x^3, \qquad (5.3.26)$$

with $x = \{\exp(382.5\ K/T) - 1\}$ and $b_0 = 0.275\ dm^3 \cdot mol^{-1}$.

Deviations of the pseudo-experimental quantity T_a from equation (26) and (16) are shown in figure 5.15 and are generally in agreement to within the standard deviations. The uncertainty in T_a arises almost entirely from that in $RT\gamma_a$ and varies rapidly from less than 0.01 $dm^6 \cdot mol^{-2}$ at the higher temperatures to about 0.1 $dm^6 \cdot mol^{-2}$ at 250 K, reflecting the decline in the accessible pressure range. No other alternative solution for C was attempted here. However, elsewhere estimates for C were determined using

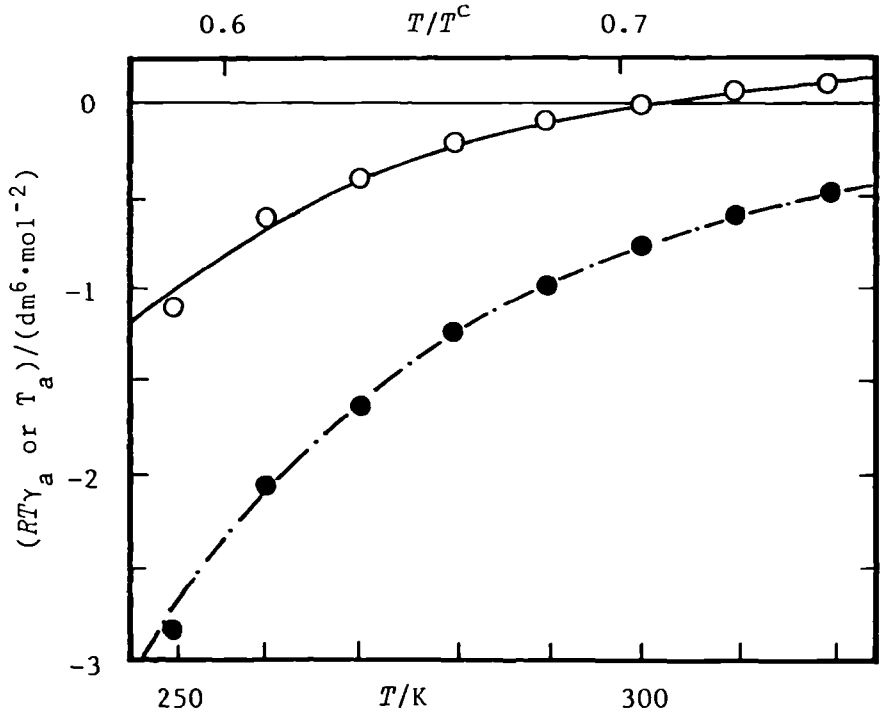

Figure 5.14. γ_a, the third acoustic virial coefficients, and derived quantities T_a for *n*-butane. ● , $RT\gamma_a$; ○ , T_a; —· —, calculated from equations (15) and (16) { or (2.3.23) and (2.3.24)} with (23), (24) and (26); ———, calculated from equations (16) with (23) and (26).

the Lennard-Jones (12,6) function.[39] Not surprisingly, the fit with two adjustable parameters was rather less good than that obtained with (17) and the maximum deviation of T_a was -0.22 $dm^6 \cdot mol^{-2}$ at 250 K. The resulting third virial coefficients are indistinguishable above 290 K, while at lower temperatures the results deviate and are 0.13 $dm^6 \cdot mol^{-2}$ less negative at 250 K. To a considerable extent, the differences arise from the very low weight given to the lowest temperature in the analysis; an unweighted adjustment of ε and σ for the (12,6) function gave values of C that lie within 0.04 $dm^6 \cdot mol^{-2}$ of equation (26). These differences between the square-well and (12,6) model evaluations of C provide an estimate of the likely systematic error associated with

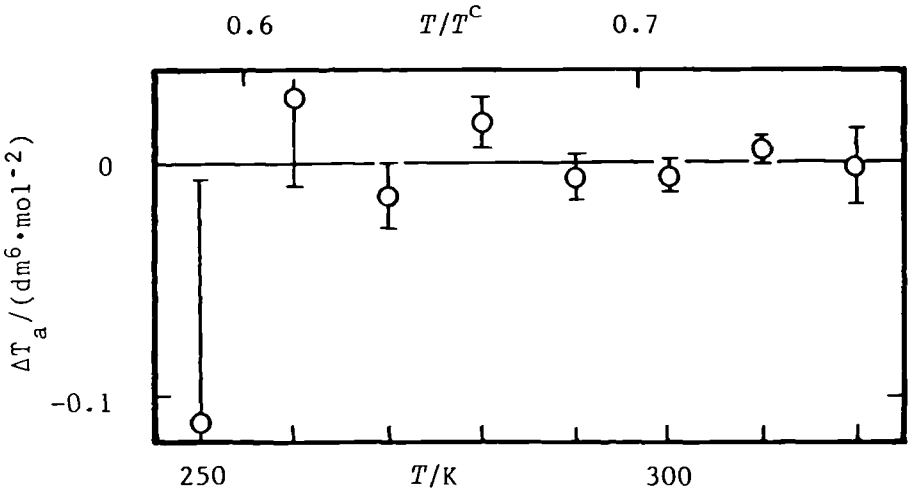

Figure 5.15. Deviations $\Delta T_a = \{T_a - T_a \text{ (calc.)}\}$ of T_a from equation (16) with (26) and experimental γ^{pg}.

the imposition of a particular functional form. The only independent estimate of C known is that given by Scott and Dunlap:[56] $C = (-0.4 \pm 0.4)$ $dm^6 \cdot mol^{-2}$ at 303 K which is in agreement with equation (26). In table 5.3 values of B and C calculated from equations (24) and (26) respectively at the experimental temperatures are given.

5.3.3 Methylpropane

The thermal conductivity of methylpropane has been measured by a number of workers between 293 and 630 K and 2.2 to 557 $kg \cdot m^{-3}$. Nieuwoudt *et al.* recommended the following expression for the thermal conductivity at zero density:

$$\kappa(T/T^c, \rho=0) = (T/T^c)^{\frac{1}{2}}/\{C_1 + C_2(T^c/T)^2 + C_3(T^c/T)^5\}, \quad (5.3.27)$$

in which $T^c = 407.84$ K,[61] $C_1 = 8.255070$ $m \cdot K \cdot W^{-1}$, $C_2 = 28.843455$ $m \cdot K \cdot W^{-1}$, and $C_3 = -1.89677$ $m \cdot K \cdot W^{-1}$. Equation (27) is consistent to a few per cent with the measurements of Nieuwoudt *et al.*[57], Karzaryen and Ryabstev,[58] and Lambert *et al.*[59]

The dilute gas viscosities reported by Abe *et al.*[62] were used by Sengers and co-workers to evaluate the adjustable parameters C_4 and C_5 in the functional form

$$\eta(T/T^c) = (T/T^c)^{\frac{1}{2}}/\{C_4 + C_5 T^c/T\}, \quad (5.3.28)$$

and found $C_4 = 0.0533$ $Pa^{-1} \cdot s^{-1}$ and $C_5 = 0.0434$ $Pa^{-1} \cdot s^{-1}$; the maximum fractional deviation of the experimental values

Table 5.3 Second and third virial coefficients from equations (24) and (26).

T/K	B/(cm^3·mol^{-1})	C/(dm^6·mol^{-2})	T/K	B/(cm^3·mol^{-1})	C/(dm^6·mol^{-2})
250	-1081.5	-0.616	260	-979.5	-0.485
270	-892.4	-0.324	280	-817.6	-0.210
290	-752.6	-0.129	300	-695.9	-0.071
310	-646.0	-0.030	310	-601.8	0.000_2

was 0.004.[57] Equation (28) also reproduces the $\eta(T)$ reported by Titani,[63] and Agayev and Yusibora[64] to within 2 per cent from 275 to 500 K which is within the error assigned to the measurements. Nieuwoudt *et al.*[57] report that the measurements of Lambert *et al.*[59] and Sage *et al.*[65] are in poor agreement with (28). The density dependence of η and κ are both insignificant in our density range of 0.1_5 to 2.5 kg·m^{-3}.

The residual experimental half widths, after allowance for classical bulk adsorption, were analysed using equation (5) to give a bulk viscosity and the average excess loss term b_r for each isotherm. The terms η_b and b_r were always significant at a probability of 0.99 but the term representing the error in κ was never significant. As with *n*-butane, b_r was about 3×10^{-6} above 261.4 K (the normal boiling temperature) which again suggests that large values of b_r may be associated with precondensation. Figure 5.16

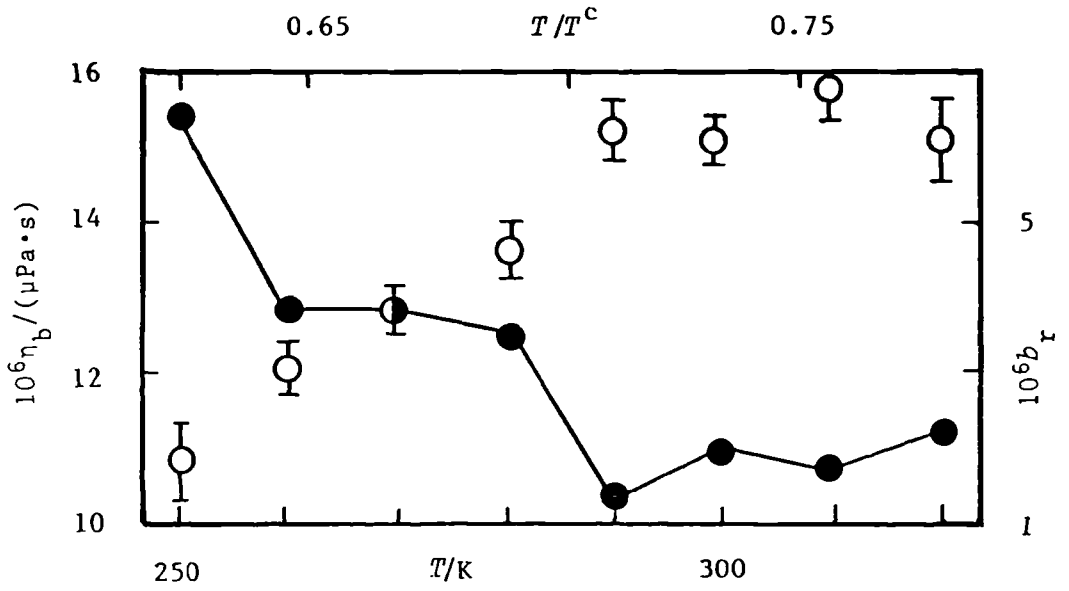

Figure 5.16. Bulk viscosities η_b (left-hand axis) and average fractional excess half widths b_r (right-hand axis) for methylpropane. ○ , η_b from analysis including b_r; ●——● , b_r. The error bars represent one standard deviation; T^c is given in table 4.2.

---

shows η_b and b_r as a function of temperature. If vibrational-vibrational energy transfer is rapid compared with translational-vibrational exchange then η_b (300 K) gives a relaxation time of 1.9 ns at 101.3 kPa. Figure 5.17 shows the quantity $\Delta g/f$ obtained after allowance for η_b, but not the empirical b_r.

The mean speeds of sound $\langle u \rangle$ at each pressure calculated from N radial resonance frequencies are given in table 5.4, along with standard deviations s of the mean on eight isotherms covering the temperature range from 251 to 320 K. Small corrections were applied to reduce all values to the stated

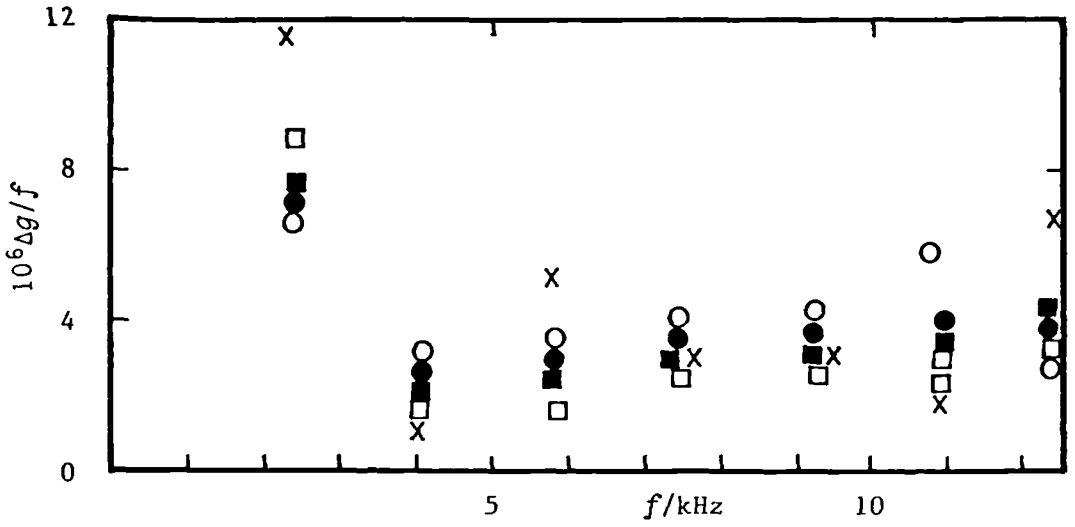

Figure 5.17. Fractional excess half widths $\Delta g/f$ for the lowest seven radial modes in methylpropane at 260 K determined from equation (5) with the bulk absorption (4) accounted for with κ and η from equatons (27) and (28) using η_b from the analysis including b_r. ○ , 54.1 kPa; ● , 42.5 kPa; ■ , 29.7 kPa; □ , 17.4 kPa; X , 8.0 kPa.

---

temperature using equation (22), and the radius a was obtained from equation (7). The maximum pressure was restricted to the lesser of 0.6 $p^{1+g(66)}$ (to avoid the known effects of precondensation) and 115 kPa (the greatest pressure measurable with the quartz-spiral gauge).

All observations of (u/a), weighted according to equation (1), were considered for the regression analysis to determine the $C_{p,m}^{pg}$ and the second and third acoustic virial coefficients. Below 300 K, three terms were sufficient to fit the $\{u(p)/a\}_T^2$ to within experimental error but at higher temperatures four terms were required. Consequently, the

Table 5.4. Mean values of u with standard deviations s determined from N radial modes, and deviations δ from equation (6) at temperatures T and pressures p for methylpropane. The coefficients of equation (6) can be obtained form equations (2.3.20) to (2.3.22).

T / K	p / kPa	u / m•s^{-1}	$10^6 s(u)/u$	N	$10^6 \delta(u^2)/u^2$
251.000	31.751	197.3534	1.9	7	0.8
	27.972	197.6310	1.6	7	-1.0
	23.638	197.9479	2.1	7	2.0
	21.530	198.1009	1.5	7	-0.3
	18.686	198.3065	1.5	7	-3.9
	15.314	198.5504	1.4	7	4.9
	11.719	198.8074	2.8	7	-2.4
	7.682	199.0913	4.8	7	(a)
	6.222	199.1988	5.7	7	-1.6
260.000	54.050	199.2989	1.7	7	-0.5
	47.782	199.7275	1.7	7	2.5
	42.492	200.0861	1.7	7	-0.1
	36.180	200.5111	1.6	7	-0.8
	29.657	200.9469	1.3	7	-0.2
	22.837	201.3986	1.3	7	-0.7
	17.834	201.7277	0.9	7	0.9
	11.935	202.1128	2.4	7	0.3
	8.027	202.3663	1.9	7	-0.6
	5.032	202.5598	5.0	7	-0.5
270.000	81.632	201.4390	1.3	7	0.2
	68.822	202.2443	1.6	7	-14.9

T / K	p / kPa	u / m•s^{-1}	$10^6 s(u)/u$	N	$10^6 \delta(u^2)/u^2$
270.000	60.199	202.7850	1.8	7	21.8
	52.080	203.2840	1.0	7	0.8
	45.304	203.6986	0.9	7	-2.5
	31.898	204.5106	0.8	7	-4.3
	17.509	205.3692	1.7	7	-7.5
	10.459	205.7862	0.8	7	1.8
	6.221	206.0355	3.0	7	8.6
280.000	107.997	203.8664	2.2	7	(a)
	100.507	204.3044	1.1	7	(a)
	90.362	204.8906	1.4	7	-1.0
	80.098	205.4778	1.3	7	0.7
	69.704	206.0667	1.0	7	0.7
	60.090	206.6064	1.0	7	0.1
	50.566	207.1364	0.9	7	-0.5
	38.710	207.7897	1.0	7	-1.8
	29.990	208.2661	0.6	7	1.2
	19.940	208.8091	1.0	7	(a)
	11.929	209.2401	1.8	7	0.3
	5.972	209.5603	8.0	5	(a)
290.000	103.817	208.0797	2.5	7	(a)
	93.465	208.6221	1.9	7	-0.8
	83.304	209.1485	2.4	7	-0.4
	72.200	209.7192	1.1	7	1.1
	62.780	210.1995	1.6	7	1.8

T / K	p / kPa	u / m•s^{-1}	$10^6 s(u)/u$	N	$10^6 \delta(u^2)/u^2$
290.000	51.965	210.7464	0.7	7	0.1
	42.869	211.2028	0.9	7	-2.0
	32.842	211.7026	1.4	7	-0.7
	22.389	212.2195	2.0	7	0.0
	12.890	212.6856	1.8	7	0.4
	6.921	212.9776	3.4	7	(*a*)
300.000	111.697	211.4955	1.2	7	(*a*)
	100.152	212.0460	1.6	7	-1.9
	90.105	212.5216	1.9	7	1.3
	79.806	213.0055	1.6	7	1.3
	69.091	213.5053	1.3	7	-0.3
	57.359	214.0488	1.2	7	1.1
	49.900	214.3919	1.4	7	-0.5
	39.833	214.8525	0.6	7	-0.6
	29.923	215.3029	1.2	7	-0.9
	19.804	215.7599	1.5	7	0.1
	10.658	216.1703	3.8	7	0.8
	5.925	216.3833	3.6	4	(*a*)
310.000	113.027	215.1862	1.7	7	3.2
	100.027	215.7510	1.4	7	1.4
	86.848	216.3191	1.6	7	-1.4
	79.355	216.6401	1.7	7	-3.5
	70.015	217.0389	1.8	7	-0.1
	59.433	217.4881	1.4	7	3.7

T / K	p / kPa	u / m·s^{-1}	$10^6 s(u)/u$	N	$10^6 \delta(u^2)/u^2$
310.000	50.292	217.8735	1.2	7	3.2
	39.872	218.3105	1.6	7	4.4
	29.929	218.7242	0.8	7	-2.0
	20.110	219.1309	2.6	7	-3.6
	9.347	219.5752	5.5	4	5.4
320.000	113.393	218.8263	1.5	7	(*a*)
	100.049	219.3567	1.5	7	(*a*)
	90.058	219.7514	1.6	7	-1.1
	80.067	220.1440	1.8	7	0.9
	69.708	220.5490	1.7	7	1.4
	58.833	220.9720	1.3	7	0.7
	49.850	221.3196	1.1	7	-2.0
	39.799	221.7075	1.6	7	0.9
	29.802	222.0910	2.5	7	-1.3
	19.856	222.4697	6.1	7	(*a*)
	9.292	222.8732	16.2	6	1.5

(*a*), pressure omitted from final analysis.

Table 5.5 Perfect-gas heat capacities, second and third acoustic virial coefficients, and standard deviations s obtained by analysis of N modes for methylpropane. The resonator radius $a(T)$ required to determine $C_{p,m}^{pg}(T)$ was given by equation (7). The quoted uncertainties are one standard deviation.

T/K	N	$C_{p,m}^{pg}/R$	$\beta_a/(cm^3 \cdot mol^{-1})$	$\gamma_a/(cm^3 \cdot mol^{-1} \cdot kPa^{-1})$	$10^6 s(u^2)/u^2$
251.000	53	10.0896 ± 0.0012	-1467.9 ± 1.3	-0.877 ± 0.029	4.5
260.000	67	10.3707 ± 0.0003	-1365.4 ± 0.3	-0.654 ± 0.005	3.6
270.000	60	10.7120 ± 0.0008	-1264.7 ± 0.5	-0.500 ± 0.006	10.1
280.000	53	11.0290 ± 0.0003	-1173.7 ± 0.1	$-0.392 \pm 0.001_2$	2.2
290.000	60	11.3241 ± 0.0004	-1094.2 ± 0.2	-0.297 ± 0.002	3.1
300.000	67	11.6737 ± 0.0004	-1022.7 ± 0.2	$-0.235 \pm 0.001_4$	3.0
310.000	71	11.9869 ± 0.0006	-957.0 ± 0.2	-0.191 ± 0.002	4.3
320.000	53	12.2920 ± 0.0011	-900.7 ± 0.4	-0.128 ± 0.003	4.4

pressure range was truncated to produce the best three-term equation and the results of the analysis are given in table 5.5;[§] the pressures that were omitted for three-term fits are indicated in table 5.4. $C_{p,m}^{pg}$, β_a, and γ_a provided by four-term and three-term fits over the whole pressure range, for each of the isotherms between 300 and 320 K, are reported in table 5.6. The greatest changes arising from truncation of the pressure range in $C_{p,m}^{pg}$ and β_a for three-term fits are only 0.0013 R and 0.9 $cm^3 \cdot mol^{-1}$; γ_a is also in good agreement. Had the four-term

[§]The coefficients reported in tables 5.5 and 5.6 were all significant at a probability of 0.009.

Table 5.6. $C_{p,m}^{pg}$, β_a and γ_a from n-term fits ($n = 3$ and 4) with equation (6) over the whole experimental pressure range for the isotherms between temperatures T of 300 and 320 K, and standard deviations s. All quoted uncertainties are one standard deviation.

T/K	n	$C_{p,m}^{pg}/R$	$\beta_a/(cm^3 \cdot mol^{-1})$	$\gamma_a/(cm^3 \cdot mol^{-1} \cdot kPa^{-1})$	$10^6 s(u^2)/u^2$
300.000	3	11.6740 ± 0.0014	-1022.4 ± 0.1	-0.233 ± 0.001	3.2
310.000	3	11.9872 ± 0.0007	-956.8 ± 0.2	-0.193 ± 0.002	4.0
320.000	3	12.2933 ± 0.0009	-899.6 ± 0.3	-0.138 ± 0.002	4.6
300.000	4	11.6729 ± 0.0006	-1023.9 ± 0.4	-0.209 ± 0.007	2.9
310.000	4	11.9904 ± 0.0012	-955.0 ± 0.2	-0.256 ± 0.002	3.2
320.000	4	12.2909 ± 0.0014	-902.4 ± 0.7	-0.090 ± 0.011	4.1

analysis been adopted with a complete complement of pressures, the estimates of $C_{p,m}^{pg}$ and β_a would have differed by 0.0035 R and 2.0 $cm^3 \cdot mol^{-1}$ from those given in table 5.5. All the $C_{p,m}^{pg}(T)$ and $\beta_a(T)$ reported in tables 5.5 and 5.6 agree within uncertainty estimates based on a 0.999 confidence interval for N degrees of freedom. Useful comparisons cannot be made between apparent γ_a from three-term fits and those given by four-term analyses with equation (6). The differences $\Delta(u/a)$ between the experimental results and the three-term equation for the first seven radial modes are shown in figure 5.18 for the isotherm at 260 K; the range and distribution are similar to those expected from the work with argon.

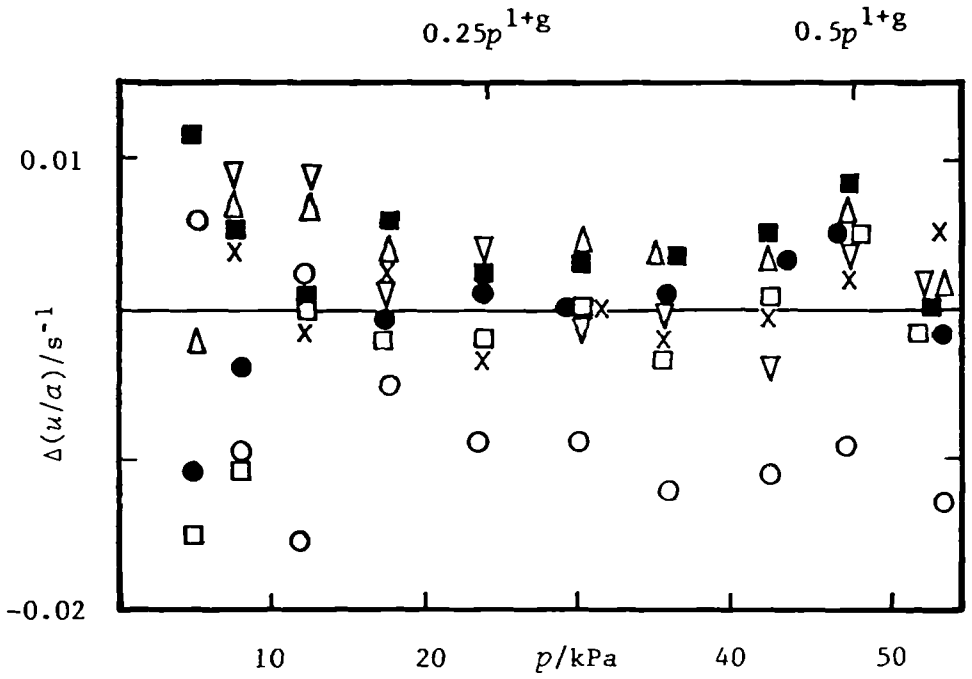

Figure 5.18. Deviations $\Delta(u/a) = [(u/a) - \{u(\text{calc.})/a\}]$, for individual resonant modes in methylpropane at 260 K from equation (6) with coefficients obtained from equations (2.3.20) to (2.3.22) and table 5.5. ○ , (0,2); ● , (0,3); □ , (0,4); ■ , (0,5); Δ , (0,6); ∇ , (0,7); X , (0,8). The vapour pressure was taken from reference (66).

The values of $C^{pg}_{p,m}$ given in table 5.5 are represented by

$$C^{pg}_{p,m}/R = 2.03 + 0.03211\ (T/\text{K}), \qquad (5.3.29)$$

with a standard deviation of 0.013 R. If the mole fraction impurity of 10^{-3}, given in table 4.4, were n-butane then the molar heat capacity derived from the measurements would change by only 0.0001 R but dimethylpropane would be more serious producing a change of about 0.033 R. Figure 5.19 shows the molar heat capacity from table 5.5 as deviations from

equation (29) together with some of the results in the literature. The flow-calorimetric measurements of Ernst and Büsser[69] are in excellent agreement with equation (29); at 293 K their results differ by only 0.009 R and at 313 K by 0.021 R, although at higher temperatures the differences are 0.06 R. The results reported by Wacker *et al.*[68] are about 0.04 R high in the overlapping temperature range and 0.06 R above the extrapolation of

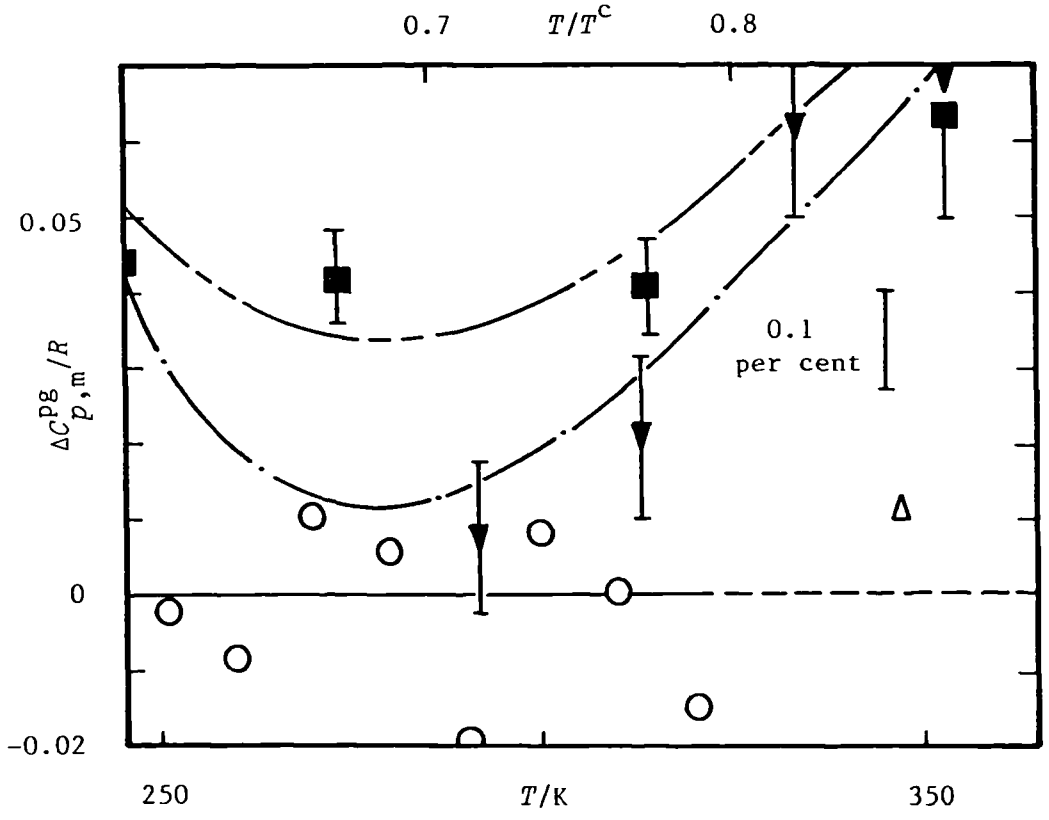

Figure 5.19. Deviation $\Delta C^{pg}_{p,m} = \{C^{pg}_{p,m} - C^{pg}_{p,m}(\text{calc.})\}$ of experimental heat capacities at constant pressure from equation (29). ○ , This work; ■ , reference 68; ▼ ,reference 69; Δ , reference 35; — · — , reference 38; — — — , equation (30) and (31) with constants from table 5.7.[70,71] T^c was taken from table 4.2.

equation (29). Dailey and Felsing[35] at 347.6 K are 0.015 R above the value obtained by extrapolation of equation (29). The heat capacities reported by Sage *et al.*[67] are in poor agreement (differences as large as 0.53 R) with all the above measurements. The comprehensive correlation of thermodynamic properties, due to Scott,[36] provides $C^{pg}_{p,m}$ which are virtually identical with the measurements of Wacker *et al.*[68] The calculations of Chen *et al.*[38] are also shown in figure 5.19. Although the torsional modes of the 3 methyl groups have been adequately assigned spectroscopically, the required estimates of the interaction energies between these groups are unknown.[38] Consequently, Chen *et al.*[38] assumed that each methyl group rotated independently, and the constants in an empirical expression for the potential-energy barrier were adjusted to give the best fit to thermodynamic properties, principally $C^{pg}_{p,m}$ from references (68) and (69). Therefore, it is not surprising to see agreement between Chen *et al.*[38] and equation (29) in the order of 0.5 per cent in the common temperature range.

Wilhoit,[70] {a co-author of reference (38)} has proposed for non-linear polyatomic molecules with N atoms the empirical expression

$$C^{pg}_{p,m}(T)/R = 4 + (3N - 6)y^2\{1 + (y - 1)\sum_{i=0}^{n} a_i y^i\}, \qquad (5.3.30)$$

to correlate $C^{pg}_{p,m}(T)$, in which

$$y = T/(T + T'_B), \qquad (5.3.31)$$

Table 5.7. Constants T_B' and $a_{i,B}$ (i = 0,1,2,3.) for substances B with N_B atoms, required to calculate $C_{p,m}^{pg}$ from equations (30) and (31).

B	N_B	T_B'/K	a_0	a_1	a_2	a_3
CH_4 [a]	5	240	2.156	-9.436	30.834	-25.830
n-C_4H_{10} [a], [b]	14	130	5.7560	-29.220	56.412	-32.440
$CH_3CHCH_3CH_3$	15.10994	120	6.7270	-29.350	51.175	-26.661
n-C_5H_{12}	17	220	-3.6540	15.289	-14.153	1.286
$CH_3CHCH_3CH_2CH_3$	17	500	-1.0025	0.8897	-2.5972	0.0447
$CH_3C(CH_3)_2CH_3$ [a]	17	130	0.0670	-2.9780	17.174	13.669

[a] Taken from reference 71. [b] Based on $C_{p,m}^{pg}$ from reference 38.

where T_B' and the a_i's from (30) are constants;[70,71] values of these constants when n = 3 are given in table 5.7 for the pure hydrocarbons on which measurements are reported in this Chapter and Chapter Six. Replacement of 4 with 4.5 and (3N - 6) with (3N - 5) in equation (30) was found sufficient by Wilhoit[70] for the correlation of $C_{p,m}^{pg}(T)$ for linear molecules. This approach is particularly useful over a wide temperature range.[71]¶ The heat capacities predicted from equations (39) and (31) with constants from table 5.7 are

¶This method of estimating perfect-gas molar heat capacities at constant pressure has been adopted by British Gas PLC.

less than 0.5 per cent greater than (29) between 250 and 340 K and are shown in figure 5.19; the parameters given in table 5.7, including N, were adjusted to best represent the $C^{pg}_{p,m}$ information reported in references (38), (68), and (69).

The square-well potential expression for B, using experimental β_a and γ^{pg} from table 5.5 gave

$$B(T)/(cm^3 \cdot mol^{-1}) = 270.3 - 192.13 \exp(460\ K/T), \qquad (5.3.32)$$

with a standard deviation of 0.62 $cm^3 \cdot mol^{-1}$ in β_a (about 0.06 per cent). Figure 5.20 shows deviations of β_a from equations (2.3.23) and (32) with experimental γ^{pg}. To verify, albeit crudely, the informal solution of (2.3.23) provided by (32), the power series in T approach was also applied. The resulting equation

$$B(T)/(cm^3 \cdot mol^{-1}) = -45.15 \times {}^{6}(K/T)^2 - 3.224 \times 10^{9}(K/T)^3, \qquad (5.3.33)$$

fits β_a with a standard deviation of 1.2 $cm^3 \cdot mol^{-1}$. Estimates of B from (33) are compared with equation (32) in figure 5.21 between 250 and 450 K. In the experimental temperature range (250 to 320 K), the two solutions agree to better than 10 $cm^3 \cdot mol^{-1}$ (about 1 per cent), and to within 5 $cm^3 \cdot mol^{-1}$ between 320 and 450 K. The second virial coefficients reported by other workers are plotted, as deviations from equation (32), in figure 5.22 where the ordinate scale has been compressed by a factor of 40 compared with figure 5.20.

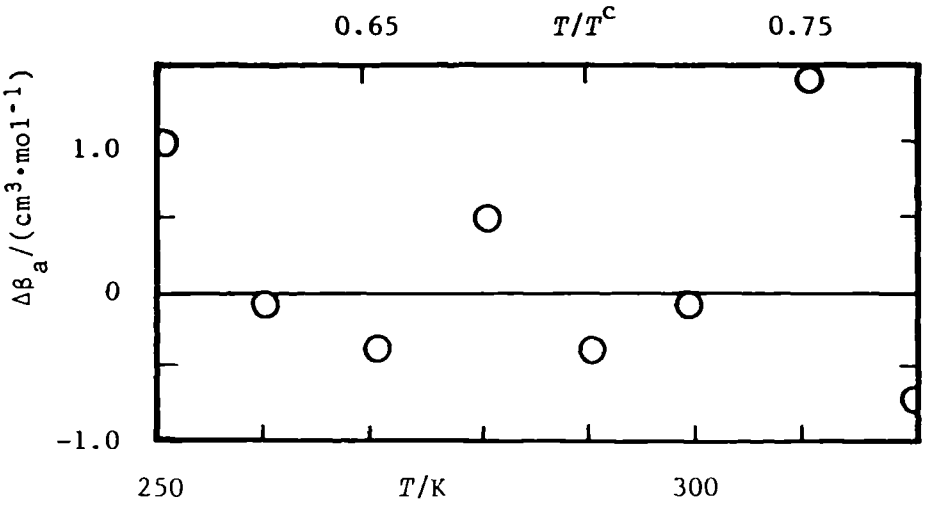

Figure 5.20. Deviations $\Delta\beta_a = \{\beta_a - \beta_a(\text{calc.})\}$ of experimental second acoustic virial coefficients of methylpropane from equation, (2.3.23) using (32) and γ^{pg} obtained from $C^{pg}_{p,m}$ given in table 5.5 combined with equation (2.3.20).

The correlation of Das *et al.*[73] lies above equation (32) by about 20 $cm^3 \cdot mol^{-1}$ at temperatures greater than 450 K but is too low in the overlapping temperature range. By contrast the measurements of Huff and Reed[72] above 444 K deviate by only 3 $cm^3 \cdot mol^{-1}$ (within their estimated uncertainty) from (32), while at lower temperatures this positive deviation increases to almost 50 $cm^3 \cdot mol^{-1}$. The most recent results of Strein *et al.*,[50] consistently show deviations between -50 and -40 $cm^3 \cdot mol^{-1}$, and appear to contain a systematic error.

The experimental quantity $RT\gamma_a$ was used in conjunction with equations (32) and (15), and the $C^{pg}_{p,m}$ from table 5.5,

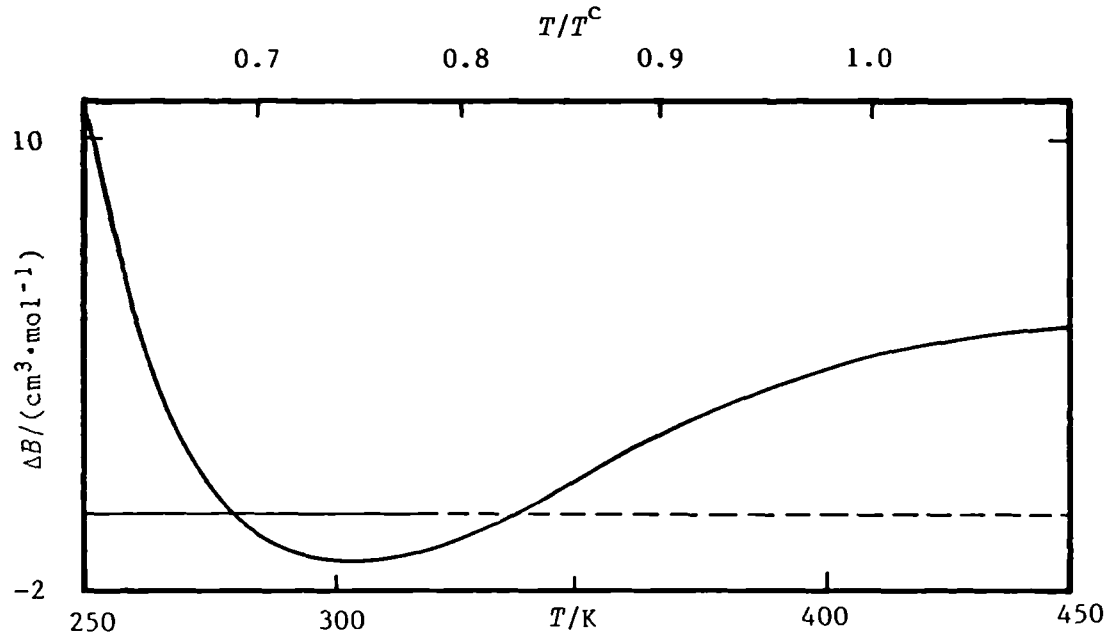

Figure 5.21. Deviations ΔB = [B {equation (33)} - B {equation (32)}] as a function of T for methylpropane, ———. T^c was taken from table 4.2.

---

to calculate T_a and subsequently to determine the three adjustable parameters in the square-well potential expression for C with the result:

$$C/b_0^2 = 0.625 - 2.0020x + 7.3956x^2 - 5.0635x^3, \qquad (5.3.34)$$

with $b_0 = 0.218\ \mathrm{dm^3 \cdot mol^{-1}}$ and $x = \{\exp(250.3\ \mathrm{K}/T) - 1\}$. T_a and $RT\gamma_a$ are shown as functions of temperature in figure 5.23. As for B no physical significance is attached to the parameters of the square-well model. Deviations of T_a from (34) and (16) are shown in figure 5.24 and generally agree within one standard deviation. Although there is a

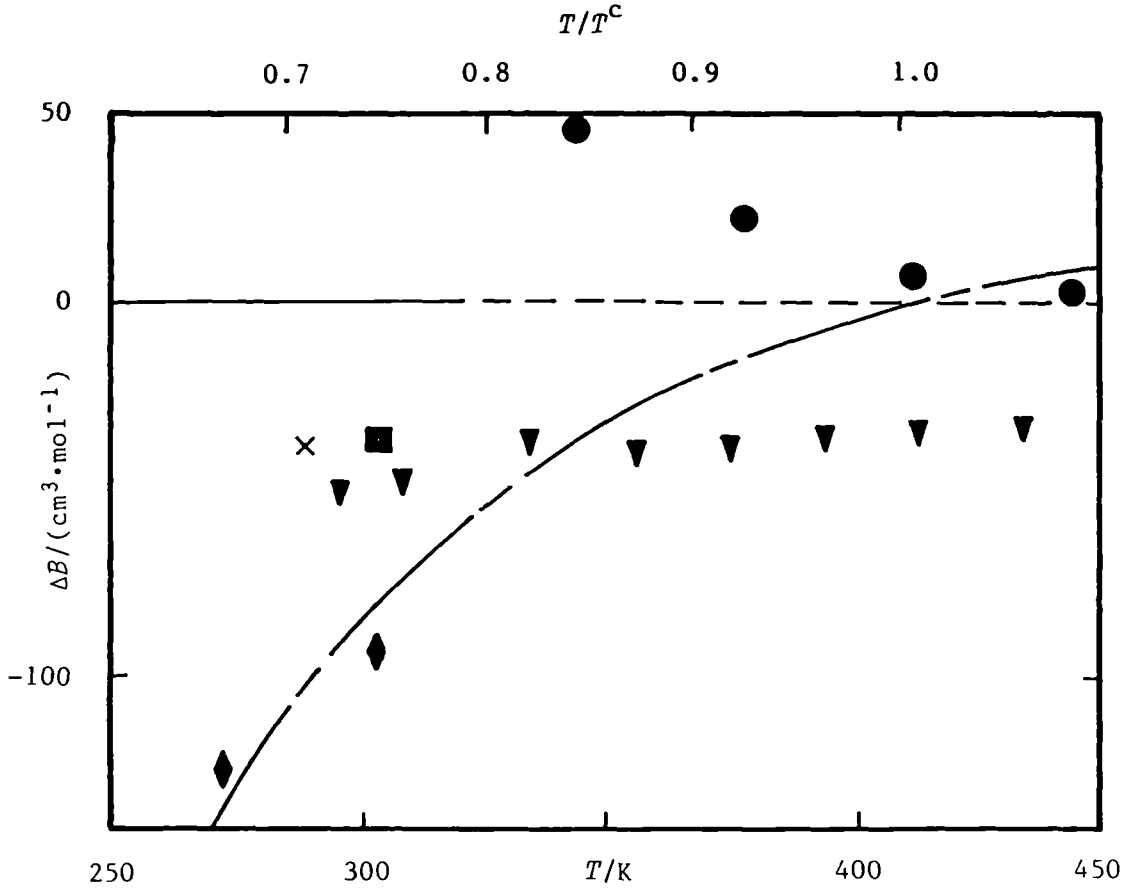

Figure 5.22. Deviations $\Delta B = \{B - B(\text{calc.})\}$, of second (p,V_m,T) virial coefficients from equation (32). ● , Reference 72; ♦ , reference 40; ▼ , reference 50; X , reference 43; ■ , reference 41; —— – ——, reference 73.

---

larger discrepancy at 310 K, removal of this point did not significantly alter the value of C obtained from the analysis. Consequently, the $RT\gamma_a$ (310 K) was retained in the regression. The origin of this uncertainty is unclear. None of the workers whose second virial coefficients are given in the comprehensive review of Dymond and Smith

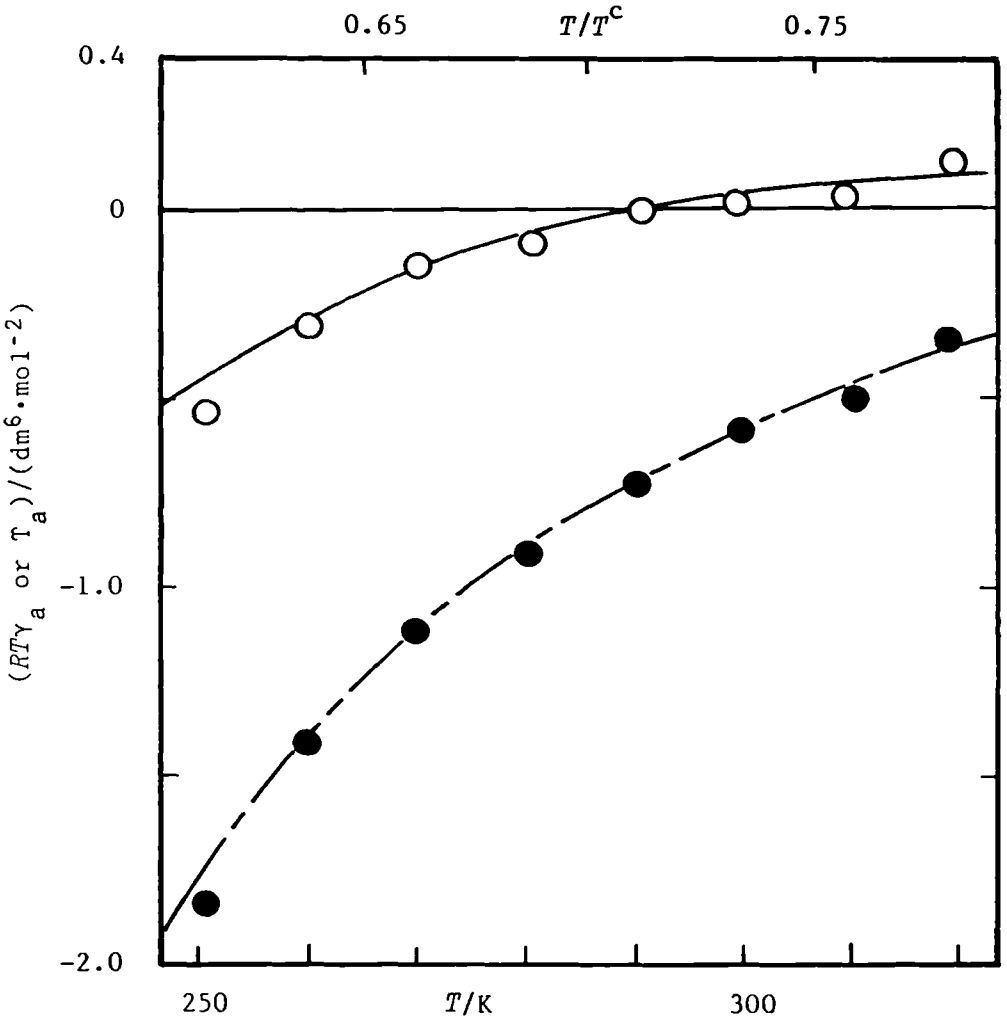

Figure 5.23. The apparent third acoustic virial coefficient γ_a, provided by three-term fits with equation (6), and derived quantities τ_a for methylpropane. ● , $RT\gamma_a$; ○ , τ_a; —·—, calculated from equation (15) and (16) {or (2.3.23) and (2.3.24)} with (29), (32) and (34); ———, calculated from equations (16) with (29) and (34).

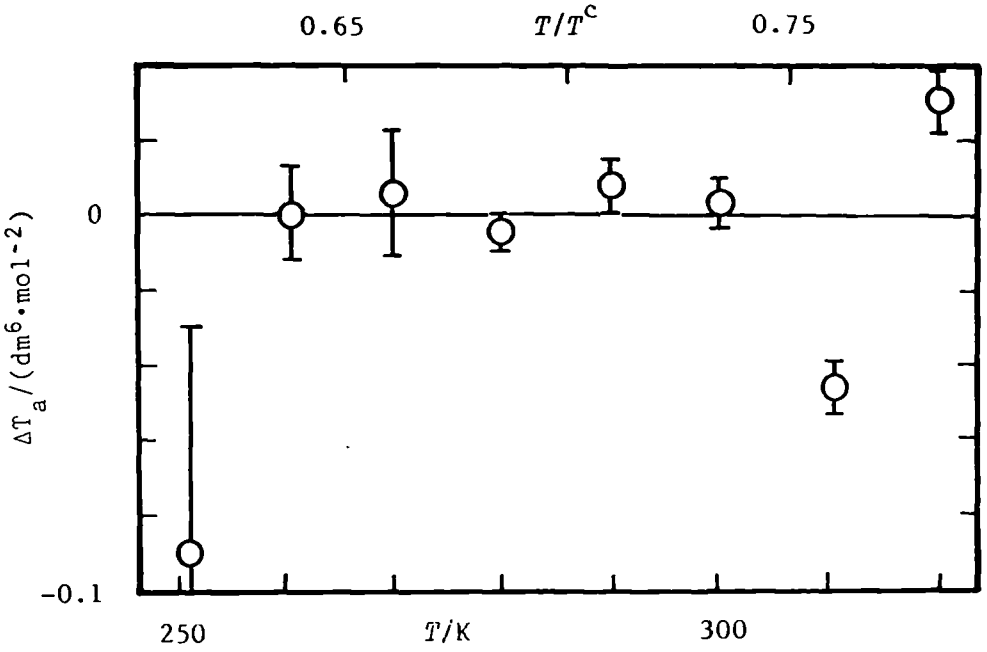

Figure 5.24. Deviations $\Delta T_a = \{T_a - T_a(calc.)\}$ of T_a from equations (16) with (34) and experimental γ^{pg}.

report values of C.

In table 5.8 values of B and C calculated from equations (32) and (34) are reported at the experimental temperatures.

Table 5.8 Second and third virial coefficients from equations (32) and (34).

T/K	$B/(cm^3 \cdot mol^{-1})$	$C/(dm^6 \cdot mol^{-2})$	T/K	$B/(cm^3 \cdot mol^{-1})$	$C/(dm^6 \cdot mol^{-2})$
251	-930.6	-0.308	260	-856.8	-0.223
270	-785.3	-0.152	280	-723.0	-0.099
290	-668.3	-0.060	300	-619.9	-0.030
310	-577.0	-0.007_3	320	-538.6	0.009_7

5.3.4 *n*-Pentane

Table 5.9 lists mean values of u for each pressure along the seven isotherms between 270 and 330 K, together with standard deviations and the number of modes from which they were determined. The corrections required to provide (u/a) were calculated using the transport properties discussed below.

The thermal conductivities of Gray *et al.*[74] at 323.15 and 373.15 K give for equation (20)

$$\kappa/(\mathrm{mW \cdot m^{-1} \cdot K^{-1}}) = 16.76\ (T/323.15\ \mathrm{K})^{1.938},$$

which fits the measurements of Carmichael *et al.*[75] between 277 and 344 K to 3 per cent.

Shear viscosities of *n*-pentane were obtained from

$$\eta/(\mu\mathrm{Pa \cdot s}) = 0.311 + 0.02305\ (T/\mathrm{K}), \qquad (5.3.35)$$

which fits the results of Diaz Peña and Cheola[30] to 0.05 μPa·s over the temperature range 205 to 423 K.

The residual experimental line widths were analysed with equation (5). Terms representing the bulk viscosity and the empirical b_r were sufficient to fit Δg to within experimental error except for the 290 K isotherm, for which the further term b_2 (for the (0,2) mode) was also significant at a probability greater than 0.99; use of b_2 at 290 K altered η_b by less than 0.2 μPa·s. It is possible that the need for b_2 at this temperature only may have arisen from the movement of a transducer due to a sudden pressure change. The bulk viscosities determined in the

Table 5.9. Mean speeds of sound u with standard deviations s determined from N radial modes, and deviations δ from equation (6) with the leading three terms at temperatures T and pressures p for n-pentane.

$\frac{T}{K}$	$\frac{p}{kPa}$	$\frac{u}{m \cdot s^{-1}}$	$\frac{10^6 s(u)}{u}$	N	$\frac{10^6 \delta(u^2)}{u^2}$
270.000	12.640	182.0275	6.9	7	(a)
	10.933	182.2129	5.1	7	-2.0
	9.536	182.3626	4.2	7	3.3
	6.468	182.6867	4.1	5	-0.1
	5.952	182.7407	3.5	5	-1.4
	4.458	182.8966	3.6	5	-2.2
	3.024	183.0458	3.4	5	3.2
	1.521	183.2003	3.6	4	-0.3
280.000	20.645	184.5748	5.6	7	(a)
	18.966	184.7425	4.5	7	(a)
	17.375	184.8942	4.2	7	-1.8
	16.002	185.0263	3.7	7	0.7
	14.454	185.1726	3.5	7	(a)
	13.060	185.3072	3.2	7	1.0
	11.745	185.4321	2.9	7	2.2
	10.045	185.5923	2.2	7	-2.5
	8.619	185.7263	2.4	7	-4.1
	7.012	185.8776	2.5	7	4.2
	5.503	186.0177	3.5	7	-2.5
	4.018	186.1559	2.0	7	0.8

$\frac{T}{K}$	$\frac{p}{kPa}$	$\frac{u}{m \cdot s^{-1}}$	$\frac{10^6 s(u)}{u}$	N	$\frac{10^6 \delta(u^2)}{u^2}$
290.000	28.248	187.2661	4.1	7	-1.7
	25.836	187.4727	3.6	7	(a)
	23.577	187.6729	3.1	7	3.7
	20.941	187.9002	2.6	7	-0.0
	17.556	188.1907	2.3	7	-1.1
	14.593	188.4124	1.9	7	-5.8
	12.459	188.6250	1.6	7	2.9
	9.960	188.8362	1.8	7	3.4
	7.557	189.0377	1.9	7	-2.5
	5.515	189.2086	2.2	7	-2.9
	3.263	189.3969	3.3	5	3.2
300.000	46.801	189.0388	6.0	5	(a)
	42.923	189.3537	4.9	7	-2.4
	38.628	189.6983	3.4	7	-2.3
	34.911	189.9950	2.8	7	0.9
	30.898	190.3132	2.3	7	2.0
	26.879	190.6297	2.3	7	0.9
	19.873	191.1768	1.6	7	-0.7
	14.869	191.5640	1.1	7	-1.3
	9.880	191.9471	1.0	7	-1.5
	5.061	192.3147	2.2	7	2.1
310.000	65.948	190.9904	5.2	7	(a)
	59.820	191.4477	3.8	7	(a)
	52.083	191.0191	3.3	7	-4.4

T / K	p / kPa	u / m·s^{-1}	$10^6 s(u)/u$	N	$10^6 \delta(u^2)/u^2$
310.000	47.839	192.3301	2.6	7	0.7
	40.834	192.8399	2.1	7	(a)
	35.946	193.1913	1.7	7	0.8
	29.208	193.6731	2.4	7	-2.3
	20.947	194.2585	1.4	7	-2.2
	13.891	194.7537	0.8	7	-1.1
	6.146	195.2922	0.8	7	1.3
320.000	55.503	195.0669	2.8	7	(a)
	44.706	195.7845	2.3	7	-0.6
	40.029	196.0923	2.0	7	0.5
	34.829	196.4325	1.7	7	-1.0
	29.826	196.7584	1.4	7	0.8
	24.940	197.0748	1.3	7	0.1
	19.960	197.3956	1.0	7	-1.1
	14.936	197.7177	0.9	7	-0.7
	9.982	198.0338	0.7	7	1.0
	4.913	198.3560	2.7	7	(a)
330.000	88.095	196.2528	3.3	7	-2.4
	79.951	196.7630	2.7	7	0.7
	69.934	197.3850	2.4	7	3.9
	49.368	198.6423	2.5	7	-0.0
	39.826	199.2173	1.7	7	-1.0
	29.749	199.8188	1.8	7	-2.0

$\frac{T}{K}$	$\frac{p}{kPa}$	$\frac{u}{m \cdot s^{-1}}$	$\frac{10^6 s(u)}{u}$	N	$\frac{10^6 \delta(u^2)}{u^2}$
330.000	19.962	200.3995	1.3	5	(*a*)
	9.878	200.9886	1.7	3	3.4

(*a*), pressure omitted from analysis.

analysis are shown in figure 5.25 together with b_r and b_2 (290 K). A large increase in b_r is observed below 290 K, but at higher temperatures b_r is about 5×10^{-6}. Since the term b_h was not significant for any isotherm, the estimates for the thermal conductivity were sufficiently accurate for the analyses. Assuming that the vibrational states of *n*-pentane are strongly coupled, the bulk viscosities provide a relaxation time t = 0.9 ns at 300 K and 101.3 kPa; this value is in agreement with the literature value of 1.1 ns.[32]

The excess losses, calculated after allowance for the bulk viscosity but not b_r, is shown in figure 5.26 for the isotherm at 270 K which is the worst case.

In the regression analysis to determine heat capacities and acoustic virial coefficients, a full

compliment of (u/a) observations were used even though table 5.9 reports only mean values at each temperature and pressure. Below 300 K only the three leading terms in the infinite series (6) had coefficients which were significant at a probability of 0.999. Although the pressure range is small at the lower temperatures, the third acoustic virial coefficient is correspondingly large and systematic deviations from a two-term fit

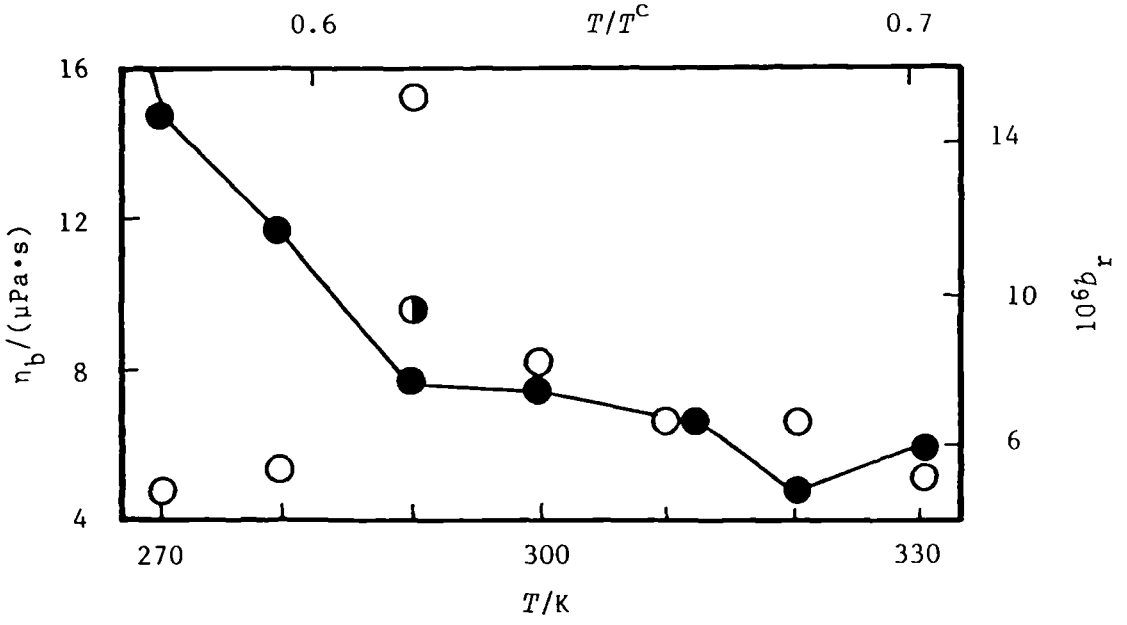

Figure 5.25. Bulk viscosities η_b (left-hand axis) and average excess half widths b_r (right-hand axis) for *n*-pentane with b_2 for 290 K.

○ , η_b from analysis including b_r; ●——● b_r; ◑ b_2 provided by analysis including η_b and b_r, for which the right-hand ordinate scale applies.

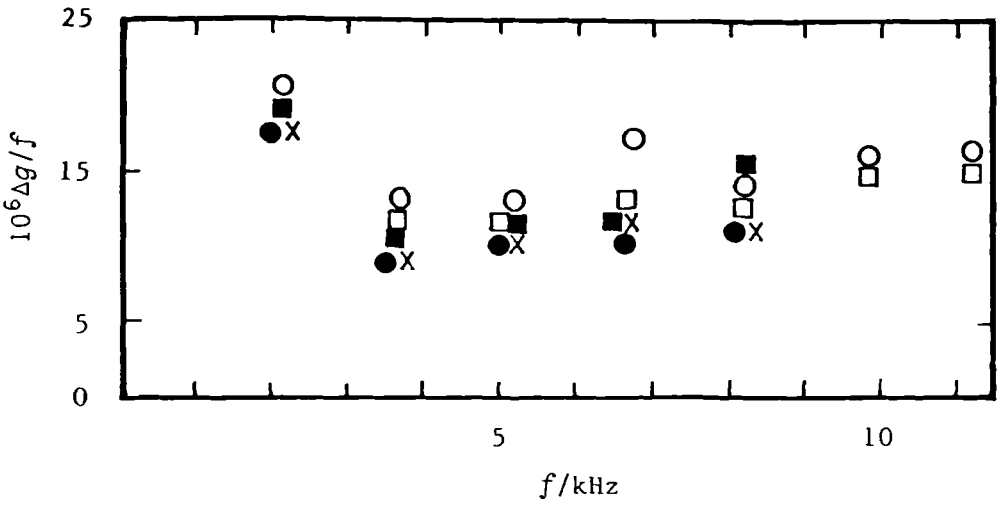

Figure 5.26. Fractional excess half widths $\Delta g/f$ for the lowest seven radial modes in *n*-pentane at 270 K including η_b in the bulk absorption. ○ , 10.9 kPa; ● , 5.95 kPa; ■ , 3.0 kPa; □ ; 9.5 kPa; X , 6.5 kPa.

---

exceed the discrepancies between individual modes at any one pressure by more than a factor of five. By contrast, the deviations shown in figure 5.27 from the three-term equation are comparable with the distribution of results obtained from the seven modes studied at each pressure. At the highest pressure (u/a) increased by 0.05 s^{-1} between the (0,2) and (0,8) {excluding the (0,5) mode which had a low weight} modes the results are clearly affected by precondensation; this pressure of 12.6 kPa, which corresponds to about 0.6 $p^{l+g,(76,77)}$ was omitted from the regression analysis. Although the (0,2) mode

gave values of (u/a) that were consistently 0.2 s^{-1} less than the mean of the remaining modes, omission of this mode did not alter significantly the estimates of heat capacity or acoustic virial coefficients. Between 300 and 320 K, the best three-term equations gave values of the second acoustic virial coefficient and heat capacity

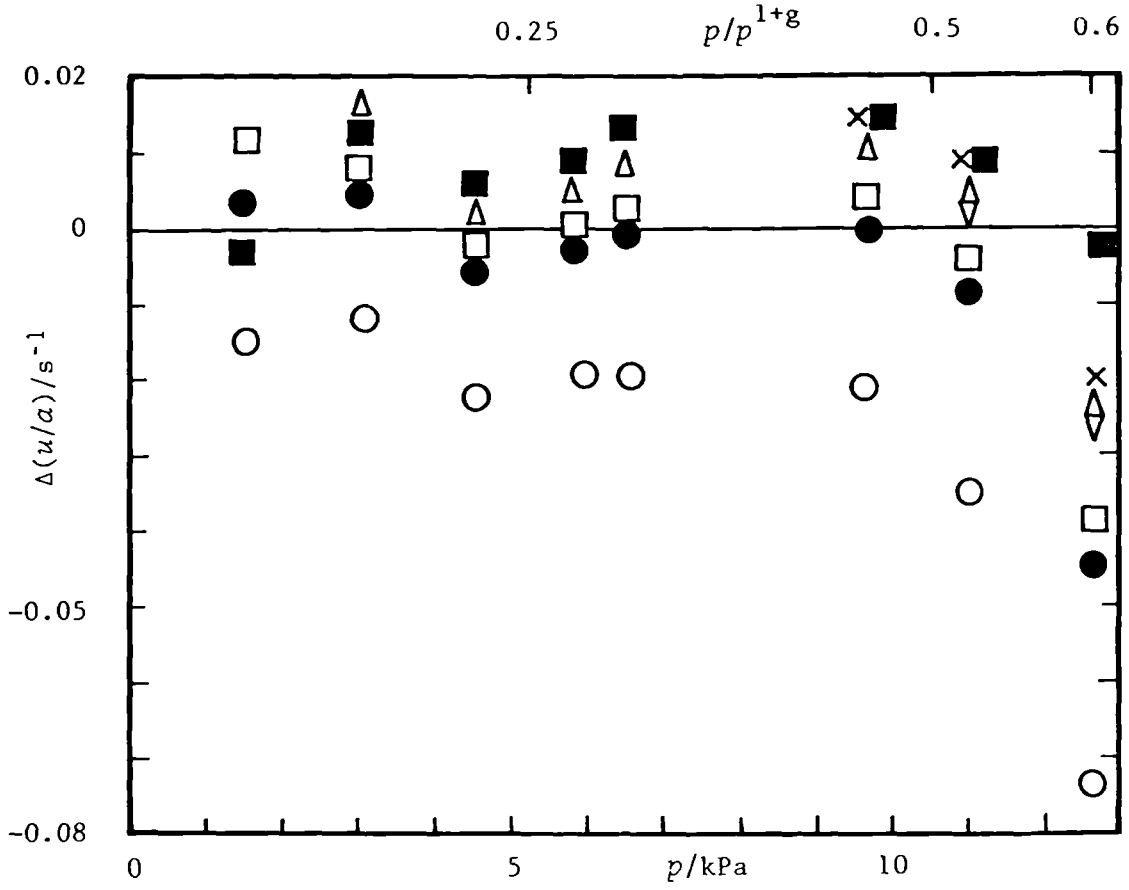

Figure 5.27. Deviations $\Delta(u/a) = [(u/a) - \{u(\text{calc.})/a\}]$, for individual modes in *n*-pentane at 270 K, from equation (6) with coefficients adjusted to fit the results below 12 kPa. ○ , (0,2); ● , (0,3); □ , (0,4); ■ , (0,5); Δ , (0,6); ▽ , (0,7); X , (0,8). The vapour pressure was calculated from references (4), (76) and (77).

Table 5.10 Perfect-gas heat capacities, second and third acoustic virial coefficients, and standard deviations s obtained by analysis of N modes for n-pentane. The resonator radius $a(T)$ required to determine $C_{p,m}^{pg}(T)$ was given by equation (7). The quoted uncertainties are one standard deviation.

T/K	N	$C_{p,m}^{pg}/R$	$\beta_a/(cm^3 \cdot mol^{-1})$	$\gamma_a/(cm^3 \cdot mol^{-1} \cdot kPa^{-1})$	$10^6 s(u^2)/u^2$
270.000	35	13.4200 ± 0.0020	-2495.8 ± 4.6	-5.103 ± 0.347	8.0
280.000	60	13.7770 ± 0.0017	-2286.5 ± 2.4	-2.724 ± 0.108	6.2
290.000	65	14.0817 ± 0.0010	-2100.9 ± 1.0	-1.642 ± 0.031	5.7
300.000	60	14.4999 ± 0.0010	-1949.9 ± 0.6	-1.144 ± 0.013	5.2
310.000	46	14.8422 ± 0.0009	-1807.1 ± 0.4	-0.853 ± 0.007	4.1
320.000	53	15.2300 ± 0.0010	-1686.1 ± 0.5	-0.611 ± 0.009	3.0
330.000	42	15.6352 ± 0.0017	-1571.5 ± 0.4	-0.538 ± 0.004	4.9

differing between 4 and 11 $cm^3\ mol^{-1}$ and 0.0002 and 0.0032 R from those of the four-term equation, and by no more than 2 $cm^3 \cdot mol^{-1}$ and 0.0017 R from three-term equations covering the full pressure range. The differences between all the three estimates are less than the combined uncertainties estimated at a probability of 0.999.

The results of the analysis for n-pentane are given in table 5.10 together with the number N of resonance frequencies in the final regression and the standard deviations of the fits.

The $C^{pg}_{p,m}$ may be represented to 0.02 R by

$$C^{pg}_{p,m}/R = 0.04546\ (T/K) + 0.226 \times 10^8\ (K/T)^3, \qquad (5.3.36)$$

and are shown as deviations from this equation in figure 5.28. If the impurity with a mole fraction of 10^{-4} reported in table 4.5 were a butane, then the heat capacity derived from the measurements would change by 0.004 R, although another pentane would produce an insignificant change. The values of $C^{pg}_{p,m}$ given in table 5.10 are in excellent agreement with

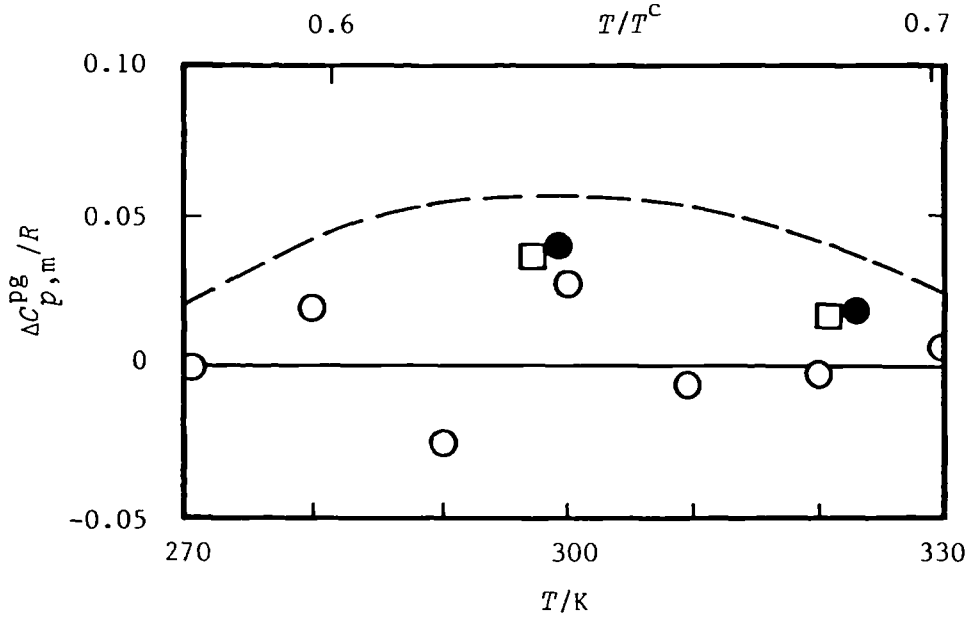

Figure 5.28. Deviations $\Delta C^{pg}_{p,m} = \{C^{pg}_{p,m} - C^{pg}_{p,m}(\text{calc.})\}$ of experimental heat capacities at constant pressure from equation (36) in the experimental temperature range. ○ , This work; ● , reference 36; □ , reference 78; - - -, calculated using equation (30)and (31) with constants from table 5.7.[70,71]

the flow-calorimetric measurements of Hossenlopp and Scott.[78] Not surprisingly the correlations based on these flow-calorimetric results due to Scott,[36] and Wilhoit[70] (using the constants in table 5.7) are also in excellent agreement. Although the errors in acoustics and flow calorimetry are very different, an unweighted regression with the combining results covering the temperature range 270 to 323 K gives

$$C_{p,m}^{pg}/ = 0.0479\ (T/K) - 17.09 \times 10^{-8}\ (T/K)^3 + 15.49 \times 10^{6}\ (K/T)^3, \qquad (5.3.37)$$

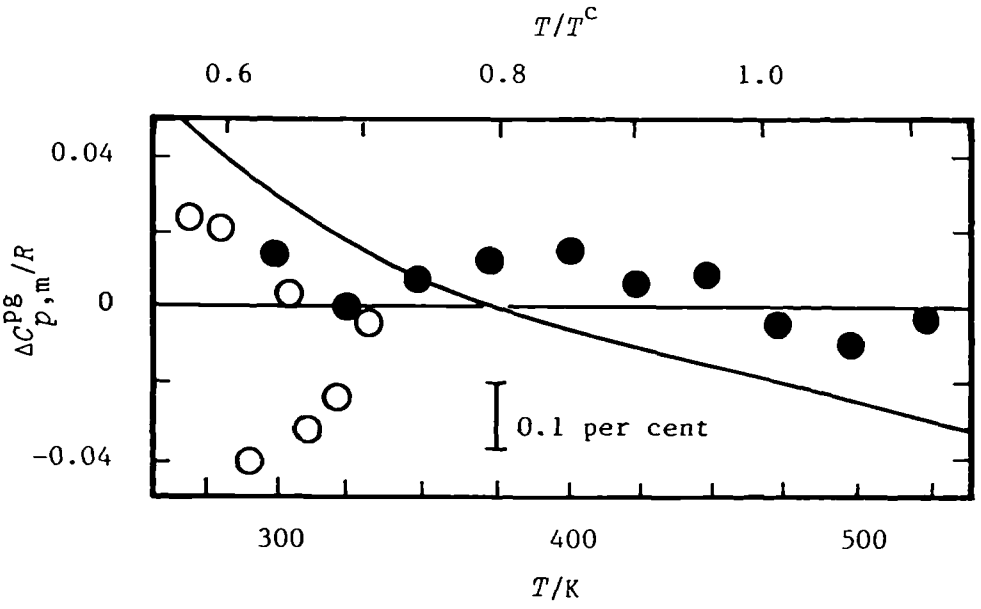

Figure 5.29. Deviations $\Delta C_{p,m}^{pg} = \{C_{p,m}^{pg} - C_{p,m}^{pg}(\text{calc.})\}$, of experimental $C_{p,m}^{pg}$ for *n*-pentane from equation (37). O , This work; ● , reference 78; ———, equations (30) and (31) with constants from table 5.7. T^c was taken from table 4.2.

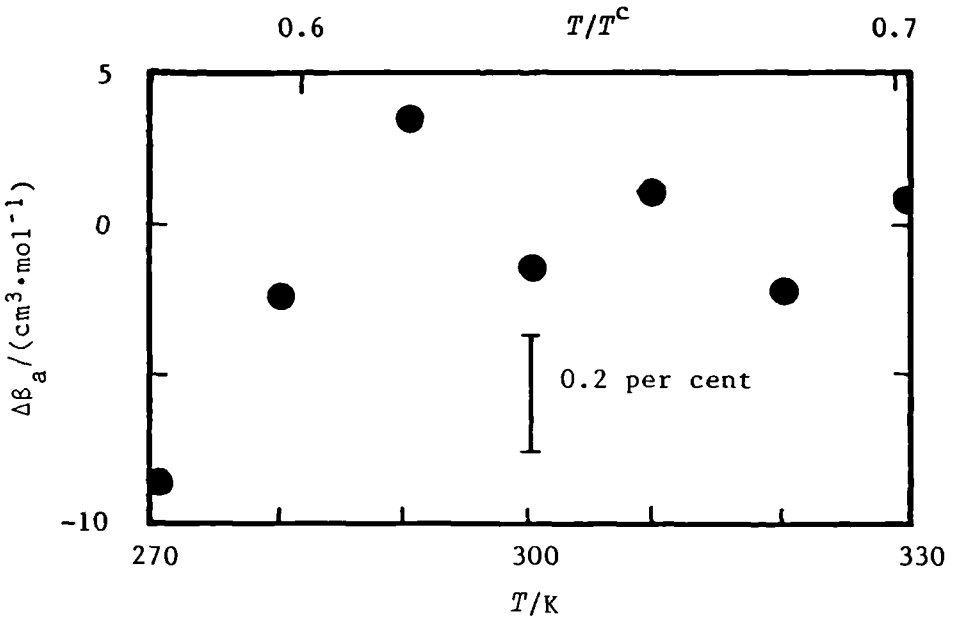

Figure 5.30. Deviations $\Delta\beta_a = \{\beta_a - \beta_a(\text{calc.})\}$, of experimental β_a from equation (2.3.23) using (38) and experimental γ^{pg}.

---

with a standard deviation of only 0.02 R (about 0.1 per cent). The calorimetric results show a systematic deviation from equation (37), which implies that the functional form is not entirely satisfactory, while the random scatter of the acoustic results suggests the possibility of variations in impurities.

The experimental β_a and γ^{pg} of table 5.10 when used with the square-well potential expression for B gave

$$B(T)/(cm^3 \cdot mol^{-1}) = 400.0 - 249.07 \exp(550\ K/T), \qquad (5.3.38)$$

with a standard deviation in β_a of 2.2 $cm^3 \cdot mol^{-1}$. The differences between the experimental β_a and those calculated

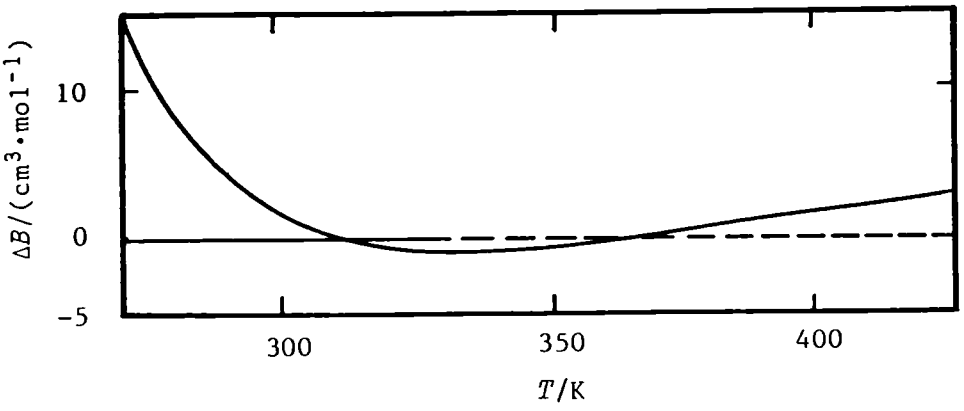

Figure 5.31. Deviations ΔB = B(alt.) - B(calc.) of the alternative solution to B(alt.) given by (39) of equation (2.3.23) from equation (38).

---

from equations (38) and (2.3.23) using experimental γ^{pg} are given in figure 5.30 and, although the value at 270 K is 8.4 $cm^3 \cdot mol^{-1}$ (about 0.3 per cent) low it still lies within the uncertainty estimate based on a confidence interval of 0.999.

When represented by a polynomial in temperature, the selected functional form

$$B(T)/(cm^3 \cdot mol^{-1}) = - 60.57 \times 10^6 \ (K/T)^2 - 13.05 \times 10^9 \ (K/T)^3, \quad (5.3.39)$$

fitted β_a to 2.2 $cm^3 \cdot mol^{-1}$. As figure 5.31 shows, the virial coefficients calculated from equations (38) and (39) agree to within 0.6 per cent (about 15 $cm^3 \cdot mol^{-1}$ at 270 K) over the experimental temperature range and differ by less than

3 $cm^3 \cdot mol^{-1}$ when extrapolated to 425 K. The second virial coefficients reported by other workers are plotted as deviations from equation (38), in figure 5.32 for the temperature range 260 to 425 K where the ordinate scale has been compressed by a factor of 8 compared with figure 5.30. The values of B derived by Hossenlopp and Scott[78] from their enthalpies of evaporation show a discontinuity below 283 K where the discrepancies are +60 $cm^3 \cdot mol^{-1}$, although above this temperature the deviations (5 to -30 $cm^3 \cdot mol^{-1}$) are much smaller and are less than the estimated error in their results. The results of Hajjar *et al.*[81] from low pressure (p, V_m, T) studies lie within 10 $cm^3 \cdot mol^{-1}$ of equation (38) even when the equation is extrapolated almost 150 K to 473 K. The measurements reported by McGlashan and Potter agree with (38) to within their precision of 20 $cm^3 \cdot mol^{-1}$. Equation (38) extrapolates to join the recommendations of Dymond and Smith[82] above 340 K to within their estimated errors but, for the correlation of Das *et al.*,[82] agreement with equation (38) is not achieved until 450 K. Both these correlations are based on the measurements of Beattie *et al.* between 473 and 573 K; the differences between the original measurements and the extrapolated equation (38) are less than 8 $cm^3 \cdot mol^{-1}$. By contrast at lower temperatures all three correlations[78,82,84] shown in the figure are much too low. The measurements of Schäffer and co-workers[46] show deviations between -140 and -220 $cm^3 \cdot mol^{-1}$; clearly there are serious differences for both B and dB/dT between

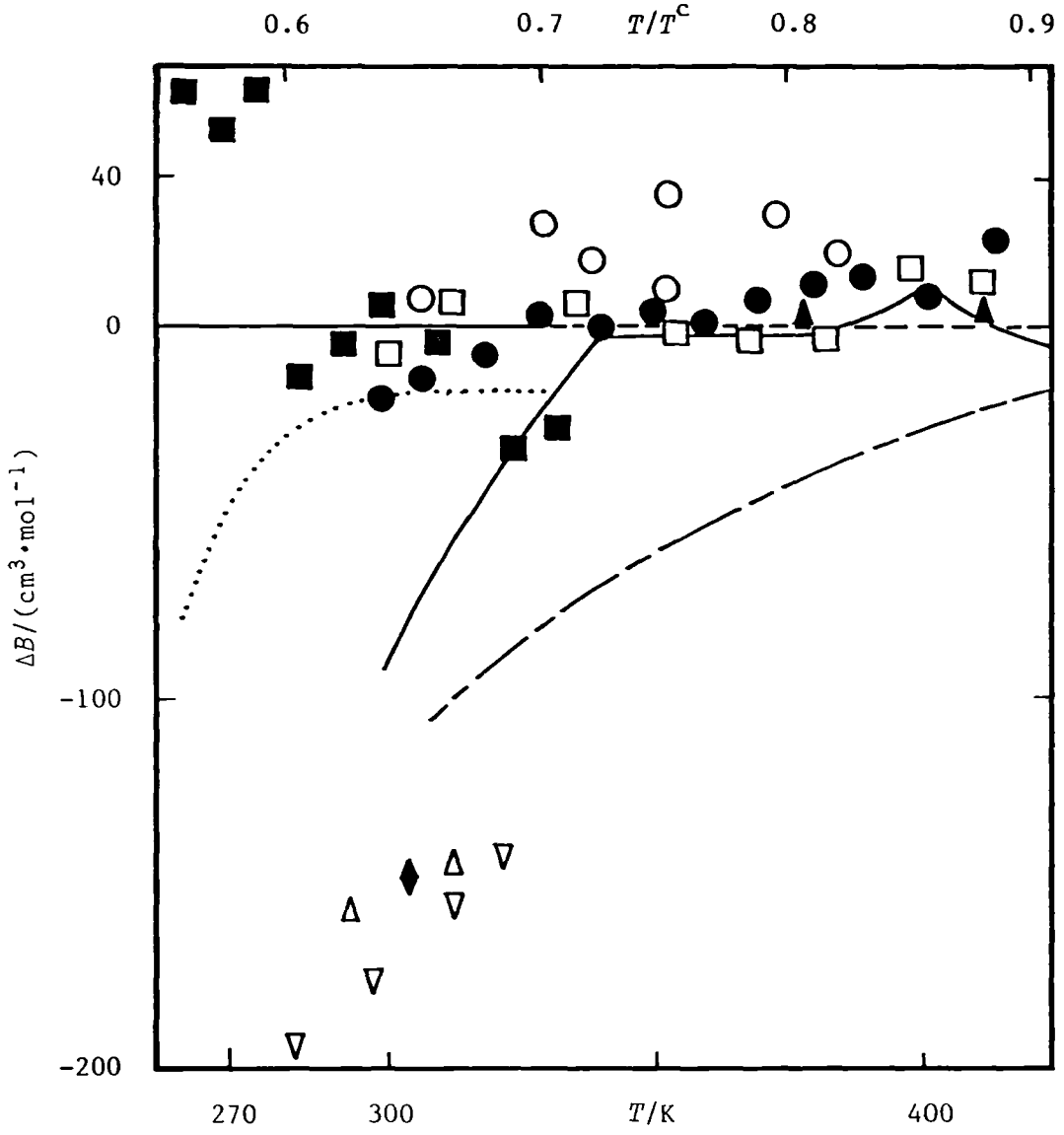

Figure 5.32. Deviations $\Delta B = \{B - B(\text{calc.})\}$, of second virial coefficients from equation (38). ♦ , Reference 40; ▲ , reference 72; ○ , reference 79; ● , reference 44; ▽ , reference 46; △ , reference 80; □ , reference 81; ■ , reference 78; — - —, reference 82; ———, reference 83;····, reference 78.

these measurements and those reported here.

With the quantity T_a calculated from equations (38) and (15) analysis of the experimental γ_a in terms of the square-well potential for C gave

$$C(T)/b_0^2 = 0.625 - 0.01876x + 2.261_3 \times 10^{-4}x^2 - 7.538 \times 10^{-7}x^3, \qquad (5.3.40)$$

where $b_0 = 0.297\ \mathrm{dm^3 \cdot mol^{-1}}$ and $x = \{\exp(2100\ \mathrm{K}/T) - 1\}$; the standard deviation in T_a was $0.06\ \mathrm{dm^6 \cdot mol^{-2}}$. Figure 5.33 illustrates the exceptionally good agreement, compared with that obtained for *n*-butane and methylpropane as discussed earlier in this chapter, between the experimental and calculated values of $RT\gamma_a$ and T_a at low temperatures. As with B no physical significance is attached to the parameters in the square-well model. Deviations of T_a from (40) and (16) are shown in figure 5.34 and generally are less than one standard deviation. The discrepancy at 310 K might be attributed to a systematic error induced by an inappropriate truncation of the pressure range to produce a three-term equation. However, removal of this point from the analysis did not alter significantly the value of C at other temperatures. Dymond and Smith[38] do not report any values of C in their comprehensive review of virial coefficients.

The values of B and C calculated from equations (38) and (40) are listed in table 5.11 at the experimental temperatures.

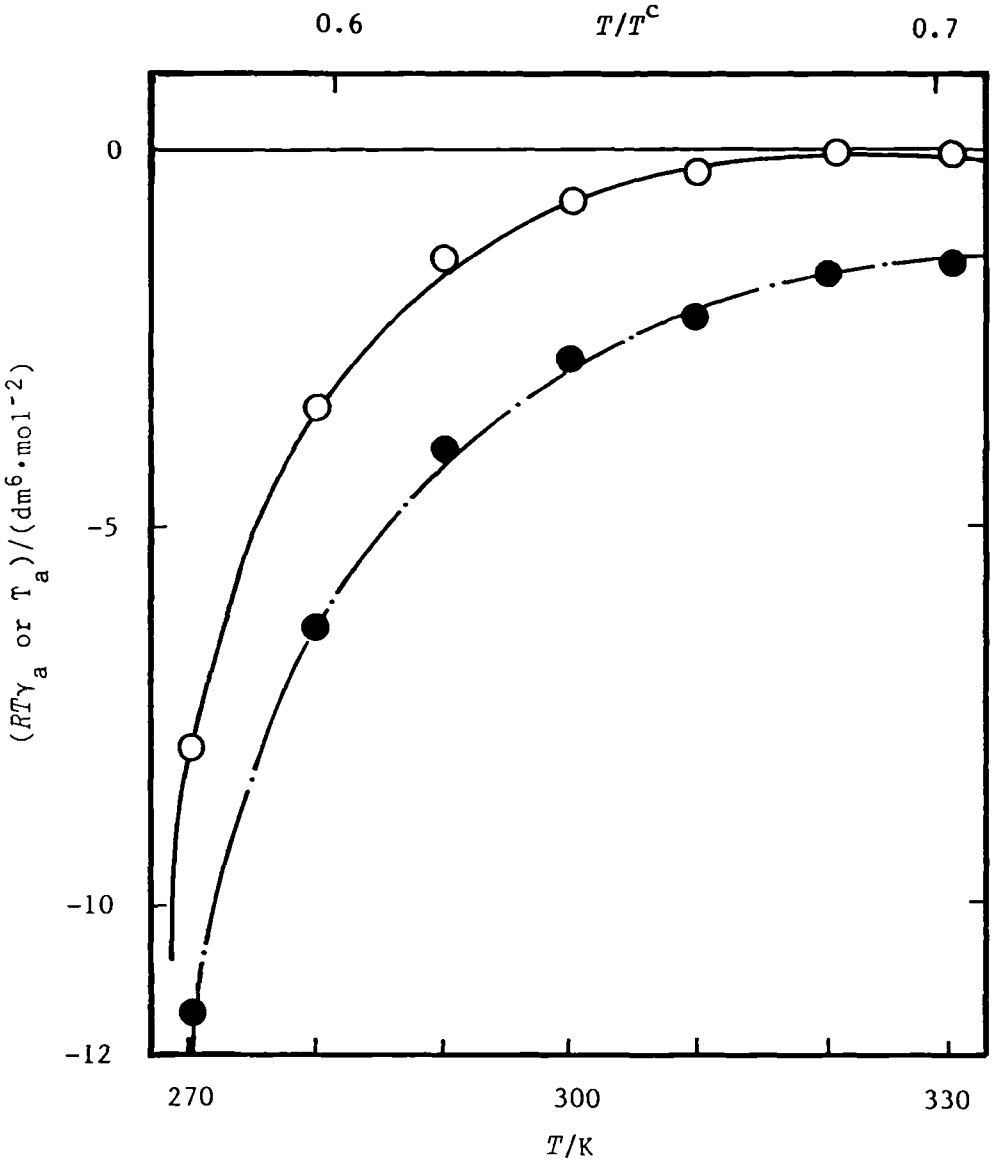

Figure 5.33. Apparent γ_a and derived quantity T_a for *n*-pentane. ● , $RT\gamma_a$; ○ , T_a; —·—, calculated from equation (15) and (16) with (36), (38) and (40); ———, calculated from equations (16) with (36) and (40).

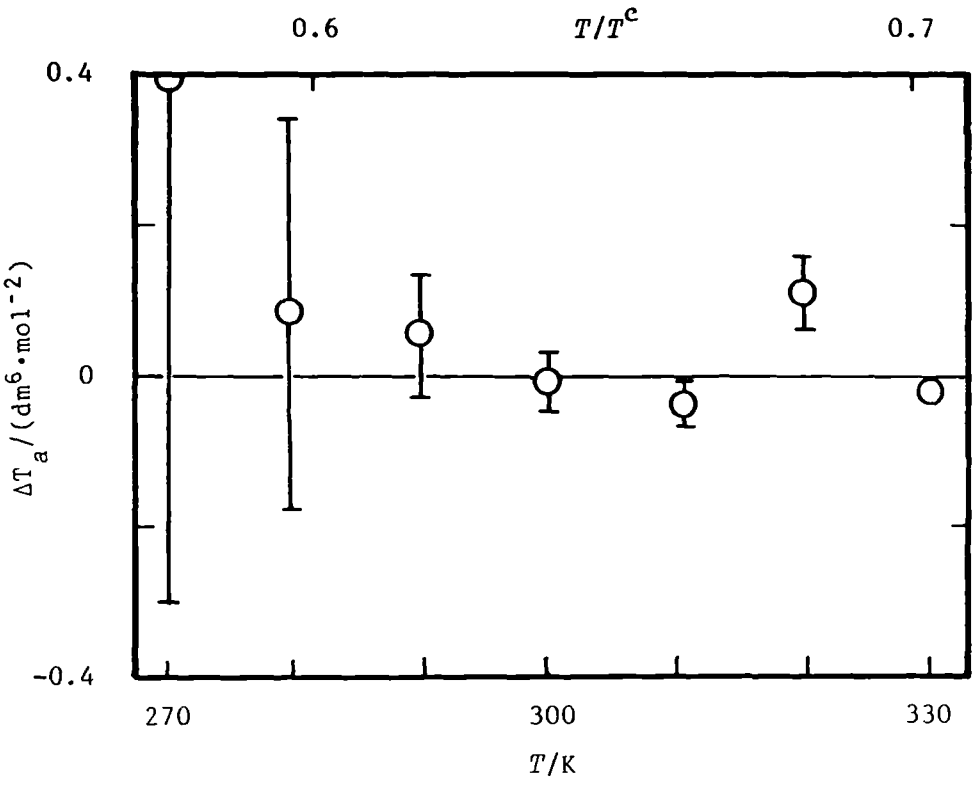

Figure 5.34. Deviations $\Delta T_a = \{T_a - T(calc.)\}$ of T_a from equation (16) with (40) and experimental γ^{pg}.

Table 5.11 Second and third virial coefficients from equations (38) and (40).

T/K	$B/(cm^3 \cdot mol^{-1})$	$C/(dm^6 \cdot mol^{-2})$	T/K	$B/(cm^3 \cdot mol^{-1})$	$C/(dm^6 \cdot mol^{-2})$
270	-1509.8	-7.934	280	-1375.8	-3.302
290	-1259.5	-1.440	300	-1157.8	-0.653
310	-1068.4	-0.306	320	-989.2	-0.147
330	-918.7	-0.072			

5.3.5 Methylbutane

Vapour pressure

The vapour pressures of methylbutane were determined as described in section two and are listed in table 5.12. The vapour pressures of water, which was used as the reference fluid, were calculated from the boiling temperatures using the tenth order Chebyshev series given by Ambrose.[86] The measurements covered the range $14.8 < p/\text{kPa} < 205$ and are described by an Antoine equation:

$$\ln(p^{g+l}/\text{kPa}) = 13.67562 - 2376.152/\{(T/\text{K}) - 38.646\}, \quad (5.3.41)$$

to 12 Pa in pressure or 5.0 mK in the temperature; the calculated normal boiling temperature is 300.993 K. The deviations of the experimental $p^{l+g}(T)$ from equation (41) are given in table 5.12 and shown in figure 5.35. The greatest deviation is 32 Pa at 323 K but this corresponds to a combined error in the boiling temperature of only 5 mK. Figure 5.35 shows that the ebulliometric results of Willingham *et al.*,[3] which cover the temperature range $289.4 \leqslant T/\text{K} \leqslant 301.7$, are in excellent agreement with the observations listed in table 5.12. The measurements of Schumann *et al.*[88] show deviations from equation (41) of between -38 and 271 Pa in the overlapping temperature range, while those of Silberberg and co-workers[87] at 323.15 K lies 99 Pa above (41). Since an extrapolation

Table 5.12. Vapour pressures p^{l+g} and deviations Δp from equation (41) for methylbutane at temperatures T.

T/K	p^{l+g}/kPa	Δp/Pa	T/K	p^{l+g}/kPa	Δp/Pa
255.109	14.861	4.7	290.006	68.204	5.5
257.986	17.155	-2.1	291.312	71.607	-6.6
258.008	17.176	0.3	296.079	85.227	-9.4
261.882	20.724	-3.8	296.087	85.256	-4.9
261.923	20.761	-7.4	301.267	102.275	-10.6
265.161	24.179	-1.8	301.266	102.282	-0.1
266.472	25.679	-6.4	305.827	119.347	-18.4
272.886	34.195	19.4	306.673	122.760	-3.6
276.157	39.309	9.3	309.904	136.415	-21.3
277.167	40.999	-1.3	311.422	143.422	-1.1
279.062	44.359	9.5	316.996	170.538	-14.8
282.596	51.177	0.5	317.003	170.588	-1.5
282.598	51.178	-2.6	323.086	204.771	15.3
286.525	59.726	5.8	323.092	204.824	32.2[a]

[a] omitted from figure 5.35.

of an Antoine equation above a reduced temperature of about 0.75 is often unreliable,[6] no comparison was attempted with the work of Silberberg *et al.*[87] above 348 K.

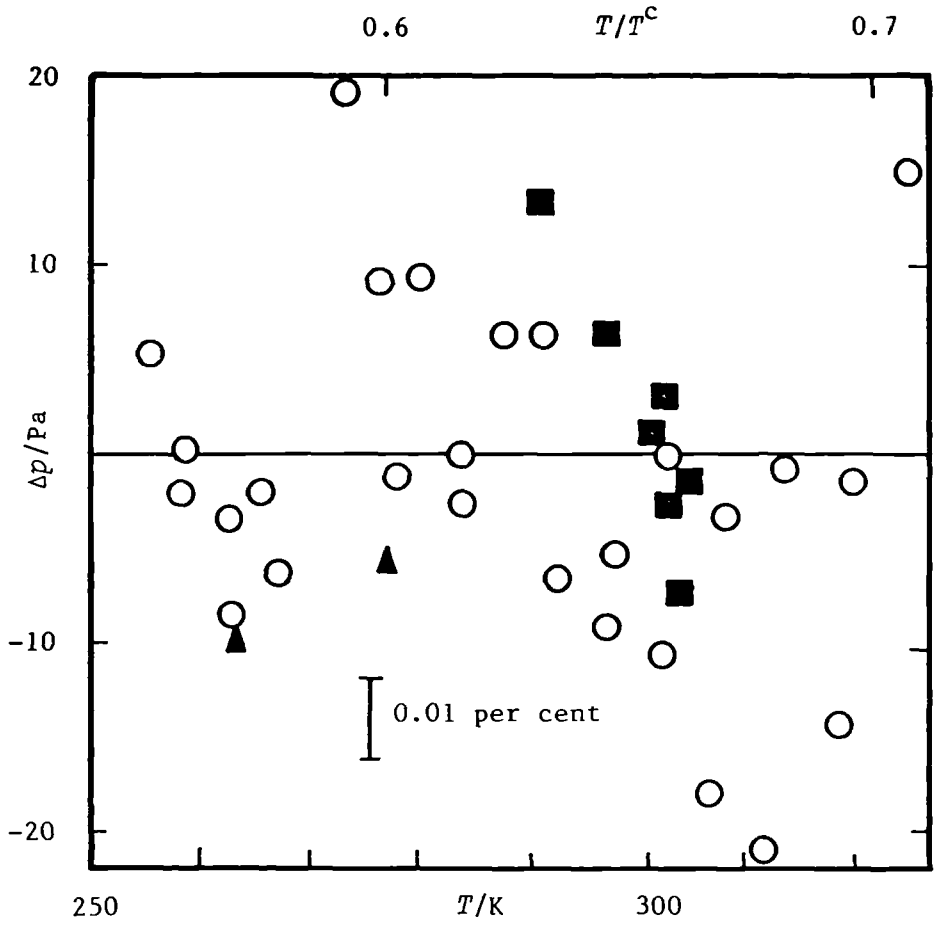

Figure 5.35. Deviations $\Delta p^{l+g} = \{p^{l+g} - p^{l+g}$ (calc.)$\}$ from equation (41). ○ , This work; ■ , reference 4; ▲ , reference 88. Deviations for several results of reference 88 are too large to be plotted on the figure.

Acoustic results

Seven isotherms between 260 and 320 K were studied for methylbutane, at pressures never greater than 60 per cent of the vapour pressure. The resonance frequencies were corrected to obtain the quantity (u/a), as described previously.

The transport properties used in the calculation of corrections are discussed below.

Parkinson and Gray[25] reported thermal conductivities for methylbutane at 323.15 and 373.15 K which can be described by equation (20) with n = 1.919 and $\kappa(T_2 = 323.15\ \mathrm{K}) = 17.49\ \mathrm{mW \cdot m^{-1} \cdot K^{-1}}$. The shear viscosities of Lambert *et al.*[59] in the temperature range 325.15 to 351.15 K, can be represented to 0.02 μPa·s by

$$\eta/(\mu\mathrm{Pa\ s}) = 1.17 + 0.0208\ (T/\mathrm{K}), \qquad (5.3.42)$$

which was extrapolated to the experimental temperatures.

Mean values of the speed of sound, calculated using the radius a given by equation (7), are reported in table 5.13 for each (p,T) state investigated, together with fractional standard deviations and the number of modes from which they were determined.

The bulk viscosities determined from analysis of the excess half width using equation (5), including the term b_r, are shown in figure 5.37. Assuming the vibrational states of methylbutane are strongly coupled, η_b give the quantity $t\rho$ which can be represented to 0.04 $\mathrm{ns \cdot kg \cdot m^{-3}}$ by

$$t\rho = -2.89 + 0.0212\ (T/\mathrm{K}), \qquad (5.3.43)$$

between 270 and 320 K; $t\rho$ at 260 K lies about 30 per cent below the value extrapolated from equation (43). The temperature dependence of $t\rho$ given by equation (43)

indicates that the interactions during molecular collisions are not purely repulsive. For the densities and frequencies studied in this work, u is not altered significantly by vibrational relaxation. As shown in figure 5.36, at 310 and 320 K the term b_r was about 3×10^{-6} or roughly equal to the value estimated from a typical isotherm in argon; at lower temperatures b_r

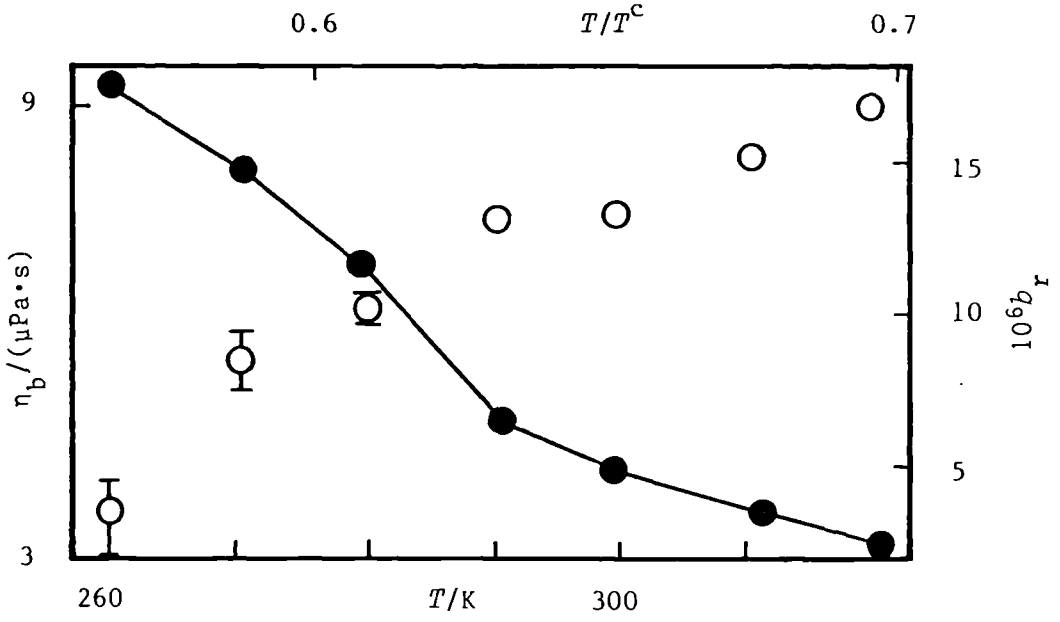

Figure 5.36. Bulk viscosities η_b (left-hand axis) and average excess half widths b_r (right-hand axis) for methylbutane obtained from residual experimental half widths after allowance for classical absorption, coupling tubes and thermal boundary layer with equation (5). O , η_b from analysis including b_r, and ●—● b_r. T^c from table 4.2.

Table 5.13. Mean speeds of sound u with standard deviations s determined from N radial modes {using equation (7) for a}, and deviations δ from equation (6) with three terms for methylbutane at temperatures T and pressures p.

T / K	p / kPa	u / m·s^{-1}	$10^6 s(u)/u$	N	$10^6 \delta(u^2)/u^2$
260.000	11.068	179.0757	9.2	7	(a)
	9.780	179.2162	8.0	5	-4.1
	8.945	179.3062	7.3	5	-1.6
	7.945	179.4135	3.5	4	3.5
	6.935	179.5206	3.3	4	2.8
	5.871	179.6321	6.3	5	-3.9
	4.904	179.7335	5.9	5	-1.2
	3.901	179.8380	5.2	5	2.1
	2.808	179.9505	6.4	2	-0.4
270.000	17.292	181.7648	6.5	7	(a)
	16.451	181.9034	5.9	7	-1.9
	14.793	182.0678	4.9	7	-0.2
	13.243	182.2157	4.4	7	-1.6
	11.486	182.3836	4.3	7	10.1
	9.784	182.5436	3.9	7	3.2
	8.407	182.6718	4.3	7	-8.3
	6.728	182.8288	4.1	5	-5.5
	4.974	182.9920	4.2	5	-0.5
	3.379	183.1396	4.0	5	4.8
280.000	27.376	184.2775	4.6	7	-3.0
	25.018	184.4840	1.4	6	5.3

T / K	p / kPa	u / m·s^{-1}	$10^6 s(u)/u$	N	$10^6 \delta(u^2)/u^2$
280.000	22.422	184.7087	3.7	7	-1.0
	19.786	184.9365	3.6	7	2.9
	17.330	185.1470	3.6	7	0.4
	14.753	185.3667	3.7	7	-1.8
	12.293	185.5754	3.3	7	-2.4
	9.531	185.8087	1.2	6	0.5
	7.026	186.0190	0.9	6	2.3
290.000	39.963	186.6076	3.8	7	-2.4
	36.276	186.9018	3.3	7	1.6
	32.098	187.2327	2.7	7	2.7
	28.293	187.5319	2.6	7	1.8
	24.341	187.8404	2.4	7	-1.8
	20.189	188.1625	2.0	7	-3.9
	15.979	188.4878	2.0	7	4.3
	11.612	188.8213	1.9	7	-3.4
	8.085	189.0898	0.7	6	0.1
	3.890	189.4068	5.1	6	1.4
300.000	58.361	188.5973	3.2	7	(a)
	51.630	189.0929	1.0	6	(a)
	45.897	189.5102	1.0	6	(a)
	39.810	189.9505	0.4	6	-1.6
	34.199	190.3528	1.6	7	1.4
	27.993	190.7941	1.2	7	1.6
	21.860	191.2265	1.0	7	-0.9
	15.956	191.6398	0.8	7	-0.4

T / K	p / kPa	u / m·s^{-1}	$10^6 s(u)/u$	N	$10^6 \delta(u^2)/u^2$
300.000	9.891	192.0611	0.5	7	0.1
	4.014	192.4663	0.3	4	1.6
310.000	80.921	190.4371	2.6	7	(a)
	69.802	191.1951	1.8	7	(a)
	61.254	191.7718	1.9	7	(a)
	54.151	192.2452	1.5	7	(a)
	46.057	192.7808	1.4	7	-0.0
	37.685	193.3280	1.2	7	-0.9
	29.761	193.8417	0.8	7	0.2
	21.665	194.3621	1.2	7	0.6
	13.908	194.8564	0.6	7	-0.8
	6.484	195.3260	0.8	7	0.5
320.000	76.840	194.1016	0.8	6	(a)
	69.888	194.5301	0.6	6	(a)
	62.610	194.9752	0.6	6	(a)
	54.840	195.4468	0.6	6	-0.9
	47.320	195.8997	1.4	7	1.0
	39.863	196.3454	1.2	7	0.5
	32.466	196.7843	1.0	7	-1.0
	25.894	197.1718	0.9	7	-1.0
	17.935	197.6380	0.8	7	0.5
	8.613	198.1812	1.0	7	(a)

(a), pressure omitted from final analysis.

increased, particularly rapidly below 290 K, reaching 17×10^{-6} at 270 K.

Figure 5.37(a) shows, for the isotherm at 270 K, the quantity $\Delta g/f$ (after allowance for η_b but not b_r). Clearly, except for the lowest pressure (3.4 kPa), $\Delta g/f$ declines with decreasing pressure and, although the (0,2) modes shows the same trend as observed previously, there is also some evidence for a frequency dependence; for the adjacent isotherm at 260 and 280 K these trends are magnified and reduced respectively. However, figure 5.37(b) shows $\Delta g/f$ at 300 K (after allowance for η_b but not b_r) and, except for the mode (0,2), this quantity is approximately independent of pressure and frequency as expected.

Figures 5.38 and 5.39 show, for the isotherms at 270 and 300 K, the deviations of the (u/a) obtained for each mode from that calculated using the final three-term smoothing equation. At both temperatures the highest pressure is about 60 per cent of the vapour pressure and (u/a) increases by 0.06 s^{-1} at 270 K and 0.03 s^{-1} at 300 K between the (0,2) and (0,8) modes; this clearly shows the effect of precondensation. At 300 K this systematic discrepancy between modes has disappeared by 0.25 p^{1+g} but for the 270 K isotherm the negative deviation of the (0,2) mode persists to the lowest pressures (similar behaviour was observed for *n*-pentane). These isotherms span approximately the same fractions of the vapour pressure

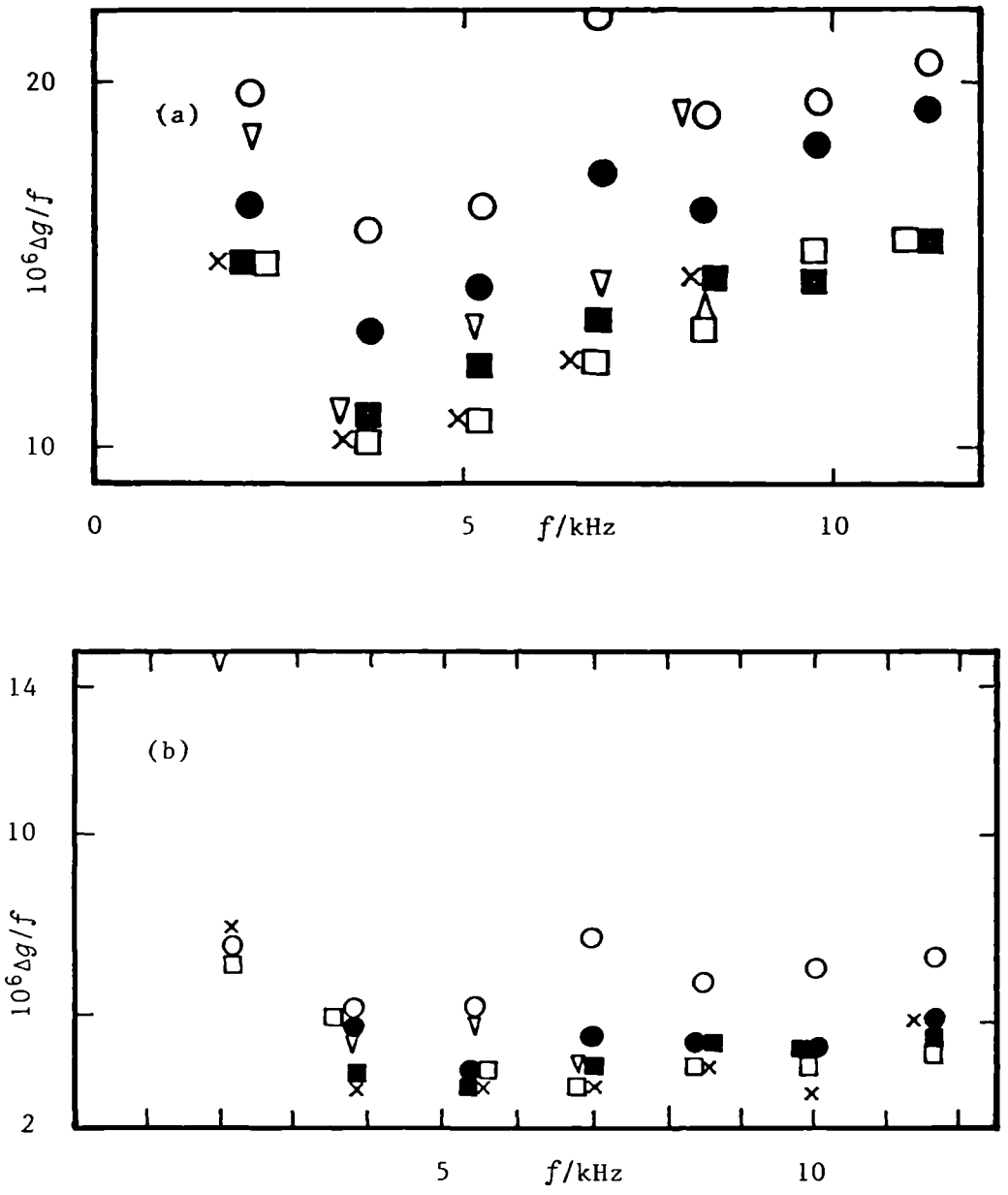

Figure 5.37. Fractional excess half widths $\Delta g/f$ for the lowest seven radial modes in methylbutane including η_b in equations (2) and (4), without b_r. (a) $\Delta g/f$ at 270 K. ○ , 17.9 kPa; ● , 16.5 kPa; ■ , 13.2 kPa; □ , 9.8 kPa; X , 6.7 kPa; ▽ , 3.4 kPa. (b) $\Delta g/f$ at 300 K. ○ , 58.4 kPa; ● , 45.9 kPa; ■ , 39.8 kPa; □ , 28.0 kPa; X , 16.0 kPa; ▽ , 4.0 kPa.

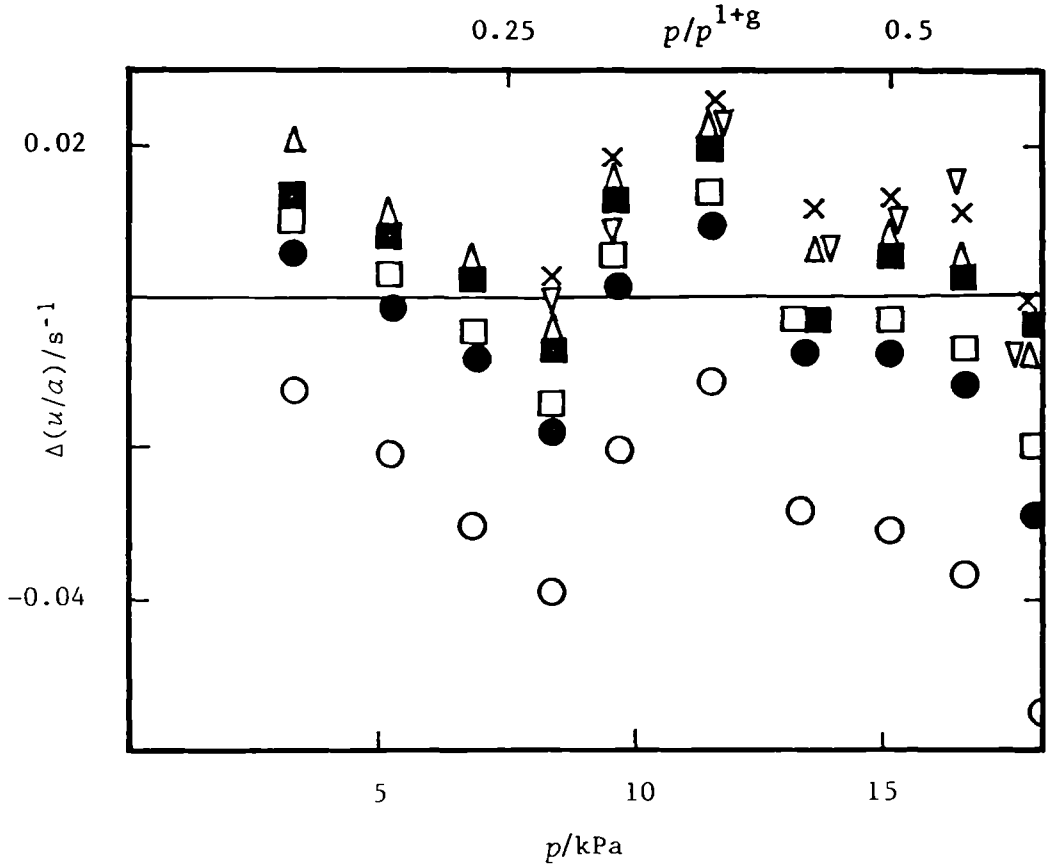

Figure 5.38. Deviations $\Delta(u/a) = [(u/a) - \{u(\text{calc.})/a\}]$, for individual modes in methylbutane at 270 K, from equation (6) with the leading three-term, for which the coefficients given in table 5.14 were adjusted to fit the results below 16.5 kPa. ○ , (0,2); ● , (0,3); □ , (0,4); ■ , (0,5); Δ , (0,6); ▽ , (0,7); X , (0,8). The vapour pressure was calculated from equation (41).

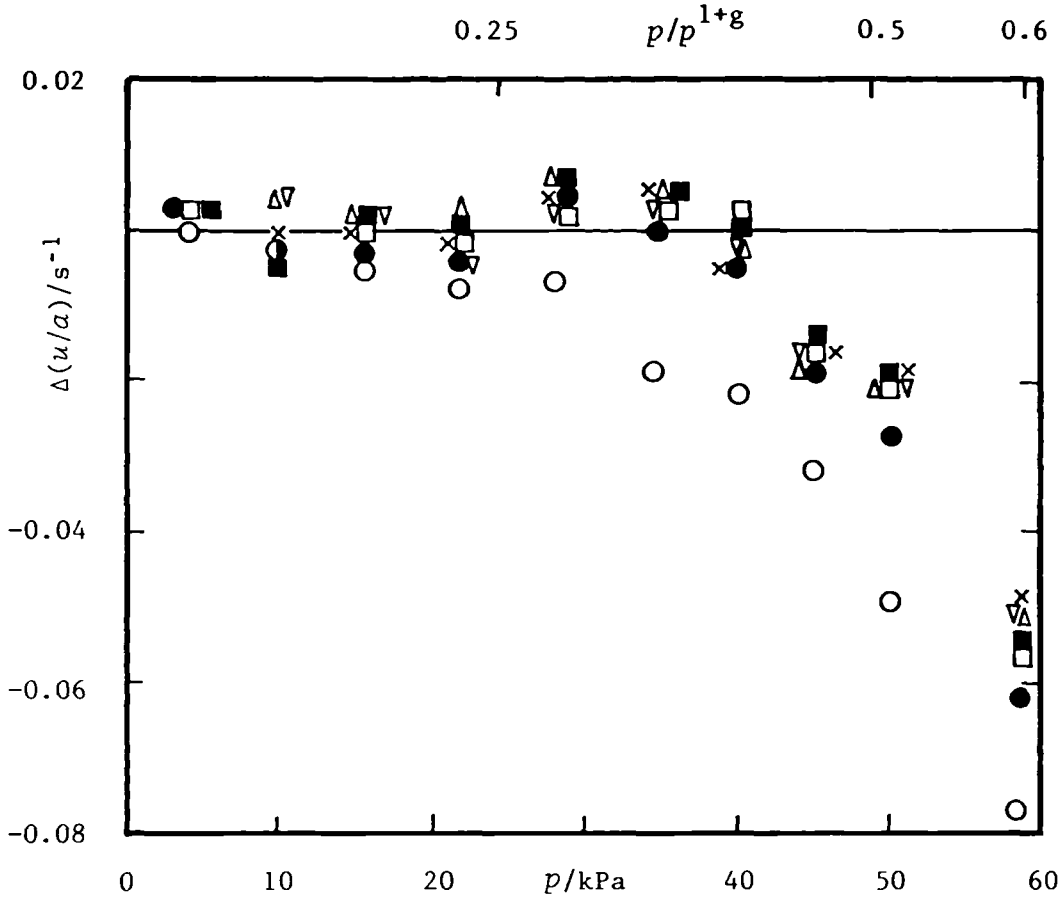

Figure 5.39. Deviations $\Delta(u/a) = [(u/a) - \{u(\text{calc.})/a\}]$, for individual modes in methylbutane at 320 K from equation (6) with the leading three-term, in which the coefficients reported in table 5.14 were adjusted to fit the results below 42 kPa. ○ , (0,2); ● , (0,3); □ , (0,4); ■ , (0,5); Δ , (0,6); ∇ , (0,7); X , (0,8). The vapour pressure was calculated from equation (41).

(and so the effects of precondensation should be roughly comparable) and the differences between the final pressures of an isotherm are not sufficiently large that the behaviour of the (0,2) mode at 270 K can be explained in terms of an increased demand on the acoustic model. Similar observations may be made of the 260 K isotherm and also for *n*-pentane.

Between 300 and 320 K four-term fits were required with equation (6) to represent adequately the (u/a) observations at all experimental pressures. Subsequently the pressure range was progressively truncated so as to produce the best three-term equation. (In figure 5.39 the pressures at 45.9 and 51.6 kPa were omitted to obtain the best three-term equation while the results at 58.4 kPa were omitted because of precondensation.) Where some of the higher pressures were omitted to obtain the best three-term equations, the values of $C_{p,m}^{pg}$ and β_a differ by no more than 0.003 R (0.02 per cent) and 3.3 $cm^3 \cdot mol^{-1}$ (0.2 per cent) from those obtained with a four-term fit of all pressures except those affected by precondensation. The pressures omitted from the final regression analysis are indicated in table 5.13.

The results of the analysis are given in table 5.14 together with the number of resonance frequencies in the final regression. The coefficients, which were all significant at a probability of 0.999 and were insensitive to further truncation of the pressure range, are expressed

Table 5.14 Perfect-gas heat capacities, second and third acoustic virial coefficients, and standard deviations s obtained by analysis of N modes for methylbutane. The resonator radius $a(T)$ required to determine $C_{p,m}^{pg}(T)$ was given equation (7). The quoted uncertainties are one standard deviation.

T/K	N	$C_{p,m}^{pg}/R$	$\beta_a/(cm^3 \cdot mol^{-1})$	$\gamma_a/(cm^3 \cdot mol^{-1} \cdot kPa^{-1})$	$10^6 s(u^2)/u^2$
260.000	27	12.8743 ± 0.0063	-2415.8 ± 15.5	-8.0 ± 1.3	10.6
270.000	54	13.2546 ± 0.0026	-2223.8 ± 3.9	-3.46 ± 0.19	10.0
280.000	57	13.6352 ± 0.0022	-2055.0 ± 1.8	-1.835 ± 0.005	6.6
290.000	65	14.0209 ± 0.0010	-1901.1 ± 0.7	-1.224 ± 0.001	5.9
300.000	42	14.4114 ± 0.0005	-1767.9 ± 0.3	-0.833 ± 0.007	2.1
310.000	39	14.8053 ± 0.0005	-1647.7 ± 0.3	-0.602 ± 0.005	2.1
320.000	38	15.2062 ± 0.0013	-1536.0 ± 0.5	-0.509 ± 0.007	2.0

as perfect gas heat capacities at constant pressure and acoustic virial coefficients.

Regression analysis of the heat capacities in table 5.14 when weighted by their standard deviations gave

$$C_{p,m}^{pg}/R = 0.0436\ (T/K) + 396\ (K/T); \qquad (5.3.44)$$

the coefficients were significant at a probability better than 0.999. The experimental results are compared with this equation in figure 5.40(a); the maximum deviation is only 0.005 R and the weighted standard deviation of the fit is 0.0015 R (about 0.01_1 per cent). Therefore, the heat capacities of methylbutane are internally consistent at a

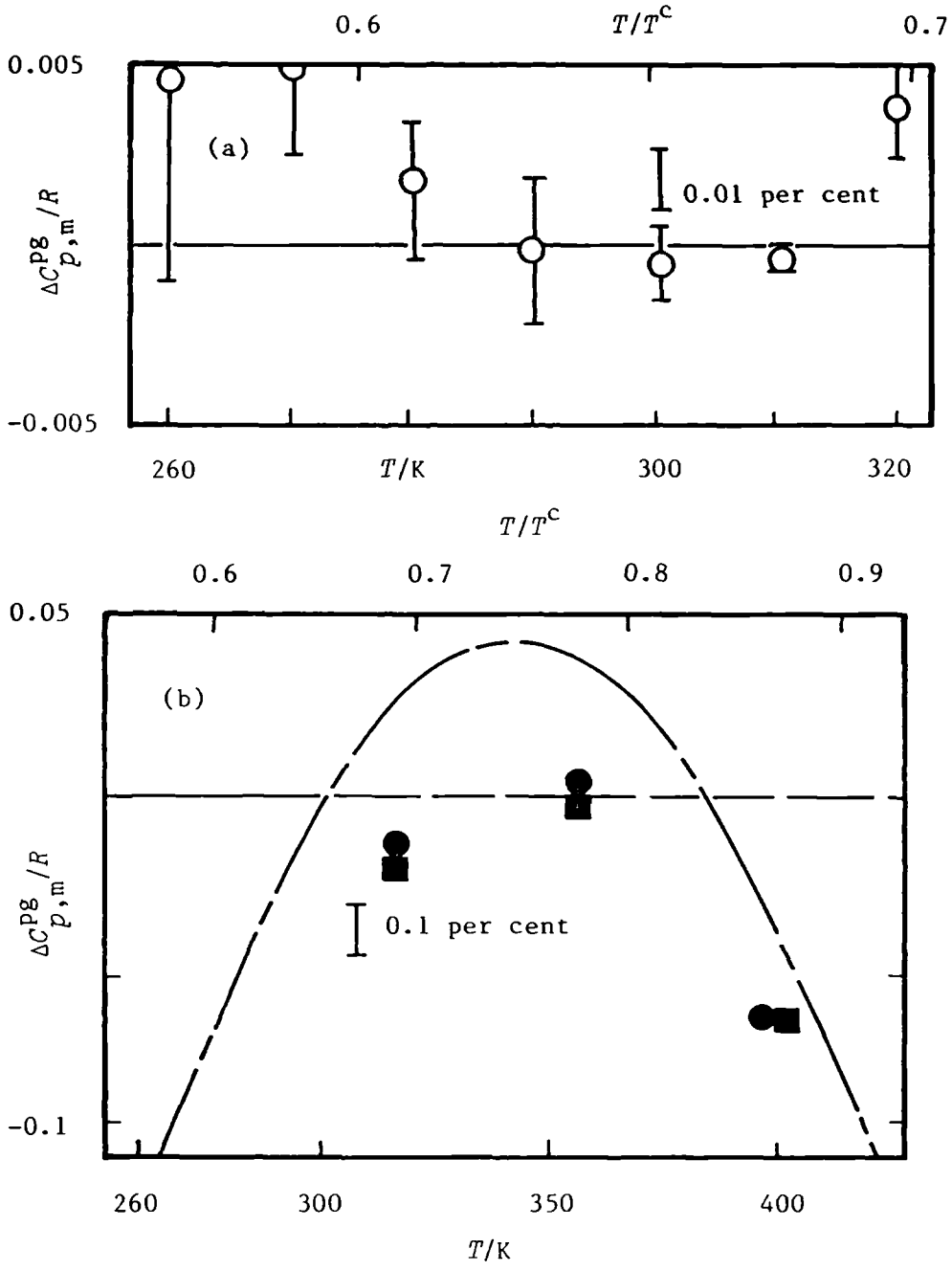

Figure 5.40. (a), Deviations $\Delta C^{pg}_{p,m} = C^{pg}_{p,m} - C^{pg}_{p,m}$(calc.) of experimental molar heat capacities at constant pressure from equation (44). (b), Deviations $\Delta C^{pg}_{p,m} = C^{pg}_{p,m} - C^{pg}_{p,m}$(calc.) of literature heat capacities from equation (44), where the ordinate scale has been compressed by a factor of 10 compared with (a). ■ , Reference 89; ● , reference 36; — – — calculated using equations (30) and (31) with constants from table 5.7.[70,71]

level which is about a factor of 10 better than the other hydrocarbons discussed here. Methylbutane is particularly suited to purification by fractional distillation and great care was taken. Excluding air and water, the mole fraction was greater than 0.9999. The maximum deviation of 0.005 R could result from variations in the mole fraction of air by 4×10^{-5} or of water by 3×10^{-5}. Although the standard deviations quoted in table 5.14 for $C^{pg}_{p,m}/R$ exceed the most optimistic estimate (about $C^{pg}_{V,m}\ \delta u/u \approx 26 \times 10^{-6}\ R$) they are remarkably small considering that, at 260 K for example, the 1 Pa resolution in the pressure gauge represents up to 350×10^{-6} of the pressure.

Assuming the second (p, V_m, T) virial coefficients may be represented by the expression derived from the square-well Potential. Weighted non-linear regression using the results of table 5.14 gave

$$B(T)/(\mathrm{cm}^3 \cdot \mathrm{mol}^{-1}) = 753.2 - 473.19 \exp(400\ \mathrm{K}/T), \quad (5.3.45)$$

with a standard deviation of 1.1 $\mathrm{cm}^3 \cdot \mathrm{mol}^{-1}$ (about 0.05 per cent). The power series in temperature representation for B, equation (13), gave

$$B(T)/(\mathrm{cm}^3 \cdot \mathrm{mol}^{-1}) = 85.6 \times 10^3\ (\mathrm{K}/T) - 119.43 \times 10^6\ (\mathrm{K}/T)^2, \quad (5.3.46)$$

also with a standard deviation of 1.1 $\mathrm{cm}^3 \cdot \mathrm{mol}^{-1}$ in β_a. Figure 5.41 shows deviations of β_a from equations (2.2.34) and (45). The variation, which is less than 1 per cent,

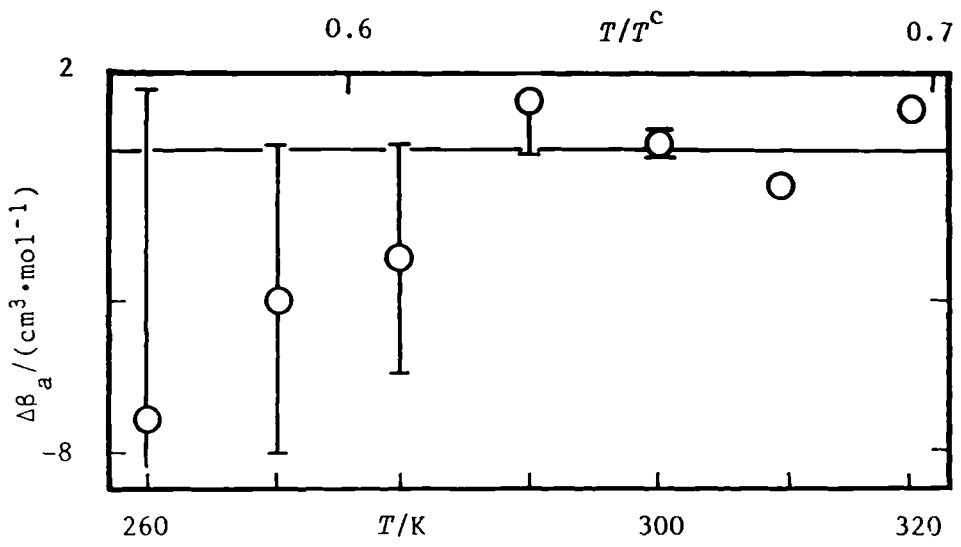

Figure 5.41. Deviations $\Delta\beta_a = \{\beta_a - \beta_a(\text{calc.})\}$, of experimental β_a from equations (2.3.23) using (45) and experimental γ^{pg}.

---

in estimates of B given by equations (45) and (46) as solutions for (2.3.23) are shown in figure 5.42(a).

The second virial coefficients reported by other workers are plotted as deviations from equation (45) in figure 5.42(b). Over the experimental temperature range the values derived by Scott *et al.*[89] from their enthalpies of vaporation show discrepancies of about -90 $cm^3 \cdot mol^{-1}$, and the measurement reported by Mason and Eakin[43] lies 121 $cm^3 \cdot mol^{-1}$ below equation (45). The only (p, V_m, T) measurements at higher temperatures cited by Dymond and Smith[92] are those of Silberberg and co-workers;[87] their second virial coefficients agree with (45) to within

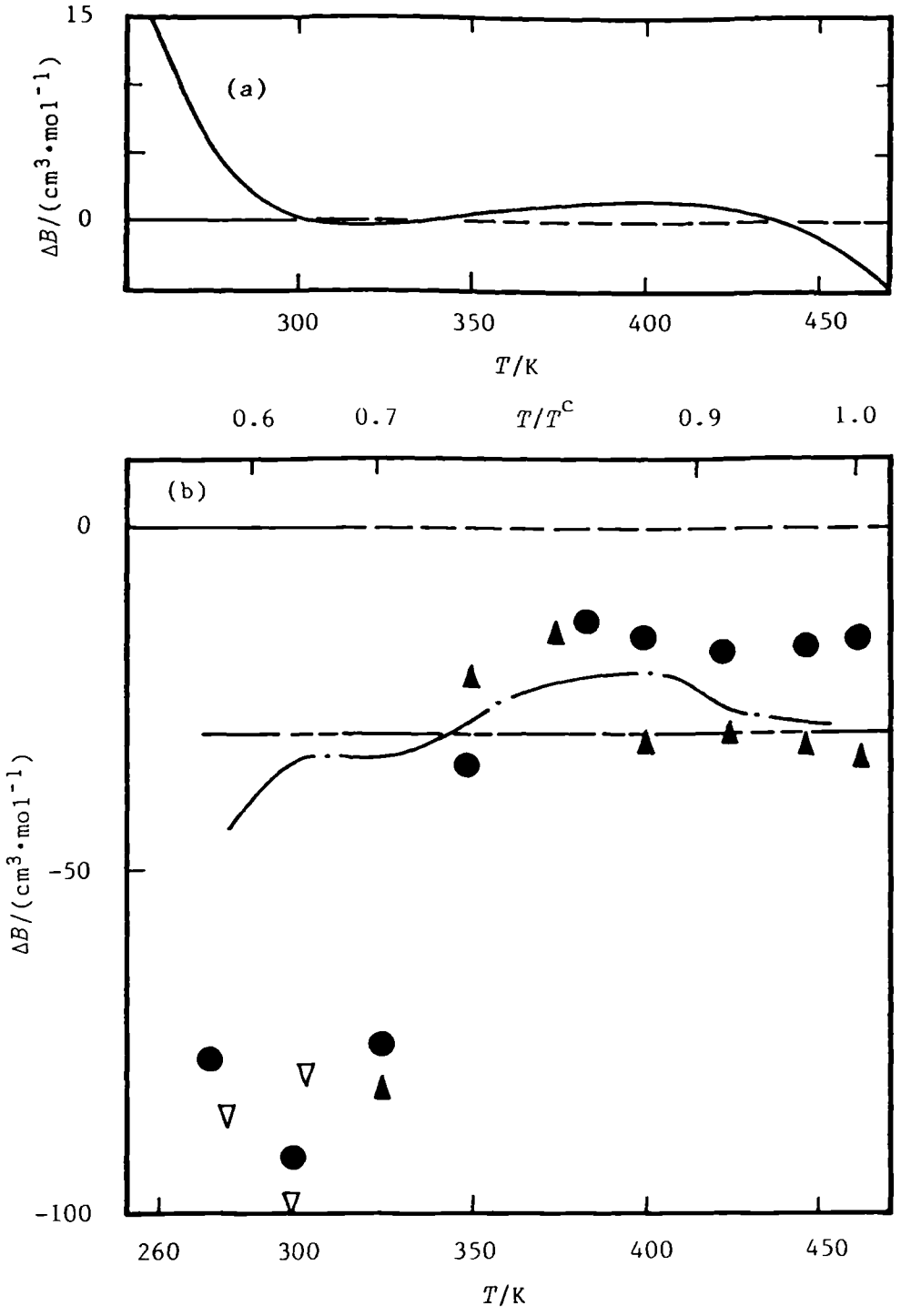

Figure 5.42. (a), Deviations ΔB = B(alt.) - B(calc.) of the alternative solution to B(alt.) given by (46) of equation (2.3.23) from equation (45). (b), Deviations ΔB = {B - B(calc.)}, of second virial coefficients from equation (45). ▲ , Reference 87; ▽ , reference 89; ● , reference 90; — — — —, reference 91; —• —. reference 92.

their stated bounds and show deviations of -80 $cm^3 \cdot mol^{-1}$ at 343.15 K and about -40 $cm^3 \cdot mol^{-1}$ between 348.15 and 473.15 K. Silberberg, Lin and McKetta have subsequently reanalysed these measurements and estimate the error to be less than 2 per cent.[90] The recent correlation of Das *et al.*[19] appear to contain a systematic error; Dymond and Smith's recommendations are derived from this correlation.[92]

The experimental quantity $RT\gamma_a$ is shown in figure 5.43 together with the derived quantity T_a obtained using equations (45) and (15) and the experimental γ^{pg}. The uncertainty in T_a arises almost entirely from that in $RT\gamma_a$ and varies rapidly from less than 0.02 $dm^6 \cdot mol^{-2}$ at the higher temperatures to 2.8 $dm^6 \cdot mol^{-2}$ at 260 K (about 16 per cent), reflecting the decrease in the accessible pressure range. If it is assumed that the third virial coefficient C can be represented by the square-well model analytic expression (15), then weighted non-linear regression with T_a and experimental γ^{pg} gives

$$C/b_0^2 = 0.625 - 1.5006 \times 10^{-2}x + 1.4458 \times 10^{-4}x^2 - 3.8625 \times 10^{-7}x^3, \qquad (5.3.47)$$

where $x = \{\exp(1790\ K/T) - 1\}$ and $b_0 = 0.232\ dm^6 \cdot mol^{-2}$, with a standard deviation of 0.01 $dm^6 \cdot mol^{-2}$ in T_a. Deviations of T_a from values calculated using equations (16) and (47) are less than one standard deviation. The

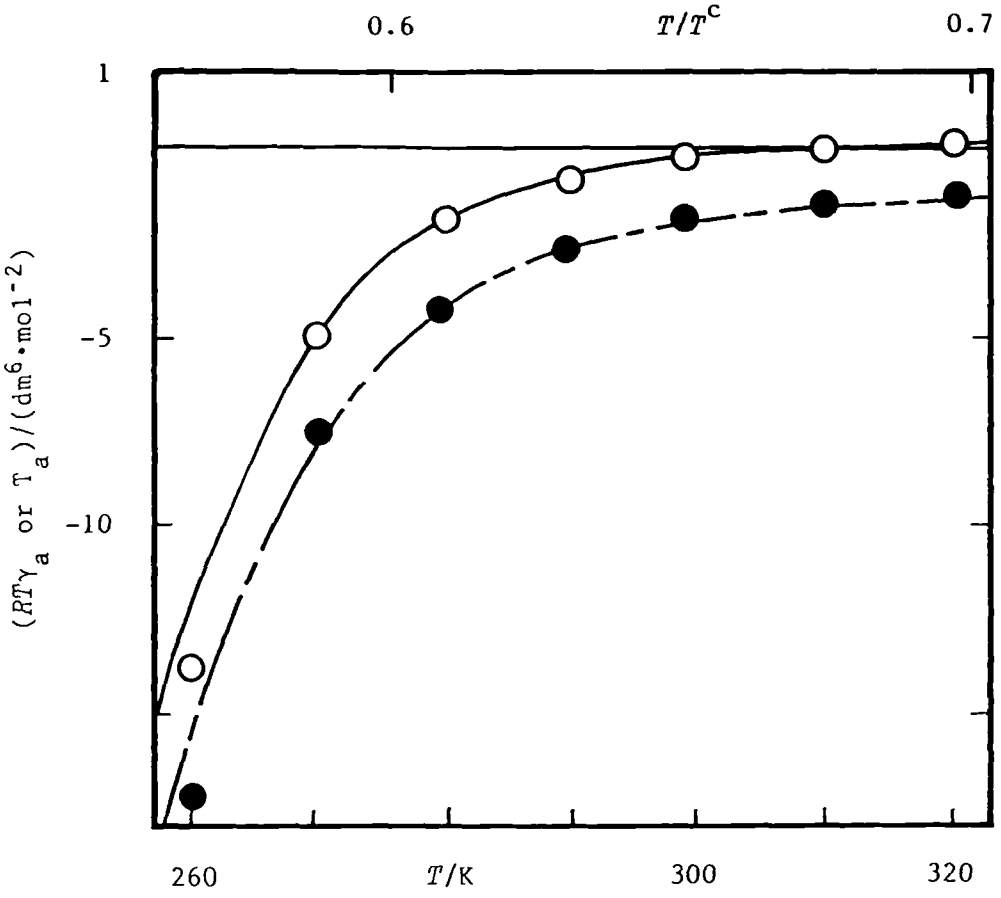

Figure 5.43. Third acoustic virial coefficients γ_a and derived quantities T_a for methylbutane. ● , $RT\gamma_a$; ○ , T_a; ——·—— calculated from equations (15) and (16) with (44), (45) and (47); ———, calculated from (16) with (44) and (47). T^c from table 4.2.

(p, V_m, T) measurements of Silberberg and co-workers,[87] as reanalysed by Silberberg, Lin and McKetta,[90] give the values of C which are compared in figure 5.44 with those calculated from equation (47); no other values of C are cited by Dymond and Smith in their comprehensive review.[92]

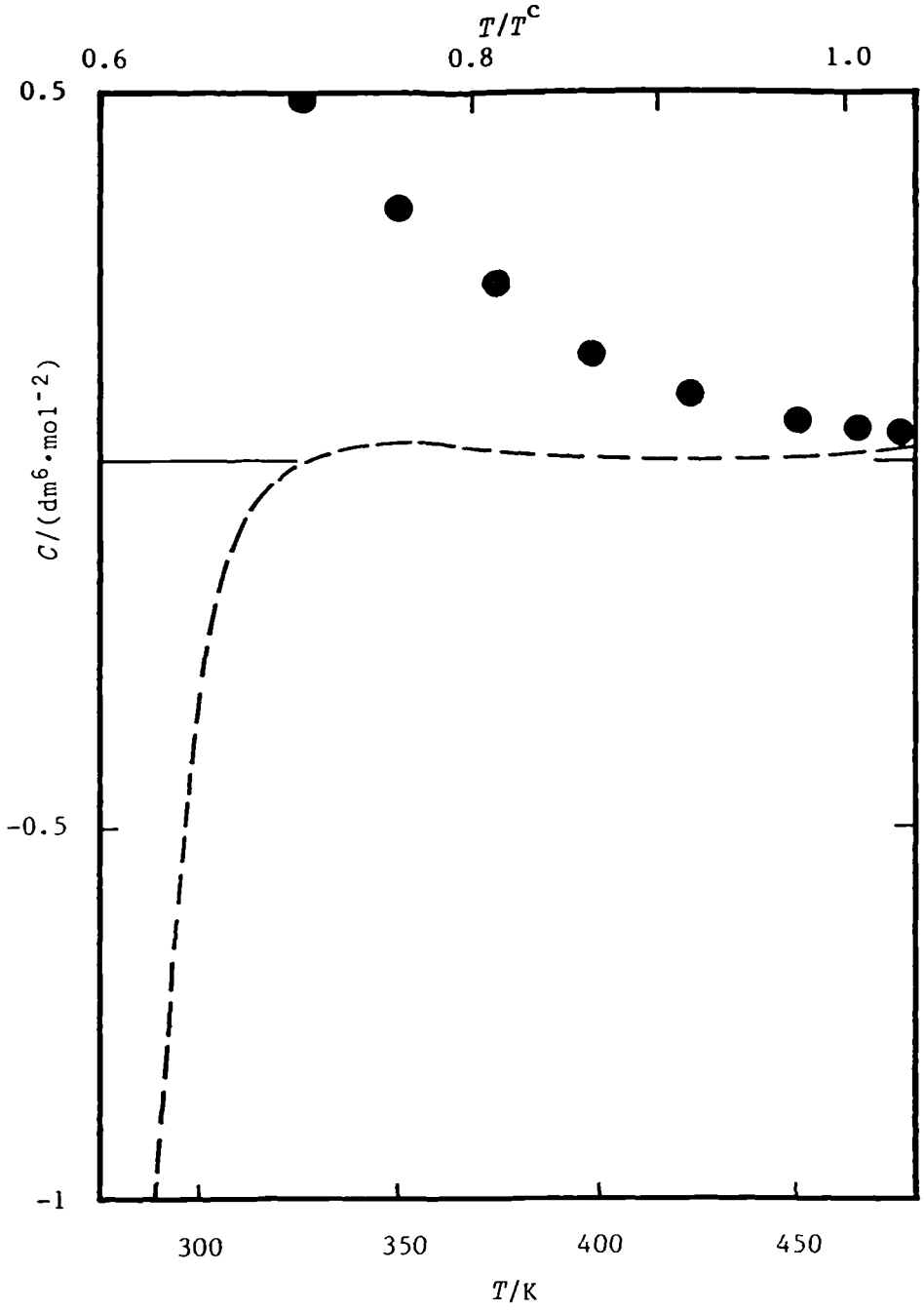

Figure 5.44. Third (p,V_m,T) virial coefficients, ● , references 87 and 90; - - - - , this work equation (47).

Table 5.15 Second and third virial coefficients from equations (45) and (47).

T/K	B/(cm^3·mol^{-1})	C/(dm^6·mol^{-2})	T/K	B/(cm^3·mol^{-1})	C/(dm^6·mol^{-2})
260	-1450.6	-12.6365	270	-1328.5	-5.1014
280	-1221.3	-2.0862	290	-1126.3	-0.8451
300	-1041.9	-0.3267	310	-966.3	-0.1109
320	-898.4	-0.0238			

Values of B and C calculated from equations (45) and (47) are listed in table 5.15 at the experimental temperatures.

5.3.6 Dimethylpropane

These measurements have been reported elsewhere,[93] and a reprint of this publication is given in Appendix A.1. In this section additional comparisons and analysis are reported.

As for the other hydrocarbons discussed here the correlation for $C_{p,m}^{pg}$ due to Wilhoit[70] (see equations (30) and (31) and table 5.7) is remarkably successful and deviates by between -0.08 R and 0.03 R from equation (A1.36) which fits the acoustic[93] and flow calorimetric[78] results.

In Appendix 1 the third coefficient C' was estimated from equation (2.3.35) using experimental γ_a, and $C_{p,m}^{pg}$ and the smoothing equation (A1.37) for B by imposing the functional form $C' = A\exp(B/T)$. Here the alternative functional form, equation (17), has been chosen for C with

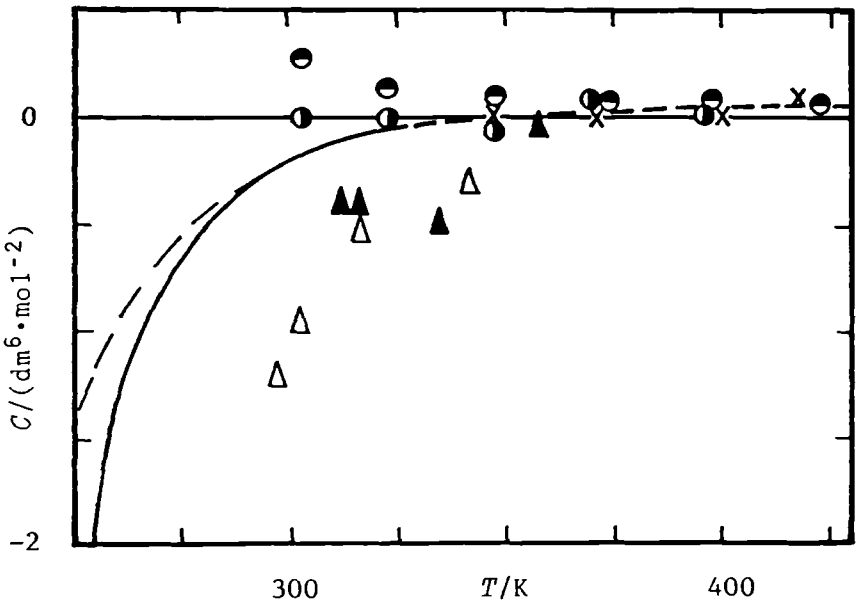

Figure 5.45. Third (p,V_m,T) virial coefficients. ◑ , Reference 95; ◓ , reference 90; X , reference 94; Δ , reference 96; ▲ , reference 97; - - - -, equation (A1.39) with (A1.37) and (A1.38); ———, equation (48).

---

the result

$$C/b_0^2 = 0.625 - 0.3762x + 0.0991x^2 - 6.9458 \times 10^{-3}x^3, \quad (5.3.48)$$

where $x = \{\exp(820\ \mathrm{K}/T) - 1\}$, $b_0 = 0.169\ \mathrm{dm^3 \cdot mol^{-1}}$; the weighted standard deviation of T_a was $0.019\ \mathrm{dm^6 \cdot mol^{-2}}$. Figure 5.45 compared the two methods of estimating C. The results are indistinguishable above 290 K, even when extrapolated to 425 K, but at lower temperatures the curves separate and at the lowest experimental temperature (250 K) the deviation has reached $0.33\ \mathrm{dm^6 \cdot mol^{-2}}$. Although this

represents about 18 per cent of C, the agreement is remarkably good in view of the maximum pressure of 14.3 kPa for the 250 K isotherm {γ_a (250 K), consequently, had a low weight in both analyses} and the differences in the functional forms adopted for C' or C. Figure 5.45 also shows the third virial coefficients obtained from (p,V_m,T) measurements; these are discussed in Appendix 1.

5.3.7 Methanol

Table 5.16 lists mean value of u for each pressure on the nine isotherms between 280 and 329 K, together with fractional standard deviations and number of radial modes from which they were determined; small corrections have been applied to reduce all values to the stated temperatures for each isotherm. The maximum pressure for an isotherm was always less than 60 per cent of the vapour pressure; the vapour pressure was taken from reference (98).

The virial coefficients used in the calculation of the corrections for the thermal boundary layer were estimated from a preliminary analysis of the acoustic measurements and an expression given by Francis and Phutela.[99] Although these values of B are rather uncertain, their omission from the analysis had no significant effect. The transport properties used in the calculations are discussed below.

The four shear viscosity measurements on methanol between 308.15 and 350.95 K reported by Craven and Lambert,[101]

Table 5.16. Mean speeds of sound u with standard deviations s determined from N radial modes, and devitions δ from equation (53) with the leading three terms at temperatures T and pressures p for methanol. $A_3 = \delta_a A_0/(RT)$ in equation (53).

T / K	p / kPa	u / m·s^{-1}	$10^6 s(u)/u$	N	$10^6 \delta(u^2)/u^2$
280.000	3.002	297.1741	2.9	3	(a)
	2.980	297.6215	1.6	4	(a)
	2.652	298.1773	1.5	2	-8.6
	2.443	298.4986	8.8	5	8.6
	2.173	298.8467	18.6	5	7.5
	1.980	299.0524	9.9	5	-16.2
	1.797	299.2466	11.0	5	(a)
	1.412	299.5100	9.4	5	5.5
285.000	4.238	299.5294	6.0	5	(a)
	3.882	300.0605	3.5	4	4.6
	3.605	300.4294	6.5	5	-5.2
	3.243	300.8591	2.0	3	(a)
	2.920	301.1638	1.3	3	-5.8
	2.648	301.3942	3.5	4	6.4
	2.224	301.6905	2.5	4	9.5
	1.898	301.8722	8.6	5	-5.5
	1.592	302.0167	13.4	5	-0.7
290.000	5.890	301.5005	4.7	5	(a)
	5.231	302.2362	3.5	5	(a)
	4.954	302.5330	4.6	5	(a)

T / K	p / kPa	u / m·s^{-1}	$10^6 s(u)/u$	N	$10^6 \delta(u^2)/u^2$
290.000	4.478	302.9714	4.2	5	0.0
	4.001	303.3759	4.7	5	(a)
	3.496	303.7338	3.9	5	(a)
	2.997	304.0012	4.3	5	-0.2
	2.485	304.2330	1.4	3	0.5
	1.979	304.4149	5.9	5	-0.1
	1.512	304.5544	7.7	5	(a)
295.000	7.745	303.5692	2.6	5	(a)
	7.075	304.2099	2.3	5	(a)
	6.390	304.7928	2.5	5	(a)
	5.694	305.2992	2.8	5	4.1
	4.940	305.7565	2.7	5	-11.3
	4.256	306.1003	2.5	5	9.6
	3.506	306.4001	4.5	5	-6.3
	2.793	306.6328	10.5	5	10.1
	2.081	306.8156	17.3	5	-9.4
	1.357	306.9741	5.8	5	12.0
300.000	10.180	305.6294	2.1	5	(a)
	9.327	306.2868	2.8	4	(a)
	8.556	306.8184	2.6	5	(a)
	7.641	307.3711	1.6	5	(a)
	6.729	307.8394	1.9	5	1.0
	5.987	308.1635	2.0	5	-2.9
	4.960	308.5366	2.1	5	2.3
	3.877	308.8478	2.9	4	-0.9

T / K	p / kPa	u / m·s^{-1}	$10^6 s(u)/u$	N	$10^6 \delta(u^2)/u^2$
300.000	2.887	309.0752	4.1	4	-2.3
	1.910	309.2606	22.3	5	1.3
305.000	13.952	307.2262	1.2	5	(a)
	13.211	307.6811	1.2	5	(a)
	11.962	308.4444	1.3	5	(a)
	10.807	309.0736	1.3	5	(a)
	9.601	309.6397	1.7	5	2.9
	8.659	310.0256	1.7	5	-3.0
	7.482	310.4362	1.8	5	-7.0
	6.067	310.8422	3.0	5	11.1
	4.580	311.1760	3.8	4	-5.4
	3.505	311.3757	4.4	3	(a)
310.000	17.157	309.5951	2.6	5	(a)
	15.740	310.3136	1.3	5	(a)
	14.347	310.9502	0.9	5	(a)
	12.982	311.5038	1.3	5	(a)
	11.528	312.0190	0.4	5	1.3
	9.812	312.5321	1.0	5	-3.2
	8.325	312.9017	1.2	5	0.7
	6.755	313.2272	2.9	5	$0.\bar{8}$
	5.307	313.4796	0.7	4	1.9
	3.720	313.7147	4.7	4	-1.8
	2.338	313.8960	5.9	2	4.6

T / K	p / kPa	u / m·s^{-1}	$10^6 s(u)/u$	N	$10^6 \delta(u^2)/u^2$
315.000	19.568	312.4680	2.3	5	(*a*)
	17.164	313.3265	1.7	5	(*a*)
	15.461	313.8539	1.6	5	(*a*)
	13.481	314.3862	1.1	5	2.0
	9.517	315.2167	1.7	5	-3.4
	7.585	315.5282	1.4	5	-0.4
	6.198	315.7234	2.1	5	1.1
	4.582	315.9251	7.8	5	4.0
	2.720	316.1371	8.3	3	6.1
320.000	22.444	315.0924	1.8	5	(*a*)
	20.544	315.6082	1.5	5	(*a*)
	18.184	316.1765	1.3	5	(*a*)
	16.521	316.5308	1.4	5	2.5
	14.503	316.9130	1.1	5	-4.1
	11.909	317.3359	0.9	5	-1.3
	10.267	317.5691	1.9	5	2.3
	8.135	317.8378	1.3	5	2.2
	6.166	318.0588	2.2	5	-0.0
	4.313	318.2488	7.0	5	-2.3
	2.733	318.4019	4.7	3	1.2

(*a*), pressure omitted from final analysis.

can be represented to 0.03 μPa•s by

$$\eta/(\mu Pa \cdot s) = 0.03286\ (T/K), \qquad (5.3.49)$$

which was used to estimate η at the required temperatures.

The thermal conductivity measurements reported by Renner, Kucera, and Blander[102] at five temperatures between from 306.9 to 345.1 K at pressures in the range $73 \leqslant p/kPa \leqslant p^{1+g}$ were analysed using the adaptive regression algorithm.[16] At each temperature a constant and a term in p^3 were the only terms required from the array p^{-3} to p^3; each term entered with a high degree of significance (>0.99). The results of these analyses are given in table 5.17. These $\kappa(T,p=0)$ estimates may be represented by

$$\kappa(T,p=0)/(mW \cdot m^{-1} \cdot K^{-1}) = 0.1818 \times 10^{-3}\ (T/K)^2, \qquad (5.3.50)$$

to 0.09 $mW \cdot m^{-1} \cdot K^{-1}$. For the pressure range covered by the acoustic measurements the pressure dependence of κ is small, for example, κ(306.9 K, 10 kPa) differs from $\kappa(T,p=0)$ by 2 per cent. More recently, Frurip, Curtiss and Blander[103] reported thermal conductivities $\kappa(T,p)$ of gaseous methanol in the temperature range 337.6 to 419.9 K, from which they obtained $\kappa(T,p=0)$ and subsequently the simple expression:

$$\kappa(T,p=0)/(mW \cdot m^{-1} \cdot K^{-1}) = -16.40 + 0.1025\ (T/K). \qquad (5.3.51)$$

Equation (51) is in good agreement with the measurements of several other workers.[104-106]

In preliminary analyses of excess line widths using equation (5) at 315 and 320 K using κ from equation (51),

Table 5.17. $\kappa(T, p = 0)$ and pressure dependence a_1 of the equation $\kappa(T, p) = \kappa(T, p=0) + a_1 p^3$, obtained from analysis of the $\kappa(T, p)$ measurements reported by Renner *etal.*[102] for methanol at temperatures T.

T/K	$\kappa(T, p= 0)/(mW \cdot m^{-1} \cdot K^{-1})$	$10^6 a_1/(mW \cdot m^{-1} \cdot K^{-1} \cdot kPa^{-1})$
306.9	17.00	373.0
316.6	18.28	118.1
326.6	19.50	34.98
337.4	20.71	9.991
345.1	21.59	4.699

it was found necessary to include the terms $b_b(\eta_b)$, b_b', and b_h. However, the values of b_h so obtained implied that the thermal conductivities should be increased by about 2.6_5 $mW \cdot m^{-1} \cdot K^{-1}$ or very close to those calculated from equation (50). Consequently, for the remaining analyses, κ was taken from equation (50) and then the term b_h was not required. Below 295 K if all pressures were considered, b_b' (the apparent density dependence of η_b) was the only significant term in the analysis of Δg when κ was estimated with equation (50); at 280 K B_b' reached 600 $\mu Pa \cdot s^{-1}$. However, the resulting $\Delta g/f$ showed a systematic undulation which implied that the choice of just b_b' was not entirely suitable; selection of an additional term (none of which were significant at a probability of 0.99) did not alter this trend. If the

vibrational states of methanol are assumed to be strongly coupled, the value of η_b at 305 K gave $t\rho$ = 1.9 ns·kg·m^{-3} or a relaxation time t = 1.4 ns at 101.3 kPa, which does not compare well with the literature value of 2.3 ns.[107]

Blander *et al.*,[102,103] in both series of $\kappa(T,p)$ measurements, suggested that a tetrameric species in the gas contributes mainly to the pressure dependence observed in the thermal conductivity. Spectroscopic observations[108,109] favour a monomer, dimer, tetramer model, whereas the (p,V_m,T) measurements of Christian and co-workers[110] (performed with a Burnett apparatus) were interpreted in terms of monomer, trimers, and octamers; their later gas density results were presented as further evidence for the preferential formation of trimers.[111] On the basis of quantum mechanical calculations, Curtiss[112] predicted that cyclic polymers $(CH_3OH)_n$ were more stable than chain structures and that c-$(CH_3OH)_4$ was the most favoured. Less sophisticated techniques would indicate that any cyclic n-mer contains n hydrogen bonds compared with $(n-1)$ for chains. Therefore c-$(CH_3OH)_3$ has the largest energy advantage but the bonds are under considerable strain. Consequently, the term in p^2 was omitted from the smoothing equation for $(u/a)^2$ which then has the form:

$$(u/a)^2 = (A_0/a^2) + (A_1/a^2)p + (A_3/a^2)p^3. \qquad (5.3.53)$$

The terms p^5 and p^7 were available in the regression as an extension of the odd powers in the pressure series.

Even at 280 K, where the pressure range was only 1.6 kPa, the leading three terms of equation (53) were required to describe adequately the measurements (each term was significant at a probability level of 0.999) which demonstrates the extreme curvature of the isotherm. At higher temperatures it was necessary to progressively truncate the pressure range to obtain the best three-term equation. All the (u/a) measurements below about 2 kPa received a weight according to equation (1) less than unity in the regression analysis, which reflects the extreme difficulty in acoustic measurements under these conditions. Additional problems were experienced at 280, 285, and 290 K for which the pressure measurements were affected by an unexplained instability in the pressure transducer. Table 5.16 gives the fractional deviation of the mean u^2, at each pressure included in the final analyses, from equation (53) with the coefficients given in table 5.18.

The deviations of (u/a) for each mode from the finally adopted three-term equation are shown in figure 5.46. At the higher pressures these are comparable with the distribution expected from previous measurements but, at the lower pressures are rather larger. At 310 K, where the vapour pressure is about 29 kPa, the terms in p^5 and p^7 were required to describe the complete isotherm. Figure 5.47 shows the deviations for each mode from this smoothing equation and the discrepancies between modes are comparable or less than the systematic variations of

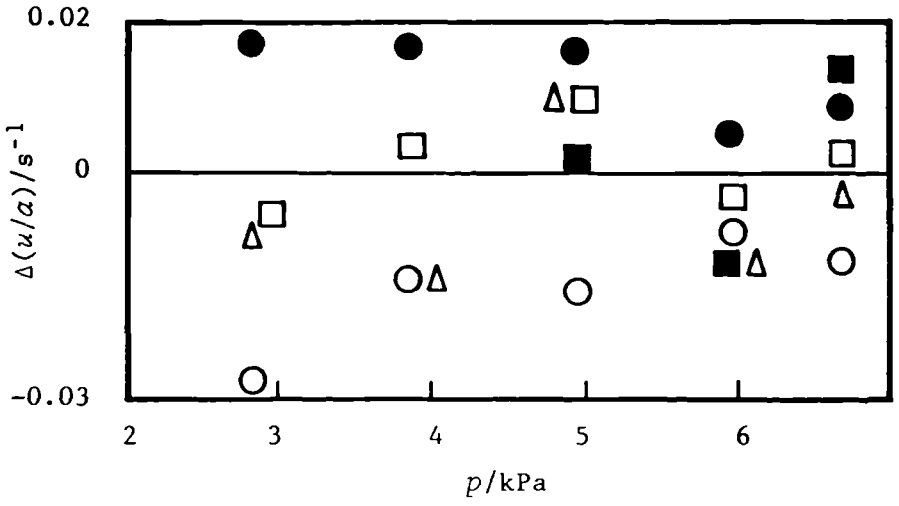

Figure 5.46. Deviations $\Delta(u/a) = [(u/a) - \{u(\text{calc.})/a\}]$, for individual modes in methanol at 300 K, from equation (53) with the leading three-terms which have coefficients adjusted to fit results below 7 kPa. ○ , (0,2); ● , (0,3); □ , (0,4); ■ , (0,5); Δ , (0,6).

$\langle u/a \rangle_p$ as a function of pressure. Both figures 5.46 and 5.47 give no indication of dispersion and this is true for all isotherms.

In table 5.18 are given heat capacities and acoustic virial coefficients determined for methanol, together with the number N of modes in each regression analysis and the standard deviations of the fit.

The perfect gas heat capacities at 310 and 320 K obtained from two to five parameter fits with progressive

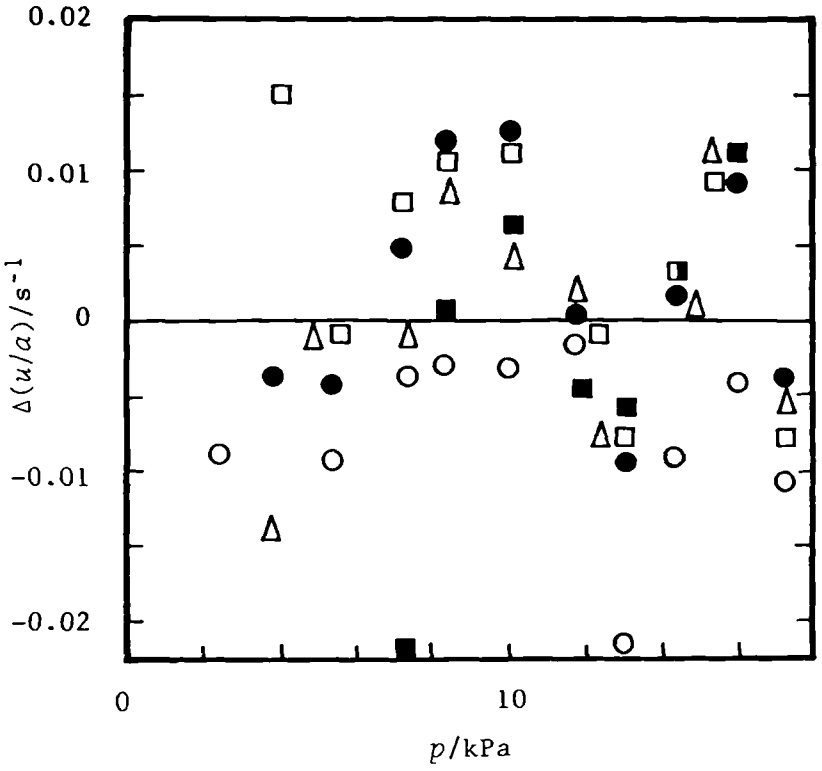

Figure 5.47. Deviations $\Delta(u/a) = [(u/a) - \{u(\text{calc.})/a\}]$, for each radial mode at 310 K, from equation (53) with the leading five-terms for which the coefficients were obtained from regression analysis of all pressures. ○ , (0,2); ● , (0,3); □ , (0,4); ■ , (0,5); Δ , (0,6).

---

truncation of the pressure range are shown in figures 5.48 as a function of the mean value of the pressure retained in the data set. These plots show that the apparent $C_{p,m}^{pg}$ for each order fit extrapolates to the same value at zero mean pressure limit. These extrapolated values are listed

Table 5.18. Perfect-gas heat capacities, second and fourth acoustic virial coefficients, and standard deviations s obtained by analysis of N modes in methanol using equation (53) with the first three terms at temperatures T. The quoted uncertainties are one standard deviation. The fourth acoustic virial coefficient is given by $\delta_a = RT A_3/A_0$.

T/K	N	$C_{p,m}^{pg}/R$	β_a/(cm^3·mol^{-1})	δ_a/(cm^3·mol^{-1}·kPa^{-2})	$10^6 s(u^2)/u^2$
280.000	19	5.1885 ± 0.0045	−3366 ± 175	−1035.4 ±13.2	25.8
285.000	27	5.2148 ± 0.0012	−3599 ± 36	−403.9 ± 1.4	13.4
290.000	14	5.2542 ± 0.0011	−2797 ± 28	−192.04 ± 0.79	8.6
295.000	27	5.2928 ± 0.0013	−2679 ± 26	−82.42 ± 0.49	15.9
300.000	25	5.3293 ± 0.0011	−2377 ± 17	−38.19 ± 0.19	4.8
305.000	21	5.3657 ± 0.0011	−2127 ± 12	−18.003 ± 0.080	8.5
310.000	25	5.4044 ± 0.0003	−1893.1 ± 3.1	−8.736 ± 0.016	4.5
315.000	27	5.4463 ± 0.0004	−7688.9 ± 4.2	−4.401 ± 0.016	6.8
320.000	35	5.4871 ± 0.0002	−1525.3 ± 1.9	−2.250 ± 0.005	6.1

in table 5.18 and shown in figure 5.49 as deviations from the recent IUPAC correlation;[100] a systematic discrepancy is apparent. The IUPAC correlation was based mainly on previously published calculations from spectroscopic data,[113] for which the required vibrational wavenumbers were taken from those selected by Shimanouchi.[114] Mole fractions of 5×10^{-4} of air or water would give deviations from IUPAC of $-0.02\ R$ and $-0.006\ R$, compared with the observed differences

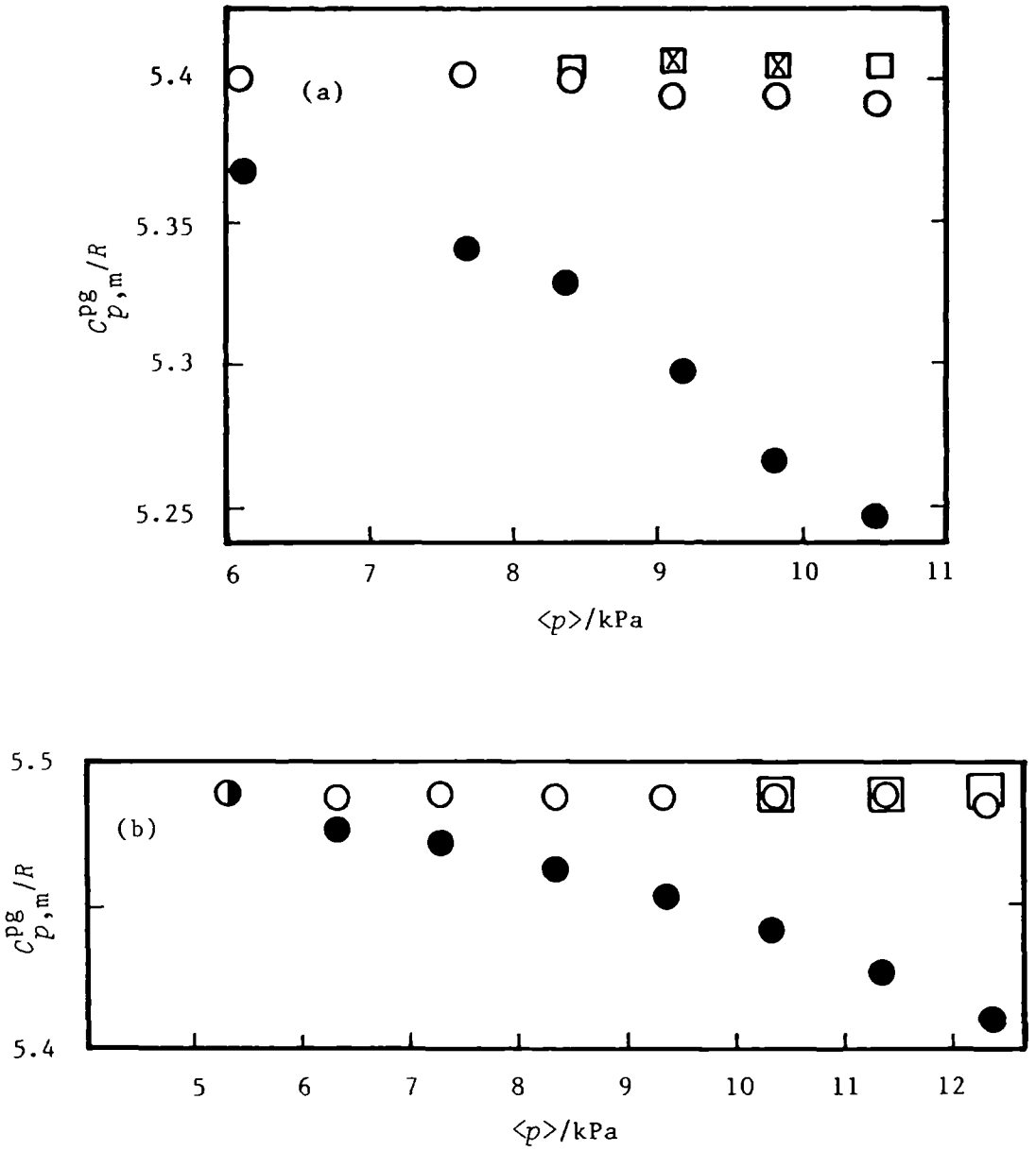

Figure 5.48. Perfect-gas molar heat capacities at constant pressure from various orders of fit as a function of the mean pressure used in the regression analysis for the isotherms at (a) 310 K and (b) 320 K . ● , Two-term fit; ○ , three-term fit; □ , four-term fit; X , five-term fit.

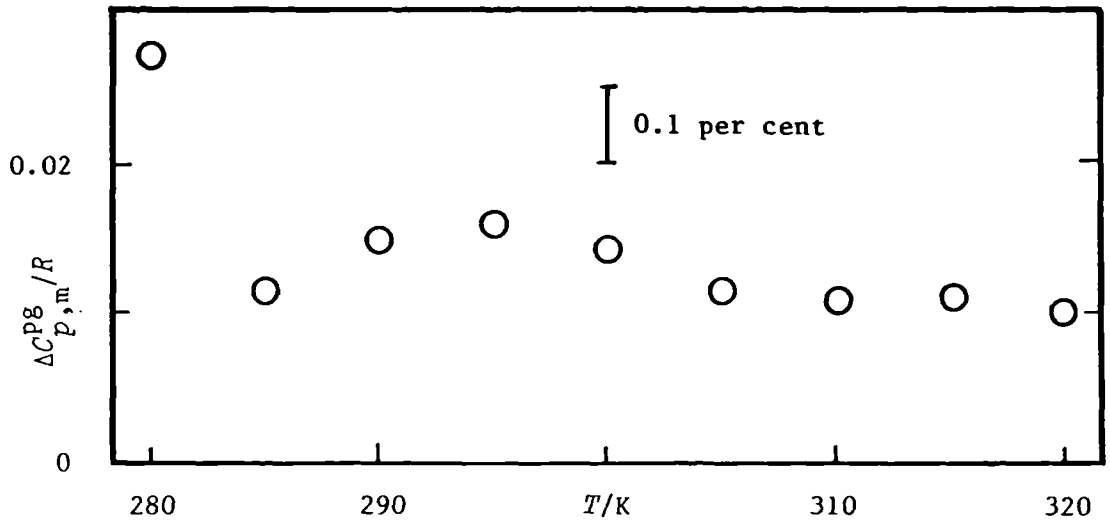

Figure 5.49. Deviations $\Delta C^{pg}_{p,m} = C^{pg}_{p,m} - C^{pg}_{p,m}(\text{IUPAC})$ of $C^{pg}_{p,m}$ given in table 5.16 from reference (100).

---

of about 0.012 R. However, as noted earlier argon was used in the drying procedure and a mole fraction of 0.005 of Ar would account for the discrepancy. (Note that since $M(\text{Ar}) > M(CH_3OH)$ the presence of argon may increase the apparent heat capacity even though u is increased.)

No attempt has been made to estimate (p, V_m, T) virial coefficients from the acoustic coefficients; such an analysis would possibly require the relevant expression derived from the Stockmayer Potential energy function.[115] Furthermore no analysis has been attempted using the adaptive regression analysis to provide information concerning the best combination of powers in pressure required to accommodate the $u(p)_T$ measurements.

REFERENCES

1. Trusler, J.P.M. Ph.D. Thesis, University of London 1984.
2. Ewing, M.B.; McGlashan, M.L.; Trusler, J.P.M. *Metrologia* 1986, 22, 93.
3. Willingham, C.B.; Taylor, W.J.; Pignocco, J.M.; Rossini, F.D. *J. Res. Nat. Bur. Stand.* (US) 1945, 35, 219.
4. Ambrose, D.; Sprake, C.H.S.; Townsend, R. *J. Chem. Thermodynamics* 1972, 4, 247.
5. Ambrose, D. *J. Phys. E.* 1968, 1, 41.
6. Ambrose, D. *Specialist Periodical Reports, Chemical Thermodynamics, Volume 1.* McGlashan, M.L.: Senior Reporter. Chemical Society: London. 1973, Chapter 7, p.240-246.
7. Ambrose, D. *Experimental Thermodynamics, Volume II, Experimental Thermodynamics of Non-Reacting Fluids.* Le Neindre, B.; Vodar, B.: Editors. For IUPAC. Butterworths: London. 1975, Chapter 13 p.626-634.
8. Mehl, J.B.; Moldover, M.R. *J. Chem. Phys.* 1982, 77, 455.
9. Maitland, G.C.; Rigby, M.; Smith, E.B.; Wakenham, W.A. *Intermolecular Forces. Their Origin and Determination.* Clarendon: Oxford. 1981, p.571.
10. Kroger, F.R.; Swenson, C.A. *J. Appl. Phys.* 1977, 48, 853.
11. Aziz, R.A.; Chen, H.H. *J. Chem. Phys.* 1977, 67, 5719.
12. Maitland, G.C.; Smith, E.B. *Mol. Phys.* 1971, 22, 861.
13. Aziz, R.A.; Slaman, M.J. *Mol. Phys.* 1986, 58, 679.
14. Trusler, J.P.M. Private communication.

15. Moldover, M.R.; Trusler, J.P.M.; Edwards, T.J.; Mehl, J.B.; Davis, R. *J. Res. Natl. Bur. Std. (U.S.)* Mar/Apr 1988 (in press).

16. Ewing, M.B. Unpublished work.

17. Bruch, L.W. *Phys. Rev.* 1969, 178, 303.

18. Bruch, L.W. *Phys. Rev. A* 1970, 2, 2167.

19. Mehl, J.B.; Moldover, M.R. *Proc. Eighth Symp. on Thermodphysical Prop.* Sengers, J.V.: Editor. Am. Soc. Mech. Eng.: New York. 1982, p.134.

20. Ewing, M.B.; McGlashan, M.L.; Trusler, J.P.M. *Mol. Phys.* 1987, 60, 681.

21. Boyd, M.E.; Mountain, R.D. *Phys. Rev. A* 1970, 2, 2164.

22. McGlashan, M.L. *Chemical Thermodynamics.* Academic Press: London, 1979, Chapter 12, p.173-174.

23. Mason, E.A.; Spurling, T.H. *Encyclopedia of Physical Chemistry and Chemical Physics.* Volume 10.2, *The virial equation of state.* Rowlinson, J.S.: Editor. Pergamon: Oxford. 1969, Chapter 4, p.192.

24. Barker, J.A.; Monaghan, J.J. *J. Chem. Phys.* 1962, 36, 2558.

25. Parkinson, C.; Gray, P.J. *Chem. Soc. Faraday Trans. 1* 1972, 28, 1065.

26. Owen, E.J.; Thodos, G. *Am. Inst. Chem. Eng.* 1960, 6, 676.

27. Carmichael, L.T.; Sage, B.H. *J. Chem. Eng. Data* 1964, 9, 511.

28. Reference (9), p.564.

29. Kestin, J.; Khalifa, H.E.; Wakenham, W.A. *J. Chem. Phys.* 1977, 66, 1132.

30. Diaz Peña, M.; Cheda, J.A.R. *An. R. Soc. Españ. Fis. Quim.* 1975, 71, 34.

31. Hilderbrand, J.H. *Proc. Natl. Acad. Sci. U.S.A.* 1976, 73, 4302.

32. Lambert, J.D. *Vibrational and rotational relaxation in gases.* Clarendon Press: Oxford. 1977, p.65.

33. Kratzke, H.; Spillner, E.; Müller, S. *J. Chem. Thermodynamics* 1982, 14, 1175.

34. Sage, B.H.; Webster, D.C.; Lacey, W.N. *Ind. Eng. Chem.* 1937, 29, 1309.

35. Dailey, B.P.; Felsing, W.A. *J. Am. Chem. Soc.* 1943, 65, 44.

36. Scott, D.W. *J. Chem. Phys.* 1974, 60, 3144.

37. Haynes, W.M.; Goodwin, R.D. *Thermophysical properties of normal butane from 135 to 700 K at pressures to 70 MPa.* NBS monograph 169, 1982.

38. Chen, S.S.; Wilhoit, R.C.; Zwolinski, B.J. *J. Phys. Chem. Ref. Data* 1975, 4, 859.

39. Ewing, M.B.; Goodwin, A.R.H.; McGlashan, M.L.; Trusler, J.P.M. *J. Chem. Thermodynamics* 1988, 20, 000.

40. Jessen, F.W.; Lightfoot, J.H. *Ind. Eng. Chem. Ind. Edn.* 1938, 39, 312.

41. Kretschmer, C.B.; Wiebe, R. *J. Am. Chem. Soc.* 1951, 73, 3778.

42. Gunn, R.D. MSc Thesis, University of California, Berkeley 1958.

43. Mason, D.McA.; Eakin, B.E. *J. Chem. Eng. Data* 1961, 6, 499.

44. McGlashan, M.L.; Potter, D.J.B. *Proc. Roy. Soc. A* 1962, 267, 478.

45. Tripp, T.B.; Dunlap, R.D. *J. Phys. Chem.* 1962, 66, 635.

46. Kapallo, W.; Lund, N.; Schäfer, K. *Z. Phys. Chem.* (Frankfurt) 1963, 37, 196.

47. Bottomley, G.A.; Spurling, T.H. *Aust. J. Chem.* 1964, 17, 501.

48. Jones, A.E.; Kay, W.B. *Am. Inst. Chem. Eng.* 1967, 13, 720.

49. Lichtenthaler, R.N.; Schäfer, K. *Ber. Bunsenges. Phys. Chem.* 1969, 73, 42.

50. Strein, K.; Lichtenthaler, R.N.; Schramm, B.; Schäfer, K. *Ber. Bunsenges. Phys. Chem.* 1971, 75, 1308.

51. Schäfer, K; Schramm, B.; Navarro, J.S.V. *Z. Phys. Chem.* (Frankfurt) 1974, 93, 203.

52. Bottomley, G.A.; Nairn, D.B. *Aust. J. Chem.* 1977, 30, 1645.

53. Das, T.R.; Reed, C.O.; Jr.; Eubank, P.T. *J. Chem. Eng. Data* 1973, 18, 244.

54. Dymond, J.H.; Smith, E.B. *The virial coefficients of pure gases and mixtures.* Clarendon Press: Oxford. 1980, p.114.

55. Beattie, J.A.; Stockmayer, W.H. *J. Chem. Phys.* 1942, 10, 473.

56. Scott, R.L.; Dunlap, R.D. *J. Phys. Chem.* 1962, 66, 639.

57. Nieuwoudt, J.C.; Le Neindre, B.; Tufeu, R.; Sengers, J.V. *J. Chem. Eng. Data* 1987, 32, 1.

58. Kazaryan, V.A.; Ryabstev, N.J. *Gazov. Dela* 1969, 10, 27.

59. Lambert, J.D.; Cotton, K.J.; Pailthorpe, M.W.; Robinson, A.M.; Scrivins, J.; Vale, W.R.F.; Young, R.M. *Proc. R. Soc. A* 1955, 231, 280.

60. Nietode Castro, C.A.; Tufeu, R.; Le Neindre, B. *Int. J. Thermophysics* 1983, 4, 11.

61. Levelt Sengers, J.M.H.; Kamgar-Parsi, B.; Sengers, J.V. *J. Chem. Eng. Data* 1983, 28, 354.

62. Abe, Y.; Kestin, J.; Khalifa, H.E.; Wakenham, W.A. *Physica A* 1979, 97, 296.

63. Titani, T. *Bull. Chem. Soc. Jpn.* 1930, 5, 98.

64. Agayev, N.A.; Yusibova, A.D. *Gazov. Promst* 1969, 14, 41.

65. Sage, B.H.; Yale, W.D.; Lacey, W.H. *Ind. Eng. Chem.* 1939, 31, 223.

66. Waxman, M.; Klein, M. *Nat. Bur. Stand. NBSIR* 81-2435, 1982.

67. Sage, B.H.; Lacey, W.N. *Ind. Eng. Chem.* 1938, 30, 673.

68. Wacker, P.F.; Cheney, R.K.; Scott, R.B. *J. Res. Nat. Bur. Stand.* 1947, 38, 651.

69. Ernst, G.; Büner, J. *J. Chem. Thermodynamics* 1970, 3, 673.

70. Wilhoit, R.C. Ideal gas thermodynamic functions. TRC Current Data News 1975, 3, 2.

71. Harmens, A. Proc. NPL Conf. *Chemical thermodynamics data on fluids and fluid mixtures; their estimation, correlation and use.* London. 1978, p.112.

72. Huff, J.A.; Reed, T.M. *J. Chem. Eng. Data* 1963, 8, 306.

73. Das, T.R.; Reed, C.O.,Jr.; Eubank, P.T. *J. Chem. Eng. Data* 1973, 18, 253.

74. Gray, P.; Holland, S.; Maczek, A.O.S. *Trans. Faraday Soc.* 1970, 66, 107.

75. Carmichael, L.T.; Sage, B.H.; Jacobs, *J. Chem. Eng. Data* 1969, 14, 31.

76. Osborn, A.G.; Douslin, D.R. *J. Chem. Eng. Data* 1974, 19, 114.

77. Ambrose, D. Equations for the correlation and estimation of vapour presures. NPL report Chem.114 1980, p.9.

78. Hossenlopp, I.A.; Scott, D.W. *J. Chem. Thermodynamics* 1981, 13, 415.

79. Garner, M.D.G.- McCoubrey, J.C. *Trans. Faraday Soc.* 1959, 55, 1524.

80. Ratzsch, M.; Bittrich, H.-J. *Z. Phys. Chem.* 1965, 228, 81.

81. Hajjar, R.F.; Kay, W.B.; Leverett, G.F. *J. Chem. Eng. Data* 1969, 14, 377.

82. Das, T.R.; Reed, C.O.,Jr.; Eubank, P.T. *J. Chem. Eng. Data* 1977, 22, 3.

83. Reference 54, p.135.

84. Beattie, J.A.; Levine, S.W.; Douslin, D.R. *J. Am. Chem. Soc.* 1952, 74, 4778.

85. Ambrose, D.; Sprake, C.H.S. *J. Chem. Soc. A* 1971, 1263.

86. Ambrose, D. Based on measurements reported by Osborne, N.S.; Meyers, C.H. *J. Res. Nat. Bur. Stand.* (US). 1934, 13, 1.

87. Silberberg, I.H.; McKetta, J.J.; Kobe, K.A. *J. Chem. Eng. Data* 1959, 4, 323.

88. Schumann, S.C.; Aston, J.G. *J. Am. Chem. Soc.* 1942, 64, 1039.

89. Scott, D.W.; McCullough, J.P.; Williamson, K.D.; Waddington, G. *J. Am. Chem. Soc.* 1951, 73, 1707.

90. Silberberg, I.H., Lin, D.C.K.; McKetta, J.J. *J. Chem. Eng. Data* 1967, 12, 226.

91. Das, T.R.; Reed, C.O.,Jr.; Eubank, P.T. *J. Chem. Eng. Data* 1977, 2, 9.

92. Reference 54, p.138.

93. Ewing, M.B.; Goodwin, A.R.H., McGlashan, M.L.; Trusler, J.P.M. *J. Chem. Thermodynamics* 198719, 721.

94. Dawson, P.P.; Silberberg, I.H.; McKetta, J.J. *J. Chem. Eng. Data* 1973, 18, 7.

95. Perez, Masià, A.; Diaz Peña, M.; Burriel Lluna, J.A. *An. R. Soc. Españ. Fis. Quim.* 1964, 603, 229.

96. Ewing, M.B.; Marsh, K.N. *J. Chem. Thermodynamics* 1979, 11, 793.

97. Toczylkin, L.S. Ph.D. Thesis, University of London. 1984.

98. Ambrose, D.; Sprake, C.H.S. *J. Chem. Thermodynamics* 1976, 2, 631.

99. Francis, P.G.; Phutela, R.C. *J. Chem. Thermodynamics* 1979, 11, 747.

100. Craven, R.J.B.; de Reuck, K.M. *Int. J. Thermophysics* 1986, 7, 541.

101. Craven, P.M.; Lambert, J.D. *Proc. Roy. Soc. A* 1951, 205, 439.

102. Renner, T.A.; Kucera, G.H.; Blander, M. *J. Chem. Phys.* 1977, 66, 177.

103. Frurip, P.J.; Curtiss, L.A.; Blander, M. *Int. J. Thermophysics* 1981, 2, 115.

104. Vines, R.G. *Aust. J. Chem.* 1953, 6, 1.

105. Vines, R.G.; Bennett, L.A. *J. Chem, Phys.* 1954, 22, 360.

106. Lambert, J.D.; Staines, E.N.; Woods, S.D. *Proc. Roy. Soc. A* 1950, 200, 262.

107. Ener, C.; Busala, A.; Hubbard, J.C. *J. Chem. Phys.* 1955, 23, 155.

108. Fletcher, A.N. *J. Phys. Chem.* 1971, 75, 1808.

109. Inskeep, R.G.; Kelliher, J.M.; McMahan, P.E.; Somers, B.G. *J. Chem. Phys.* 1958, 28, 1033.

110. Tucker, E.E.; Farnham, S.B.; Christian, S.D. *J. Chem. Phys.* 1969, 73, 3820.

111. Cheam, V.; Farnham, S.B.; Christian, S.D. *J. Chem. Phys.* 1970, 74, 4157.

112. Curtiss, L.A. *J. Chem. Phys.* 1977, 67, 1144.

113. Chen, S.S.; Wilhoit, R.C.; Zwolinski, B.J. *J. Phys. Chem. Ref. Data* 1977, 6, 105.

114. Shimanouchi, T. NSRDS-NBS 1972, 39, 63.

115. Reference 9, p.149-152.

CHAPTER SIX

HIGH PRESSURE MEASUREMENTS

6.1 INTRODUCTION

The speed of sound u is an important quantity in the gas industry since, in addition to the usual thermophysical properties that can be obtained from $u(p)_T$ measurements, sonic nozzles offer a useful secondary method of flow measurement.

An apparatus, based on a spherical resonator, that is suitable for measurements in gaseous mixtures between 250 and 350 K at pressures up to 21 MPa is described.

This chapter reports results of acoustic measurements at pressures below 7 MPa for argon and the industrially important fluids methane, natural gas, and air;

measurements with a natural gas and compressed air were made at 255 K, which is a typical throat temperature obtained with sonic nozzles. Measurements with argon were performed to characterize the resonator and to study the model used to account for acoustic energy losses in the resonator. The speed of sound, for the industrially important fluids, was compared with estimates obtained from several equations of state, including the two recent equations developed specifically for natural gas for G.R.I. (AGA8) and G.E.R.G.

6.2 APPARATUS

Spherical resonator

The spherical resonator used for the measurements reported in this chapter is shown in figure 6.1. Two hemispheres with nominal internal radius of 40 mm were machined from a cylindrical bar of aluminium alloy (AlSiMgMn) using a worm driven turning tool. The external surface was turned with a spherical turning tool so that the radius was 50.2 mm. Before commencing machining the northern hemisphere, the transducer ports M and S were drilled at an angle $\pi/2$ apart and then reamered to have a nominal diameter of 10 mm at the inner surface. Approximately 5 mm from the inner surface of the resonator, these holes were threaded using a 26 t.p.i. 3/4" diameter tap. Each port had a smooth base D so that the transducer could be sealed in to the resonator with either a viton elastomer 'O'-ring or a PTFE coated stainless steel torus filled with

nitrogen. The hemispheres were both cut off near the equator so that the polar depth was about 3 mm greater than the radius. In this way, any rounding of the equatorial edge, resulting from polishing, could be removed in the final dimensional adjustment. Tooling marks were reduced, but not removed, by mechanical polishing with: (1), 600 grit silicon carbide paper; (2), 1200 grit silicon carbide paper; and (3), "Solvol autosol" metal polish. More recently, this proprietary polish has been found to be detrimental to the surface finish and Al_2O_3 in various particle sizes (5 μm to 0.3 μm diameter) has been preferred. The 3 mm × 7 mm interlocking step, which aligned the two hemispheres, was machined so that the polar depth for each hemisphere equalled half its equatorial diameter and contact was made only on the inner edge. Mechanical measurements gave a = (40.00 ± 0.02) mm for each hemisphere. Prior to final assembly the 1 mm diameter gas filling tube was drilled. The hemispheres were joined near the equator by an electron-beam weld, which penetrated about 7 mm (as indicated by a cylindrical test piece) into the wall, and formed a spherical resonator which a helium leak detector showed was vacuum tight. Before welding, it was extremely difficult to identify the interior equatorial join when viewed through the transducer ports. Although the welding did not obviously distort the external surface, the internal join appeared to be more prominent and a slight mismatch could be detected using a plastic probe. Closer visual

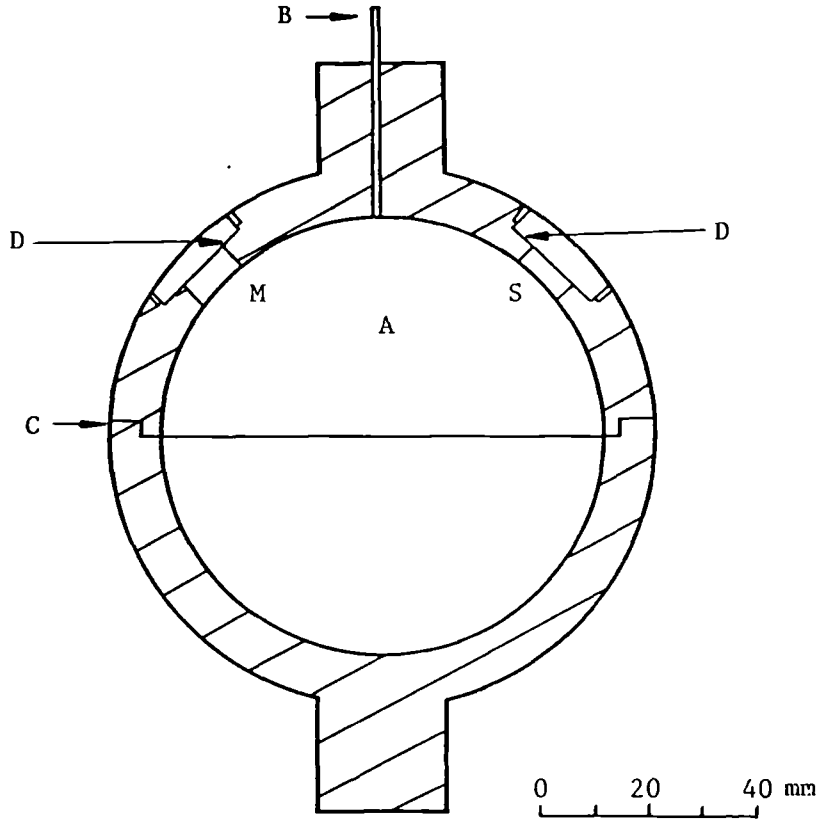

Figure 6.1. Cross sectional view of the spherical resonator, constructed from two aluminium hemispheres, joined at C by an electron beam weld. The source S was positioned at an angle $\pi/2$ from the microphone M; both transducers were located with 3/4" diameter 26 t.p.i. threads. The gas entered the cavity A via tube B.

inspection suggested that the welding had pulled the join together and had extruded a small seam. It should be noted that the welding beam had been directed at the exterior join of the interlocking step and, consequently, when it refroze, the stresses at the join would have been asymmetric. At any rate, this geometric imperfection is minor and the effect on the quality of the acoustic results should be insignificant. The external spherical surface was then turned to give a wall thickness of 10 mm except for the 20 mm long by 25.4 mm diameter bosses located at the north and south poles. Finally the 40.09 mm long gas filling tube was completed with a 0.99 mm internal diameter stainless steel tube forced 5 mm into the northern boss.

The fractional change in a as a function of pressure is given by

$$\delta a/a = (x_1 p_1 - x_0 p_0)/3, \qquad (6.2.1)$$

in which

$$x_1 = \{1 - 2\sigma + t^3(1 + \sigma)/2\}/\{(t^3 - 1)E\} \qquad (6.2.2)$$

and

$$x_0 = 3(1 - \sigma)t^3/\{2(t^3 - 1)E\}, \qquad (6.2.3)$$

where $t = b/a$ is the ratio of inner to outer radii, ϕ is Poisson's ratio and E is Young's modulus.[1] In equation (2) p_0 refers to the pressure acting on the outer surface at $r = b$ and p_1 the internal gas pressure. For the aluminium alloy resonator discussed above with $t = 1.25$ and $E = 7.03 \times 10^{10}$ Pa, $\delta a/a = 55 \times 10^{-6}$ when $p_0 = 0.1$ MPa and $p_1 = 7$ MPa, but

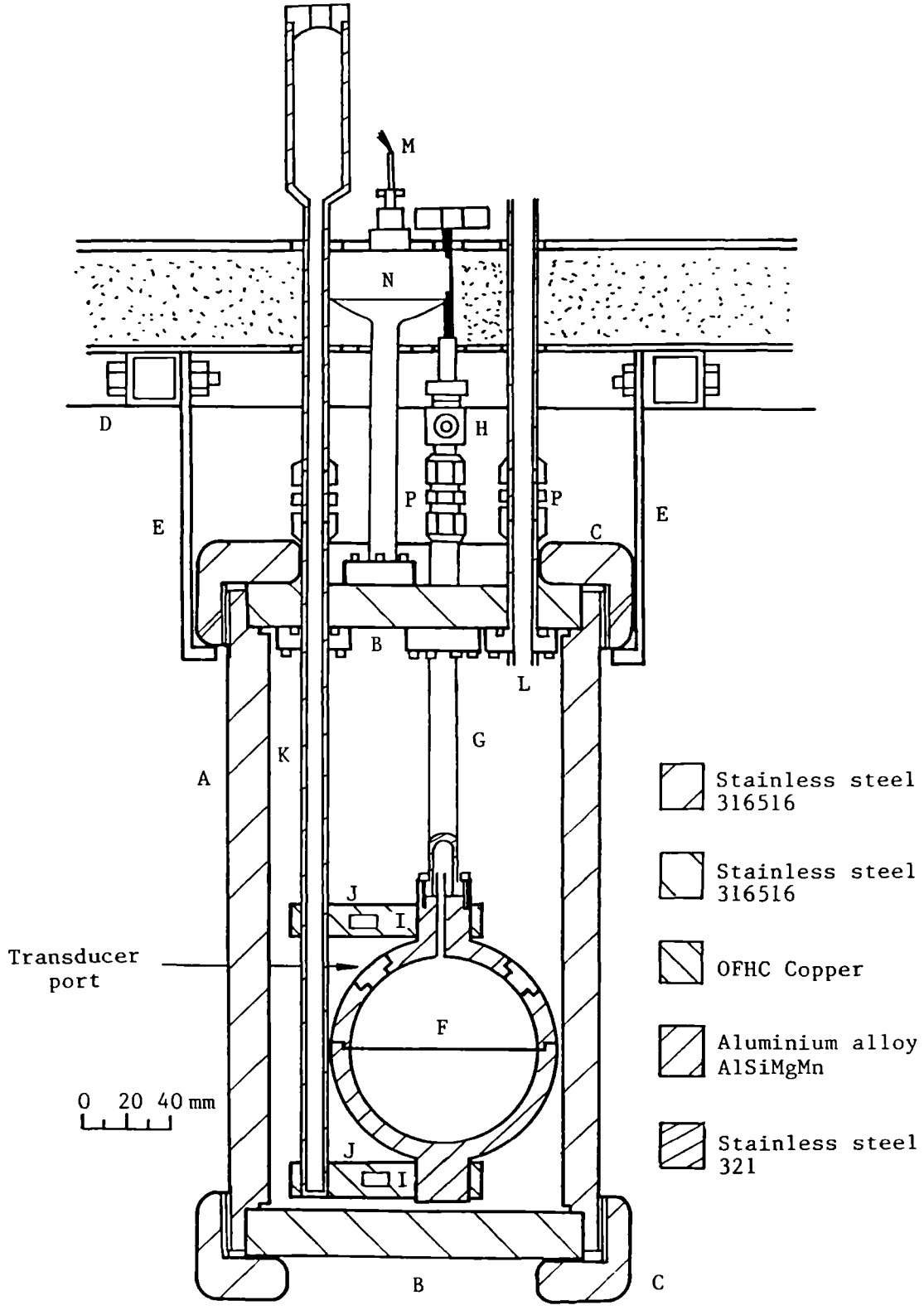

Figure 6.2. For description see subsequent page.

Figure 6.2. High-pressure apparatus. The pressure vessel consisting of cylinder A, end covers B, and end caps C were suspended in a stirred fluid thermostat from a square-sectioned frame D using aluminium plates E. The sample passed to the resonator F through tube G via H, a bellows sealed, all welded, stainless steel valve (Nupro SS-8BAW-TW). The resonator heaters I were mounted on copper blocks J, which connected the sphere to the thermometer well K. This well K, held the long-stem resistance thermometer (LN7080308) with its platinum sensing element located about the resonators equator; to improve thermal contact the well was filled with ethanol or *n*-octane dependant on the operating temperature. The nitrogen gas required for pressure compensation of the resonator, entered the vessel via tube L. The necessary electrical connections were made using two hermitically sealed lead-throughs M, housed in a smaller end cover-and-cap arrangement N. The thermostat was insulated with Kaowool blanket O, sandwiched between aluminium sheets. The joints P were made with stainless steel Swagelock couplings suitable for 12.7 mm diameter tubing.

$\delta a/a = -9.7 \times 10^{-6}$ when $p_0 = p_1 = 7$ MPa; the advantages of pressure compensation are obvious. Furthermore, for measurements with gaseous substances such as CH_4 or natural gas a separate pressure vessel offers additional protection against leakage.

Pressure vessel

The pressure vessel, shown in figure 6.2, was designed to operate up to 673 K and a pressure of 7 MPa when constructed from 316S16[2] and 321S12[2] austenitic

stainless steel; the stainless steels 316S16 and 321S12 have similar thermal expensivities,[3] and tend not to 'cold-weld'. Since the design of a pressure vessel is quite a complex task, only the simple formula (given in table 6.1) required to design and evaluate individual components are used for the following brief discussion of the vessel. Detailed information for design and use of pressure vessels can be found in the literature,[4-6] which should be consulted if a pressure vessel is to be constructed. A further useful guide for the assessment of pressure vessels has been produced by the High Pressure Technology Association.[7] The maximum allowable design stress S at 673 K was taken as 120 $MN \cdot m^{-2}$ for both 316S16 and 321S12 stainless steels. At lower temperatures larger values of S are applicable;[6] austenitic stainless steels do not suffer brittle fracture and therefore can be used for cryogenic pressure vessels. A wall thickness of 4 mm is sufficient to contain 7 MPa in a cylinder of internal diameter 130 mm, but to secure end caps and to locate seals about a further 10 mm was required. Rather than weld additional pieces to a thin-walled cylinder, the cylinder was machined to include the sealing surfaces, from a seamless drop-forged tube of 316S16 stainless steel. The minimum of material was removed over the entire length of this tube resulting in a cylinder with an internal diameter of 133.7_1 mm and a wall thickness of 16.4_6 mm. In each end of the tube a recess was cut to hold 20 mm of the 22 mm thick end cover, which was machined from 316S16

Table 6.1 Equations to assess individual pressure vessel components B.[5,7,10]

B	Equations	Symbol	Definition
Cylindrical shell thickness when subject to internal pressure.[5]	$t = pd_i/(2SE - p)$	t	wall thickness.
		p	pressure.
		d_i	internal diameter.
		S	maximum allowed stress.
Spherical shell thickness, when subject to internal pressure.[5]	$t = pd_i/(4SE - p)$	E	welded joint efficiency factor. Unity for radiographed welds, 0.75 for uninspected welds.
		G	diameter of gasket reaction.
Minimum thickness of flat circular cover.	$t_{min} = \{1.909Wh_G/(GS)\}^{\frac{1}{2}}$	W	design bolt load for bolting up condition.
(1) bolted.[5]		h_G	radial distance from gasket load reaction to bolt circle.
(2) unbolted.[5]	$t = G(Cp/S)^{\frac{1}{2}}$		$C = 0.30$.
Thread shear stress σ_y for screw plugged/end cap closures.[7,10]	$\sigma_y = d_S^2 p/(2d_t l_t)$	d_S	effective diameter of seal.
		l_t	thread length.
Combined bending and longitudinal stress of an undercut.[10]	$\sigma_{cbd} = 4pd_i^2/(d_0^2 - d_{uc}^2)$	d_t	mean diameter of threaded portion of closure.
		d_0	outside diameter.
		d_{uc}	undercut diameter.

bar stock, leaving 2 mm protruding so that they could be secured on to the seal with threaded end caps. The main advantage of threaded end caps over screw plugged closures arises from the position of the thread. For end caps the thread is on the least stressed outer surface, while with screw plugs the thread is cut on the highly stressed inner surface. Consequently, end caps reduce the possibility of failure due to fatigue. The important dimensions required to design end caps are the thickness of the internal load-bearing flange, and the flange fillet radius; these dimensions have been discussed by Allison and Bacchus.[8] The geometric complexity of the problem precludes the application of analytical methods for detailed stress analysis. When end caps are used to maintain a fluid tight seal an important consideration is the flange deflection as a function of pressure. This displacement can be easily estimated using methods described by Harvey,[9] and at 7 MPa should not amount to more than 0.2 mm for the vessel descibed here. Since the presence of sharp corners on the cover and cap can act as fatigue crack initiators,[7] these have been removed from this vessel. Although the adequacy of a particular thread can be assessed by traditional methods (equation given in table 6.1), and the average load per thread estimated, this is not sufficient for the safest thread evaluation. Fryer and Smith[10] have recently shown that, for a conventional buttress thread, the load on the first and second threads are 3.5 and 2.5 times greater than the average respectively. Cray,[11] has

reported finite element analysis which indicates the first engaged turn of a V-shaped thread is less stressed than the corresponding buttress thread. However, the results of thread fatigue tests as a function of the number of pressurization cycles, between 13 and 203 MPa have indicated a V cross-sectioned thread is slightly more likely to fail.[13] An ISO metric coarse thread with a pitch of 3 mm and internal angle of $\pi/3$ (the thread had a depth of 1.8_4 mm), was screw-cut on the cylinder and end caps over a length of 20 mm. Since a single turn could withstand working pressure, then no permanent deformation should occur. Consequently, this arrangement reduces the possibility of thread seizure; the threads were also coated with an antilocking agent. To prevent thread failure due to bending stresses, which according to both classical and finite element analyses can be a factor of 3 greater than longitudinal tensile stress, the undercut prior to the first thread needs to be well proportioned with a good smooth surface finish.[12] The threads on this vessel have all been appropriately undercut.

In the top cover 4 equally spaced holes, centred on a circle of diameter 262 mm, were drilled to provide clearance holes for 12.7 mm tubing. To accommodate for the presence of holes, the end cover was stiffened by flanges, which were designed in accordance with BS 5500,[6] machined from 321 stainless steel and attached to the internal face with six 3 mm diameter bolts; these bolts were also used to compress the sealing ring (either a viton 'O'-ring or

PTFE coated stainless steel torus) situated between the end cover and flange. To each of these flanges was welded a tube, with an external diameter of 12.7 mm and 1.6 mm thick walls, which served to: (1), allow sample gas to pass to the resonator; (2), allow nitrogen into the pressure vessel; and (3), hold the long-stem platinum resistance thermometer. Two further holes were drilled to have a 6 mm diameter, separated from the other holes by at least the necessary 25 mm, were sealed to flanges(of identical design to those mentioned previously) to which were welded further sections of tubing. Each of these two tubes, of sufficient length to reach ambient temperature, were welded to a holder for an electrical lead through. The electrical lead through consisted of 3 pins hermetically sealed into a steel case, and were capable of withstanding 17 MPa between 245 and 365 K.

The seal grooves were designed primarily for the PTFE coated stainless steel pressure sealed rings (supplied by Fothergill Engineering plc) but were, in general, also adequate for the alternative viton rings according to BS 1806.[12] However, the cylinder to end cover "groove" had no internal wall and additional steel support rings were required when viton 'O'-rings were used.

The completed pressure vessel was hydrostatically tested at six evenly spaced presures up to 21 MPa,[13,14] with the electrical lead throughs replaced by steel discs. At each pressure the cylinder dilation as a function of height and the end cap distortion were determined. After

a change in pressure a 1 h adjustment period was allowed before measurements were taken. Dimensional measurements were performed on decreasing as well as increasing the pressure and, in both cases, the results were essentially identical. The hydrostatic pressure test was repeated twice. Below 7 MPa the cylinder diameter did not alter significantly, while the end caps were each displaced by 0.12 mm over the whole internal load bearing flange. At a pressure of 21 MPa the cylinder diameter had increased evenly along its height by 0.03_5 mm and the load bearing flange had been displaced by 0.2 mm.

Transducers

Both transducers were sealed devices mounted in special plugs that screwed into ports in the wall of the resonator. Some gap between the transducer body and port is necessary, but the circumference of π cm implies that the gap should be small if the surface area of the annular slot exposed to the sound field is not to be excessive. To prevent binding in the port, the transducer body was fabricated from brass. A nominal clearance of 10 μm allowed the transducer to be inserted and removed without difficulty.

The electrostatic source transducer is shown in figure 6.3. The active element was a 6 mm diameter disc of 12 μm thick polyester film (Melinex, ICI plc) coated with 50 μm layer of aluminium on the side facing into the sphere; the active surface exposed was 2 mm in diameter. The back electrode was fabricated from brass, and had six 0.3 mm diameter holes drilled to a depth of 0.5 mm on its front

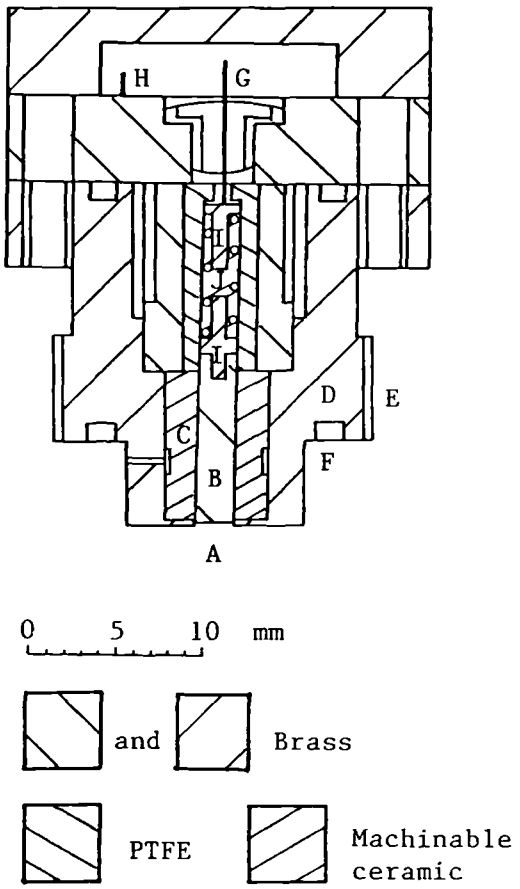

Figure 6.3. Electrostatic capacitance transducer used in high pressure apparatus : A, 50 nm aluminium coating on a 12 μm thick polyester film disc of diameter 6 mm; B, brass rod machined in end A, five equally spaced holes of 0.25 mm diameter drilled to a depth of 1 mm; C, machinable ceramic insulating sleeve; D, brass body; E, 26 t.p.i. 3/4" British standard brass thread; F, groove suitable for PTFE coated metallic and viton 'o' cross section sealing rings; G, ceramic sealed one pin electrical lead through; H, earth connection point; I, electrical contacts; J, spring which exerts a force of about 1 N (RS components plc) and ensures continued contact between film and brass rod.

face to increase the compliance of the polyester film. Electrical contact to the back electrode was by means of a steel spring soldered to the electrical feed through mounted on the back cover of the transducer body. The spring also served to maintain slight tension in the polyester-film membrane. A hole of diameter 0.3 mm drilled through the side of the transducer body allowed equilibration of the static pressure by leakage through the annular gap around the port. The transducer was biased with 200 V dc and operated with an excitation signal of up to 60 V rms at the measurement frequency. The efficiency of the device varied considerably with the fluid density and was greatest near 60 $kg \cdot m^{-3}$. Many similar devices have been reported in the literature.[15-19]

The perturbation to the resonance frequencies of the gas within the spherical enclosure arising from the volume V_{tr} trapped behind the membrane may be estimated from

$$\Delta f_{tr}/f = -(2/3)\{\gamma/\gamma_{eff}\}(V_{tr}/V), \qquad (6.2.4)$$

where γ_{eff} is the real part of the effective heat capacity ratio of the gas trapped behind the membrane.[20] Since compression of the gas in this gap is nearly isothermal $\gamma_{eff} \approx 1$. For the dimensions used in this work, the perturbation should always be less than 1×10^{-6}.

A detector transducer similar to that in the 60 mm sphere was used. The electret microphone capsule was mounted in a brass body, as shown in figure 6.4, and was electrically insulated from the resonator body to prevent

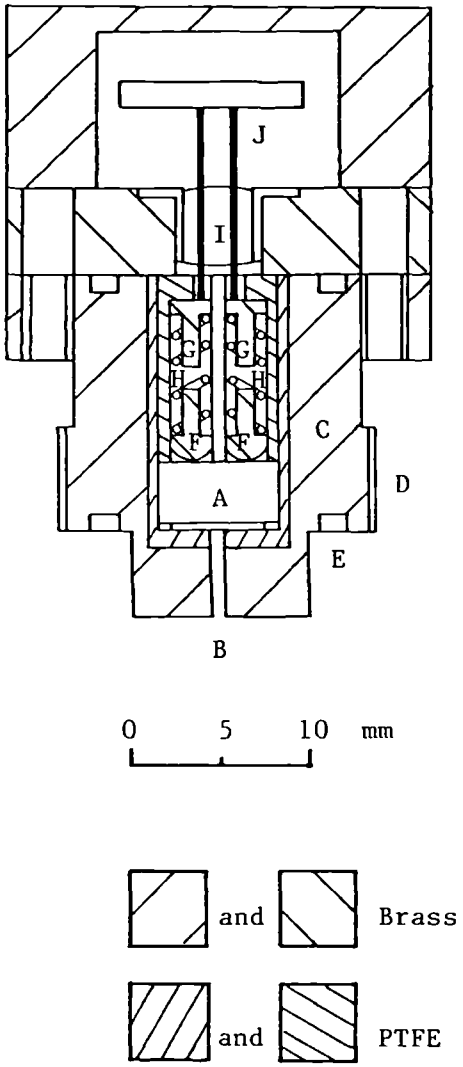

Figure 6.4. Sound detector used in high pressure apparatus : A, Capsule electret film microphone (supplied by Maplin Electronics plc), with built in leakage track for pressure equalization across diaphragm; B, 0.7 mm diameter, 4 mm long cylindrical wave-guide; C, brass body; D, 26 t.p.i. 3/4" British standard brass thread; E, groove suitable for PTFE coated metallic and viton 'o' cross section sealing rings; F and G, brass electric contacts; H, spring; I, ceramic sealed two pin electrical lead through; J, circuit board containing 1 kΩ resistor and 4.7 μF tantalun.

ground loops. The microphone was coupled to the interior of the resonator by a 0.7 mm diameter cylindrical waveguide of length 4 mm. The active element of the microphone was separated from the front of the capsule by a small volume of approximately 15 mm^3. The Helmholtz resonance frequency of this arrangement is well below the frequency of the lowest mode of the resonator. Thus, the perturbation caused by the detector was dominated by that of the open tube alone.

6.3 EXPERIMENTAL AND ANALYSIS

Before a series of measurements, the sphere was baked at 350 K, using the heaters mounted on the copper blocks shown in figure 6.2, until the pressure indicated by an ionization gauge in the pumping line had been below 1 mPa for 24 h. The resonator was filled with sample in approximately 100 kPa steps (as indicated by the differential pressure transducer), between which the pressure difference was balanced by the addition of nitrogen to the surrounding vessel. This stepwise procedure, which prevented overloading of the pressure transducer, was repeated until the pressure was about 7 MPa.

Preliminary acoustic measurements on mode (0,2) were used to estimate the position of the modes (0,3) to (0,8). These estimates of f_{0n}, which took into account the effects of shell motion {with the isolated mode approximation equation (3.4.31)}, the coupling and filling tubes, and the thermal-boundary-layer, were used to select the range of

frequencies over which the measurements would be made for each mode. Acoustic measurements were then made with the Network Analyser under the control of the microcomputer in the manner described in Chapter Four.

The pressure of the gas sample was determined, before and after the acoustic measurements, as described in Chapter Four. The pressure was then slowly decreased in the resonator by about 100 kPa, the sphere was sealed, and the pressure in the containment vessel decreased so as to renull the differential pressure transducer. This process was repeated until the pressure had been decreased by about 700 kPa. The sphere temperature was returned to within a few millikelvin of the set point temperature using the sphere heaters powered by a servo loop activated by the output from the Tinsley resistance bridge. A period of about 2 h was required to reach thermal equilibrium after a pressure change of 700 kPa.

Analysis

The measurements of f_{0n} were corrected as described in Chapters Five and Three, to provide the quantity (u/a). However, since the effect of shell motion was large at these densities this correction was made with equations (3.4.29) and (3.4.21) to (3.4.28) which are derived from the exact theory of elasticity for a perfect isotropic sphere and include the effect of radiation from the external surface.

The excess half widths reported in the following sections were calculated with allowance for classical bulk

absorption, losses at the surface, and the coupling and filling tubes, but not radiative losses from the shell. For the methane isotherms and those determined with a natural gas and dry air the quantity t_ρ, where t is the vibrational relaxation time and ρ the mass density, was determined by analysis of the residual experimental half width assuming the vibrational states are strongly coupled according to equations (5.3.5) and (3.3.12). The quantity $t\rho$ and any apparent density dependence so determined was used to make allowance for the effect of vibrational relaxation on the speed of sound using equation (3.3.11).

6.4 RESULTS

6.4.1 Argon

Table 6.2 lists the resonance frequencies and half widths determined in argon along four isotherms between 255 and 300 K, together with the quantity (u/a) and the speed of sound u; u was calculated using $a(T,p)$ which was obtained from $a(T,\ p=0)$, determined in analysis of the results combined with the linear hydrostatic compressibility $\{1/a(\partial a/\partial p)_T\}$ calculated assuming the wall was constructed from pure aluminium using equations (6.2.1) to (6.2.3). Small corrections have been applied to reduce all values of (u/a) to the stated temperature for each isotherm. Two isotherms were studied at 273.16 K: one with the acoustic transducers described in section (6.3.3), and the other for evaluation of a prototype source transducer. At pressures below 250 kPa, this transducer, which had an active element

Table 6.2 Resonance frequencies f_{0n} and half widths g_{0n} fractional excess half widths $\delta = 10^6 \Delta g / f$, experimental quanties (u/a) and speeds of sound u for the n-th radial mode at temperatures T and pressures p in argon. The radius $a = a(T,p)$ was calculated using $a_u(T,p = 0)$ and equations (6.2.1) to (6.2.3).

p / kPa	n	f_{0n} / s^{-1}	g_{0n} / s^{-1}	δ	(u/a) / s^{-1}	$10^3 a$ / m	u / $m \cdot s^{-1}$
			$T/K = 255.000$				
7022.029	2	5419.045	0.394	17	7579.844 [c]	39.97321	302.9907
	3	9316.926	0.491	11	7580.195		303.0048
	4	13150.367	0.589	9	7580.224		303.0059
	5	16962.931 [b]	1.051	31	7580.293		303.0087
	6	20762.022 [b]	6.059	264	7579.318 [c]		303.9697
5808.954	2	5385.319	0.368	12	7532.707 [c]	39.97328	301.1070
	3	9258.895	0.462	7	7532.986		301.1182
	4	13068.527	0.566	8	7532.995		301.1185
	6	20633.767	3.439	138	7532.150 [c]		301.0848
	7	24408.492 [b]	0.916	11	7533.616 [c]		301.1434
	8	28049.131 [b]	2.225	55	7503.543 [c]		299.9412
5137.365	2	5370.183	0.356	9	7511.249 [c]	39.97332	300.2495
	3	9232.829	0.454	6	7511.474		300.2585
	4	13031.795	0.568	8	7511.486		300.2590
	6	20576.337	2.121	74	7510.701 [c]		300.2276
	7	24340.798 [b]	0.993	14	7512.018 [c]		300.2803

p / kPa	n	f_{0n} / s^{-1}	g_{0n} / s^{-1}	δ	(u/a) / s^{-1}	$10^3 a$ / m	u / $m \cdot s^{-1}$
5137.365	8	27968.437 [b]	1.821	40	7480.451 [c]	39.97332	299.0185
4593.837	2	5359.493	0.350	8	7496.123 [c]	39.97335	299.6451
	3	9214.424	0.461	6	7496.312		299.6527
	4	13005.865	0.569	7	7496.328		299.6533
	6	20536.412 [b]	1.533	45	7495.801 [c]		299.6322
	7	24293.308 [b]	0.877	9	7496.868 [c]		299.6749
4101.097	2	5351.000	0.352	7	7484.256	39.97338	299.1710
	3	9199.771	0.454	5	7484.390		299.1763
	4	12985.246	0.579	7	7484.421		299.1776
	5	16750.387	0.860	18	7484.461		299.1792
	7	24255.297	0.831	7	7484.739 [c]		299.1903
	8	27865.850	1.363	23	7451.057 [c]		297.8439
3266.735	2	5339.317	0.359	6	7467.624	39.97342	298.5065
	3	9179.682	0.466	4	7467.730		298.5107
	4	12956.947	0.593	7	7467.758		298.5118
	5	16713.995	0.805	14	7467.790		298.5131
	6	20460.433 [b]	1.154	25	7467.431		298.4987
	7	24203.457	0.840	6	7468.131 [c]		298.5267
	8	27803.386	1.658	32	7433.002 [c]		297.1225
2608.368	2	5322.166	0.373	5	7457.409	39.97346	298.0984
	3	9167.361	0.490	4	7457.473		298.1010

p / kPa	n	f_{0n} / s^{-1}	g_{0n} / s^{-1}	δ	(u/a) / s^{-1}	$10^3 a$ / m	u / m·s^{-1}
2608.368	4	12939.620	0.633	7	7457.509	39.97346	298.1024
	5	16691.729	0.806	11	7457.533		298.1034
	6	20433.641	0.990	15	7457.264 [c]		298.0926
	7	24171.745	0.874	4	7457.787 [c]		298.1135
1593.229 [a]	2	5325.099	0.421	3	7447.249	39.97351	297.6927
	3	9155.205	0.559	3	7447.265		297.6934
	4	12922.487	0.714	6	7447.269		297.6935
	5	16669.756	0.844	7	7447.280		297.6939
	6	20407.407	0.930	6	7447.134		297.6881
	7	24140.699	0.937	2	7447.401		297.6988
	8	27870.396	2.410	52	7448.336 [c]		297.7361
790.353 [a]	2	5321.482	0.540	1	7442.077	39.97356	297.4863
	3	9149.033	0.725	2	7442.073		297.4861
	4	12913.941	0.888	3	7442.121		297.4880
	5	16658.848 [b]	0.951	1	7442.121		297.4880
	6	20394.500	1.132	2	7442.041		297.4849
	7	24125.591	1.218	1	7442.163		297.4897
	8	27853.513	1.951	23	7442.621 [c]		297.5080
189.479	2	5319.969	1.037	1	7440.417	39.97359	297.4202
	3	9146.617	1.402	3	7440.389		297.4190
	4	12910.678	1.709	3	7440.418		297.4202
	5	16654.831 [b]	1.843	6	7440.416		297.4201

p / kPa	n	f_{0n} / s^{-1}	g_{0n} / s^{-1}	δ	(u/a) / s^{-1}	$10^3 a$ / m	u / m·s^{-1}
115.850	2	5319.673 [b]	1.308	1	7440.355	39.97359	297.4177
	3	9146.212	1.798	4	7440.317		297.4162
	4	12910.183	2.145	0	7440.342		297.4172
	5	16654.267 [b]	2.372	8	7440.339		297.4171
63.342	2	5319.288 [b]	1.815	7	7440.310	39.97360	297.4160
	3	9145.799 [b]	2.404	1	7440.324		297.4165
	5	16653.866 [b]	3.379	4	7440.453 [c]		297.4217
			T/K = 273.160 [d]				
6924.972 [a]	2	5632.829	0.321	3	7879.432 [c]	39.98792	315.0821
	3	9684.224	0.477	8	7879.621		315.0896
	4	13668.783	0.507	3	7879.680		315.0920
	5	17631.159	0.736	12	7879.601		315.0888
	6	21584.659	1.595	47	7880.500 [c]		315.1248
6342.753	2	5614.048	0.319	2	7852.895 [c]	39.98795	314.0212
	3	9651.958	0.501	11	7853.083		314.0287
	4	13623.207	0.510	3	7853.090		314.0289
	5	17572.595	0.749	12	7853.051		314.0274
	6	21513.130	1.633	48	7853.888 [c]		314.0609
5790.772	2	5598.438	0.316	1	7830.919 [c]	39.98798	313.1386
	3	9625.053	0.460	6	7830.934		313.1432

p / kPa	n	f_{0n} / s^{-1}	g_{0n} / s^{-1}	δ	(u/a) / s^{-1}	$10^3 a$ / m	u / $m \cdot s^{-1}$
5790.772	4	13585.266	0.557	6	7830.930	39.98798	313.1431
	5	17523.868	0.776	14	7830.933		313.1432
	6	21453.551	1.746	53	7831.690 [c]		313.1735
5124.476	2	5581.221	0.324	2	7806.534 [c]	39.98802	312.1678
	3	9595.452	0.463	6	7806.627		312.1715
	4	13543.641	0.534	4	7806.677		312.1735
	5	17470.234	0.755	12	7806.646		312.1723
	6	21387.815	1.582	45	7807.252 [c]		312.1965
4392.389	2	5564.463	0.332	2	7782.775 [c]	39.98806	311.2181
	3	9566.669	0.460	4	7782.867		311.2217
	4	13503.033	0.511	1	7782.891		311.2227
	5	17417.992	0.704	8	7782.857		311.2213
	6	21323.789	1.460	39	7783.312 [c]		311.2395
	7	25219.622	1.059	11	7783.300 [c]		311.2391
3720.628	2	5550.902	0.345	2	7763.547 [c]	39.98810	310.4495
	3	9543.355	0.482	5	7763.616		310.4522
	4	13470.175	0.544	2	7763.635		310.4529
	5	17375.833	0.806	13	7763.645		310.4534
	6	21272.291	1.331	32	7764.032 [c]		310.4688
	7	25159.738	0.958	5	7764.074 [c]		310.4705
3002.582	2	5538.247	0.354	2	7745.639 [c]	39.98814	309.7337
	3	9521.568	0.510	5	7745.660		309.7336

p / kPa	n	f_{0n} / s^{-1}	g_{0n} / s^{-1}	δ	(u/a) / s^{-1}	$10^3 a$ / m	u / m·s^{-1}
3002.582	4	13439.509	0.564	1	7745.692	39.98814	309.7345
	5	17336.327	0.759	8	7745.666		309.7358
	6	21223.978	1.277	28	7745.962 [c]		309.7466
	7	25103.577	0.963	3	7746.045 [c]		309.7499
2295.899	2	5527.610	0.390	2	7730.591	39.98815	309.1322
	3	9503.313	0.535	4	7730.612		309.1330
	4	13413.815	0.609	1	7730.649		309.1345
	5	17303.325	0.786	6	7730.630		309.1338
	6	21183.661	1.147	18	7730.852 [c]		309.1427
	7	25056.793	0.972	1	7730.971 [c]		309.1474
1667.122	2	5519.656	0.546	2	7719.253	39.98821	308.6791
	3	9489.646	0.612	6	7719.250		308.6790
	4	13394.560	0.692	2	7719.275		308.6800
	5	17278.631	0.846	5	7719.269		308.6798
	6	21153.525	1.177	15	7719.435 [c]		308.6364
	7	25021.878	1.037	2	7719.574 [c]		308.6919
975.569	2	5512.320	0.542	3	7708.883	39.98825	308.2647
	3	9477.079	0.714	2	7708.867		308.2641
	4	13376.907	0.851	2	7708.895		308.2652
	5	17255.998	1.012	4	7708.892		308.2651
	6	21125.711 [b]	1.310	12	7708.919		308.2662
248.466	2	5505.860	0.984	1	7700.239	39.98827	307.9192

p / kPa	n	f_{0n} / s^{-1}	g_{0n} / s^{-1}	δ	(u/a) / s^{-1}	$10^3 a$ / m	u / m·s^{-1}
248.466	3	9466.182	1.318	2	7700.229	39.98827	307.9188
	4	13361.697	1.596	2	7700.252		307.9198
	5	17236.653	1.860	2	7700.273		307.9206
	6	21102.242	2.291	10	7700.250		307.9197
	7	24963.019	2.416	-19	7700.439 [c]		307.9272
206.440	2	5505.478	1.079	2	7699.820	39.98827	307.9025
	3	9465.561	1.449	3	7699.807		307.9020
	4	13360.849	1.753	2	7699.829		307.9028
	5	17235.571	2.026	1	7669.844		307.9034
	6	21100.897 [b]	2.364	4	7699.802		307.9018
153.455	2	5504.960	1.224	1	7699.290	39.98827	307.8813
	3	9464.741	1.652	0	7699.280		307.8809
	4	13359.746	2.030	2	7699.304		307.8818
	5	17234.201	2.362	1	7699.321		307.8825
	6	21099.331	2.933	12	7699.300		307.8817
101.646	2	5504.404	1.520	1	7698.806	39.98827	307.8619
	3	9463.902	2.057	3	7698.798		307.8616
	4	13358.652	2.515	2	7698.826		307.8627
	5	17232.833	2.922	1	7698.830		307.8629
	6	21097.757	3.588	11	7698.819		307.8625
43.284 [a]	2	5503.397	2.353	3	7698.534	39.98827	307.8511
	3	9462.546	3.137	-4	7698.570		307.8525

p / kPa	n	f_{0n} / s^{-1}	g_{0n} / s^{-1}	δ	(u/a) / s^{-1}	$10^3 a$ / m	u / $m \cdot s^{-1}$
43.284 [a]	4	13356.974	3.953	2	7698.598	39.98827	307.8536
	5	17230.840	4.624	-3	7698.588		307.8532
	6	21095.718	5.785	16	7698.655 [c]		307.8559
			T/K = 273.160 [e]				
6894.966 [a]	2	5630.771	0.312	1	7876.433	39.98806	314.9633
	3	9680.635	0.473	8	7876.579		314.9691
	4	13663.691	0.500	2	7867.622		314.9708
	5	17624.571	0.731	11	7876.530		314.9672
6271.313	3	9648.903	0.509	11	7850.603	39.98810	313.9307
	4	13618.909	0.507	3	7850.614		313.9311
	5	17567.073	0.739	12	7850.579		313.9297
5871.067 [a]	2	5603.259	0.311	1	7837.643	39.98812	313.4126
	3	9633.352	0.461	6	7837.769		313.4176
	4	13596.930	0.515	3	7837.741		313.4165
	5	17538.816	0.757	13	7837.710		313.4153
5589.780 [a]	2	5592.947	0.317	1	7823.080	39.98813	312.8304
	3	9615.617	0.444	4	7823.193		312.8349
	4	13572.012	0.555	6	7823.215		312.8358
	5	17506.682	0.749	12	7823.160		312.8336

p / kPa	n	f_{0n} / s^{-1}	g_{0n} / s^{-1}	δ	(u/a) / s^{-1}	$10^3 a$ / m	u / $m \cdot s^{-1}$
4869.252	2	5575.366	0.324	1	7798.195	39.98817	311.8356
	3	9885.398	0.475	7	7798.290		311.8394
	4	13529.426	0.502	1	7798.313		311.8403
	5	17451.918	0.744	11	7798.268		311.8385
4222.437 [a]	2	5560.858	0.329	1	7777.632	39.98821	311.0136
	3	9560.449	0.462	4	7777.700		311.0163
	4	13494.250	0.514	1	7777.712		311.0168
	5	17406.699	0.697	8	7777.680		311.0155
3473.029	2	5546.392	0.341	1	7757.074	39.98825	310.1918
	3	9535.553	0.484	4	7757.098		310.1928
	4	13459.188	0.535	1	7757.118		310.1936
	5	17361.613	0.693	6	7757.087		310.1923
2826.949	2	5535.431	0.365	1	7741.634	39.98829	309.5747
	3	9516.743	0.502	4	7741.662		309.5758
	4	13432.683 [b]	0.669	8	7741.676		309.5763
	5	17327.515	0.757	8	7741.634		309.5747
2119.151	2	5525.209	0.400	2	7727.145	39.98832	308.9956
	3	9499.172	0.542	3	7727.147		308.9957
	4	13407.966	0.626	1	7727.173		308.9967
	5	17295.804	0.806	6	7727.151		308.9958

p / kPa	n	f_{0n} / s^{-1}	g_{0n} / s^{-1}	δ	(u/a) / s^{-1}	$10^3 a$ / m	u / $m \cdot s^{-1}$
1451.355	2	5517.125	0.456	1	7715.676	39.98836	308.5372
	3	9485.303	0.611	2	7715.668		308.5369
	4	13388.450	0.728	2	7715.691		308.5378
	5	17270.798	0.878	4	7715.689		308.5378
717.482	2	5509.806	0.620	4	7705.426	39.98840	308.1277
	3	9472.797	0.811	2	7705.413		308.1271
	4	13370.894	0.990	3	7705.437		308.1281
	5	17248.325	1.151	4	7705.445		308.1284
	6	21116.391	1.425	10	7705.459		308.1290
214.000	2	5505.484	1.060	2	7699.796	39.98843	307.9027
	3	9465.644	1.369	-3	7699.849		307.9049
	4	13360.846 [b]	1.732	3	7699.804		307.9031
	5	17235.561	1.993	1	7699.819		307.9037
	6	21100.934	2.429	9	7699.797		307.9028
172.560	2	5505.085	1.174	1	7699.419	39.98843	307.8877
	3	9464.923	1.584	3	7699.405		307.8871
	4	13359.964 [b]	1.867	2	7699.419		307.8877
	6	21099.658	2.705	9	7699.425		307.8879
124.141	2	5504.585	1.382	1	7698.949	39.98843	307.8689
	3	9464.145	1.862	2	7698.934		307.8683
	4	13359.007 [b]	2.309	5	7698.993		307.8707
	5	17233.211	2.637	1	7698.978		307.8701

p / kPa	n	f_{0n} / s^{-1}	g_{0n} / s^{-1}	δ	(u/a) / s^{-1}	$10^3 a$ / m	u / m·s^{-1}
124.141	6	21098.168	3.241	11	7698.961	39.98843	307.8694
70.764	2	5503.871	1.822	1	7698.499	39.98844	307.8510
	3	9463.135	2.462	1	7698.606		307.8552
	4	13357.652	3.032	1	7698.504		307.8512
	5	17231.605	3.531	-1	7698.537		307.8525
	6	21095.646 [b]	5.057	45	7698.277		307.8421
23.789	2	5502.264 [b]	3.330	28	7697.983	39.98844	307.8303
	3	9461.049 [b]	4.497	15	7698.120		307.8358
			T/K = 300.000				
6798.196	2	5922.011	1.051	124	8283.911	40.01311	331.4650
	3	10181.374	0.442	3	8284.087		331.4721
	4	14370.073	0.856	26	8283.945		331.4664
	5	18536.197	1.395	46	8284.154		331.4748
	6	22691.116	1.150	24	8284.822 [c]		331.5015
	7	26666.532 [b]	0.834	6	8234.487 [c]		329.4874
	8	30843.613	1.366	22	8346.513 [c]		333.9700
6050.542	2	5897.886	0.945	106	8249.869 [c]	40.01315	330.1032
	3	10140.104	0.449	3	8250.184		330.1158
	4	14311.889	0.719	16	8250.029		330.1097
	5	18461.266	1.365	44	8250.199		330.1165
	6	22599.930	1.146	23	8250.861 [c]		330.1429

p / kPa	n	f_{0n} / s^{-1}	g_{0n} / s^{-1}	δ	(u/a) / s^{-1}	$10^3 a$ / m	u / $m \cdot s^{-1}$
6050.542	7	26790.279 [b]	2.374	63	8271.804 [c]	40.01315	330.9809
	8	30716.609	1.457	24	8277.146 [c]		331.1947
5273.117	2	5874.709	0.801	81	8217.047 [c]	40.01320	328.7903
	3	10100.383	0.450	2	8217.435		328.8059
	4	14255.930	0.726	15	8217.291		328.8001
	5	18389.268	1.189	33	8217.452		328.8066
	6	22512.066	1.126	22	8218.016 [c]		328.8291
	7	26685.154 [b]	4.212	132	8237.935 [c]		329.6262
	8	30917.349	8.493	249	8362.445 [c]		334.6082
4505.108	2	5853.725	0.711	64	8187.372 [c]	40.01324	327.6033
	3	10064.308	0.458	2	8187.732		327.6177
	4	14205.157	0.701	13	8187.624		327.6134
	5	18323.869	1.183	32	8187.741		327.6181
	6	22432.289	1.096	19	8188.228 [c]		327.6375
	7	26592.428 [b]	3.817	116	8208.075 [c]		328.4317
	8	30483.367	1.294	17	8178.965 [c]		327.2669
3794.813	2	5835.914	0.609	44	8162.195 [c]	40.01328	326.5962
	3	10033.686	0.476	2	8162.526		326.6094
	4	14162.066	0.693	10	8162.451		326.6064
	5	18268.425	1.140	28	8162.556		326.6106
	6	22364.594	1.033	15	8162.950 [c]		326.6264
	7	26449.444 [b]	0.002	-29	8162.837 [c]		326.6219
	8	30389.388	1.170	12	8144.615 [c]		325.8927

p / kPa	n	f_{0n} / s^{-1}	g_{0n} / s^{-1}	δ	(u/a) / s^{-1}	$10^3 a$ / m	u / $m \cdot s^{-1}$
3087.985	2	5819.570	0.547	30	8139.171 [c]	40.01332	325.6752
	3	10005.547	0.503	2	8139.441		325.6860
	4	14122.485	0.714	9	8139.403		325.6845
	5	18217.504	1.041	21	8139.496		325.6882
	6	22302.465	1.005	12	8139.819 [c]		325.7011
	7	26376.823 [b]	5.186	166	8139.544 [c]		325.6901
	8	30303.007	1.244	12	8114.565 [c]		324.6907
2368.781	2	5804.551	0.525	20	8117.882	40.01336	324.8237
	3	9979.670	0.552	2	8118.076		324.8314
	4	14086.064	0.745	8	8118.054		324.8306
	5	18170.615	1.022	16	8118.115		324.8330
	6	22245.266	1.012	9	8118.369 [c]		324.8432
	7	26309.408 [b]	4.253	128	8117.764		324.8190
	8	30223.089	1.348	13	8087.451 [c]		323.6061
1608.874	2	5790.180	0.540	12	8097.602	40.01340	324.0126
	3	9954.909	0.649	3	8097.708		324.0169
	4	14051.256	0.836	7	8097.719		324.0173
	5	18125.256	1.061	12	8097.500		324.0086
	6	22190.627	1.082	6	8097.933		324.0259
	7	26246.681 [b]	2.809	68	8097.516		324.0092
	8	30146.752	1.399	9	8062.143 [c]		322.5938
854.115	2	5777.412	0.654	7	8079.654	40.01344	323.2947
	3	9932.945	0.849	4	8079.682		323.2958

p / kPa	n	f_{0n} / s^{-1}	g_{0n} / s^{-1}	δ	(u/a) / s^{-1}	$10^3 a$ / m	u / $m \cdot s^{-1}$
854.115	4	14020.398	1.039	5	8079.716	40.01344	323.2972
	5	18086.187	1.227	6	8079.744		323.2983
	6	22142.244	1.354	5	8079.830		323.3017
	7	26191.261	2.247	33	8079.597		323.2924
	8	30079.076	1.753	8	8039.976 [c]		321.7071
224.301	2	5767.659	1.152	2	8066.413	40.01347	322.7652
	3	9916.352	1.554	3	8066.393		322.7644
	4	13997.180	1.886	3	8066.425		322.7656
	5	18056.477	2.257	6	8066.452		322.7667
	6	22106.040 [b]	2.442	0	8066.451		322.7667
	7	26150.058	2.890	6	8066.398		322.7645
	8	30028.354 [b]	2.798	-7	8023.590 [c]		321.0516
149.409	2	5766.364	1.390	1	8064.983	40.01348	322.7081
	3	9914.213	1.901	3	8064.951		322.7068
	4	13994.233	2.311	3	8064.979		322.7079
	5	18052.697 [b]	2.627	2	8064.982		322.7080
93.190	2	5765.204 [b]	1.751	3	8063.892	40.01348	322.6644
	3	9912.412	2.404	3	8063.896		322.6645
	4	13991.823	2.942	2	8063.937 [c]		322.6662
60.953	2	5764.399 [b]	2.161	5	8063.278	40.01348	322.6398
	3	9911.238	2.958	0	8063.317		322.6414
	4	13990.311 [b]	3.693	3	8063.371		322.6435

p / kPa	n	f_{0n} / s^{-1}	g_{0n} / s^{-1}	δ	(u/a) / s^{-1}	$10^3 a$ / m	u / $m \cdot s^{-1}$
60.953	5	18047.723	4.070	14	8063.322 [c]	40.01348	322.6416

[a] Pressure removed from final analysis.

[b] (u/a) received weight less than unity.

[c] (u/a) omitted from final regression analysis.

[d] Isotherm performed with transducers described in text.

[e] Isotherm performed with wave guide to microphone of length 6 mm and source with 6 mm diameter active element mounted flush with the resonator's inner surface; both devices were mounted in aluminium bodies.

of diameter 6 mm, operated with high efficiency but at higher pressures the efficiency decreased, especially at higher frequencies, until at pressures above 1 MPa the signals were too weak and unstable to be useful. These variations in efficiency are believed to have been caused by the back plate and back chamber arrangement which have been described in detail elsewhere.[66] The microphone also differed; it was coupled to the spherical cavity by a 6 mm long 1 mm diameter wave guide. This isotherm is indicated in table 6.2 and all other tables in this section by a superscript *e*.

For the thermal boundary layer correction the accommodation coefficient was taken as 0.84, as determined previously;[21] further analysis confirmed this choice of h. The thermal conductivities and shear viscosities used for the corrections are those tabulated by Maitland *et al.*;[22] the original measurements were made by Kestin and co-workers.[23,24] In contrast with the measurements discussed in Chapter Five the variation of κ and η with density is important for the results reported here. The virial coefficients required for ρ, $C_{p,m}$, and γ in the acoustic model were estimated from the results reported by Dymond and Smith in their comprehensive review.[25]

Above about 1.6 MPa the corrections to (u/a) are dominated by those due to shell motion. At these pressures $\Delta f_w/f$ ranged from 10^{-2} for the (0,8) mode at 6.8 MPa and 300 K, and 70×10^{-6} for the (0,2) mode at 1.6 MPa and 255 K. Below 250 kPa $\Delta f_w/f$ was always less than 30×10^{-6}. The speed of

sound required in this calculation was estimated from a preliminary analysis of the results.

The thermal-boundary-layer correction ranged between 22×10^{-6} for the (0,8) mode at 6.8 MPa and 300 K, and 550×10^{-6} for the (0,2) mode at 23.8 kPa and 273.16 K.

The residual experimental half widths, defined by equation (5.3.2), for the isotherm at 255 K are reported in table 6.2 and plotted in figure 6.5. Except for (0,6), $\Delta g/f$ increases linearly with pressure and may be consistent with a perturbation arising from the shell. If such an effect were due to a combination of radiation from the external surface and losses within the wall then $\Delta g/f$ would also increase as the frequency approached the radial shell resonance. Clearly this is not the case. The (0,6) mode shows a fractional excess half width which increases rapidly with pressure above about 4 MPa. A possible explanation for this observation is an overlap of the acoustic resonance with a shell resonance, which has a particularly low resonance quality factor. The (0,3) and (0,4) modes are in excellent agreement with each other, and in general $\Delta g/f$ is less than 10×10^{-6} for these modes.

The quantity (u/a) determined from each mode is shown in figure 6.6 as deviations from the mean (u/a) at each pressure. For modes (0,3) and (0,4) the values of (u/a) agree to within 5×10^{-6} at all pressures, while (0,5) mode gave values no more than 15×10^{-6} above the mean. At 6.8 MPa fractional deviations for (0,6) and (0,7) modes span 200×10^{-6}, while the (0,2) mode deviates by 50×10^{-6}.

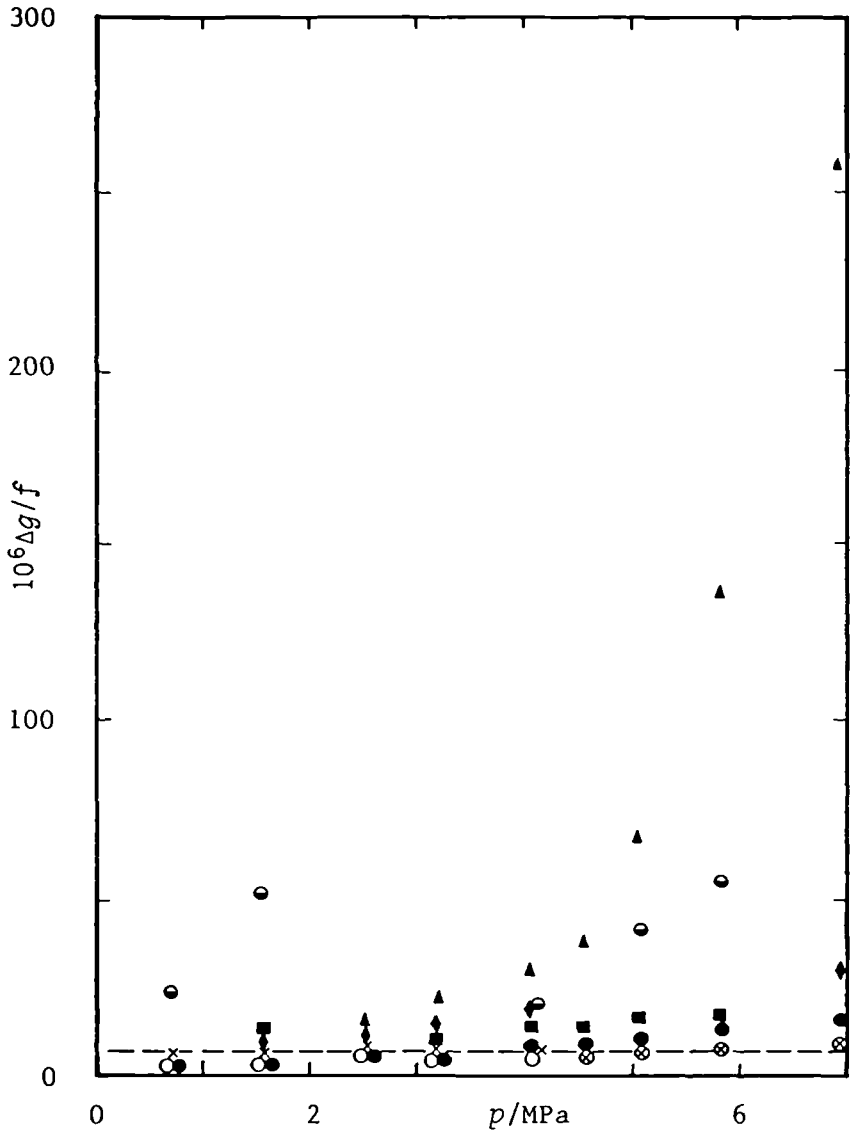

Figure 6.5. Fractional excess half widths as a function of pressure in argon at 255 K. The dotted line indicates 8×10^{-6}. ● , (0,2); ○ , (0,3); X , (0,4); ♦ , (0,5); ▲ , (0,6); ■ , (0,7); ◒ , (0,8).

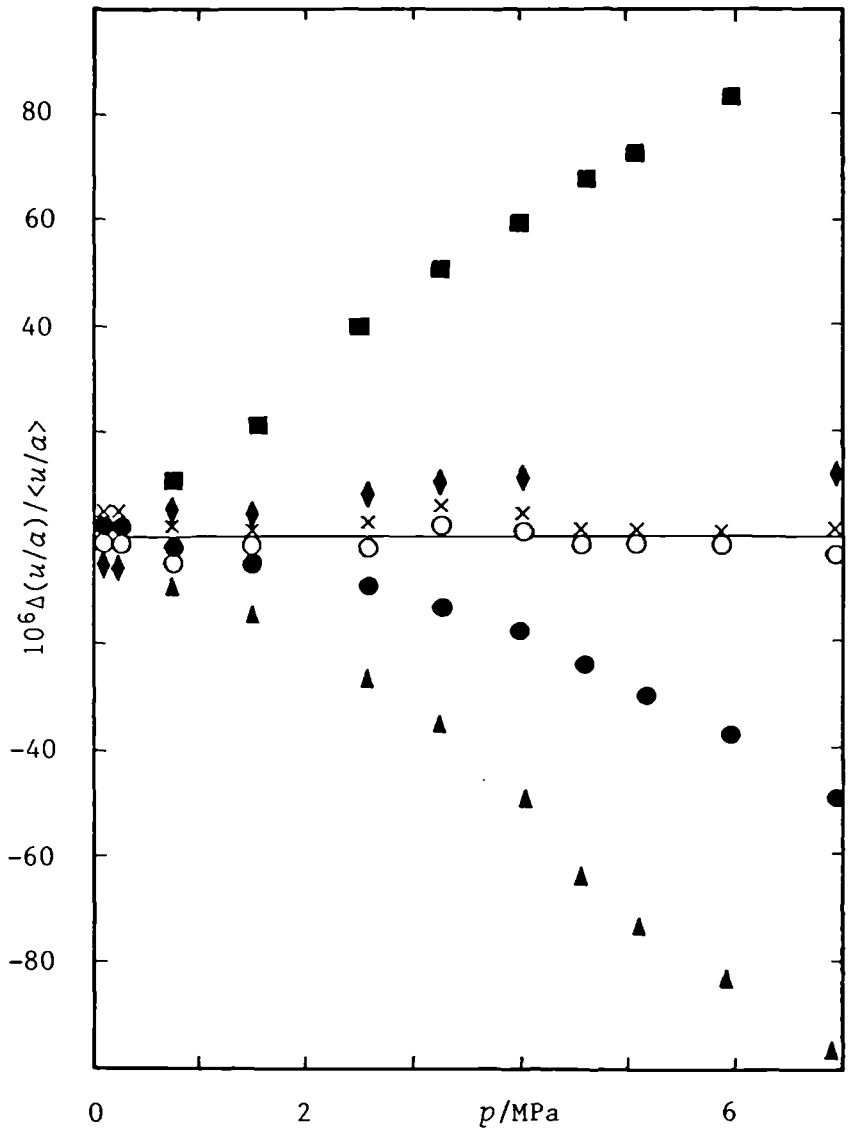

Figure 6.6. Fractional deviations $\Delta(u/a)/\langle u/a\rangle = \{(u/a) - \langle u/a\rangle\}/\langle u/a\rangle$ for individual modes in argon at 255 K, from the mean $\langle u/a\rangle$ of the modes finally selected for analysis with equation (5.3.6) at each pressure. ● , (0,2); ○ , (0,3); X , (0,4); ♦ , (0,5) Δ , (0,6); ■ , (0,7).

The deviations decrease at lower pressures: for example, at 790 kPa the variations in the (u/a) from the seven modes have decreased by a factor of 10 and at 190 kPa the remaining four observed modes span 10×10^{-6}, a further factor of 2 reduction.

Both $\Delta(u/a)$ and $\Delta g/f$ indicate a pressure dependent perturbation which might arise from coupling to shell resonances.

Mehl,[26] has developed a theory for the shell resonances of a perfect isotropic sphere. Since it was likely that the resonator was not a perfect isotropic sphere, the in phase response to 42 kHz was studied under vacuum in an attempt to monitor the shell resonances of the sphere. Figure 6.7 shows the results of such a scan at 255 K together with the shell-resonance frequencies expected from theory (see Chapter Three), and the frequency ranges for the (0,2) to (0,7) radial acoustic modes for the argon isotherms at 255 K. Although this crude experiment appears to have detected resonances which are in general close to the predicted shell resonances, it can not be expected to detect every resonance and may also detect resonances other than those attributed solely to the shell. The strong multiplet observed at about 21 kHz is associated with a shell resonance since its frequency and structure were independent of temperature and the resonator's environment (a scan with the resonator suspended by wires in an evacuated glass dessicator gave similar results). This band might be either the 7 or 9 component bending (or a combination of both) modes shifted by the holes in the resonator's wall from the

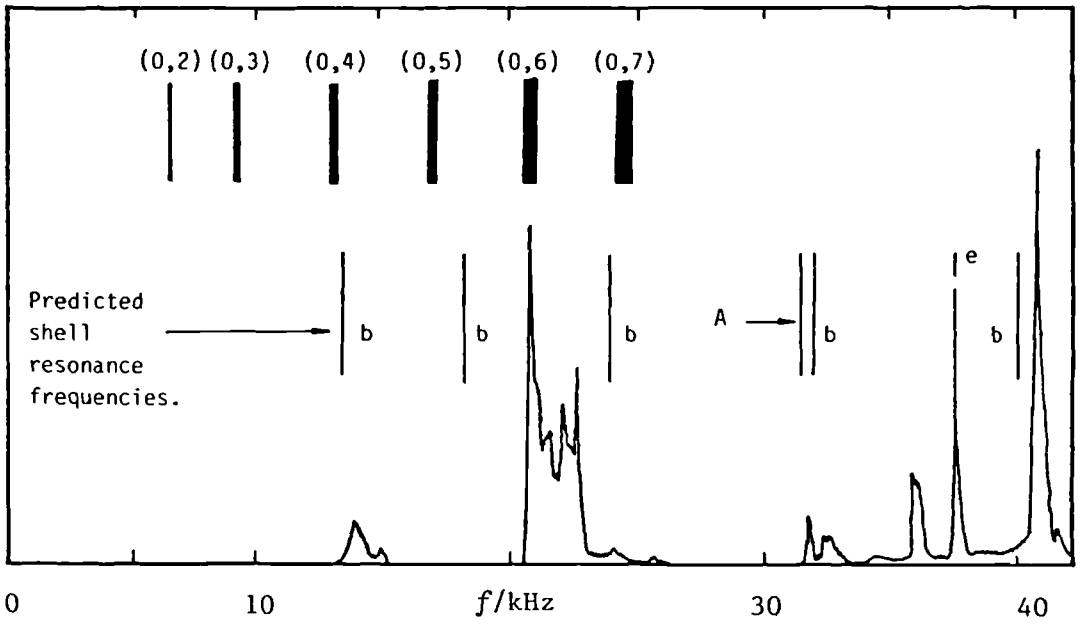

Figure 6.7. Bottom: Resonances detected using the acoustic source and microphone, in the aluminium resonator (shown in figure 6.1) at 255 K and p< 3 MPa. Middle: Shell resonances for an isotropic perfectly spherical shell constructed from aluminium with (a = 40 mm and b = 50 mm) t = 1.25 calculated from equation (3.2.27) using Λ_{ln} given in table 3.3. b, bending; e, extentional; A, breathing resonance. Top: Frequency range of the (0,2) to (0,7) acoustic modes at 255 K over the experimental pressure range.

predicted values of 18 and 24 kHz respectively. The (0,6) acoustic mode overlaps with this shell mode, and it is believed that the large pressure dependent half widths, shown in figure 6.5, and the discrepancies shown in figure 6.6 for (u/a) may be attributed to the coupling between the acoustic and shell modes. A similar, albeit

smaller, discrepancy has been observed for the (0,6) mode of the 60 mm radius resonator containing argon. The pressure dependent positive $\Delta(u/a)$ for the (0,7) acoustic mode is shown in figure 6.6. Again a possible explanation is the coupling of the radial acoustic mode to the shell mode at 21 kHz or coupling with the predicted, and possibly observed, 9 component bending mode at 23 kHz; both of these shell resonances lie below $f_{(0,7)}$ and hence would decrease the observed acoustic resonance frequency. A further possible explanation of the perturbation arises from the overlap with adjacent acoustic modes (2,5) and (13,1), although no supporting evidence was found when this hypothesis was tested by measurements over the (0,7), (2,5) and (13,1) modes at 4 MPa.

Figures 6.5 to 6.7 show that the behaviour of the (0,2) mode cannot be accounted for in terms of shell resonances and an alternative explanation must be sought. Figure 6.8 shows scans over the (0,2) and the adjacent (3,1) modes at 6.7 and 3.8 MPa. At the higher pressure the seven components of (3,1) have been split superficially into a doublet, the lower component of which is only partially resolved from the (0,2) mode. At 3.8 MPa the (3,1) is apparently no longer split and there is no evidence for coupling with the radial mode. The pressure dependence of the splitting of the mode (3,1), and its coupling with (0,2), is probably due to elastic anisotropy in the shell. The effects of transducer location will be discussed later. Below 4 MPa, (u/a) from (0,2) agrees fractionally to 20×10^{-6} with the values of

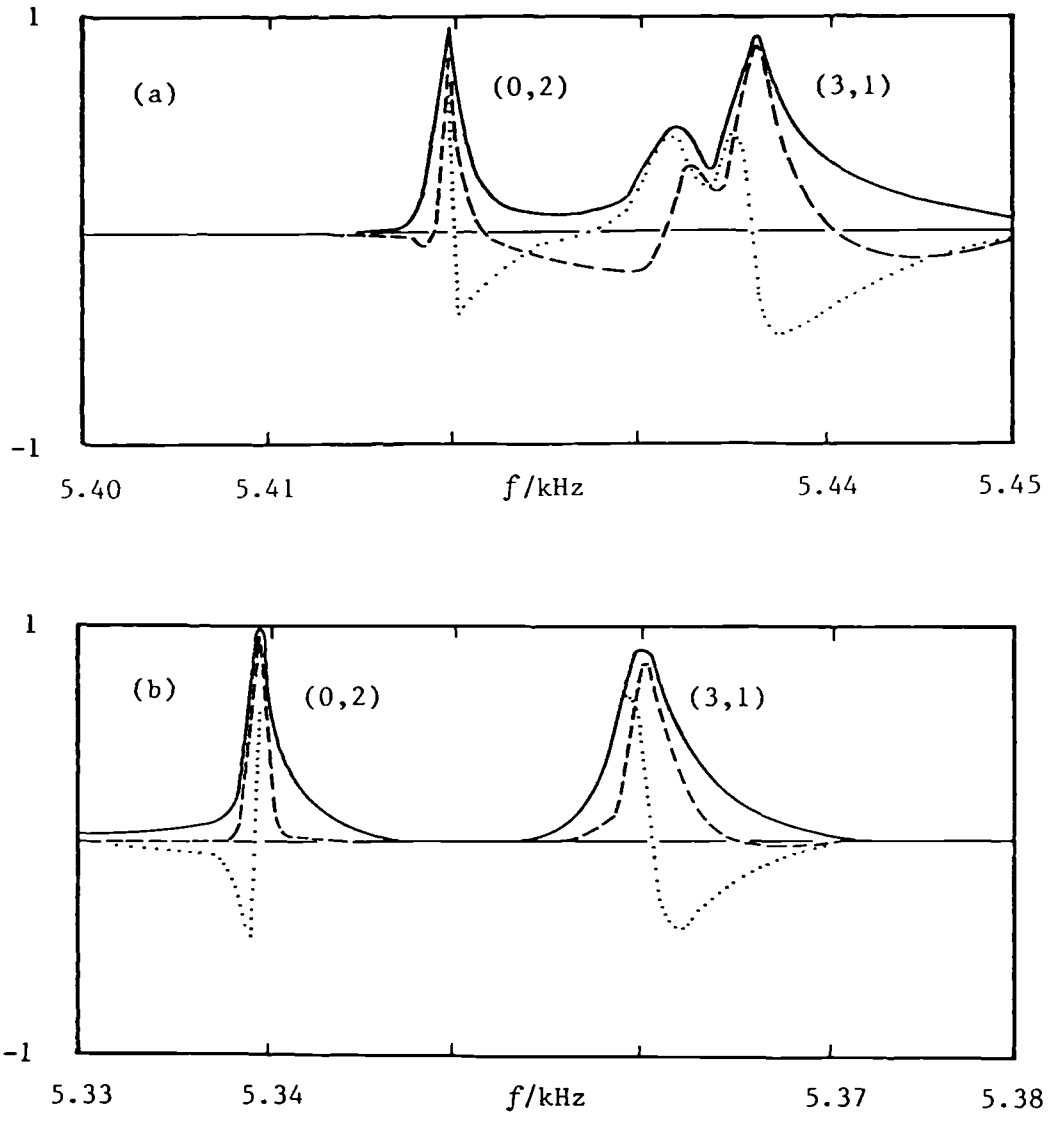

Figure 6.8. Real and imaginary components of the complex potential difference ratio w {equation (4.2.11)}, calculated from measurements of the relative amplitude $\bar{a}$ and phase ϕ between the received and reference signals at frequencies over the (0,2) and (3.1) modes in argon at 255 K. (a); At a pressure of 6.7 MPa, where the ordinate axis has been scaled to a maximum $\bar{a}$ of 0.68. (b); At a pressure of 3.8 MPa, where the ordinate axis has been scaled to a maximum $\bar{a}$ of 3.11. – – – – , Re(w); · · · · , Im(w); ———, $\bar{a}$.

(u/a) obtained from the (0,3) and (0,4) modes. The fractional excess half widths $\Delta g/f$ for (0,2) never exceed 17×10^{-6} and, again, below 4 MPa are in excellent agreement with the values obtained from (0,3) and (0,4). No attempt was made to analyse measurements over (3,1) and (0,2) with two or more terms in the summation of equation (3.4.62).

The shell resonances, in contrast with the acoustic modes are essentially independent of temperature; a shell scan at 300 K was identical to that shown in figure 6.7.

For the isotherm at 273.16 K $\Delta g/f$ is shown in figure 6.9. Again the (0,6) mode has a large pressure dependent

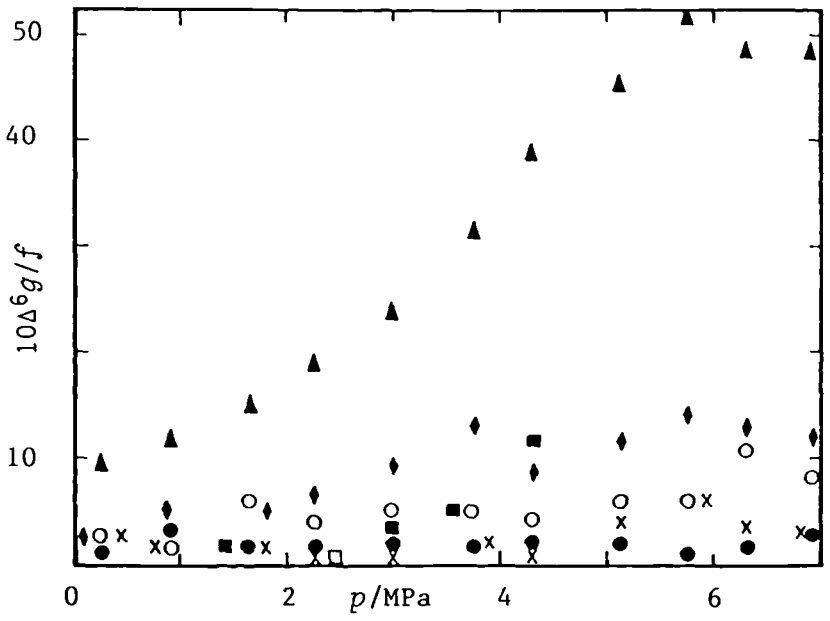

Figure 6.9. Fractional excess half widths as a function of pressure in argon at 273.16 K. ● , (0,2); ○ , (0,3); X , (0,4); ♦ , (0,5); ▲ , (0,6); ■ , (0,7).

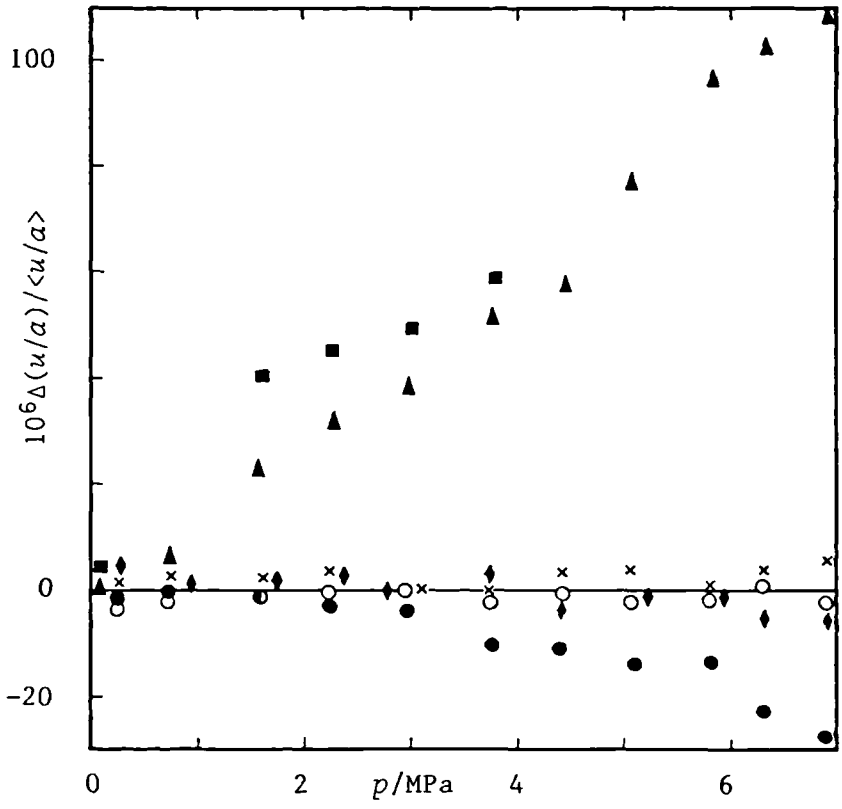

Figure 6.10. Fractional deviations $\Delta(u/a)/\langle u/a\rangle = \{(u/a) - \langle u/a\rangle\}/\langle u/a\rangle$ for individual modes in argon at 273.16 K, from $\langle u/a\rangle$ of the modes finally selected at each pressure for analysis with equation (5.3.6). ● , (0,2); ○ , (0,3); × , (0,4); ♦ , (0,5); ▲ , (0,6); ■ , (0,7).

$\Delta g/f$ exceeding 50×10^{-6} at and above 5.7 MPa. The $\Delta g/f$ for (0,6) are about a factor of 3 smaller than those observed at 255 K and similar densities. For the remaining modes $\Delta g/f$ are less than about 15×10^{-6} over the whole pressure range, and below 1 MPa they are less than 5×10^{-6}. Figure 6.10, shows for the isotherm at 273.16 K, the values of (u/a) as determined from each mode as fractional deviations from $\langle u/a\rangle$ of the modes finally selected for

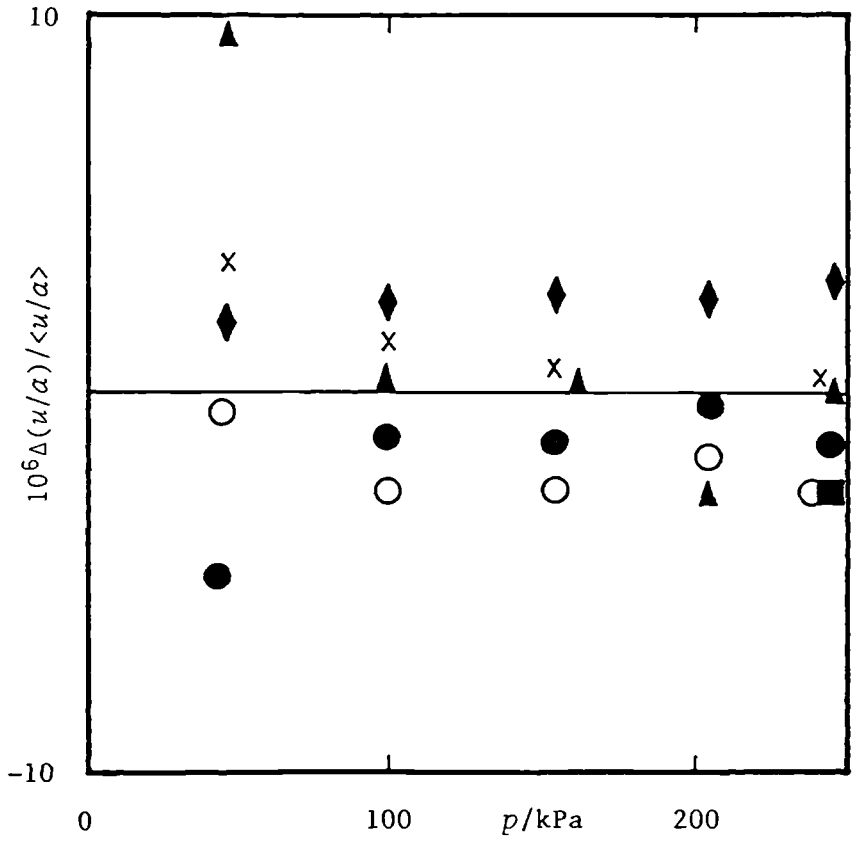

Figure 6.11. Fractional deviations $\Delta(u/a)/\langle u/a\rangle = \{(u/a) - \langle u/a\rangle\}/\langle u/a\rangle$, for the individual modes in argon at 273.16 K, from $\langle u/a\rangle$ of the modes finally selected for analysis with equation (5.3.6) at each pressure below 250 kPa.

● , (0,2); ○ , (0,3); X , (0,4); ♦ , (0,5); ▲ , (0,6); ■ , (0,7).

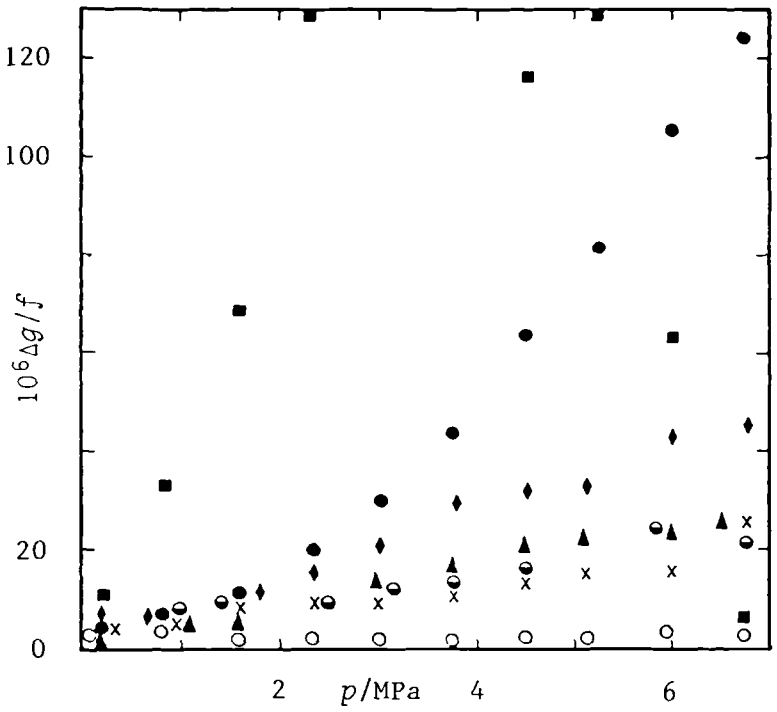

Figure 6.12. Fractional excess half widths $\Delta g/f$ as a function of pressure in argon at 300 K. ● , (0,2); ○ , (0,3); X , (0,4); ♦ , (0,5); ▲ , (0,6); ■ , (0,7); ◒ , (0,8).

---

inclusion in the regression analysis. Mode (0,6) has a large positive deviation; at 255 K this mode showed negative deviations. Such observations are consistent with $f(0,6)$ between 255 and 273.16 K passing through the shell resonance. The (u/a) for (0,3), (0,4), and (0,5) modes span about 10×10^{-6} at the highest pressure with the agreement improving at lower pressures.

The deviations in (u/a) for individual modes from $\langle u/a \rangle$ for the measurements below 250 kPa at 273.16 K are shown in figure 6.11. Between 100 and 250 kPa the deviations for the (0,2) to (0,5) modes fractionally span no more than 6×10^{-6}, and appear to be systematic; these are similar to

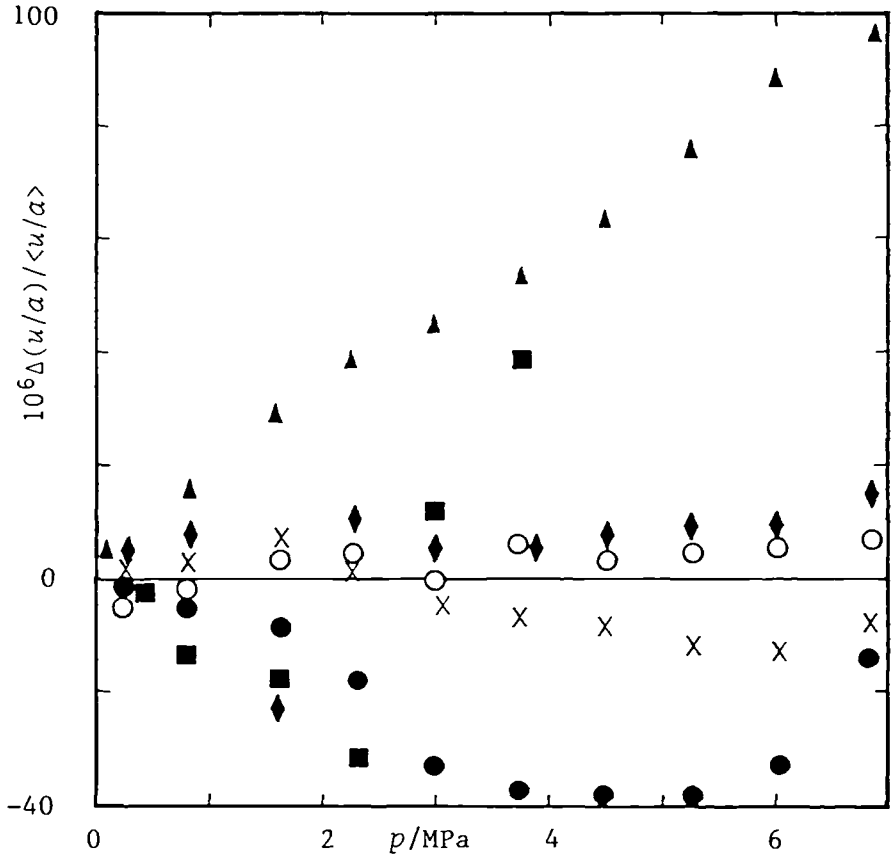

Figure 6.13. Fractional deviations $\Delta(u/a)/\langle u/a\rangle = \{(u/a) - \langle u/a\rangle\}/\langle u/a\rangle$, for individual modes in argon at 300 K, from $\langle u/a\rangle$ of the modes finally selected for analysis with equation (5.3.6) at each pressure. ● , (0,2); ○ , (0,3); X , (0,4); ♦ , (0,5); ▲ , (0,6); ■ , (0,7).

---

those observed with the 60 mm resonator at these pressures. At the lowest pressure these deviations illustrate the decline in efficiency of the transducer used to excite the sound field.

Figures 6.12 and 6.13 show, for the isotherm at 300 K, the fractional excess half widths for each mode and

deviations of (u/a) for individual modes from $\langle u/a \rangle$. For the mode (0,6) $\Delta(u/a)$ again may be attributed to coupling with a shell resonance. Before commencing measurements the sound source was removed, the film replaced, and high spots on the back plate removed. Transducer efficiency was apparently increased after this minor modification, so that the (0,7) and (0,8) modes could be studied with relative ease. The (0,8) mode occurred at frequencies between 30.1 and 30.8 kHz, which covers a range near the radial shell breathing resonance predicted at 31.2 kHz. Consequently, the (u/a) was substantially perturbed. However, the $\Delta g/f$ was similar in magnitude to that (0,4) determined for the (0,4) and (0,3) modes and did not suggest the close proximity of a shell resonance, especially not one with the same symmetry as the acoustic mode; the slight pressure dependence and small magnitude of Δg suggests a shell resonance which has a high quality factor and does not radiate significantly to the surrounding fluid. The (0,7) mode occurs at frequencies between 26.6 and 26.2 kHz and shows fractional deviations in (u/a) which are consistent with an acoustic mode whose frequency passes through that of a shell motion as the pressure is decreased. The (0,3) and (0,4) modes agree fractionally to better than 20×10^{-6} in (u/a).

Mode (0,2) showed larger $\Delta g/f$ than expected which are proportional to pressure, and also deviations in (u/a) which at the lower pressures are about a factor of 3 larger than observed at 255 K. A more obvious difference

is that $\Delta(u/a)$ is not monatonic in pressure. These differences in the behaviour of the (0,2) mode might have arisen from the replacement of the transducers which were resealed in the resonator by rotation against a rubber seal; this process may not have been reproducible in terms of the transducer orientation. It is unlikely that the threads on the transducers and in the ports are concentric and coincident with axes defining an angle of $\pi/2$. It is believed that after the source was replaced, the (3,1) mode could be excited more efficiently, which, when combined with the splitting of (3,1) with pressure, consequently produced a larger perturbation.

An attempt was made to measure the static compliance of the shell wall at 273.16 K; the method is described elsewhere.[27] The resonance frequencies of the first four radial modes were measured with a pressure of about 1494 kPa both inside and outside the resonator. The external pressure was then reduced to 211 kPa and the resonances remeasured. These results were interpreted in terms of the constant S_0' of equation (3.4.32), which varied between 11 TPa^{-1} and 16 TPa^{-1} between the (0,2) and 0,5) modes; the (0,2) mode returned 13 TPa^{-1}. The value predicted by equation (3.4.32) is 23 TPa^{-1}. No particular interpretation is placed upon these differences, and no further experiments were attempted.

These measurements with argon have been useful in characterising the resonator. The first six radial modes give values of (u/a) which agree to about 0.01 per cent over

the full pressure range to 7 MPa; coupling with the shell motions perturbs the (0,6) and (0,7) modes, especially at high pressures, while overlap with the non-radial (3,1) perturbs the (0,2) mode, again especially at high pressures. The remaining radial modes, (0,3), (0,4), and (0,5), give values of (u/a) that agree to 25×10^{-6}; the (0,5) mode was not measured at all pressures but the (0,3) and (0,4) modes were measured consistently and always agreed to 20×10^{-6} $\langle u/a \rangle$, and usually to better than 10^{-5} $\langle u/a \rangle$, over the pressure range to 7 MPa.

The experimental quantity (u/a) can be adequately represented by four terms of the infinite series (5.3.6). The results of the analysis are given in table 6.3 together with the number N of resonance frequencies in the final regression and the standard deviations. The coefficients were all significant at a probability of 0.999. Those modes which if omitted from the analysis provide a statistically significant reduction in the standard deviation of $\langle u/a \rangle$ at each pressure were removed. Also any pressure with $\langle u/a \rangle$ which deviated by more than 5 standard deviations of the fit from the smoothing equation were not retained in the regression analysis. The individual modes and complete pressures omitted from the final regression analyses are indicated in table 6.2. The similarity of the fractional standard deviation of $\langle u/a \rangle$ for the selected modes at each pressure and of (u/a) for an isotherm, show that equation (5.3.6) gives a good representation of the results. The deviations of $\langle u/a \rangle$,

Table 6.3. Coefficients for either the leading four terms of equation (5.3.6), and standard deviation s obtained by analysis of N modes for argon at temperatures T. Uncertainties are one standard deviation.

$\frac{T}{K}$	N	$\frac{10^{-6}(A_0/a^2)}{s^{-2}}$	$\frac{10(A_1/a^2)}{s^{-2}\cdot Pa^{-1}}$	$\frac{10^{8}(A_2/a^2)}{s^{-2}\cdot Pa^{-2}}$	$\frac{10^{16}(A_3/a^2)}{s^{-2}\cdot Pa^{-3}}$	$\frac{10^{6}s(u^2)}{u^2}$
255.000	30	55.35773 ± 0.00038	0.0386 ± 0.0065	3.275 ± 0.024	13.28 ± 0.23	19
273.160	52	$59.25663_9 \pm 0.00009_5$	1.4255 ± 0.0020	3.1796 ± 0.0085	9.039 ± 0.091	6
273.160[e]	50	59.25614 ± 0.00017	1.4056 ± 0.0037	3.254 ± 0.016	8.70 ± 0.18	11
300.000	49	64.99708 ± 0.00043	3.0734 ± 0.0078	3.068 ± 0.030	3.835 ± 0.030	22

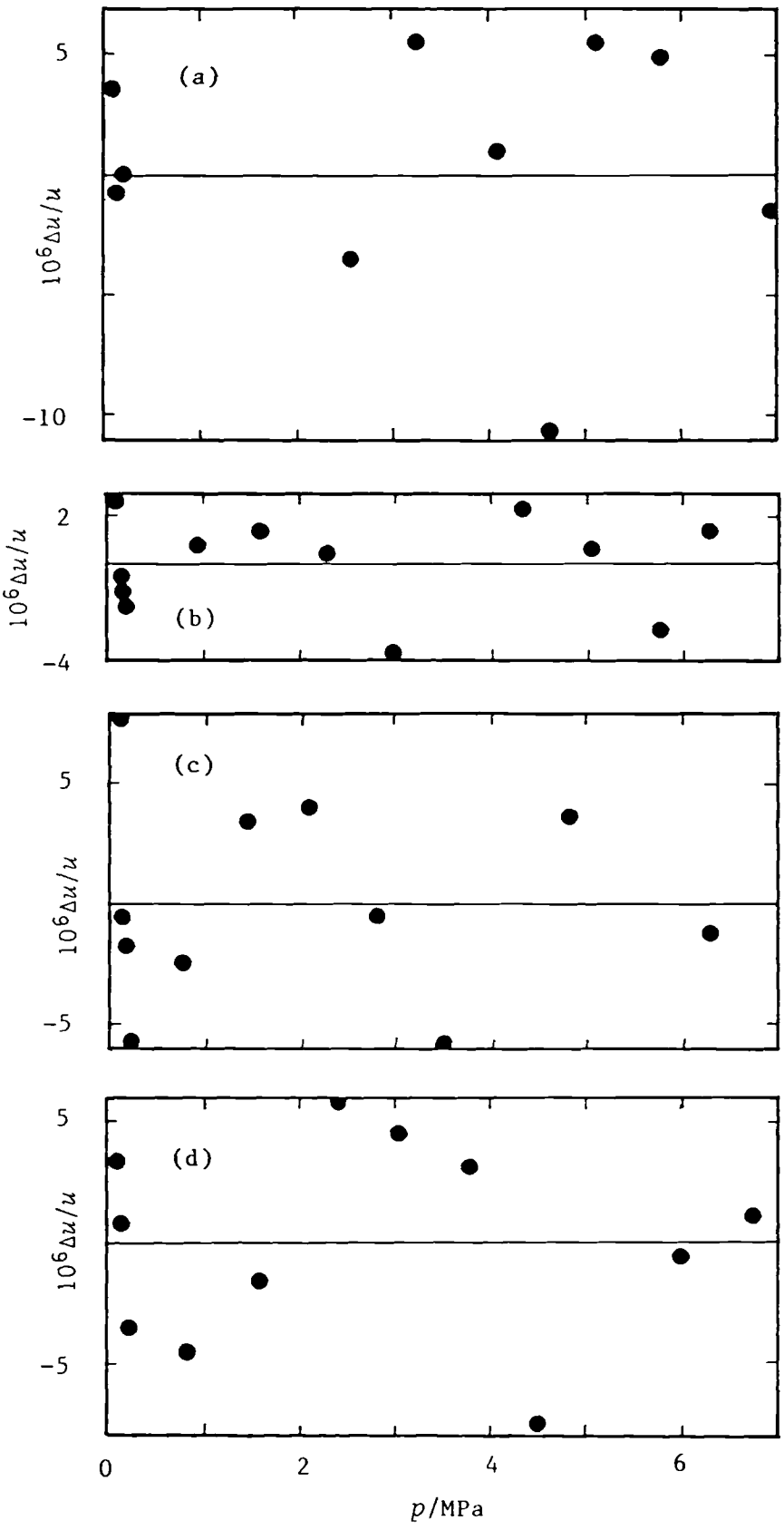

Figure 6.14. For description see subsequent page.

Figure 6.14. Fractional deviations $\Delta u/u = [\langle u/a\rangle - \{u(\text{calc.})/a\}]/\{u(\text{calc.})/a\}$, for $\langle u/a\rangle$ of selected modes in argon at each pressure from equation (5.3.6), in which the coefficients (given in table 6.4) were adjusted to fit the selected modes on each of the isotherms at : (a), 255 K; (b), 273.16 K; (c), 273.16 K^{e}; (d), 300 K.

---

of the selected modes, from the finally adopted smoothing equation are shown in figure 6.14. Clearly, the majority of the $\langle u/a\rangle$ on all isotherms lie fractionally within 5×10^{-6} of the regression equation. In particular figure 6.14(b) shows, for the best isotherm in argon, $\Delta\langle u/a\rangle$ which span fractionally only 6×10^{-6}, and in general lie within 2×10^{-6} of the smoothing equation. Since A_0 for argon is known with sufficient accuracy the radius can be obtained from the coefficient (A_0/a^2); the value of the radius so determined is given in table 6.4.

The second acoustic virial coefficients, determined from the coefficients of table 6.3 using equation (2.3.22) are reported in table 6.4, and show deviations from equation (5.3.8) of between 0.20 and 0.14 $cm^3 \cdot mol^{-1}$; equation (5.3.8) was obtained from the 12 experimental β_a provided by measurements with the 60 mm radius resonator. The β_a provided by measurements at 273.16 K with the prototype acoustic transducers is in excellent agreement with the value reported by Moldover *et al.*,[27] while the other determined at 273.16 K, although more precise, is about 0.07_5 $cm^3 \cdot mol^{-1}$ higher than their value. At a temperature near to 255 K $\beta_a = 0$.

Table 6.4 The resonators radius $a(T,p=0)$, and second acoustic virial coefficients β_a of argon at temperatures T.

T/K	a/mm	$\beta_a/(cm^3 \cdot mol^{-1})$
255.000	$39.9736_2 \pm 0.0005_5$	0.148 ± 0.025
273.160	$39.9882_7 \pm 0.0000_6$	5.464 ± 0.008
273.160[e]	$39.9884_4 \pm 0.0002_3$	5.387 ± 0.014
300.000	$40.0134_8 \pm 0.0005_3$	11.794 ± 0.030

[e] Isotherm performed with prototype transducers.

6.4.2 Methane

Resonance frequencies f and half widths g, listed in table 6.5, were measured for up to the lowest seven radial modes of the cavity along four isotherms between 255 and 350 K; usually only at the lowest pressure was it not possible to measure seven radial modes due to a combination of strong absorption and poor transducer efficiency. The isotherm at 350 K the precision of f and g was compromised by an instability in the source transducer. On this isotherm between two and four radial modes were satisfactorily measured at each pressure. Such problems prevented the measurements with argon at 350 K.

The resonance frequencies were corrected using the acoustic model described in section 2. As with argon, above 1.6 MPa the correction due to shell motion is by far the

Table 6.5. Resonance frequencies f_{0n} and half widths g_{0n}, fractional excess half widths $\delta = 10^6 \Delta g/f$, quantities (u/a), radius $a = a(T,p)$, and speeds of sound u for the n-th radial mode at temperatures T and pressures p in methane. (u/a) and u were corrected for the effect of vibrational relaxation using equation (3.3.11) with $t\rho$ obtained from analysis of δ.

p / kPa	n	f_{0n} / s^{-1}	g_{0n} / s^{-1}	δ	(u/a) / s^{-1}	$10^3 a$ / m	u / m·s^{-1}
			T/K = 255.000				
6939.689	2	6946.469	0.368	16	9716.174	39.97322	388.3868
	3	11942.136	0.526	1	9716.062		388.3823
	4	16855.078	1.422	35	9715.978		388.3789
	5	21742.810	1.810	25	9717.228 [c]		388.4289
	6	26602.256	13.287	432	9715.238 [c]		388.3493
	7	31274.008	2.161	-8	9519.033 [c]		380.5064
	8	36170.843	3.522	11	9656.260 [c]		385.9918
6331.071	2	6957.509	0.380	15	9731.338	39.97325	388.9932
	3	11961.117	0.535	2	9731.196		388.9875
	4	16881.971	1.265	23	9731.111		388.9841
	5	21777.337	1.967	29	9732.159 [c]		389.0260
	6	26646.651	11.167	349	9730.565 [c]		388.9623
	7	31605.784	7.583	161	9667.269 [c]		386.4322
	8	36226.736	3.269	0	9672.005 [c]		386.6215
5732.793	2	6978.665	0.354	9	9760.672	39.97329	390.1661
	3	11997.519	0.546	-1	9760.527		390.1603
	4	16933.482	1.233	18	9760.465		390.1578
	5	21843.874	1.732	16	9761.442 [c]		390.1969
	6	26729.890 [b]	11.707	365	9760.193 [c]		390.1470

p / kPa	n	f_{0n} / s^{-1}	g_{0n} / s^{-1}	δ	(u/a) / s^{-1}	$10^3 a$ / m	u / m·s^{-1}
5732.793	7	31416.091	2.297	-11	9565.469	39.97329	382.3632
5081.085	2	7011.445	0.356	7	9806.271	39.97332	391.9892
	3	12053.965	0.569	-2	9806.170		391.9852
	4	17013.282	1.237	15	9806.129		391.9835
	5	21946.830	1.771	13	9807.003 [c]		392.0185
	6	26861.165	11.007	332	9807.383 [c]		392.0337
	7	31562.656	2.400	-13	9663.104 [c]		386.2664
	8	36205.767 [b]	3.701	1	9667.769 [c]		386.4528
4384.756	2	7055.979	0.360	5	9868.278	39.97336	394.4682
	3	12130.618	0.602	-3	9868.219		394.4659
	4	17121.609	1.226	10	9868.199		394.4651
	5	22086.440	1.793	8	9868.906 [c]		394.4933
	6	27032.748	9.349	261	9869.250 [c]		394.5071
	7	31762.184	2.530	-17	9756.324 [c]		389.9930
	8	36736.609 [b]	4.292	8	9810.652 [c]		392.1647
3613.728	2	7114.720	0.384	5	9950.053	39.97340	397.7375
	3	12231.644	0.657	-4	9949.991		397.7350
	4	17264.274	1.329	12	9949.952		397.7334
	5	22270.473	1.896	4	9950.536 [c]		397.7568
	6	27263.485 [b]	9.191	243	9952.565 [c]		397.8379
	7	32025.436	2.945	-17	9855.346 [c]		393.9517
	8	36738.024 [b]	7.226	73	9811.619 [c]		392.2038

p / kPa	n	f_{0n} / s^{-1}	g_{0n} / s^{-1}	δ	(u/a) / s^{-1}	$10^3 a$ / m	u / $m \cdot s^{-1}$
2696.945	2	7195.056	0.426	3	10062.152	39.97345	402.2189
	3	12369.822	0.788	-4	10062.098		402.2168
	4	17459.428	1.566	8	10062.053		402.2150
	5	22522.286	2.192	0	10062.515 [c]		402.2335
	6	27571.819 [b]	5.543	87	10064.152 [c]		402.2989
	7	32385.890	3.520	-23	9977.529 [c]		398.8363
	8	37150.705 [b]	8.385	76	9922.869 [c]		396.6513
1749.148	2	7285.469	0.526	1	10188.335	39.97350	407.2634
	3	12525.336	1.055	-4	10188.290		407.2616
	4	17679.201 [b]	2.085	8	10138.314		407.2626
	5	22805.826 [b]	2.853	-7	10188.616 [c]		407.2747
	6	27918.705 [b]	5.128	29	10139.631 [c]		407.3152
	7	32791.279	5.143	-23	10108.595 [c]		404.0760
	8	37930.209 [b]	8.226	13	10132.036 [c]		405.0130
963.891	2	7365.724	0.757	1	10300.301	39.97355	411.7396
	3	12663.378	1.679	-2	10300.249		411.7375
	4	17874.305	3.154	3	10300.334		411.7409
	5	22805.826 [b]	2.853	-88	10138.007 [c]		407.2508
	6	28227.188	7.273	8	10300.987 [c]		411.7670
	7	33152.347 [b]	8.881	-24	10222.950 [c]		408.6476
	8	38030.363 [b]	14.210	39	10159.236 [c]		406.1007
234.144	2	7443.189	2.273	4	10408.635	39.97359	416.0705
	3	12796.956 [b]	5.829	12	10408.655		416.0713

p / kPa	n	f_{0n} / s^{-1}	g_{0n} / s^{-1}	δ	(u/a) / s^{-1}	$10^3 a$ / m	u / m·s^{-1}
234.144	4	18063.617 [b]	10.868	9	10408.874 [c]	39.97359	416.0801
171.372 [a]	2	7450.153 [b]	2.975	6	10418.450	39.97359	416.4629
	3	12809.342 [b]	7.892	26	10418.654		416.4710
	4	18082.311 [b]	14.241	-6	10419.374 [c]		416.4998
98.161 [a]	2	7457.966 [b]	5.016	40	10429.111	39.97360	415.8890
	3	12818.160 [b]	11.532	-90	10424.979		416.7239
46.952 [a]	2	7495.513 [b]	11.960	335	10480.939 [c]	39.97360	418.9608
	3	13039.929 [b]	35.502	697	10601.778		423.7912
	4	18404.422 [b]	60.473	502	10595.622 [c]		423.5451
	5	23709.756 [b]	91.409	304	10574.466 [c]		422.6995
			T/K = 273.160				
7090.309	2	7345.026	0.376	8	10273.645	39.98788	410.8213
	3	12627.310	0.639	0	10273.565		410.8181
	4	17822.068	1.816	41	10273.568		410.8182
	5	22988.179 [b]	2.026	16	10274.427 [c]		410.8526
	6	28137.321 [b]	12.812	371	10280.200 [c]		411.0834
	7	33067.205	2.491	-22	10178.586 [c]		407.0346
6557.275	2	7346.951	0.401	10	10276.067	39.98791	410.9184
	3	12630.652	0.663	1	10275.981		410.9150
	4	17826.768	1.875	43	10275.909		410.9121

p / kPa	n	f_{0n} / s^{-1}	g_{0n} / s^{-1}	δ	(u/a) / s^{-1}	$10^3 a$ / m	u / $m \cdot s^{-1}$
6557.275	5	22994.805	1.988	12	10276.862 [c]	39.98791	410.9502
	6	28143.608	12.646	363	10281.274 [c]		411.1266
	7	33075.032 [b]	2.434	-87	10182.875 [c]		407.1918
	8	38257.143 [b]	3.514	-21	10215.958 [c]		408.4148
5678.638 [a]	2	7362.195	0.406	9	10297.045	39.98796	411.7578
	3	12656.945	0.684	-1	10296.979		411.7552
	4	17864.124	1.847	37	10296.950		411.7540
	5	23043.192 [b]	1.994	8	10297.760 [c]		411.7864
	6	28205.085 [b]	12.438	349	10302.066 [c]		411.9588
	7	33142.399 [b]	2.608	-28	10207.060 [c]		408.1595
	8	38006.006 [b]	5.818	32	10149.461 [c]		405.8562
4842.183	2	7390.002	0.407	6	10335.569	39.98800	413.2987
	3	12704.815	0.722	-2	10335.510		413.2964
	4	17931.834	1.978	39	10335.476		413.2950
	5	23130.918	2.149	8	10336.259 [c]		413.3263
	6	28153.874	2.671	-5	10281.446 [c]		411.1345
	7	33565.936 [b]	5.982	-7	10342.387 [c]		413.5714
	8	38158.558 [b]	8.108	-75	10190.897 [c]		407.5136
4367.669	2	7410.415	0.422	6	10363.936	39.98803	414.4334
	3	12739.895	0.730	-4	10363.841		414.4296
	4	17981.497	1.946	34	10363.845		414.4298
	5	23194.769	1.979	-4	10364.424 [c]		414.4529
	6	28390.997	9.948 [b]	245	10367.741 [c]		414.5855

p / kPa	n	f_{0n} / s^{-1}	g_{0n} / s^{-1}	δ	(u/a) / s^{-1}	$10^3 a$ / m	u / $m \cdot s^{-1}$
4367.669	7	33356.970 [b]	3.091	-29	10278.148 [c]	39.98803	411.0029
	8	38803.684 [b]	5.668	9	10353.825 [c]		414.4289
3673.080	2	7445.892	0.445	5	10413.228	39.98807	416.4049
	3	12800.993	0.796	4	10413.184		416.4031
	4	18067.982	1.972	24	10413.261		416.4062
	5	23306.174	2.266	-1	10413.611 [c]		416.4202
	6	28528.393 [b]	8.323	176	10416.747 [c]		416.5456
	7	32926.796	3.888	-18	10145.022 [c]		405.6798
3023.069	2	7484.123	0.470	3	10466.422	39.98810	418.5323
	3	12866.720	0.882	-5	10466.342		418.5291
	4	18161.030	2.146	26	10466.512		418.5366
	5	23426.471	2.583	0	10466.832 [c]		418.5487
	6	28676.236 [b]	7.133	118	10469.636 [c]		418.6609
	7	33093.826 [b]	4.417	-21	10199.246 [c]		407.8485
	8	38645.622 [b]	7.384	18	10322.329 [c]		412.7703
2066.315	2	7548.176	0.553	1	10555.685	39.98816	422.1024
	3	12976.923	1.141	-5	10555.615		422.0996
	4	18316.628	2.344	11	10555.712		422.1035
	5	23627.510	3.158	-9	10555.943 [c]		422.1127
	6	28922.605	6.640	61	10557.914 [c]		422.1915
	7	33974.301	5.706	-29	10475.140 [c]		418.8815
	8	39298.122 [b]	8.239	-13	10497.359 [c]		419.7700

p / kPa	n	f_{0n} / s^{-1}	g_{0n} / s^{-1}	δ	(u/a) / s^{-1}	$10^3 a$ / m	u / $m \cdot s^{-1}$
1578.204	2	7582.785	0.662	2	10605.352	39.98818	424.0887
	3	13038.155	1.403	-4	10605.258		424.0850
	4	18402.624 [b]	2.683	4	10605.050		424.0766
	5	23739.306	3.976	-6	10605.536 [c]		424.0961
	6	29059.455 [b]	7.428	49	10606.925 [c]		424.1516
	7	34134.001 [b]	7.316	-21	10525.472 [c]		420.8944
	8	39157.920 [b]	12.647	47	10460.186 [c]		418.2838
1554.117	2	7585.616	0.652	1	10607.892	39.98819	424.1903
	3	13041.299	1.416	-4	10607.793		424.1864
	4	18407.683	2.778	8	10607.940		424.1922
	5	23745.092	3.972	-9	10608.089 [c]		424.1982
	6	29066.767	7.163	38	10609.532 [c]		424.2559
	7	34142.472	7.508	-23	10528.120 [c]		421.0004
	8	39492.733 [b]	10.214	-19	10549.664 [c]		421.8619
995.153	2	7628.736	0.880	1	10668.076	39.98822	426.5973
	3	13115.488	2.041	-1	10667.973		426.5931
	4	18512.551	3.794	2	10668.130		426.5995
	5	23880.391 [b]	5.862	-5	10668.120		426.5990
	6	29233.293	9.661	32	10699.080 [c]		426.6374
	7	34336.417 [b]	11.433	-17	10589.016 [c]		423.4359
	8	39716.862 [b]	15.784	-2	10609.852 [c]		424.2690
598.578	2	7660.472	1.292	2	10712.383	39.98824	428.3693
	3	13170.186	3.170	5	10712.328		428.3671

p / kPa	n	f_{0n} / s^{-1}	g_{0n} / s^{-1}	δ	(u/a) / s^{-1}	$10^3 a$ / m	u / $m \cdot s^{-1}$
598.578	4	18589.808	5.845	4	10712.435	39.98824	428.3714
	5	23980.401 [b]	9.270	-0	10712.428		428.3762
	6	29356.937	14.588	33	10713.105 [c]		428.3982
	7	34479.129 [b]	18.910	2	10633.586 [c]		425.2183
	8	39882.320 [b]	25.276	10	10654.087 [c]		425.0382
223.337 [a]	2	7691.212 [b]	2.943	11	10755.431	39.98826	430.0909
	3	13223.273 [b]	7.865	33	10755.333		430.0870
	4	18665.640 [b]	14.366	12	10755.662		430.1002
	5	24071.243 [b]	23.968	39	10752.112		429.9582
	6	29787.396 [b]	41.134	237	10868.251 [c]		434.6025
	7	35137.340 [b]	71.439	687	10835.796 [c]		433.3046
	8	39729.411 [b]	59.842	-72	10611.612 [c]		424.3398
			T/K = 300.000				
7119.451	2	7844.202	0.407	11	10971.925	40.01310	439.0207
	3	13485.373	0.667	3	10971.819		439.0165
	4	19032.861	1.778	38	10971.856		439.0180
	5	24547.082	2.005	16	10972.350 [c]		439.0377
	6	29884.846	2.058	-8	10936.702 [c]		437.6113
	7	35312.928	3.776	19	10882.625 [c]		435.4476
	8	40505.155 [b]	6.422	59	10817.434 [c]		432.8391
6252.065	2	7849.244	0.415	10	10964.516	40.01315	438.7248
	3	13476.920	0.700	2	10964.406		438.7204

p / kPa	n	f_{0n} / s^{-1}	g_{0n} / s^{-1}	δ	(u/a) / s^{-1}	$10^3 a$ / m	u / $m \cdot s^{-1}$
6252.065	4	19021.204	1.806	35	10964.465	40.01315	438.7227
	5	24532.768	2.180	18	10964.892 [c]		438.7398
	6	29865.053	2.314	-6	10924.569 [c]		437.1263
	7	35289.530	3.855	14	10876.565 [c]		435.2056
	8	40478.640 [b]	7.266	71	10810.781 [c]		432.5734
5530.865	2	7842.703	0.428	10	10968.982	40.01319	438.9039
	3	13482.912	0.735	1	10968.858		438.8989
	4	19029.803	1.831	32	10968.895		438.9003
	5	24544.529	2.272	16	10969.326 [c]		438.9177
	6	29877.595	2.469	-8	10925.852 [c]		437.1781
	7	35303.818	4.115	13	10881.961 [c]		435.4220
	8	40834.837 [b]	4.602	-5	10906.391 [c]		436.3994
4885.080	2	7851.170	0.457	11	10980.546	40.01322	439.3670
	3	13497.533	0.791	1	10980.434		439.3625
	4	19050.617	1.849	27	10980.480		439.3644
	5	24571.674	2.327	11	10980.797 [c]		439.3771
	6	29909.542	2.788	-6	10935.002 [c]		437.5446
	7	35341.087	4.373	10	10894.390 [c]		435.9197
	8	40538.923 [b]	8.101	71	10827.607 [c]		433.2474
4093.793	2	7867.947	0.465	7	11003.666	40.01327	440.2926
	3	13526.473	0.871	1	11003.581		440.2892
	4	19091.680	1.894	21	11003.644		440.2917
	5	24625.290	2.615	12	11003.958 [c]		440.3043

p / kPa	n	f_{0n} / s^{-1}	g_{0n} / s^{-1}	δ	(u/a) / s^{-1}	$10^3 a$ / m	u / $m \cdot s^{-1}$
4093.793	6	29972.406	3.741	13	10955.149 [c]	40.01327	438.3513
	7	35415.607	4.795	6	10918.486 [c]		436.8842
	8	40964.427 [b]	5.439	-13	10941.746 [c]		437.8157
3391.270	2	7888.228	0.504	6	11031.781	40.01330	441.4180
	3	13561.391	0.979	0	11031.691		441.4144
	4	19141.071	2.039	16	11031.721		441.4156
	5	24689.437	2.853	7	11031.976 [c]		441.4258
	6	30050.844 [b]	5.355	49	10981.500 [c]		439.4151
	7	35505.910	5.358	2	10947.338 [c]		438.0391
	8	40728.409 [b]	9.855	70	10879.053 [c]		435.3069
2626.517	2	7915.476	0.586	7	11069.597	40.01335	442.9316
	3	13608.379 [b]	1.224	4	11069.570		442.9305
	4	19207.483	2.331	12	11069.549		442.9297
	5	24775.614	3.374	4	11069.752		442.9378
	6	30154.530 [b]	6.059	43	11016.762 [c]		440.7175
	7	35627.770 [b]	6.546	1	10985.941 [c]		439.5843
	8	40868.403 [b]	10.954	58	10916.850 [c]		436.8196
1850.820	2	7948.142	0.711	5	11115.005	40.01339	444.7490
	3	13664.569	1.553	2	11114.946		444.7466
	4	19287.113	2.949	9	11115.000		444.7488
	5	24878.793	4.420	1	11115.115		444.7534
	6	30278.906 [b]	7.082	22	11059.253 [c]		442.5182
	7	35774.192 [b]	8.607	-6	11032.076 [c]		441.4308

p / kPa	n	f_{0n} / s^{-1}	g_{0n} / s^{-1}	δ	(u/a) / s^{-1}	$10^3 a$ / m	u / $m \cdot s^{-1}$
1850.820	8	41036.540	13.544	47	10962.153	40.01339	438.6329
1136.012	2	7982.297	0.988	5	11162.455	40.01343	466.6481
	3	13723.356	2.310	2	11162.384		446.6453
	4	19370.376 [b]	4.228	1	11162.491		446.6495
	5	24986.741 [b]	6.471	-11	11162.555		446.6521
	6	30409.465 [b]	10.161	9	11103.527 [c]		444.2902
	7	35926.861 [b]	13.206	-12	11079.888 [c]		443.3443
	8	41986.952 [b]	23.040	119	11216.297 [c]		448.8025
239.419	2	8029.311 [b]	3.533	5	11228.207	40.01348	449.2797
	3	13804.743 [b]	9.186	-6	11228.263		449.2819
	4	19791.986 [b]	22.580	214	11382.299 [c]		456.3407
	5	25482.016 [b]	43.087	514	11354.394 [c]		455.4454
	6	31086.362 [b]	45.505	32	11239.921 [c]		454.3288
171.068	2	8033.060 [b]	4.822	12	11233.486	40.01348	449.4908
	3	13811.715 [b]	14.496	127	11233.762		449.5019
	4	19797.162 [b]	28.555	163	11407.184 [c]		456.4411
	5	25495.382 [b]	58.575	668	11387.405 [c]		455.6498
98.797 [a]	2	8036.700 [b]	8.392	69	11238.451	40.01348	449.6895
	3	13762.892 [b]	48.173	1946	11193.188		447.8785
	4	19800.439 [b]	49.336	312	11407.031		456.4350
	5	25512.205 [b]	90.564	767	11391.413		455.8102

p / kPa	n	f_{0n} / s^{-1}	g_{0n} / s^{-1}	δ	(u/a) / s^{-1}	$10^3 a$ / m	u / $m \cdot s^{-1}$
			T/K = 350.000				
7175.305	2	8592.326	0.405	0	12018.225	40.05948	481.4438
	3	14771.352 [b]	0.936	3	12018.102		481.4389
	6	32602.278	3.051	-8	11868.273 [c]		475.4368
	7	39034.837 [b]	6.759	57	12035.358 [c]		482.1301
6202.121	2	8592.326	0.424	-1	11989.875	40.05953	480.3088
	3	14737.177 [b]	1.010	4	11989.162		480.3042
	4	20797.290 [b]	6.518	232	11988.653		480.2598
	6	32524.125	3.213	-19	11840.307 [c]		474.3171
5134.144	2	8558.520	0.445	-2	11969.993	40.05959	479.5130
	3	14713.470	1.031	-1	11969.871		479.5081
	6	32470.969	3.727	-17	11824.863 [c]		473.6991
4137.587	2	8553.468	0.503	-2	11962.530	40.05964	479.2147
	3	14704.805	1.157	-2	11962.336		479.2069
	4	20754.038 [b]	4.145	97	11962.184		479.2008
	5	26799.416 [b]	6.120	103	11962.686 [c]		479.2209
	6	32450.403 [b]	4.398	-16	11821.698 [c]		473.5730
	7	38851.331	10.047	86	11980.528 [c]		479.9357
3164.101	2	8555.168	0.618	2	11964.425	40.05970	479.2913

p / kPa	n	f_{0n} / s^{-1}	g_{0n} / s^{-1}	δ	(u/a) / s^{-1}	$10^3 a$ / m	u / m·s^{-1}
3164.101	3	14707.927	1.369	-2	11964.307	40.05970	479.2865
	4	20758.723[b]	3.815	61	11964.115		479.2788
	6	32455.607[b]	5.144	-23	11828.035[c]		473.8275
	7	37829.435[b]	7.241	-24	11665.639[c]		467.3220
2082.221	2	8564.154	0.769	-2	11976.623	40.05976	479.7806
	3	14723.528	1.897	1	11976.531		479.7769
	4	20781.313	4.097	30	11976.446		479.7735
1258.873[a]	2	8575.391	1.131	1	11991.870	40.05980	480.3919
	3	14742.954[b]	2.705	-7	11991.776		480.3882
	4	20809.328[b]	5.630	19	11991.857		480.3914
	5	26841.813[b]	9.617	42	11991.921		480.3940
660.657	2	8585.933	1.920	4	12006.712	40.05984	480.9869
	3	14761.372[b]	4.896	2	12006.758		480.9888
	4	20836.615[b]	9.782	25	12007.422		481.0154
	5	26877.333[b]	14.559	-19	12007.118[c]		481.0032
214.957[a]	2	8594.560[b]	5.426	45	12018.842	40.05986	481.4731
	3	14781.510[b]	13.751	2	12022.869[c]		481.6344

[a] Pressure omitted from final analysis.

[b] (u/a) received weight less than unity in regression.

[c] (u/a) omitted from regression analysis.

largest and, for the highest pressure at 255 K, was only 25 per cent less than that in argon (for a similar frequency) even though the density in methane is only 67 kg·m^{-3} compared with 141 kg·m^{-3} for argon. This reflects the dependence of $\Delta f_w/f$ on $\rho_g u_g^2$. The measurements cover the frequency range between 6.9 and 42 kHz, and the calculated (and applied) shell corrections $\Delta f_w/f$ varies between -1.3×10^{-2} for (0,7) at 7.0 MPa and 255 K and 3.0×10^{-3} for (0,6) at 300 K and 7.1 MPa; the predicted shell breathing resonance occurs between (0,6) and (0,7). For mode (0,3) at the highest density (67 kg·m^{-3} at 255 K and 7.0 MPa) attained in these measurements a 0.4 per cent uncertainty in the mass density would result in a fractional error in u of 1×10^{-6}, while at 934 kPa a 2.5 per cent uncertainty in ρ was required. The speed of sound used in the calculation of Δf_w was obtained from preliminary analysis of modes (0,3) and (0,4). The virial coefficients used to calculate ρ, $C_{p,m}$, and γ are discussed below.

Douslin *et al.*[28] reported second and third virial coefficients, which were obtained from analyses of their precise (p,V_m,T) measurements for methane. In the temperature range 273.15 to 498.15 K their determinations of B can be represented to 0.03 cm^3·mol^{-1} (about 0.06 prt cent at 273.16 K) by

$$B/(\mathrm{cm}^3\cdot\mathrm{mol}^{-1}) = 216.65 - 167.762 \exp(130\ \mathrm{K}/T), \quad (6.4.1)$$

and their third virial coefficients, omitting the value at

448.15 K, are given by

$$C/(\mathrm{cm}^6\cdot\mathrm{mol}^{-2}) = 1028.1 + 148.3x + 17.7x^2 - 1.505x^3, \quad (6.4.2)$$

with a standard deviation of 1.2 $\mathrm{cm}^6\cdot\mathrm{mol}^{-2}$ where $x = \{\exp(610\ \mathrm{K}/T) - 1\}$. Both equations (1) and (2) were determined using unweighted non-linear regression and have been used for extrapolation to the experimental temperatures.

The transport properties used to account for losses at the surface, the effects of coupling and filling tubes and classical bulk absorption were taken from reference (22); the original measurements were made by Kestin and co-workers.[29-31] At a density of 67 $\mathrm{kg}\cdot\mathrm{m}^{-3}$ the thermal conductivity increased by 14 per cent, and the shear viscosity by 11 per cent, over the zero-density value. The thermal boundary layer correction $\Delta f_h/f$, with an accommodation coefficient of unity, covered the range 9×10^{-6} for (0,8) at 7.2 MPa and 300 K to 115×10^{-6} for (0,2) at 98 kPa and 255 K. An error of 3 per cent in κ would lead to a fractional error in u of 10^{-6} in the worst case.

The quantities $t\rho$ and their apparent density dependence, determined from the residual experimental line widths, are reported in table 6.6. In this analysis, it was not necessary to allow for an additional term representing a constant fractional excess half width, as was the case for the 60 mm resonator. At 350 K the measured values of g were of sufficient precision, despite the instability in the source transducer discussed previously,

Table 6.6. The quantity $t\rho$, where t is the vibrational relaxation line and ρ the main-density, and $\{\partial(t\rho)/\partial\rho\}T$ for methane, obtained at temperatures T from analysis of the excess half widths Δg assuming the vibrational states couple strongly.

T/K	$t\rho$/μs•kg•m^{-3}	$\{\partial(t\rho)/\partial\rho\}_T$/ns
255.000	2.233 ± 0.028	29.3 ± 3.4
273.160	1.738 ± 0.003	26.3 ± 3.0
300.000	1.319 ± 0.012	5.9 ± 1.6
350.000	0.7805 ± 0.0089	8.1 ± 0.7

to require terms representing $t\rho$ and $\{\partial(t\rho)/\partial\rho\}_T$ in the analysis. The vibrational relaxation times reported by other workers are plotted in figure 6.15, with those values obtained from this work, at a pressure of 101.3 kPa. At 300 K the value reported by Cottrell and Matheson,[32] obtained from speed dispersion measurements, agrees with our value within the standard deviation assigned to their value; the purity of the two samples was similar. The values derived by Cottrell and Martin,[34] from their speed dispersion measurements and those determined by Edmonds and Lamb,[33] from their absorption measurements were obtained with samples which were likely to be severely

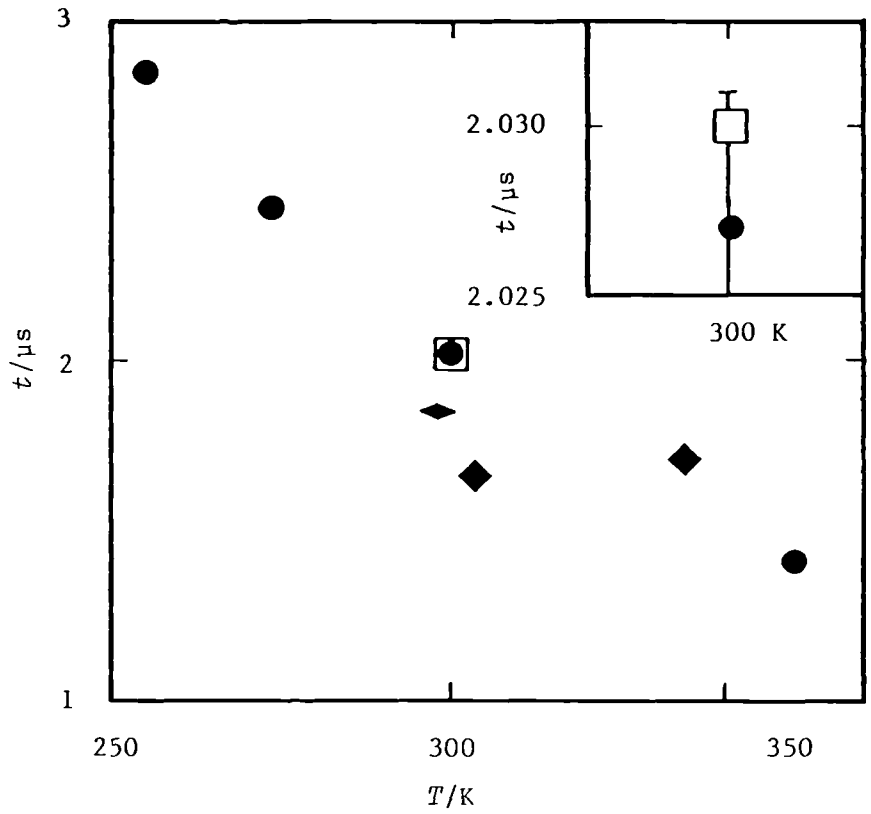

Figure 6.15. Vibrational relaxation times t for methane at 101.3 kPa, assuming the vibrational states are strongly coupled. ● , This work; □ , reference 32; ◆ , reference 33; ◆ , reference 34.

---

contaminated.[35] The relaxation times determined in this work decline with increasing temperature, as predicted by the Landau and Teller theory,[36] which assumes the interactions during a collision are purely repulsive.

The excess losses (after allowance for vibrational relaxation absorption) are illustrated in figures 6.16 and 6.17 for the isotherms at 255 and 300 K respectively. At 255 K, clearly the mode (0,6) is severely perturbed; $\Delta g/f$ exceeds 360×10^{-6} at 5.7 MPa and declines to about

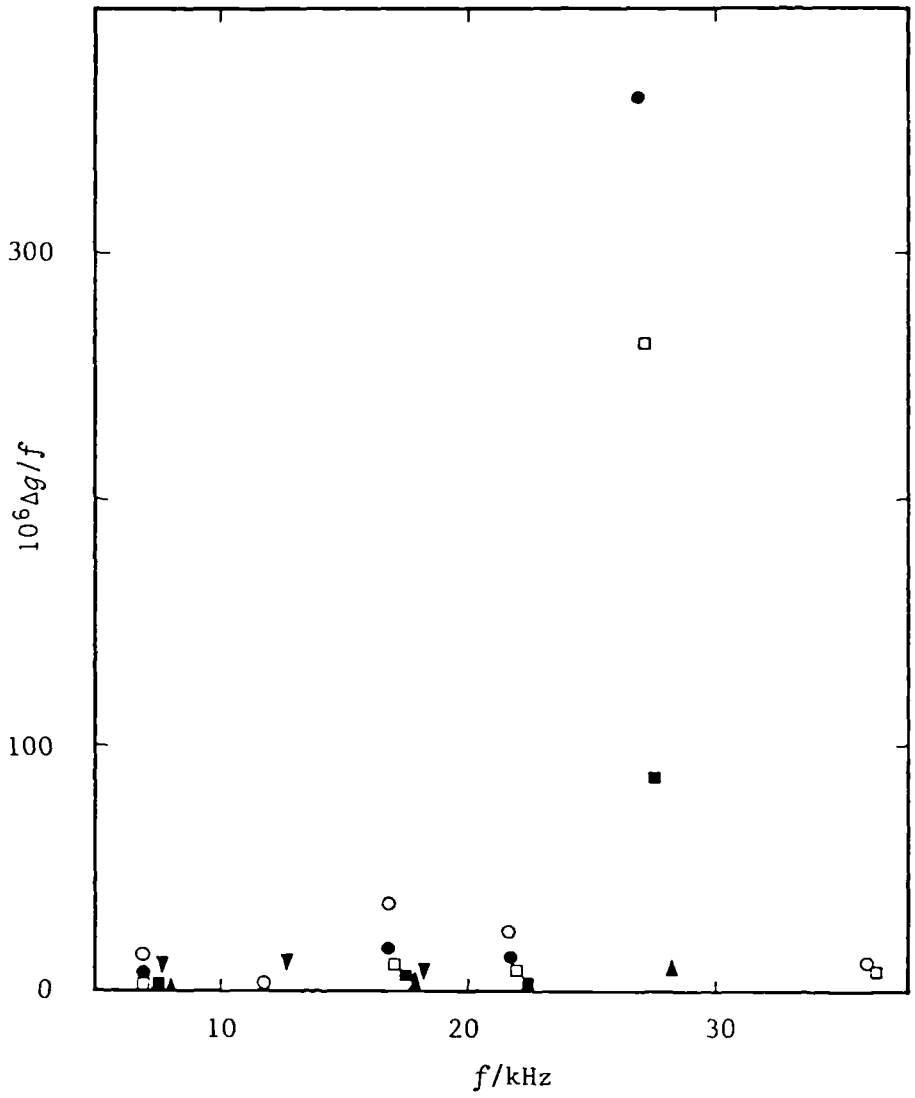

Figure 6.16. Fractional excess half widths for the radial modes listed in table 6.5 in methane at 255 K. ○ , 6940 kPa; ● , 5733 kPa; □ , 4385 kPa; ■ , 2997 kPa; ▲ , 964 kPa; ▼ , 234 kPa.

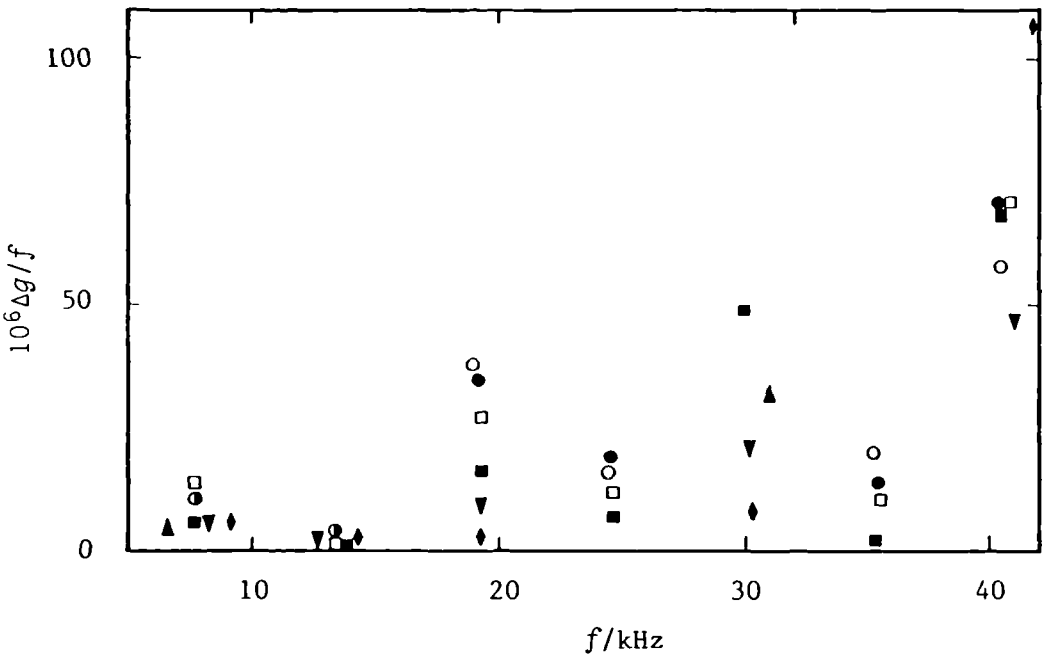

Figure 6.17. Fractional excess half widths for the lowest seven radial modes in methane at 300 K. ○ , 7120 kPa; ● , 6252 kPa; □ , 4885 kPa; ■ , 3391 kPa; ▼ , 1851 kPa; ♦ , 1136 kPa; ▲ , 239 kPa.

10×10^{-6} at 964 kPa. The large losses might be explained in terms of the coupling between acoustic and shell resonances. Further evidence to support this suggestion is provided in figure 6.18 for the deviation of (u/a) from $\langle u/a \rangle$ of the selected modes. $\Delta(u/a)$ for (0,6) can be qualitatively understood in terms of an acoustic resonance which traverses a shell resonance through the pressure range of the experiment; three values of $\Delta(u/a)$ exceed $200 \times 10^{-6}(u/a)$ between about 1.75 and 3.6 MPa, consequently, they have been omitted from figure 6.18. However, it is not clear, from the evidence in figure 6.7, which shell mode this would correspond to at a frequency near 27 kHz. For (0,5), $\Delta(u/a)$ increases linearly reaching $1.2 \times 10^{-4}(u/a)$ at 6.9 MPa; this discrepancy may be associated with coupling to the shell resonance centred on 21 kHz. The pressure dependence of the excess losses are in general as anticipated from previous measurements with argon, illustrated in figures 6.5, 6.9, and 6.12 in similar frequency ranges. At 300 K the excess losses for the acoustic modes (0,4) near 19 kHz, (0,6) near 30 kHz, and (0,8) near 41 kHz, may possibly suggest coupling to the shell breathing resonance predicted at 31.2 kHz and the resonances observed (and shown in figure 6.7) near 21 and 41 kHz; $\Delta(u/a)$ for modes (0,4), (0,6), and (0,8) are consistent with this hypothesis. The small $\Delta g/f$ and $\Delta(u/a)$ for (0,2) compared with those observed with argon might be attributed to precise transducer alignment and the factor of about 2 reduction in density. For the other isotherms, the acoustic

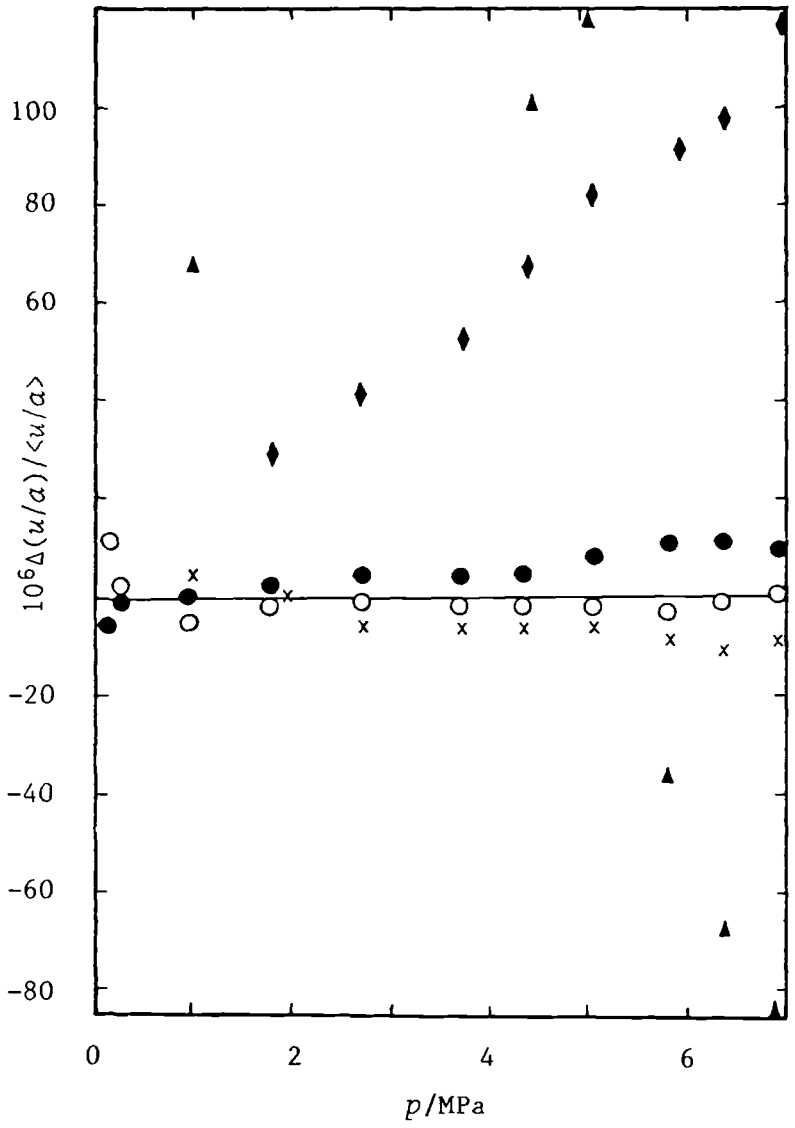

Figure 6.18. Fractional deviations $\Delta(u/a)/\langle u/a\rangle = \{(u/a) - \langle u/a\rangle\}/\langle u/a\rangle$, for individual modes in methane at 255 K, from $\langle u/a\rangle$ of the modes finally selected at each pressure for analysis with equation (5.3.6). ● , (0,2); ○ , (0,3); X , (0,4); ♦ , (0,5); ▲ , (0,6).

measurements which occur at frequencies close to an observed resonance associated with the shell, show excess losses and discrepant (u/a) dependent on pressure. Such observations in conjunction with those made for the measurements with argon assist in selecting modes for inclusion in the regression analysis with equation (5.3.6) and also the excess losses to determine $t\rho$.

The correction applied to (u/a) for speed dispersion arising from vibrational relaxation was not significant at frequencies less than 30 kHz and pressures greater than 2 MPa. For mode (0,3) at 171 kPa and 300 K, this correction contributed fractionally 46×10^{-6} to u. Below 171 kPa the measurements were adversely affected by a combination of transducer inefficiency and considerable sound attenuation.

Table 6.5 lists values of the speed of sound calculated using $a(T,p)$, which was obtained from $a(T,p=0)$, determined from measurements with argon, and the linear hydrostatic compressibility of the resonator's wall using equations (6.2.1) to (6.2.3). At 350 K the radius was obtained by extrapolation of a(273.16 K, p=0) with the linear thermal expansivity of aluminium estimated from the precise measurements[37] reported by Kroger and Swenson below 320 K.

To accommodate the (u/a), corrected to the stated temperature for each isotherm reported in table 6.5, between four and five of the leading terms of the infinite series (5.3.6) were required. The results of this analysis for methane are given in table 6.7 together with the number N of resonance frequencies in the final regression

Table 6.7. Coefficients for either the leading four or five terms of equation (5.3.6), and standard deviations s obtained by analysis of N modes for methane at temperatures T. Uncertaintities are one standard deviation.

$\frac{T}{K}$	N	$\frac{10^{-6}(A_0/a)}{s^{-2}}$	$\frac{(A_1/a^2)}{s^{-2}\cdot Pa^{-1}}$	$\frac{10^{8}(A_2/a^2)}{s^{-2}\cdot Pa^{-2}}$	$\frac{10^{15}(A_3/a^2)}{s^{-2}\cdot Pa^{-3}}$	$\frac{10^{21}(A_4/a^2)}{s^{-2}\cdot Pa^{-4}}$	$\frac{10^{6}s(u^2)}{u^2}$
255.000	24	109.0804 ± 0.0018	-3.1832 ± 0.0032	8.72 ± 0.17	2.28 ± 0.34	1.057 ± 0.023	13.9
273.160	30	116.2482 ± 0.0024	-2.5517 ± 0.0041	9.393 ± 0.021	4.12 ± 0.43	4.750 ± 0.0029	14.3
300.000	29	126.4937 ± 0.0017	-1.7743 ± 0.0026	8.75 ± 0.13	5.31 ± 0.26	0.065 ± 0.017	10.4
350.000	15	144.6169 ± 0.0041	-7.457 ± 0.0044	7.95 ± 0.13	2.92 ± 0.11	————	22.1

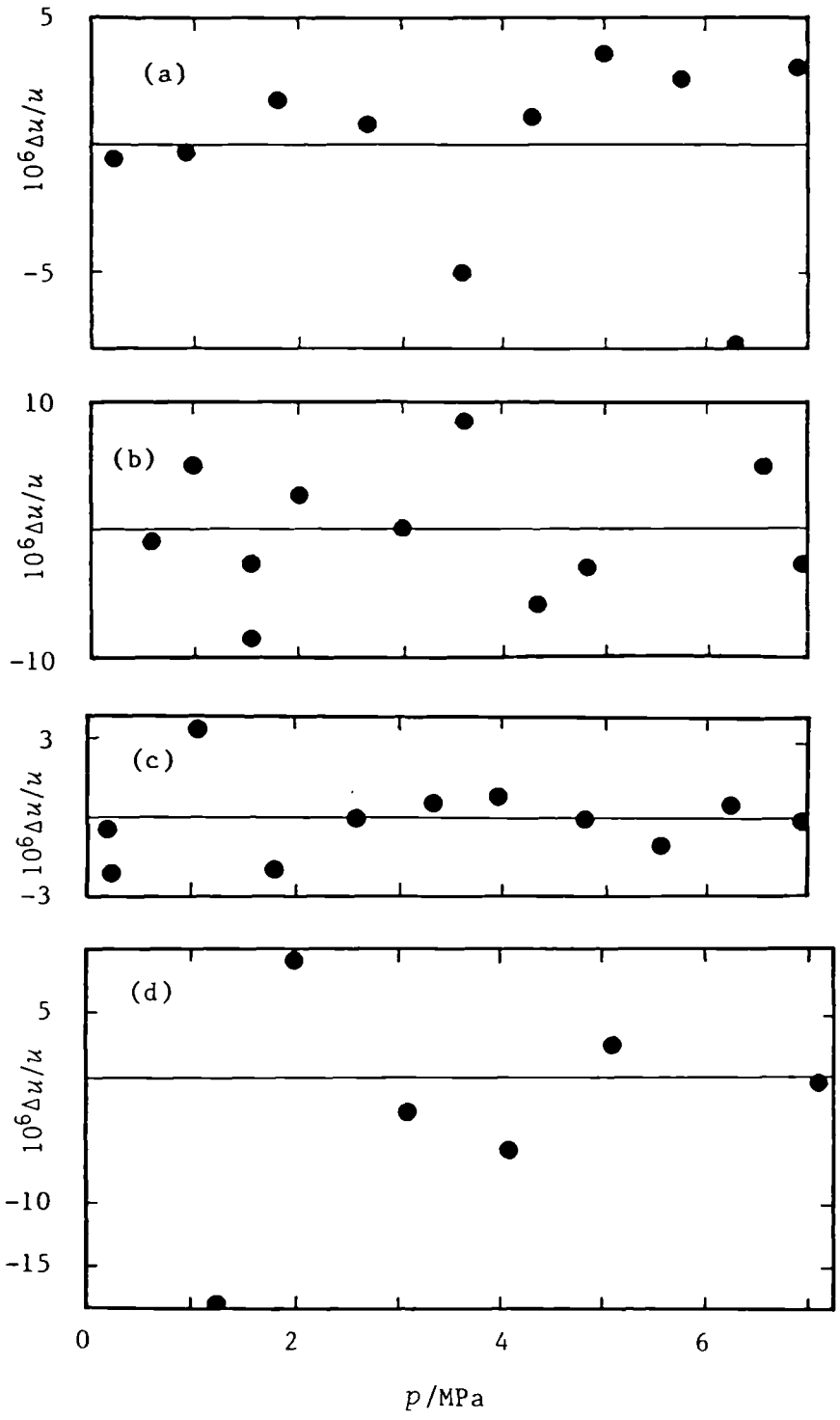

Figure 6.19. For description see subsequent page.

Figure 6.19. Fractional deviations $\Delta u/u = [\langle u/a \rangle - \{u(\text{calc.})/a\}]/\{u(\text{calc.})/a\}$, for $\langle u/a \rangle$ of selected modes in methane at each pressure from equation (5.3.6), in which the coefficients (given in table 6.7) were adjusted to fit the selected modes on each of the isotherms at : (a),255 K; (b),273.16 K; (c),300 K; (d),350 K.

---

and the standard deviations; the coefficients were all significant at a probability of 0.999. Those modes and pressures omitted from the regression are indicated in table 6.5, along with the corrected frequencies which received a weight, according to equation (5.3.1), less than unity. The deviations of $\langle u/a \rangle$, for the selected modes, from the finally adopted smoothing equations, are shown in figure 6.19. At 300 K the $\langle u/a \rangle$ show a systematic undulation from the smoothing equation above 2.5 MPa, although they are only about $\pm 1 \times 10^{-6}$ of (u/a) which is exceptional. Typically, the fractional deviations of $\langle u/a \rangle$ span 10×10^{-6}.

The perfect gas molar heat capacities and second acoustic virial coefficients determined from the regression are reported in table 6.8. Figure 6.20 shows the heat capacities are deviations from the correlation due to Wilhoit.[38] The correlation in a fit to the calculations of McDowell and Kruse which are based on spectroscopic information include anharmonicity, centrifugal distortion, vibration-rotation interactions, and quantum effects

Table 6.8. Perfect-gas molar heat capacities $C^{pg}_{p,m}$ at constant pressure and second β_a acoustic virial coefficients obtained from equation (2.3.20) and (2.3.21) using $(A_0(T)/a^2)$ and $(A_1(T)/a^2)$ from table 6.7. The gas constant R was taken as 8.31441 $J \cdot K^{-1} \cdot mol^{-1}$.

T/K	$C^{pg}_{p,m}/R$	$\beta_a/(cm^3 \cdot mol^{-1})$
255.000	4.13623 ± 0.00042	-61.871 ± 0.058
273.160	4.19443 ± 0.00056	-49.853 ± 0.080
300.000	4.30494 ± 0.00037	-34.987 ± 0.051
350.000	4.57883 ± 0.00093	-15.006 ± 0.008

cover the range 50 to 5000 K and are shown in figure 6.20. In general the measurements of $C^{pg}_{p,m}$ are in good agreement with the calculations based on spectroscopic information; at 300 K the results differ by 0.0019 R (about 0.05 per cent). In particular, at 273.16 K the experimental value is 0.0013_6 R below the correction, while the value reported by McDowell and Kruse[39] at 273.15 K lie 0.0013_9 R below. However, the measurement at 350 K lies 0.07 R above the correlation and clearly is inconsistent with the observations at lower temperatures. It is believed likely that the discrepancy arose from a combination of uncertainty

in the resonator's radius and the instability associated with the source transducer.

The experimental second acoustic virial coefficients are compared with equations (1) and (2.3.23) in figure 6.21. The results show deviations between 0.1 $cm^3 \cdot mol^{-1}$ (about 0.2 per cent) at 273.16 K and 0.7 $cm^3 \cdot mol^{-1}$ (about

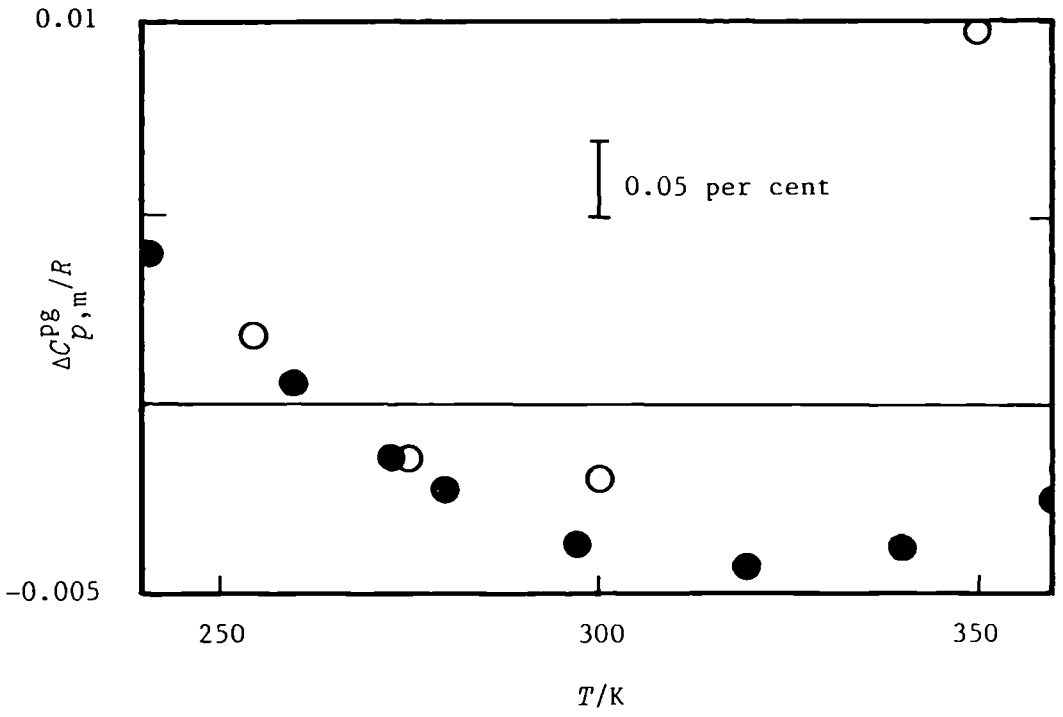

Figure 6.20. Deviations $\Delta C^{pg}_{p,m} = C^{pg}_{p,m} - C^{pg}_{p,m}$(calc.) of perfect gas molar heat capacities of constant pressure for methane, from the Wilhoit correlation given by equation (5.4.30) and (5.3.31), for which the coefficients are given in table 5.7. ○ , This work; ● , calculated from spectroscopic information.[39]

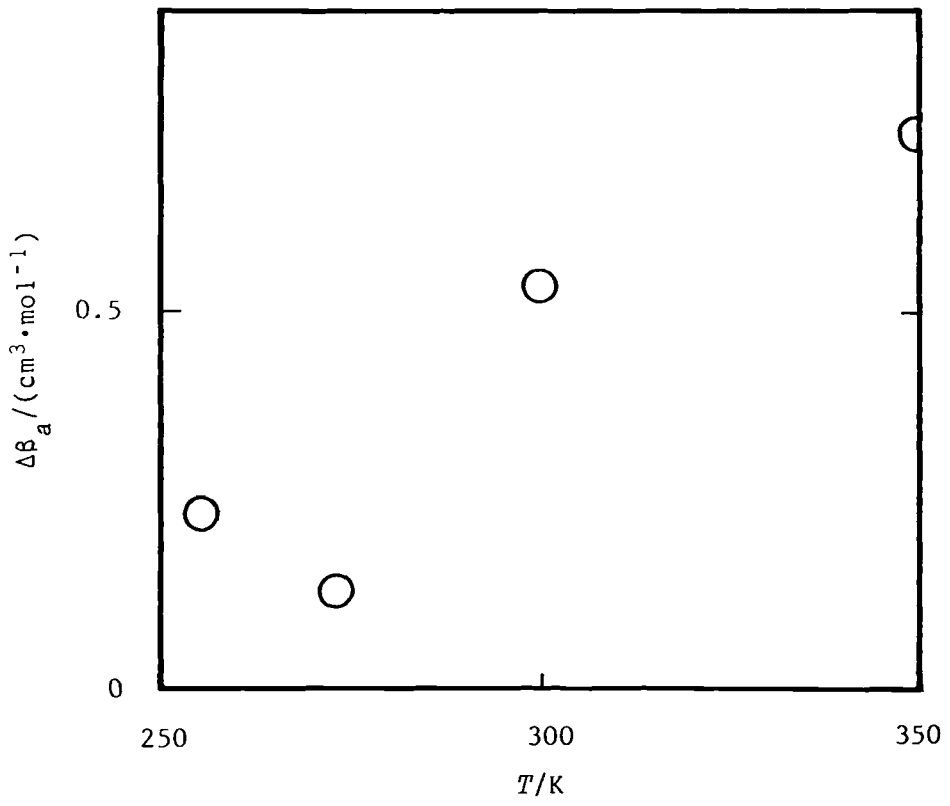

Figure 6.21. Deviations $\Delta\beta_a = \{\beta_a - \beta_a(\text{calc.})\}$ of experimental second acoustic virial coefficients of methane from equation (2.3.23), and (1) with γ^{pg} calculated from equation (5.3.30) and (5.3.31) using the coefficients given in table 5.7.

4.8 per cent) at 350 K. Neither formal solution of equation (2.3.23) by means of numerical integration with boundary conditions obtained from precise (p, V_m, T) measurements nor semi-empirical methods involving explicit assumptions about the functional form of B have been attempted.

6.4.3 Natural gas

Acoustic measurements have been performed on a sample, taken from the British Gas plc national transmission system at their Bishop Auckland test facility, of a natural gas which originated from the British Gas St Fergus field situated in the North Sea. The results are reported in table 6.9 for pressures between 0.06 and 6.69 MPa on an isotherm at 255 K. The gaseous mixture was supplied in 4 cylinders each with different compositions.† The contents of these ampoules were combined by distillation and the mole fraction composition of the final gaseous mixture, assumed to be the mean of those four individual ampoules, is given in table 6.10; subsequent analysis of the used material indicated this assumption was satisfactory.

The acoustic model has been applied without any additional corrections which may be applicable for a gaseous mixture; the most important known correction to high density measurements arise from shell motion which should not depend on composition. The measurements do not appear to be perturbed more than those previously obtained in this temperature and pressure range.

The mass density required in the acoustic model is discussed below. At fourteen equally spaced pressures between 0.5 and 7 MPa, values of ρ were estimated from the

---

†The glc analyses were performed by British Gas Engineering Research Station according to their usual procedures; report number 348-351.

Table 6.9. Resonance frequencies f_{0n} and half widths g_{0n}, fractional excess half widths $\delta = 10^6 \Delta g/f$, quantities (u/a), radius $a = a(T,p)$, and speed of sound u for the n-th radial mode at temperatures T and pressures p in a natural gas with the composition given in table 6.10. The radius was calculated using $a(T, p = 0)$ from table 6.4 and equations (6.2.1) to (6.2.3).

p / kPa	n	f_{0n} / s^{-1}	g_{0n} / s^{-1}	δ	(u/a) / s^{-1}	$10^3 a$ / m	u / $m \cdot s^{-1}$
6685.647	2	6627.523	0.394	19	9269.212 [c]	39.97327	370.5207
	3	11393.656	0.390	-3	9268.914		370.5088
	4	16081.363	0.845	15	9268.459		370.5106
	5	20741.763 [b]	3.259	117	9268.532 [c]		370.4935
	6	25388.898	1.082	1	9269.397 [c]		370.5281
	7	29838.388	1.686	9	9227.511 [c]		368.8538
	8	34510.374	1.114	-19	9209.186 [c]		368.1213
6067.038	2	6649.213	0.348	13	9299.428 [c]	39.97330	371.7288
	3	11430.986	0.412	0	9299.140		371.7173
	4	16134.039	0.776	11	9299.132		371.7170
	5	20811.102	2.222	68	9299.236		371.7212
	6	25472.790	0.971	-4	9299.520 [c]		371.7325
	7	29934.600	1.321	-2	9256.249 [c]		370.0028
	8	34622.292 [b]	1.088	-18	9240.573 [c]		369.3762
5498.734	2	6679.578	0.306	7	9341.660 [c]	39.97333	373.4173
	3	11482.921	0.387	-2	9341.133		373.3962
	4	16207.358	0.758	11	9341.096		373.3947
	5	20905.382	2.143	64	9340.993		373.3906

p / kPa	n	f_{0n} / s^{-1}	g_{0n} / s^{-1}	δ	(u/a) / s^{-1}	$10^3 a$ / m	u / $m \cdot s^{-1}$
5498.734 [a]	6	25589.648	1.176	5	9341.635 [c]	39.97333	373.4163
	7	30070.348	1.142	-6	9298.084 [c]		371.6754
	8	34779.689	1.364	-9	9283.825 [c]		371.1054
4724.319	2	6733.066	0.293	6	9416.792	39.97337	376.4209
	3	11575.320	0.360	-4	9416.599		376.4132
	4	16337.624	0.747	10	9416.427		376.4064
	5	21075.648	2.299	72	9417.228		376.4384
	6	25760.338	9.613	333	9403.858 [c]		375.9039
	7	30309.547	1.286	-1	9374.107 [c]		374.7147
	8	35057.233	1.137	-14	9360.106 [c]		374.1550
3956.061	2	6798.803	0.278	3	9508.185	39.97342	380.0746
	3	11688.486	0.361	-4	9508.090		380.0708
	4	16497.728	0.724	9	9508.086		380.0707
	5	21281.896	1.813	49	9508.673 [c]		380.0942
	6	26048.321	1.440	8	9508.097 [c]		380.0711
	7	30604.467	0.956	-11	9470.543 [c]		378.5700
	8	35398.696	0.931	-20	9452.394 [c]		377.8445
2973.273	2	6894.498	0.274	2	9641.937	39.97347	385.4217
	3	11853.023	0.357	-4	9641.821		385.4171
	4	16730.010	0.719	8	9641.779		385.4154
	5	21581.047	1.450	31	9642.030		385.4254
	6	26415.883	1.858	31	9641.672		385.4111
	7	31033.495	0.845	-15	9644.268 [c]		385.5148

p / kPa	n	f_{0n} / s^{-1}	g_{0n} / s^{-1}	δ	(u/a) / s^{-1}	$10^3 a$ / m	u / $m \cdot s^{-1}$
2973.273	8	35894.972	1.017	-17	9586.651 [c]	39.97347	383.2117
2023.194	2	6996.959	0.231	0	9785.087	39.97352	391.1444
	3	12029.265	0.392	-4	9785.005		391.1411
	4	16978.950	0.737	7	9785.000		391.1409
	5	21902.953	1.028	9	9785.470 [c]		391.1597
	6	26810.218	1.979	33	9784.878		391.1360
	7	31493.383	0.964	-13	9677.902 [c]		386.8598
	8	36427.388	1.111	-17	9730.175 [c]		388.9494
1237.864	2	7086.750	0.317	-1	9908.988	39.97357	396.0976
	3	12183.694	0.463	-3	9908.911		396.0945
	4	17197.125	0.797	5	9908.960		396.0965
	5	22184.223	0.893	-3	9909.227 [c]		396.1071
	6	27155.481	2.731	55	9908.615 [c]		396.0827
	7	31896.511	1.136	-13	9827.939 [c]		392.8578
	8	36894.197	1.433	-14	9854.232 [c]		393.9088
647.032	2	7152.972	0.400	-1	10002.672	39.97360	399.8428
	3	12297.598	0.609	-2	10002.591		399.8396
	4	17358.030	0.929	1	10002.655		399.8421
	5	22391.728	1.089	-6	10002.783		399.8472
	6	27411.590	3.640	75	10002.575		399.8389
	7	32193.903	1.648	-11	9926.611 [c]		396.8024
	8	37238.454	2.059	-12	9947.918 [c]		397.6541

p / kPa	n	f_{0n} / s^{-1}	g_{0n} / s^{-1}	δ	(u/a) / s^{-1}	$10^3 a$ / m	u / $m \cdot s^{-1}$
230.823 [a]	2	7199.731	0.668	1	10068.383	39.97362	402.4697
	3	12378.126	1.073	1	10068.330		402.4676
	4	17471.791	1.562	1	10068.382		401.4696
	5	22538.518	2.052	-3	10068.426		402.4713
	6	27593.033	3.534	27	10068.540		402.4760
	7	32404.271	3.361	-7	9994.127 [c]		399.5013
	8	37482.105	4.246	-6	10013.639 [c]		400.2814
134.505	2	7211.346	0.896	2	10084.454	39.97362	403.1122
	3	12398.152	1.494	3	10084.390		403.1096
	4	17500.086	2.232	4	10084.422		403.1109
	5	22575.127 [b]	2.911	-4	10084.478		403.1132
	6	27638.033 [b]	4.515	18	10084.569		403.1167
	7	32456.392 [b]	5.210	1	10010.526 [c]		400.1570
	8	37542.825 [b]	6.668	3	10029.664 [c]		400.9219
63.548	2	7219.122	1.391	5	10095.854	39.97362	403.5679
	3	12411.628	2.473	10	10095.770		403.5644
	4	17519.192	3.901	16	10095.790		403.5652

[a] Pressure removed from final analysis.

[b] (u/a) received weight less than unity in regression analysis.

[c] (u/a) omitted from final regression analysis.

Table 6.10. Substance B and molefraction x_B for each component in the natural gas sample used for acoustic measurements; the analysis was performed by Britsh Gas plc.

B	x_B	B	x_B
CH_4	0.93961	C_2H_6	0.04403
C_3H_8	0.00263	n-C_4H_{10}	0.00024
$CH_3CHCH_3CH_3$	0.00017	n-C_5H_{12}	0.00001
$CH_3CHCH_3CH_2CH_3$	0.00003	$CH_3C(CH_3)_2CH_3$	0.00003
Hyrdrocarbons C_n for $n \geq 6$	0.00017	N_2	0.00760
		CO_2	0.00548

GRI equation of state[¶] at 255 K; using the composition given in table 6.10 and assuming the mole fraction of C_n with $n \geqslant 6$ could be treated as n-hexane. These values of ρ could be represented to 0.001 $kg \cdot m^{-3}$ by

[¶]The GRI equation of state for natural gas has been discussed in Chapter Two. The calculations were performed with a software package, written by Savidge and called SUPER Z,[40] containing coefficients derived in 1986.

$$\rho/(\mathrm{kg\cdot m^{-3}}) = 10^6 M/\{R\ 255\ \mathrm{K\cdot MPa}/p - 69.169 - 0.8119(p/\mathrm{MPa}) + 0.0409(p/\mathrm{MPa})^2 - 8.148 \times 10^{-3}(p/\mathrm{MPa})^3 + 1.168 \times 10^{-3}(p/\mathrm{MPa})^4\} \quad (6.4.3)$$

Choice of the GL equation of state,[41] also described in Chapter Two,[§] would at the highest experimental pressure provide a density 0.4 per cent lower than the GRI estimate. Similarly, use of the McCarty-modified Benedict-Webb-Rubin[42] equation within the framework of the extended principle of corresponding states for mixtures[43] (MCSP)[§] would have predicted a value of mass density at the highest experimental pressure 0.3 per cent lower than GRI. If the differences between the values of mass density ρ obtained from GRI and that provided by either GL or MCSP (the differences in both cases are greatest at the highest experimental pressure) are taken as indication of the uncertainty in the estimation of ρ, then the estimates given by GRI are adequate for the calculations.

The $C_{p,\mathrm{m}}$ and γ for the particular gaseous mixture, given in table 6.10 (assuming x of C_n with $n \geqslant 6$ could be treated as n-hexane), were calculated at 15 equally spaced pressures between 0 and 7 MPa by the MCSP

[§]Calculations were performed with the British Gas thermophysical property estimation routine Eagle version 3.0. The required critical properties and acentric factors can be found in reference (44).

method.‡ Analysis of the results with the adaptive regression algorithm[45] offering an array of terms from p^{-3} to p^{3} gave

$$C_{p,\mathrm{m}}(255\ \mathrm{K},p)/R = 4.2193 + 0.18359(p/\mathrm{MPa}) + 0.01223(p/\mathrm{MPa})^{2} + 1.4824 \times 10^{-3}(p/\mathrm{MPa})^{3}, \qquad (6.4.4)$$

with a standard deviation of 0.0003 R in $C_{p,\mathrm{m}}/R$, and

$$\gamma(255\ \mathrm{K},p) = 1.31051_{8} + 0.04210(p/\mathrm{MPa}) + 3.178 \times 10^{-3}(p/\mathrm{MPa})^{2} + 327.4 \times 10^{-6}(p/\mathrm{MPa})^{3}, \qquad (6.4.5)$$

with a standard deviation of 7×10^{-4} in γ. All terms selected had a high degree of significance (> 0.99).

Since the transport properties were not known for this particular gaseous mixture they were estimated from a British Gas implementation of a predictive method for gaseous hydrocarbons developed at the National Bureau of Standards;[46-50] based on the extended principle of corresponding states for a van der Waals one fluid approximation with a reference equation for the thermal conductivity and viscosity of methane.[51] Experiment and calculation differ by less than 7 per cent,[50] and provided

---

‡The molar perfect gas heat capacity at constant pressure is estimated within Eagle by the correlation of Wilhoit.[38]

equivalent accuracy is achieved for the mixture defined in table 6.10, then the method is adequate for our purpose. The thermal conductivity κ and shear viscosity η were calculated at 14 equally spaced pressures between 0.5 and 7 MPa. The values of κ so determined can be represented to 0.017 $mW \cdot m^{-1} \cdot K^{-1}$ by

$$\kappa(255\ K,p)/(mW \cdot m^{-1} \cdot K^{-1}) = 29.71 + 1.3582(p/MPa) + 510 \times 10^{-6}(p/MPa)^4, \quad (6.4.6)$$

while those estimates of η so determined are given by

$$\eta(255\ K,p)/(\mu Pa \cdot s) = 9.8671 + 0.1806\ (p/MPa) + 0.01908(p/MPa)^2 + 122.2 \times 10^{-6}(p/MPa)^3, \quad (6.4.7)$$

with a standard deviation of 3.7×10^{-4} $\mu Pa \cdot s$.

Analysis of the excess half widths assuming the mixture can be considered pure methane gave $t\rho = (58 \pm 2.1)$ $ns \cdot kg \cdot m^{-3}$ and $\{\partial(t\rho)/\partial\rho\}_T = 0.9$ ns. The factor of about 40 reduction in $t\rho$ compared with the value reported in table 6.6 for methane with a mole fraction purity $x > 0.99995$, reflects the catalytic effect due to the presence of other hydrocarbons on the relaxation time of methane. The excess losses, after allowance for vibrational relaxation absorption, are reported in table 6.9.

Measurements were taken for the first seven radial modes and were selected for inclusion in the analyses of

(u/a) and the excess half widths, on the basis of information provided by the previous measurements with argon and methane at 255 K. The modes omitted from the final regression analyses are indicated in table 6.9.

Table 6.9 lists values of (u/a) to which small corrections were applied to reduce all values to exactly 255 K. The speed of sound was calculated using $a(255\ \mathrm{K},p)$ determined from the argon measurements and equations (6.4.1) to (6.4.3). For the selected modes, the effect of vibrational relaxation on the speed of sound was fractionally less than 1×10^{-6}.

The leading eight terms of equation (5.3.7) were required to accommodate the selected 34 values of $(u/a)^2$ with a fractional standard deviation of 28×10^{-6}. The coefficients, which were all significant at a probability of 0.999, are reported in table 6.11. Figure 6.22 shows values of $\langle u/a \rangle$ as determined from the modes selected at each pressure as deviations from the smoothing equation. The speed of sound varies between about 403 and 370 m s^{-1} over the experimental pressure range, and is similar to the change observed with pure methane. The need for eight terms of equation (5.3.6), for which the coefficients sign alternates (negative for odd powers in pressure), suggest that this power series expansion is not the most suitable representation of the measurements. Further analysis might be attempted with the adaptive regression algorithm in an attempt to accommodate the results with fewer terms.

Table 6.11. Coefficients of the leading eight term in equation (5.3.6) required to represent 34 measurements of (u/a) for a natural gas between 0.06 and 6.7 MPa at 255 K with a fractional standard deviation of 17.9×10^{-6} in (u/a). The coefficients were all significant at a probability of 0.999.

j	$(A_j/a^2)/s^{-2} \cdot Pa^{-j}$
0	$(102.1363 \pm 0.0019) \times 10^{6}$
1	$-(3.307_9 \pm 0.015_9)$.
2	$(2.31_5 \pm 0.32_2) \times 10^{-7}$
3	$-(1.93_{76} \pm 0.27_{00}) \times 10^{-13}$
4	$(8.73_{57} \pm 1.09_{77}) \times 10^{-20}$
5	$-(1.84_{94} \pm 0.23_{66}) \times 10^{-26}$
6	$(1.94_{94} \pm 0.25_{60}) \times 10^{-33}$
7	$-(8.06_{38} \pm 1.09_{49}) \times 10^{-41}$

The gaseous mixture defined in table 6.10 has a molar mass of 0.017012 $kg \cdot mol^{-1}$, and assuming the analysis accurately represents the gaseous mixture on which measurements were performed, then (A_0/a^2) can be expressed as the perfect gas molar heat capacity at constant pressure using the radius from table 6.5 to give

$$C^{pg}_{p,m}/R = 4.23086 \pm 0.00051, \qquad (6.4.8)$$

which is about $0.01R$ above the value estimated from the Eagle routine.

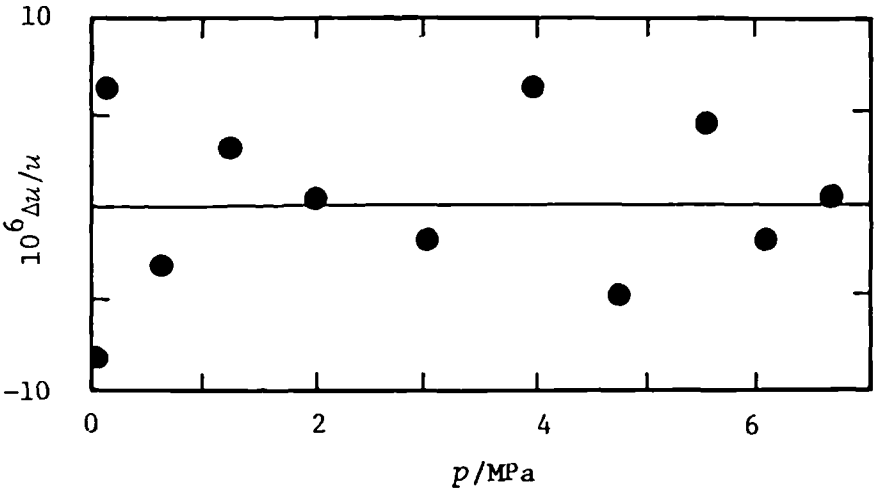

Figure 6.22. Fractional deviation $\Delta u/u = [\langle u/a \rangle - \{u(\text{calc.})/a\}]/\{u(\text{calc.})/a\}$, for $\langle u/a \rangle$ of selected modes in natural gas (the composition of which is given in table 6.10) for each pressure on the isotherm at 255 K from equation (5.3.6) in which the coefficients, given in table 6.11, were adjusted to fit the selected modes.

6.4.4 Air

Table 6.12 lists the resonance frequencies and half widths determined in Industrial quality dry air (supplied by B.O.C. plc to BS 349[53]) at 255 K, together with the quantity (u/a) and the speed of sound. Small corrections have been applied to reduce all values of (u/a) to exactly 255 K. Since no attempt was made to analyse the sample, the composition of dry air reported in table 6.13 was taken to represent the gaseous mixture studied; the mole fraction of water was quoted by the supplier to be less than 0.0001.

The thermal conductivities and shear viscosities used in the corrections were taken from values reported by Kadoya *et al.*[54] for dry air. The thermal accommodation coefficient was taken as unity. The equilibrium properties used in the acoustic model were estimated from the GL equation of state. However, the properties of xenon and krypton cannot be calculated using either GL or MCSP equations of state. Consequently the small combined mole fraction of xenon and krypton was substituted by nitrogen so that the calculations could proceed. In all 14 estimates of ρ, $C_{p,m}$, and γ were obtained between 0 and 7 MPa; for ρ the lowest pressure was 0.5 MPa. The results were then analysed using the adaptive regression algorithm the most significant terms from the array p^{-6} to p^{6} were selected. Each term selected, and retained, had a statistical significance greater than 0.99 and no significant terms remained on completion of the analyses. The estimates of ρ may be represented to 0.007 $kg \cdot m^{-3}$ by

Table 6.12. Resonance frequencies f_{0n} and half widths g_{0n}, fractional excess half widths $\delta = 10^6 \Delta g/f$, quantities (u/a), radius $a = a(T,p)$, and speeds of sound u for the n-th radial mode at temperatures T and pressures p in dry air.

p / kPa	n	f_{0n} / s^{-1}	g_{0n} / s^{-1}	δ	(u/a) / s^{-1}	$10^3 a$ / m	u / $m \cdot s^{-1}$
6880.048	2	5892.934	0.704	90	8242.681	39.97326	329.4868
	3	10131.123	0.582	35	8242.659		329.4859
	4	14299.208	0.731	33	8242.517		329.4802
	5	18445.371	1.313	55	8242.896 [c]		329.4952
	6	22580.166	1.216	39	8243.407 [c]		329.5158
	7	26533.605 [b]	3.281	110	8191.814 [c]		327.4535
	8	30431.993	1.694	43	8171.846 [c]		326.6553
5957.066	2	5853.557	0.703	90	8187.255	39.98331	327.2717
	3	10063.374	0.545	31	8187.161		327.2679
	4	14203.757	0.685	29	8187.066		327.2641
	5	18322.361	1.122	44	8187.391		327.2771
	6	22430.069	1.200	38	8187.869 [c]		327.2962
	7	26355.011 [b]	2.766	91	8135.283 [c]		325.1942
	8	30481.938	1.323	30	8181.494 [c]		327.0414
5319.556	2	5829.737	0.719	92	8153.732	39.97334	325.9319
	3	10022.441	0.531	29	8153.632		325.9279
	4	14146.079	0.643	26	8153.558		325.9250
	5	18247.975	1.060	41	8153.827		325.9357

p / kPa	n	f_{0n} / s^{-1}	g_{0n} / s^{-1}	δ	(u/a) / s^{-1}	$10^3 a$ / m	u / m·s^{-1}
5319.556	6	22339.292	1.132	35	8154.275 [c]	39.97334	325.9536
	7	26414.582 [b]	5.172	181	8153.007 [c]		325.9029
	8	30356.898	1.194	26	8138.920 [c]		325.3398
4423.070	2	5800.814	0.722	91	8112.973	39.97339	324.3030
	3	9972.854	0.506	26	8112.958		324.3024
	4	14076.217	0.600	22	8112.913		324.3006
	5	18157.913	0.968	35	8113.124		324.3091
	6	22229.252	0.994	28	8113.478 [c]		324.3232
	7	26286.476	3.356	112	8112.332 [c]		324.2774
	8	30204.952	1.159	24	8089.598 [c]		323.3687
3455.758	2	5775.287 [b]	0.604	69	8077.002	39.97344	322.8656
	3	9929.090	0.503	24	8077.057		322.8678
	4	14014.533	0.569	18	8077.015		322.8661
	5	18078.484	0.830	26	8077.207 [c]		322.8738
	6	22132.245	0.872	21	8077.477 [c]		322.8846
	7	26174.546	1.624	45	8076.723 [c]		322.8544
	8	30070.947	1.029	19	8047.380 [c]		321.6815
2784.577	2	5761.093	0.528	54	8056.883	39.97348	322.0617
	3	9904.668	0.478	20	8056.903		322.0625
	4	13980.187	0.565	16	8056.896		322.0622
	5	18034.248	0.790	22	8057.069 [c]		322.0691
	6	22078.210	0.842	18	8057.274 [c]		322.0773
	7	26112.039	1.272	31	8056.658 [c]		322.0527

p / kPa	n	f_{0n} / s^{-1}	g_{0n} / s^{-1}	δ	(u/a) / s^{-1}	$10^3 a$ / m	u / $m \cdot s^{-1}$
2784.577	8	29995.996	0.989	16	8023.844 [c]	39.97348	320.7410
1766.117	2	5744.540	0.453	34	8033.471	39.97354	321.1263
	3	9876.211	0.476	14	8033.456		321.1257
	4	13940.175	0.592	14	8033.495		321.1272
	5	17982.649	0.730	15	8033.590		321.1310
	6	22015.262	0.779	12	8033.721 [c]		321.1362
	7	26039.743	0.998	17	8033.359 [c]		321.1218
1002.136	2	5735.962	0.436	20	8021.301	39.97358	320.6401
	3	9861.506	0.537	12	8021.282		320.6394
	4	13919.442	0.658	11	8021.293		320.6398
	5	17956.048	0.818	13	8021.392		320.6437
	6	21982.814	0.798	7	8021.452		320.6461
	7	26002.795	1.008	11	8021.242		320.6378
198.578	2	5729.883	0.721	8	8013.073	39.97362	320.3116
	3	9851.194 [b]	1.000	10	8013.035		320.3100
	4	13905.104	1.250	11	8013.082		320.3119
	5	17937.629	1.482	11	8013.122		320.3135
	6	21960.562	1.725	11	8013.154		320.3148
112.919	2	5729.330	0.933	9	8012.492	39.97362	320.2884
	3	9850.341	1.303	11	8012.464		320.2873
	4	13903.966	1.640	13	8012.511		320.2891
	5	17936.247	1.978	14	8012.562		320.2912

p / kPa	n	f_{0n} / s^{-1}	g_{0n} / s^{-1}	δ	(u/a) / s^{-1}	$10^3 a$ / m	u / $m \cdot s^{-1}$
112.919	6	21958.944 [b]	2.265	12	8012.595	39.97362	320.2925
	7	25976.081	2.495	8	8012.505		320.2889
	8	29990.070	3.226	22	8012.686		320.2961
73.087	2	5728.886 [b]	1.144	10	8012.222	39.97362	320.2776
	3	9849.694	1.603	12	8012.222		320.2776
	4	13903.120	2.012	13	8012.274		320.2797
	5	17935.135 [b]	2.478	16	8012.291		320.2804
	6	21957.572 [b]	2.880	15	8012.300		320.2807
	7	25974.182 [b]	2.977	2	8012.286		320.2726
	8	29988.337 [b]	3.755	14	8012.286		320.2802
42.484	2	5728.481 [b]	1.536	22	8012.077	39.97362	320.2718
	3	9849.087 [b]	2.010	7	8012.049		320.2707
	4	13902.212	2.678	18	8012.019		320.2695
	5	17934.222	3.202	15	8012.117		320.2734
	6	21957.060 [b]	3.422	-2	8012.313		320.2815
	7	25972.943 [b]	3.535	-20	8011.892		320.2644
	8	29986.911 [b]	4.710	3	8011.984		320.2681
30.808	2	5728.180 [b]	1.781	26	8011.932	39.97362	320.2660
	3	9848.572 [b]	2.575	32	8011.837		320.2622

[a] Pressure omitted from final analysis.

[b] (u/a) received weight less than unity in regression.

[c] (u/a) omitted from regression analysis.

Table 6.13. Substance B and molefraction x_B for dry air from reference (52).

B	x_B	B	x_B
N_2	0.78102	O_2	0.20946
Ar	0.00916	CO_2	3.3×10^{-4}
Ne	1.82×10^{-5}	He	5.2×10^{-6}
CH_4	1.5×10^{-6}	H_2	0.5×10^{-6}
NO	0.3×10^{-6}	CO	0.2×10^{-6}
Kr[(a)]	1.1×10^{-6}	Xe[(a)]	0.1×10^{-6}

(a) Components not available with GL or MCSP equations of state.

$$\rho(255\ \mathrm{K},p)/(\mathrm{kg\cdot m^{-3}}) = 10^6 M/\{R\ 255\ \mathrm{K\cdot MPa}/p - 17.733 + 0.7292(p/\mathrm{MPa}) + 9.95 \times 10^{-3}(p/\mathrm{MPa})^2\}. \quad (6.4.9)$$

The $C_{p,\mathrm{m}}$ was obtained from

$$C_{p,\mathrm{m}}(255\ \mathrm{K},p)/R = 3.4874 + 0.0956(p/\mathrm{MPa}), \quad (6.4.10)$$

which represented the 14 estimates to $0.0009R$. Finally, analysis of the 14 γ estimates gave

$$\gamma(255\ \mathrm{K},p) = 1.40143 + 0.02527(p/\mathrm{MPa}) + 359 \times 10^{-6}(p/\mathrm{MPa})^2 - 44.8 \times 10^{-6}(p/\mathrm{MPa})^3, \quad (6.4.11)$$

with a standard deviation of 1.9×10^{-5} in γ. Had the MCSP method been chosen, then at 7 MPa ρ, $C_{p,\mathrm{m}}$, and γ would differ from the GL estimates by 0.8, 0.9, and -1.6 per cent respectively; at 500 kPa the differences between MCSP and GL estimates of ρ, $C_{p,\mathrm{m}}$, and γ have declined to 0.03, 0.07, and -0.2 per cent respectively. A 0.9 per cent error in ρ at 7 MPa would correspond to a fractional error in u of about 3×10^{-6} for modes (0,2) to (0,4) arising from an uncertainty in the correction for shell motion.

In the analysis of the excess half widths of the selected modes no term representing a vibrational relaxation time was found significant at a probability of 0.999, although the term accounting for the density dependence of $t\rho$ was significant at a probability of 0.9 but, was not selected. However, speed dispersion was not apparent in the frequency and pressure range of the experiment and, it was not necessary to account for the effect of vibrational relaxation on the speed of sound. The results are consistent with the presence of water which is known to act as a good catalyst for molecular energy transfer in air.[55]

The leading four terms of equation (5.3.6) were required to accommodate the selected 59 values of

Table 6.14. Coefficients of the leading four term in equation (5.3.6) required to represent 59 measurements of (u/a) for dry air between 0.03 and 6.9 MPa at 255 K with a fractional standard deviation of 19.6×10^{-6} in (u/a).

j	$(Aj/a^2)/s^{-1} \cdot Pa^{-j}$
0	$(64.1891 \pm 0.00031) \times 10^{6}$
1	$(9.409 \pm 0.059) \times 10^{-2}$
2	$(5.578 \pm 0.022) \times 10^{-8}$
3	$(1.425 \pm 0.022) \times 10^{-15}$

$(u/a)^2$ with a fractional standard deviation of 19.6×10^{-6}. The coefficients, which were all significant at a probability of 0.999, are reported in table 6.14. Figure 6.23 shows values of $\langle u/a \rangle$ as determined from the modes selected at each pressure as deviations from the smoothing equation.

Assuming the gaseous mixture has a molar mass of $0.028962\ kg \cdot mol^{-1}$, as is appropriate for the mixture compatible with the GL equation of state, then the perfect-gas molar heat capacity at constant pressure obtained from

A_0 is given by

$$C^{pg}_{p,m}/R = 3.49322 \pm 0.00008, \qquad (6.4.12)$$

and is $0.0058R$ above the value estimated from the Eagle routine.

6.5 SONIC NOZZLES

The calculation of mass flow rates, of pure gases and gaseous mixtures, through sonic nozzles invariably requires the use of an empirical equation of state and a method

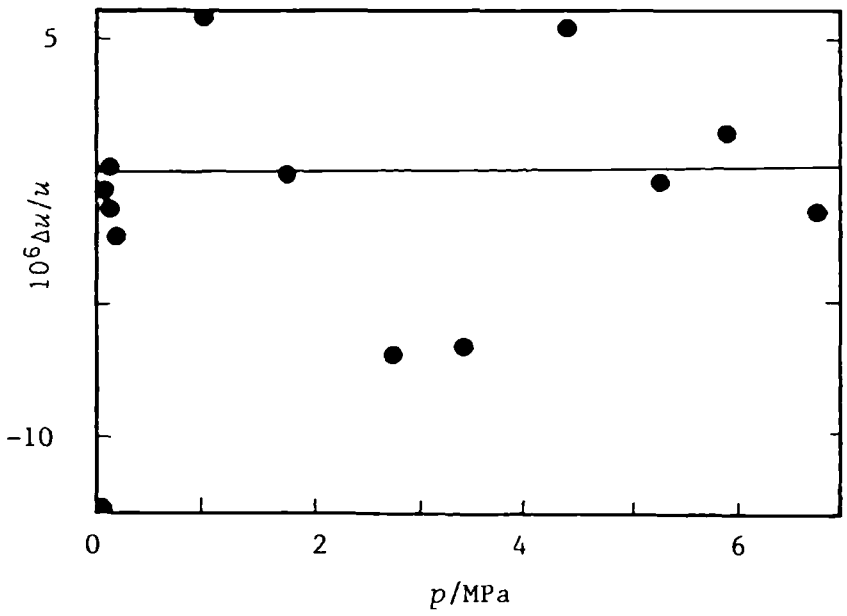

Figure 6.23. Fractional deviations $\Delta u/u = [\langle u/a\rangle - \{u(\text{calc.})/a\}]/\{u(\text{calc.})/a\}$, for $\langle u/a\rangle$ of selected modes in dry air (the composition of which is given in table 6.13) for each pressure on the isotherm at 255 K from equation (5.3.6), in which the coefficients were adjusted to fit the selected modes.

(usually a correlation) of estimating the perfect-gas heat capacity. Sonic nozzles are simple devices which are easily maintained and, consequently, may well become the flow metering standard for the gas industry.

In this section the procedure used for calculating mass transfer with sonic nozzles is reviewed, and the speed of sound determined experimentally, for the industrially important fluids discussed in section 4, are compared with estimates obtained from several equations of state; the equations of state were described in Chapter Two.

Application of the first law of thermodynamics to an amount of substance n initially present at a temperature T_1 and pressure p_1, which flows at a steady state to a position where the fluid has a temperature T_2 and pressure p_2, and assuming the duct which contains the fluid is thermally insulated then $Q = 0$ and

$$\Delta U = U(T_2,p_2) - U(T_1,p_1) = W. \qquad (6.5.1)$$

In equation (1) W is the work done and ΔU the energy change. If the fluid flow is assumed frictionless then the work done on the fluid is given by

$$W = p_2V(T_2,p_2) - p_1V(T_1,p_1) + nMg(h_1 - h_2) + \tfrac{1}{2}nm(v_1^2 - v_2^2), \qquad (6.5.2)$$

where $h_1 - h_2$ is any difference in height of the fluid between positions 1 and 2, and v_1 and v_2 are the fluid velocities. The corresponding molar enthalpy change is given by

$$\Delta H = H(T_2,p_2) - H(T_1,p_1)$$

$$= nMg(h_1 - h_2) + \tfrac{1}{2}nM(v_1^2 - v_2^2). \qquad (6.5.3)$$

Equations (2) and (3), based on reversible flow, are known to hold provided a large pressure drop exists between positions 1 and 2.[56] To achieve a pressure drop requires a change in duct cross-sectional area along the length of the duct, and to reduce the turbulence and maintain approximately frictionless flow, the cross-sectional area is necessarily a smoothly varying function of duct length.

Since the fluid flow is assumed to be adiabatic and reversible it is also isentropic; the flow must be rapid.

The mass flow rate is a constant, and for a given cross-sectional area A is proportional to the product ρA. A duct with a smoothly declining cross-sectional area, designed to drop the pressure from the plenum (position 1) to a position downstream, must also accelerate the fluid flow; such a device is called a nozzle.[56] In the region of the nozzle where the cross-sectional area has reached a minimum and is invariant, the maximum velocity which can be attained is equivalent to the speed of sound in that fluid, and is known as the throat (position 2); Venturi meters have throats but do not operate under sonic conditions. At the plenum, some way up stream from the throat, the fluid velocity is much less than the local speed of sound. A sonic nozzle is constructed from a combination of convergent and divergent nozzles.

At the plenum, provided the fluid is almost stagnant (so that $v_p \approx 0$) and sonic conditions are achieved at the throat (a sufficient pressure drop), then equation (3) reduces to

$$H(T_t,p_t) - H(T_p,p_p) \approx \tfrac{1}{2}nM\{u(T_t,p_t)\}^2, \qquad (6.5.4)$$

for a horizontal duct. In equation (4) u is the speed of sound for the fluid. Since the flow is considered to be isentropic then

$$\Delta S = S(T_t,p_p) - S(T_p,p_p) = 0. \qquad (6.5.5)$$

Equations (4) and (5) combined with an equation of state, a method of calculating perfect-gas heat capacities and a knowledge of plenum temperature T_p and pressure p_p, are sufficient to provide estimates of nozzle throat temperature T_t and pressure p_t. However, the nozzles are not perfect and it is necessary to determine a discharge coefficient C_D, which is dependent on Reynolds number $\{Rd = 4\dot{m}/(\pi d\mu)\}$, from auxiliary experiments before the mass flow rate can be obtained from

$$\dot{m} = A_t C_D \rho(T_t p_t) u(T_t,p_t). \qquad (6.5.6)$$

It is more usual to express equation (6) in terms of the measurable plenum temperature and pressure using the critical flow constant $C^\star$ or C_R:

$$\dot{m} = A_t C_D C^\star p_p/(RT_p/M)^{\frac{1}{2}}, \qquad (6.5.7)$$

$$\dot{m} = A_t C_D C_R\{\rho(T_p,p_p)p_p\}^{\frac{1}{2}}. \qquad (6.5.8)$$

C^* is related to fluid density and sound speed at the throat through

$$C^* = u(T_t, p_t)\ (T_t, p_t)\{RT_p/M\}^{\frac{1}{2}}/p_p, \qquad (6.5.9)$$

and C_R is given by

$$C_R = C^* Z_p^{\frac{1}{2}}. \qquad (6.5.10)$$

Tables of critical flow factors, mainly C^*, can be found in the literature.[57-61] More recently it has been argued that C_R is the preferred quantity for mass transfer calculations.[62] The nozzle discharge coefficient is usually determined by gravimetric analysis using air as the calibration fluid. It has been shown experimentally that C_D determined from calibration with one gas is adequate for flow rate measurements for other gases.[63]

Sonic nozzles may be operated at a plenum temperature of 300 K and a fluid pressure of up to 7 MPa. Such plenum conditions with gaseous methane would produce at the throat a gas pressure of about 5.9 MPa and a temperature of approximately 256 K; hence the choice of 255 K for the speed of sound measurements.

In order to calculate critical flow factors or mass flow rate directly, an equation of state combined with a method of predicting the perfect-gas molar heat capacity are required to provide speed of sound estimates. Consequently, it is desirable to evaluate equations of state for such calculations by comparison of speed of sound

predictions with values determined from experiment. The speed of sound has been calculated† by the following equations of state: (1), Redlick-Kwong-Soave (RK);[64] (2), GL:[41] (3), MCSP;[42,43] (4), Peng-Robinson (PR);[65] (5), GERG; and (6), GRI. Figures 6.24 to 6.26 show the speed of sound u obtained from the selected equations of state as deviations from the smoothing equations determined for methane at 255, 273.16, and 300 K. Clearly, the method of estimating the perfect-gas molar heat capacity is good, and does not lead to any significant systematic uncertainty in $u(p)$. At all three temperatures below 7 MPa the GRI provides u which differs by less than 0.05 per cent, while estimates obtained from GERG, which are valid in the temperature range 273 to 313 K, deviate by up to 1.2 per cent. Figure 6.27 shows the deviations of u calculated for the natural gas defined in table 6.10¶ from the eight term smoothing equation, not surprisingly the GRI equation provides values which differ by less than 0.05 per cent over the experimental pressure range. In figure 6.28

---

†Calculations were performed with the Eagle V.3.0 and the GRI package.[4] See Chapter Two for discussion of equations.

¶In the calculation it has been assumed that the mole fraction of C_n with $n \geqslant 6$ can be considered as n-hexane.

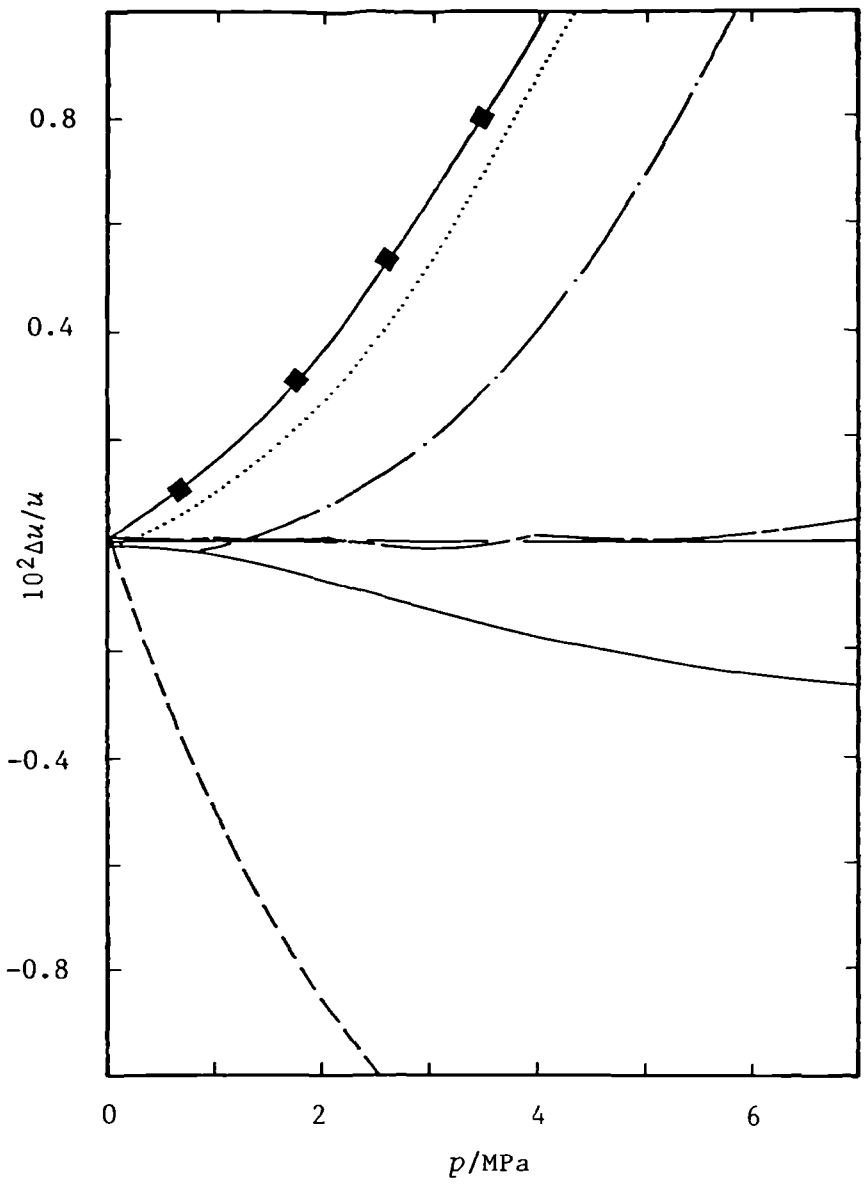

Figure 6.24. Fractional deviations $\Delta u/u = \{u(\text{e.o.s.}) - u\}/u$ for equation of state estimates of the speed of sound u(e.o.s.) for methane at 255 K, from u provided by the leading five terms of equation (5.3.6) with coefficients from table 6.7 and the resonators' radius $a(T,p)$ obtained using $a(T,p = 0)$ from table 6.4 with (6.2.1) to (6.2.3) for the pressure dependence. — – —, GRI; ————, MCSP; —·—, GL; ····· , RKS; ——■——, GERG; – – – – –, PR.

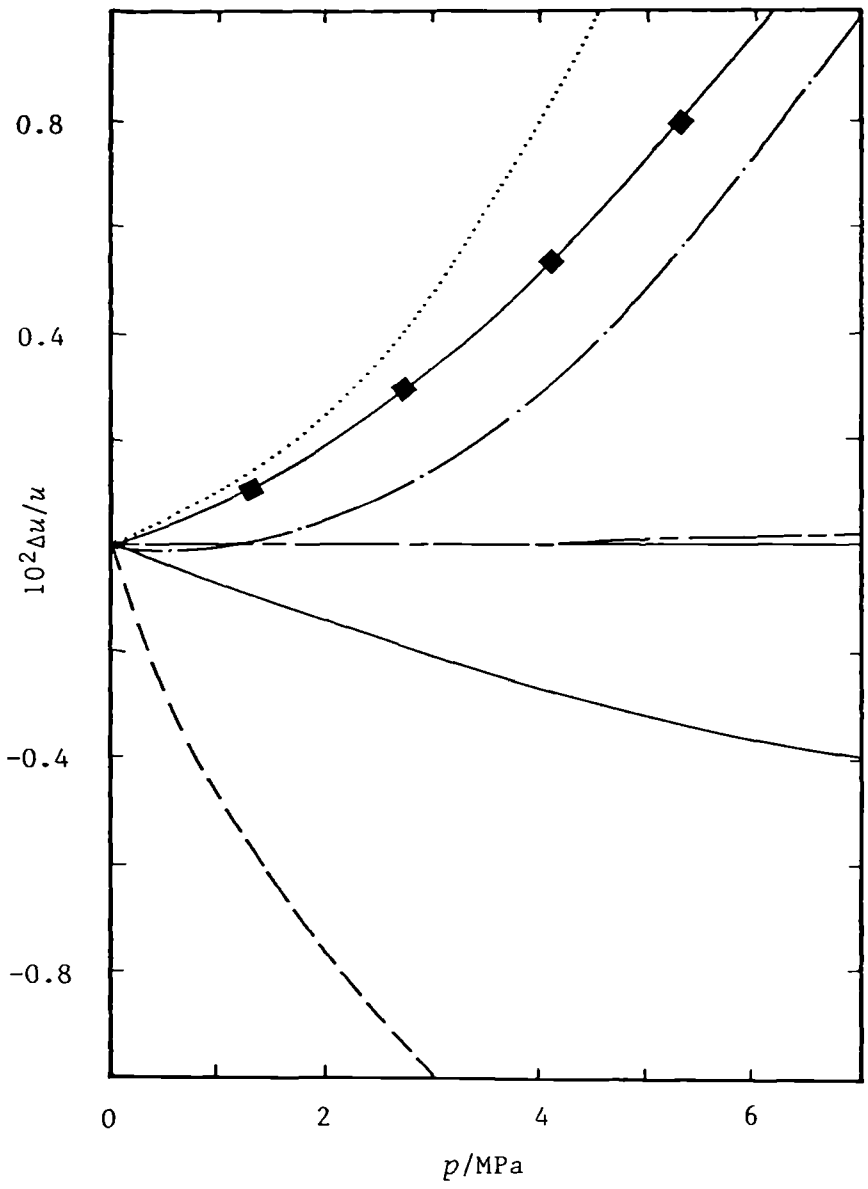

Figure 6.25. Fractional deviations $\Delta u/u = \{u(\text{e.o.s.}) - u\}/u$ for equation of state estimates of the speed of sound u(e.o.s.) for methane at 273.16 K, from u provided by the leading five terms of equation (5.3.6) with coefficients from table 6.7 and the resonators' radius $a(T,p)$ obtained using $a(T,p = 0)$ from table 6.4 with (6.2.1) to (6.2.3) for the pressure dependence. —— – ——, GRI; ————, MCSP; ——·——, G L; ·····, RKS; ——■——, GERG; – – – – – –, PR.

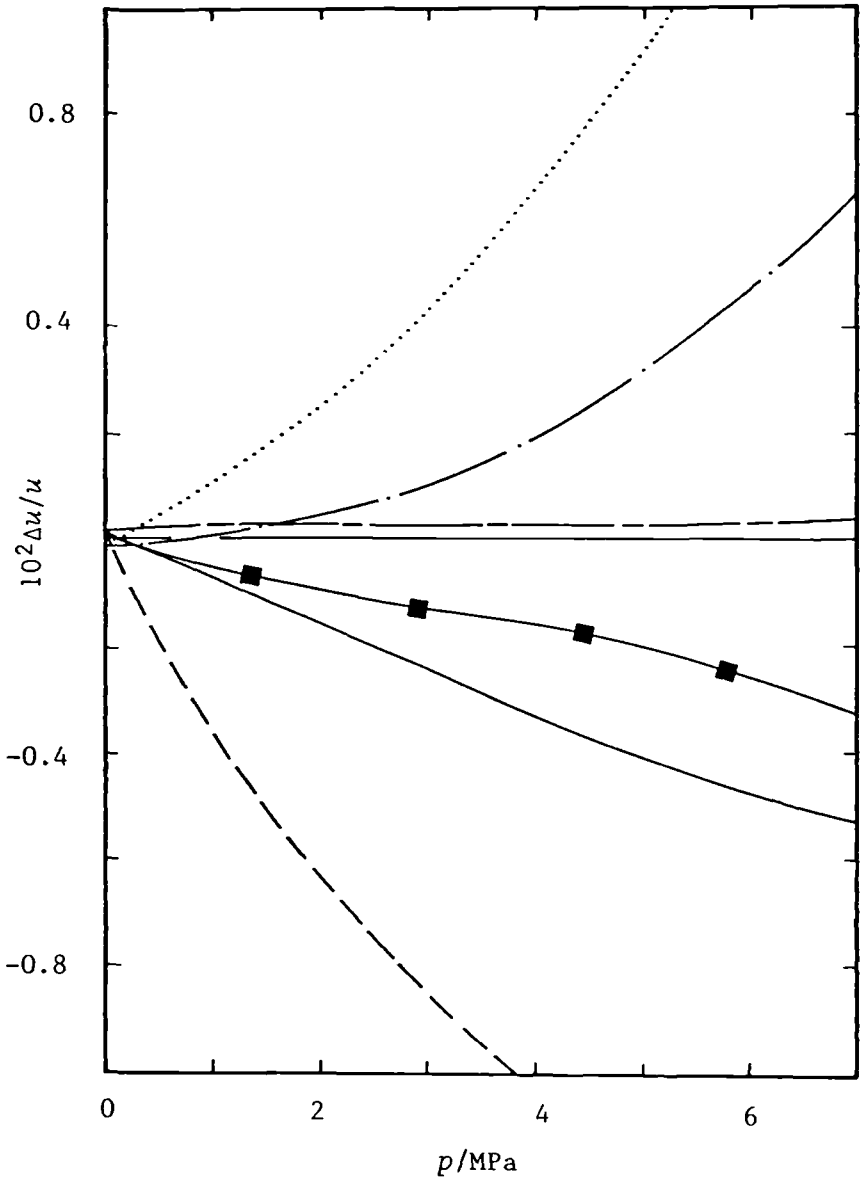

Figure 6.26. Fractional deviations $\Delta u/u = \{u(\text{e.o.s.}) - u\}/u$ for equation of state estimates of the speed of sound u(e.o.s.) for methane at 300 K, from u provided by the leading five terms of equation (5.3.6) with coefficients from table 6.7 and the resonators' radius $a(T,p)$ obtained using $a(T,p = 0)$ from table 6.4 with (6.2.1) to (6.2.3) for the pressure dependence. — – —, GRI; ——■——, GERG; ————, MCSP; —— • ——, GL; ····· ; RKS; – – – – –, PR.

are shown the deviations of predicted u[§] from the smoothing equation determined from the measurements with air at 255 K. The estimates provided by GL lie within 0.7 per cent, while those tabulated by Johnson[58] below 6 MPa lie within 0.03 per cent and at 7 MPa differ by only 0.07 per cent. Small corrections were applied using equation (5.3.9) to reduce all values reported by Johnson[58] at 460°R (equivalent to 255.556 K) to 255 K. Since argon and oxygen are components not allowed with the GRI and GERG respectively no comparison of the estimated u can be made.

In summary, the GRI provides the best estimates of u for methane and the particular natural gas studied. Consequently, this equation might well prove to be the best available for calculation of mass flow rates through sonic nozzles.

For the calibration with dry air the use of the correlation due to Johnson is not improved upon by selecting one of the other equations used here.

[§]The composition of air was taken from table 6.13 and the mole fraction of xenon and krypton were substituted with nitrogen in these calculations.

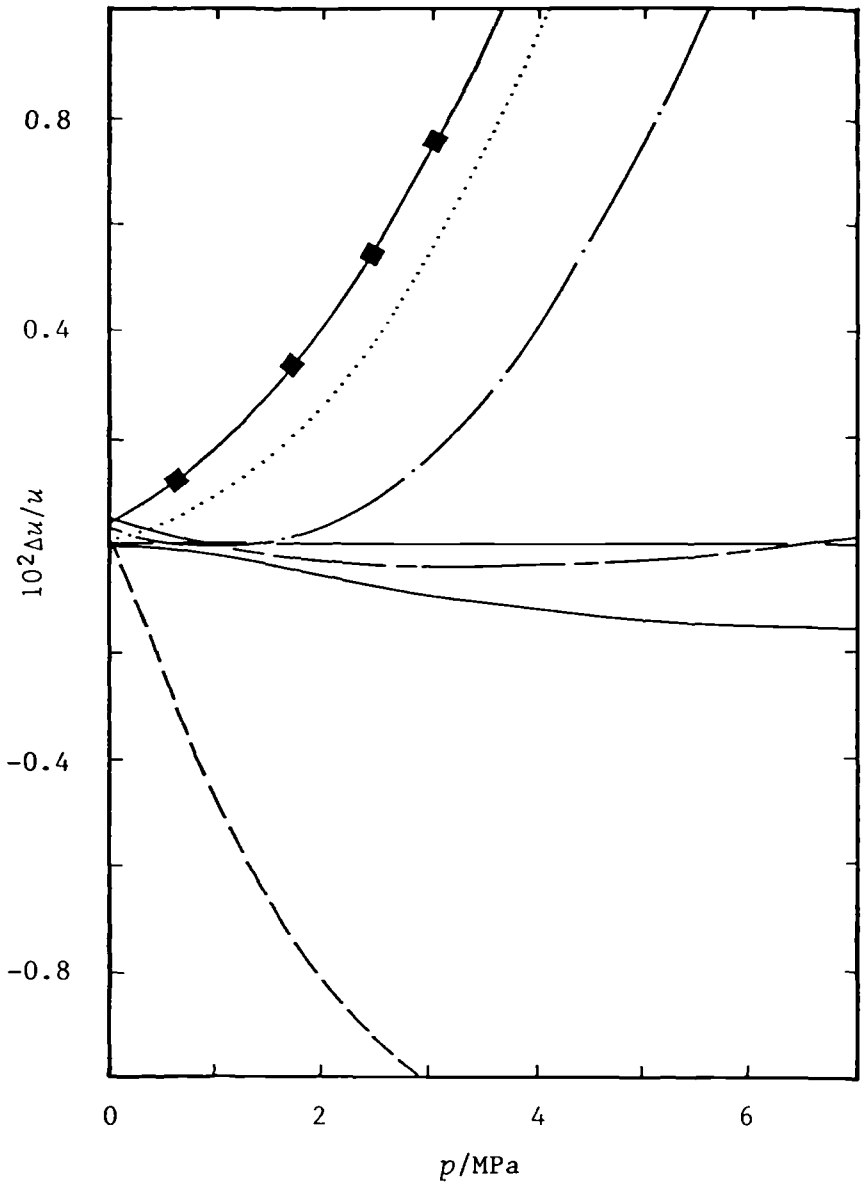

Figure 6.27. Fractional deviations $\Delta u/u = \{u(\text{e.o.s.}) - u\}/u$ for equation of state estimates of the speed of sound u(e.o.s.) for a natural gas (the composition of which is given in table 6.10) at 255 K, from u provided by the leading eight terms of equation (5.3.6) with coefficients from table 6.11 and the resonators' radius $a(T,p)$ obtained using $a(T,p = 0)$ from table 6.4 with (6.2.1) to (6.2.3) for the pressure dependence. —— – ——, GRI; ————, MCSP; ——·——, GL; ····· ; RKS; ——■——, GERG; – – – – –, PR.

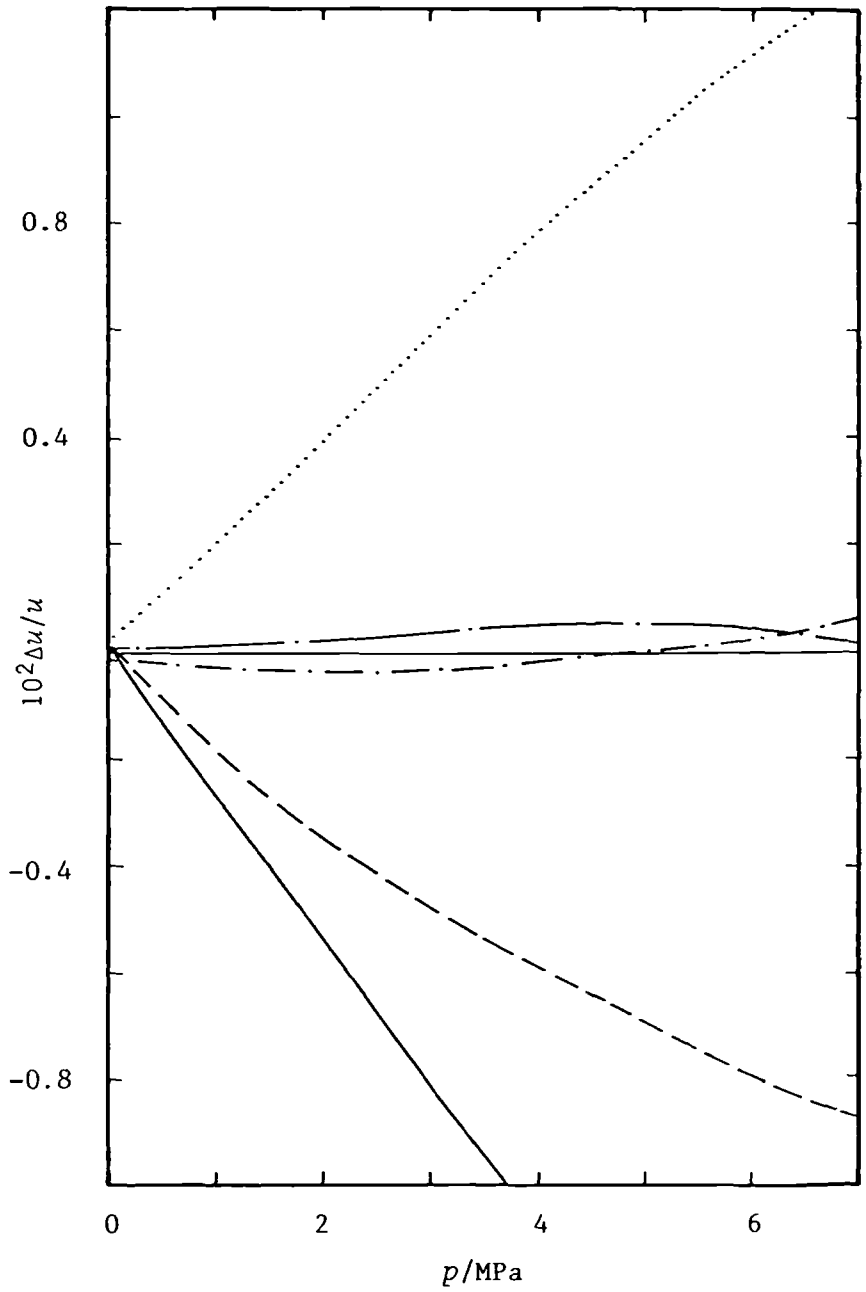

Figure 6.28. Fractional deviations $\Delta u/u = \{u(\text{e.o.s.}) - u\}/u$ for equation of state estimates of the speed of sound u(e.o.s.) for dry air (the composition of which is given in table 6.13) at 255 K, from u provided by the leading four terms of equation (5.3.6) with coefficients from table 6.14 and the resonators' radius $a(T,p)$ obtained using $a(T,p = 0)$ from table 6.4 with (6.2.1) to (6.2.3) for the pressure dependence. ——·——, GL; – – – – –, PR; ·····, RKS; ————, MCSP; —·—·—·—, estimated from reference ( ).

REFERENCES

1. Love, A.E.H. *Mathematical Theory of Elasticity* Fourth Edition. Dover: New York. 1944.
2. British Standards Institution. London. BS 970 part 4. 1971.
3. Papadakis, E.P. *Mater. Sci. Eng.* 1972, 10, 195.
4. British Standards Institution. London. BS 5500, 1976.
5. British Standards Institution. London. BS 1515, part 2, 1968.
6. American Society of Mechanical Engineers. Unifired Pressure Vessel Code. Section VIII. Division 1 and 2. 1962.
7. High Pressure Safety Code. Cox, B.G.; Saville, G.: Editors. For High Pressure Technology Association. 1975.
8. Allison, I.M.; Bacchus, K.M. *Proc. Expt. Stress Analysis* paper 13. *Inst. Mech. Eng.* 1970, 390.
9. Harvey, J.H. *The theory and design of modern pressure vessels.* Wiley: London. 1974.
10. Fryer, D.M.; Smith, C.W. Jr. *Inst. Mech. Eng.* 1977, 367.
11. Gray, M.G.; Pick, R.J. *Inst. Mech. Eng.* 1977, 353.
12. British Standards Institution. London. BS 1806.
13. Reference 7, p.85.
14. Reference 9, p.35.
15. Kuhl, W.; Schodder, G.R.; Schröder, F.-K. *Acustica* 1954, 4, 519.
16. Zahn, R. *J. Acoust. Soc. Am.* 1981, 69, 1200.
17. Matsuzawa, K. *J. Phys. Soc. Japan* 1958, 13, 1533; 1966, 15, 167.

18. Matsuzawa, K. *Japan, J. Appl. Phys.* 1978, 17, 451.

19. Sessler, G.M.; West, J.E. *J. Acoust. Soc. Am.* 1962, 34, 1774.

20. Trusler, J.P.M. unpublished notes.

21. Ewing, M.B.; McGlashan, M.L.; Trusler, J.P.M. *Metrologia* 1986, 22, 93.

22. Maitland, G.C.; Rigby, M.; Smith, E.B.; Wakenham, W.A. *Intermolecular Forces Their Origin and Determination.* Clarendon: Oxford. 1981, p.571.

23. Kestin, J.; Clifford, R.R.; Wakenham, W.A. *Physica* 1980, 100A, 349.

24. Kestin, J.; Ro, S.T.; Wakenham, W.A. *J. Chem. Phys.* 1972, 56, 4119.

25. Dymond, J.H.; Smith, E.B. *The virial coefficients of pure gases and mixtures.* Clarendon Press: Oxford, 1980. p.1

26. Mehl, J.B. *J. Acoust. Soc. Am.* 1985, 78, 785.

27. Moldover, M.R.; Trusler, J.P.M.; Edwards, T.J.; Mehl, J.B.; Davis, R. *J. Res. Natl. Bur. Std.* (U.S.) Mar/April 1988 (in press).

28. Douslin, D.R.; Harrison, R.H.; Moore, R.T. McCullough, J.P. *J. Chem. Eng. Data* 1964, 9, 358.

29. Kestin, J.; Ro, S.T.; Wakenham, W.A. *Trans. Faraday Soc.* 1971, 67, 2308.

30. Kestin, J.; Yata, J.; *J. Chem. Phys.* 1968, 49, 4780.

31. Clifford, A.A.; Kestin, J.; Wakenham, W.A. *Physica* 1979, 97A, 287.

32. Cottrell, T.L.; Matheson, A.J. *Trans. Faraday Soc.* 1962, 58, 2336.

33. Edwards, P.D.; Lamb, J. *Proc. Phys. Soc. Lond.* 1958, 72, 940.

34. Cottrell, T.L.; Martin, P.E. *Trans. Faraday Soc.* 1957, 53, 1157.

35. Cottrell, T.L.; McCoubrey, J.C. *Molecular energy transfer in gases.* Butterworths: London. 1961. p.100.

36. Lambert, J.D. *Vibrational and rotational relaxation in gases.* Clarendon Press: Oxford. 1977. p.12, 84-93.

37. Kroeger, F.R.; Swenson, C.A. *J. Appl. Phys.* 1977, 48, 853.

38. Wilhoit, R.C. *Ideal gas thermodynamic functions.* TRC Current Data News 1975. 3, 2.

39. McDowell, R.S.; Kruse, F.H. *J. Chem. Eng. Data,* 1963, 8, 547.

40. Savidge, J. University of Oklahoma.

41. Gibbons, R.M.; Laughton, A.P. *J. Chem. Soc. Faraday Trans. 2* 1984, 80, 1019.

42. McCarty, R.D. *Cryogenics* 1974, 14, 276.

43. Leach, J.W.; Chappelear, P.S.; Leland, T.W. *A.I.ch.E.J.* 1968, 14, 568.

44. Humphreys, A.E. *Some thermophysical constants of components of natural gas and cognate fluids.* GERG Tech. Monograph TPC/1. 1986. p.34-35.

45. Ewing, M.B. unpublished work.

46. Hanley, H.J.M. *Cryogenics* 1976, 16, 643.

47. Ely, J.F,; Hanley, H.J.M. *Proc. 60th Convention Gas Process. Assoc.* 1981, p.20.

48. Ely, J.F. *Proc. 61st Convention Gas Process. Assoc.* 1982, p.9.

49. Ely, J.F.; Hanley, H.J.M. *Ind. End. Chem. Fundam.* 1981, 20, 323.

50. Ely, J.F.; Hanley, H.J.M. *Ind. End. Chem. Fundam.* 1983, 22, 90.

51. Hanley, H.J.M.; McCarty, R.D.; Haynes, W.M. *Cryogenics* 1975, 15, 413.

52. Reference 44, p.31.

53. British Standards Institution. London. BS 349.

54. Kadoya, K.; Matsunaga, N.; Nagashima, A. *J. Phys. Chem. Ref. Data* 1985, 14, 947.

55. Zuckerwar, A.J.; Meredith, R.W. *J. Acoust. Soc. Am.* 1985, 78, 946.

56. Bett, K.E.; Rowlinson, J.S.; Saville, G. *Thermodynamics for chemical engineers.* Athlone Press: London. 1975, p.180.

57. Johnson, R.C. *J. Basic Eng. Trans. A.S.M.E. series D* 1964, 86, 519.

58. Johnson, R.C. N.A.S.A. TN D-2565, 1965.

59. Johnson, R.C. N.A.S.A. SP-3046, 1968.

60. Johnson, R.C. *J. Basic Eng. Trans. A.S.M.E. series D* 1970, 92, 580.

61. Johnson, R.C. N.A.S.A. SP-3074, 1972.

62. Weberg, T.; Thomassen, D. *Proc. Int. Conf. Flow Measurement* paper 4.2 1986.

63. Godt, P.W. *Proc. Ind. Symp. Sci. Contrl. Flow Measurement* 1974, 1, 263.

64. Soave, G. *Chem. Eng. Sci.* 1972, 27, 1197.

65. Peng, D.-Y.; Robinson, D.B. *Ind. Eng. Chem. Fundam.* 1976, 15, 59.

66. Zahn, R. *Acustica* 1985, 57, 200.

APPENDIX A1

O-220

J. Chem. Thermodynamics 1987, 19, 721–739

Thermophysical properties of alkanes from speeds of sound determined using a spherical resonator

I. Apparatus, acoustic model, and results for dimethylpropane

M. B. EWING, A. R. H. GOODWIN, M. L. McGLASHAN, and J. P. M. TRUSLER

Department of Chemistry, University College London, 20 Gordon Street, London WC1H 0AJ, U.K.

(Received 9 September 1986; in final form 19 November 1986)

The speed of sound in dimethylpropane between 250 and 323.15 K has been obtained from measurements of the frequencies of the radial modes of a spherical acoustic resonator; the acoustic model and the apparatus are described briefly. The radius of the resonator was obtained from the speed of sound in argon. Perfect-gas heat capacities and second and third acoustic virial coefficients for dimethylpropane have been calculated from the results, and estimates are given for the second and third (p, V_m, T) virial coefficients.

1. Introduction

Recently,[1] we published speeds of sound u in dimethylpropane obtained using a fixed-pathlength *cylindrical* resonator operating between 50 and 90 kHz, and by analysis of the results in terms of the virial expansion for the speed of sound

$$u^2 = A_0 + A_1 p + A_2 p^2 + \cdots, \tag{1}$$

obtained perfect-gas heat capacities $C^{pg}_{p,m}$, and second β_a and third γ_a acoustic virial coefficients using the relations:

$$A_0 = RT\gamma^{pg}/M, \tag{2}$$

$$\beta_a = (M\gamma^{pg})A_1 = RTA_1/A_0, \tag{3}$$

$$\gamma_a = (M/\gamma^{pg})A_2 = RTA_2/A_0, \tag{4}$$

where

$$\gamma^{pg} = 1/(1 - R/C^{pg}_{p,m}), \tag{5}$$

and M is the molar mass of the gas. Here we present much more precise results, which were anticipated in the previous paper, for u in dimethylpropane obtained

0021-9614/87/070721+19 $02.00/0

from the radial modes of a *spherical* acoustic resonator. The coefficients B and C' in the (p, V_m, T) virial expansion:

$$pV_m/RT = 1+(B/RT)p+(C'/RT)p^2+\cdots, \tag{6}$$

can be calculated from values of β_a and γ_a over a range of temperatures by solving the second-order differential equations:

$$\beta_a = 2B+2TB^{(1)}(\gamma^{pg}-1)+T^2B^{(2)}(\gamma^{pg}-1)^2/\gamma^{pg}, \tag{7}$$

$$\gamma_a = C'(\gamma^{pg}+2)+2TC'^{(1)}(\gamma^{pg}-1)+T^2C'^{(2)}(\gamma^{pg}-1)^2/2\gamma^{pg}+G, \tag{8}$$

where the superscript (i) indicates the ith temperature derivative and where the function G given by

$$\begin{aligned} RTG = B^2+(TB^{(1)})^2\{(\gamma^{pg}-1)+4(\gamma^{pg}-1)^2\}+(T^2B^{(2)})^2\{(\gamma^{pg}-1)^3/\gamma^{pg}\} \\ +4TBB^{(1)}(\gamma^{pg}-1)+2T^2BB^{(2)}(\gamma^{pg}-1)^2/\gamma^{pg} \\ +2T^3B^{(1)}B^{(2)}(\gamma^{pg}-1)^2(2\gamma^{pg}-1)/\gamma^{pg}, \end{aligned} \tag{9}$$

is independent of C' and its temperature derivatives. Although this is an indirect method of determining heat capacities and virial coefficients, the accuracy of the $C^{pg}_{p,m}$ so obtained compares very favourably with that from flow calorimetry (or calculated from spectroscopic data),[35] while the imprecision of B and C' is significantly smaller than in (p, V_m, T) measurements. In particular, the speed of sound is formally independent of the amount of substance and the spherical resonator has been operated at very low pressures and at low reduced temperatures that are inaccessible with other techniques because of the effects of adsorption.

2. Acoustic model

In the zeroth-order approximation the acoustic resonance frequencies $f^{(0)}_{ln}$ of a fluid contained in a rigid spherical cavity of radius a are given by

$$f^{(0)}_{ln} = \nu_{ln}(u/2\pi a); \quad l = 0, 1, 2, \cdots; \quad n = 0, 1, 2, \cdots, \tag{11}$$

where ν_{ln} is the n-th turning point of the spherical Bessel function of order l; the radially symmetric modes, for which $l = 0$, are particularly useful[2,3] and non-radial modes will not be considered further in this paper. Following Mehl and Moldover,[3,4] who used first-order perturbation theory to account for the energy losses in the bulk of the gas and at the wall of the resonator, a complex resonance frequency F_{0n} for the n-th radial mode may be defined by

$$F_{0n} = f_{0n}-ig_{0n} = \nu_{0n}(u/2\pi a)+\Sigma_j(\Delta f-ig)_j, \tag{12}$$

where f_{0n} and g_{0n} are the observed resonance frequency and resonance half-width and $(\Delta f-ig)_j$ is the j-th perturbation term. Although the various perturbations have been discussed in detail elsewhere,[2,3] the relevant expressions are given below for convenience. For the measurements reported here the most important loss mechanism arises from the thermal-boundary layer and the resulting perturbation

is[2]

$$(\Delta f - \mathrm{i}g)_{\mathrm{th}} = -(1+\mathrm{i})\{(\gamma-1)/2a\}(D_{\mathrm{th}}f/\pi)^{1/2} + \mathrm{i}\{(\gamma-1)/2a^2\}(D_{\mathrm{th}}/\pi) + (\gamma-1)f(l_a/a), \quad (13)$$

where $\gamma = C_{p,\mathrm{m}}/C_{V,\mathrm{m}}$ is the ratio of the molar heat capacities, D_{th} is the thermal diffusivity, and l_a is the thermal accommodation length. In equation (13), the first term is the classical expression describing the loss at a plane surface, the second term is the small correction due to the curvature of the surface, and the final term takes account of the temperature-jump effect. For a gas with molar mass M and thermal conductivity κ at mass density ρ, the thermal diffusivity and accommodation length are given by

$$D_{\mathrm{th}} = \kappa M/(\rho C_{p,\mathrm{m}}), \quad (14)$$

$$l_a = (\kappa/p)(\pi MT/2R)^{1/2}\{(C_{V,\mathrm{m}}/R) + 1/2\}^{-1}\{(2-h)/h\}, \quad (15)$$

where h is the accommodation coefficient which is sensitive to the surface finish and to the adsorbed layer of molecules.

The walls of the resonator respond elastically to the acoustic pressure but, if the motion is undamped, there is no contribution to the the half width and for the radial modes the frequency shift[3,5] is

$$\Delta f_{\mathrm{el}} = C\rho u^2 f/\{1-(f/f_{\mathrm{res}})^2\}, \quad (16)$$

where for the resonator used for this work $C = 26.9\ \mathrm{TPa}^{-1}$ and $f_{\mathrm{res}} = 21.2\ \mathrm{kHz}$.

A cylindrical tube of radius b and length L opening into the resonator gives rise to a perturbation:

$$(\Delta f - \mathrm{i}g)_{\mathrm{o}} = (ub^2/8\pi a^3)\cot\{(kL + \alpha_{\mathrm{KH}}L + \delta_L) + \mathrm{i}(\alpha_{\mathrm{KH}}L + \gamma_L)\}, \quad (17)$$

where $k = 2\pi f/u$, is the propagation constant and

$$\alpha_{\mathrm{KH}} = \{(\pi f)^{1/2}/ub\}\{D_s^{1/2} + (\gamma-1)D_{\mathrm{th}}^{1/2}\}, \quad (18)$$

is the Kirchhoff-Helmholtz tube attenuation constant; the viscous diffusivity D_s is given in terms of the shear viscosity η by

$$D_s = \eta/\rho. \quad (19)$$

The parameters γ_L and δ_L describe the change in amplitude and phase at the end of the tube remote from the resonator. For an open flanged tube:

$$\gamma_L = (kb)^2/2, \quad (20)$$

$$\delta_L = 8kb/3\pi, \quad (21)$$

while for a tube terminating in a sealed cavity of volume V with dimensions small compared with the wavelength:

$$\gamma_L = 0, \quad (22)$$

$$\delta_L = -\arctan(\pi b^2/kV). \quad (23)$$

However, if the cavity is not sealed then leakage conductance can greatly increase the terminal admittance so that

$$\gamma_L \approx \delta_L \approx 0. \tag{24}$$

Sound absorption throughout the bulk of the gas increases the half width by

$$g_b = \pi(f/u)^2\{4D_s/3 + (\gamma-1)D_{th} + \eta_b/\rho\}. \tag{25}$$

For polyatomic gases the bulk viscosity η_b arises mainly from vibrational relaxation which reduces the effective heat capacity such that, at angular frequency ω, the ratio of heat capacities becomes

$$\gamma(\omega) = \{C_{p,m} + \Sigma_j i\omega t_j C_{vib,j,m}/(1-i\omega t_j)\}/\{C_{V,m} + \Sigma_j i\omega t_j C_{vib,j,m}/(1-i\omega t_j)\}, \tag{26}$$

where the summations are over the vibrational states that relax with a characteristic time constant t_j and contribute $C_{vib,j,m}$ to the molar heat capacities at zero frequency. If it is assumed that there is a single relaxation time t arising either from one vibrational state or from a number of states coupling in series[6] then equation (26) may be written

$$\{\gamma(\omega)/\gamma\} - 1 = \omega t(\gamma-1)\Delta\{\omega t(1-\gamma\Delta) - i\}/[1 + \{\omega t(1-\gamma\Delta)\}^2], \tag{27}$$

where $\Delta = C_{vib,m}/C_{p,m}$, is the fraction of the total heat capacity that is relaxing. Equations (25) and (27) then give the contribution of vibrational relaxation to the bulk viscosity as

$$\eta_b = -i(u^2\rho/\omega)[\{\gamma(\omega)/\gamma\} - 1] = u^2\rho\Delta(\gamma-1)t, \tag{28}$$

provided that $(\omega t)^2 \ll 1$.

3. Experimental

The applications of spherical resonators as highly precise tools for the study of thermophysical properties of gases have been developed recently by Mehl and Moldover.[4] The apparatus used in the present work has been described in detail elsewhere;[2,7] only the important features are given here. Two hemispheres turned from aluminium alloy were bolted together to form a resonator with internal radius 60 mm and wall thickness 12 mm. The transducers were located at an angle of $\pi/2$ apart; the source was mounted flush with the internal surface while the microphone was fixed (but not sealed) in a small volume in the wall and coupled to the interior by a short (6 mm) wave guide. The sphere was suspended inside a cylindrical vessel which was placed in a stirred-fluid thermostat controlled to 1 mK; the corresponding temperature fluctuations, as measured with a long-stem platinum resistance thermometer (calibrated on IPTS-68) sitting in a copper block bolted to the resonator, were not greater than 0.1 mK. The acoustic resonator is a very sensitive thermometer and repeated measurements of a resonance frequency and of the resistance of the platinum thermometer indicated that the resonator and the gas reached thermal equilibrium simultaneously. The gas under study passed freely between the resonator and the containing vessel *via* a 1 mm diameter hole drilled

through the wall of the sphere. The pressure was measured with a precision of 1 Pa using a differential capacitance manometer and a quartz-spiral gauge fitted with an optical null detector. The resonance frequencies and half widths were calculated[37] from comparative measurements, performed with a network analyser, of the amplitude A and phase ϕ of the transmitted and received signals at 11 frequencies in the range $(f_{0n} \pm g_{0n})$ near each resonance. At each frequency, a time t was allowed for the acoustic pressure to stabilize such that the fractional systematic error, given approximately by $(g/f)\exp(-2\pi tg)$, in the resonance frequency was less than 10^{-7} before A and ϕ were recorded. These procedures differ only in detail from those described by Mehl and Moldover.[4]

The dimethylpropane was the dried and degassed research-grade material used previously.[1] Before a series of measurements, the apparatus was baked at 340 K under vacuum until the pressure indicated by an ionization gauge in the pumping line had been below 0.5 mPa for 24 h.

4. Results

Table 1 lists the resonance frequencies and half widths determined in dimethylpropane along eight isotherms between 250 and 323.15 K; such a temperature range corresponds to reduced temperatures between 0.58 and 0.75 and includes the normal-boiling and triple-point temperatures of dimethylpropane. Corrections were applied to obtain the quantity (u/a) as described in section 2. The accommodation coefficient was taken as 0.84 for argon, as determined previously,[2] but as unity for dimethylpropane because at high fractions of the vapour pressure the incident molecules are more likely to reach thermal equilibrium before being re-emitted from the wall. The virial coefficients required for $C_{p,m}$ and γ in the acoustic model were estimated from a preliminary analysis of the results. The transport properties used in the calculations are discussed below.

The thermal conductivities given by Parkinson and Gray[8] at 323.15 and 373.15 K show the temperature dependence predicted by Owens and Thodos[9] and consequently κ was obtained from

$$\kappa(T)/\kappa(323.15\ \mathrm{K}) = (T/323.15\ \mathrm{K})^{1.786}, \tag{29}$$

with $\kappa(323.15\ \mathrm{K}) = 18.22\ \mathrm{mW \cdot m^{-1} \cdot K^{-1}}$. The thermal conductivities given by equation (29) agree to 2 per cent with those obtained from the modified Eucken equation:[10]

$$\kappa = (\eta/M)(1.32C_{V,m} + 1.77R), \tag{30}$$

using the shear viscosities of Diaz Peña and Esteban,[11] which may be represented to 0.06 μPa·s by

$$\eta/(\mu\mathrm{Pa \cdot s}) = 1.14 + 0.01985(T/\mathrm{K}), \tag{31}$$

and the heat capacities of Hossenlopp and Scott.[12]

If the acoustic model were complete and the transport properties exact then the

TABLE 1. Resonance frequencies f_{0n} and half widths g_{0n}, fractional excess half widths $\delta = 10^6\Delta g/f$, and speeds of sound u at temperatures T and pressures p in dimethylpropane. The radius is given by equation (35)

p/kPa	f_{0n}/Hz	g_{0n}/Hz	δ	(u/a)/s^{-1}	f_{0n}/Hz	g_{0n}/Hz	δ	(u/a)/s^{-1}	f_{0n}/Hz	g_{0n}/Hz	δ	(u/a)/s^{-1}
					T = 250.000 K							
15.741 [a]	2087.181	0.144	23	2918.614	6533.769	0.455	15	2918.638	10924.947	0.906	14	2918.644
	3588.377	0.205	13	2918.623	7999.148	0.566	13	2918.640				
	5064.976	0.304	13	2918.627	9462.597	0.727	14	2918.640				
14.253	2088.888	0.147	22	2920.989	6539.104	0.468	12	2921.006	10933.861	0.953	12	2921.010
	3591.311	0.209	11	2920.995	8005.679	0.588	11	2921.008				
	5069.117	0.315	11	2920.999	9470.321	0.753	11	2921.007				
13.065	2090.228	0.152	21	2922.862	6543.296	0.487	11	2922.876	10940.864	1.006	11	2922.878
	3593.612	0.215	9	2922.866	8010.809	0.616	10	2922.877				
	5072.368	0.325	9	2922.870	9476.386	0.796	10	2922.875				
12.030	2091.390	0.156	21	2924.489	6546.931	0.507	10	2924.499	10946.942	1.066	10	2924.500
	3595.609	0.223	9	2924.490	8015.260	0.647	9	2924.500				
	5075.186	0.339	9	2924.494	9481.649	0.842	10	2924.498				
10.869	2092.682	0.162	20	2926.310	6550.975	0.541	9	2926.317	10953.698	1.154	10	2926.316
	3597.830	0.234	8	2926.309	8020.210	0.696	9	2926.318				
	5078.315	0.363	9	2926.309	9487.505	0.908	9	2926.315				
9.806	2093.855	0.169	20	2927.966	6554.658	0.577	8	2927.975	10959.845	1.254	10	2927.971
	3599.850	0.248	7	2927.967	8024.713	0.752	8	2927.974				
	5081.169	0.380	7	2927.967	9492.827	0.986	9	2927.969				
8.726	2095.054	0.180	20	2929.649	6558.410	0.629	8	2929.654	10966.133	1.381	9	2929.653
	3601.911	0.266	7	2929.648	8029.309	0.825	8	2929.653				
	5084.077	0.416	7	2929.647	9498.265	1.084	9	2929.649				
7.589	2096.310	0.191	20	2931.411	6562.345	0.696	7	2931.412	10972.719	1.553	9	2931.412
	3604.074	0.292	7	2931.410	8034.128	0.922	8	2931.412				
	5087.135	0.461	7	2931.411	9503.966	1.215	9	2931.407				
6.455	2097.554	0.208	20	2933.156	6566.273	0.791	7	2933.166	10979.260	1.797	10	2933.158
	3606.218	0.324	6	2933.156	8038.924	1.051	8	2933.162				
	5090.161	0.511	5	2933.155	9509.639	1.395	9	2933.156				
5.344	2098.763	0.230	20	2934.871	6570.068	0.921	8	2934.877	10985.621	2.134	11	2934.873
	3608.301	0.373	7	2934.871	8043.572	1.239	9	2934.875				
	5093.104	0.600	7	2934.870	9515.129	1.655	10	2934.865				
4.198	2100.006	0.262	19	2936.629	5096.149	0.725	7	2936.637	8048.360	1.530	10	2936.631
	3610.450	0.446	7	2936.634	6573.989	1.133	10	2936.636				
					T = 260.000 K							
25.100 [a]	2117.881	0.106	15	2961.501	6629.867	0.336	11	2961.531	11085.615	0.660	11	2961.536
	3641.154	0.141	5	2961.511	8116.797	0.413	10	2961.533				
	5139.469	0.198	4	2961.517	9601.751	0.525	10	2961.529				
23.341	2119.702	0.111	16	2964.061	6635.556	0.345	10	2964.084	11095.124	0.692	11	2964.088
	3644.288	0.151	6	2964.073	8123.769	0.424	9	2964.089				
	5143.878	0.212	4	2964.070	9610.007	0.534	8	2964.088				
21.284	3647.905	0.164	8	2967.027	6642.119	0.353	8	2967.028	9619.508	0.575	9	2967.029
	5148.989	0.247	9	2967.027	8131.797	0.442	7	2967.030	11106.080	0.725	10	2967.026
18.906	2124.225	0.114	12	2970.389	6649.714	0.381	8	2970.408	11118.787	0.778	8	2970.408
	3652.071	0.176	8	2970.405	8141.096	0.488	8	2970.411				
	5154.873	0.256	7	2970.406	9630.493	0.609	7	2970.405				
16.368	2126.800	0.124	13	2973.989	6657.774	0.419	8	2974.005	11132.264	0.872	8	2974.005
	3656.494	0.183	6	2974.001	8150.959	0.531	7	2974.006				
	5161.118	0.275	5	2974.002	9642.175	0.694	8	2974.004				

TABLE 1—*continued*

p/kPa	f_{0m}/Hz	g_{0m}/Hz	δ	(u/a)/s^{-1}	f_{0m}/Hz	g_{0m}/Hz	δ	(u/a)/s^{-1}	f_{0m}/Hz	g_{0m}/Hz	δ	(u/a)/s^{-1}
14.591	2128.575	0.134	14	2976.489	6663.331	0.445	6	2976.503	11141.556	0.973	10	2976.501
	3659.542	0.195	5	2976.496	8157.761	0.562	5	2976.502				
	5165.421	0.291	4	2976.497	9650.210	0.747	7	2976.497				
11.563	2131.605	0.146	13	2980.744	6672.817	0.519	5	2980.751	11157.461	1.174	9	2980.760
	3664.756	0.225	5	2980.750	8169.388	0.695	7	2980.755				
	5172.779	0.355	6	2980.749	9663.954	0.884	5	2980.746				
10.028	2133.128	0.159	14	2982.878	6677.609	0.591	6	2982.893	11165.461	1.338	11	2982.898
	3667.380	0.246	4	2982.889	8175.241	0.766	5	2982.893				
	5176.488	0.386	5	2982.889	9670.861	1.037	9	2982.878				
8.048	2135.091	0.182	15	2985.635	5181.259	0.460	6	2985.644	8182.768	0.933	7	2985.643
	3670.758	0.287	5	2985.643	6683.761	0.699	6	2985.645	9679.795	1.224	7	2985.636
					$T = 270.000$ K							
39.810[a]	2144.228	0.081	10	2998.333	6712.296	0.243	7	2998.349	11223.478	0.464	7	2998.367
	3686.449	0.115	6	2998.346	8217.727	0.298	7	2998.358				
	5203.473	0.166	6	2998.395	9721.128	0.375	7	2998.349				
36.639	2147.211	0.083	10	3002.514	6721.633	0.251	6	3002.528	11239.028	0.493	7	3002.529
	3691.578	0.118	5	3002.527	8229.143	0.305	5	3002.532				
	5210.629	0.171	5	3002.527	9734.650	0.394	6	3002.528				
33.939	2149.744	0.085	10	3006.057	6729.568	0.260	6	3006.073	11252.280	0.518	7	3006.069
	3695.933	0.120	4	3006.070	8238.852	0.325	6	3006.074				
	5216.781	0.175	5	3006.072	9746.142	0:412	6	3006.072				
29.308	2154.051	0.091	10	3012.087	6743.049	0.279	5	3012.100	11274.834	0.567	6	3012.099
	3703.338	0.128	4	3012.098	8255.358	0.354	5	3012.101				
	5227.229	0.190	4	3012.098	9765.664	0.451	5	3012.098				
25.406	2157.661	0.097	10	3017.135	6754.353	0.307	5	3017.147	11293.737	0.629	5	3017.145
	3709.545	0.139	4	3017.145	8269.198	0.389	5	3017.148				
	5235.991	0.206	4	3017.145	9782.036	0.499	5	3017.145				
21.529	2161.218	0.105	10	3022.115	6765.488	0.342	4	3022.125	11312.360	0.715	5	3022.124
	3715.659	0.153	3	3022.124	8282.830	0.438	4	3022.126				
	5244.622	0.227	3	3022.123	9798.164	0.567	5	3022.122				
17.351	2165.015	0.119	11	3027.435	6777.390	0.399	4	3027.446	11332.263	0.862	6	3027.444
	3722.192	0.174	3	3027.444	8297.401	0.522	5	3027.447				
	5253.844	0.266	3	3027.443	9815.401	0.673	5	3027.443				
13.768	2168.262	0.137	12	3031.984	6787.560	0.478	4	3031.993	11349.272	1.047	6	3031.991
	3727.776	0.204	3	3031.993	8309.855	0.623	4	3031.994				
	5261.731	0.315	3	3031.993	9830.139	0.820	5	3031.992				
10.192	2171.469	0.162	13	3036.485	6797.627	0.606	4	3036.497	11366.078	1.378	7	3036.486
	3733.293	0.250	3	3036.491	8322.168	0.805	5	3036.494				
	5269.518	0.394	3	3036.489	9844.701	1.071	6	3036.489				
5.391	2175.725	0.234	15	3042.488	5279.870	0.662	4	3042.489	8338.530	1.387	5	3042.493
	3740.616	0.399	3	3042.487	6810.982	1.050	8	3042.490	9863.909	1.763	−5	3042.440
					$T = 277.000$ K							
69.961[a]	2145.329	0.076	15	2999.870	5206.087	0.160	13	2999.903	8221.970	0.282	14	2999.911
	3688.345	0.118	14	2999.889	6715.789	0.260	19	2999.913				
60.003	2154.502	0.063	7	3012.698	5228.307	0.137	6	3012.707	8257.082	0.234	6	3012.721
	3704.112	0.095	6	3012.713	6744.457	0.196	7	3012.719				
49.993	2163.486	0.064	5	3025.261	5250.122	0.138	4	3025.276	8291.504	0.244	4	3025.278
	3719.555	0.096	3	3025.273	6772.579	0.198	4	3025.279				

TABLE 1—*continued*

p/kPa	f_{0m}/Hz	g_{0m}/Hz	δ	(u/a)/s^{-1}	f_{0m}/Hz	g_{0m}/Hz	δ	(u/a) s^{-1}	f_{0m}/Hz	g_{0m}/Hz	δ	(u/a)/s^{-1}
39.990	2172.366	0.069	4	3037.616	5271.671	0.153	3	3037.629	8325.538	0.278	3	3037.631
	3734.819	0.106	3	3037.624	6800.380	0.221	3	3037.632				
29.953	2181.037	0.079	4	3049.808	5292.720	0.183	2	3049.822	8358.783	0.341	2	3049.824
	3749.734	0.123	2	3049.821	6827.532	0.267	2	3049.825				
19.976	2189.557	0.098	4	3061.752	5313.406	0.244	2	3061.766	8391.459	0.472	3	3061.768
	3764.387	0.159	2	3061.764	6854.220	0.361	2	3061.768				
9.981	2197.971	0.148	4	3073.555	5333.853	0.409	2	3073.572	8423.758	0.841	3	3073.572
	3778.870	0.258	2	3073.571	6880.607	0.631	2	3073.575				
4.973	2202.129	0.232	5	3079.420	5343.977	0.733	3	3079.437	8439.743	1.543	1	3079.429
	3786.029	0.438	2	3079.433	6893.687	1.144	3	3079.440				
					T = 287.000 K							
72.915	2185.257	0.059	7	3055.635	5302.949	0.119	4	3055.651	8374.931	0.202	4	3055.654
	3756.985	0.085	5	3055.649	6840.726	0.164	4	3055.655				
56.954	2198.242	0.060	5	3073.860	5334.461	0.128	3	3073.875	8424.702	0.207	1	3073.878
	3779.308	0.091	3	3073.872	6881.358	0.178	2	3073.870				
42.979	2209.423	0.067	4	3089.514	5361.593	0.145	1	3089.526	8467.558	0.273	2	3089.531
	3798.531	0.103	2	3089.525	6916.372	0.217	2	3089.527				
26.983	2222.004	0.085	4	3107.093	5392.130	0.207	2	3107.104	8515.790	0.383	1	3107.108
	3820.166	0.136	2	3107.105	6955.778	0.269	−3	3107.110				
12.984	2232.783	0.131	5	3122.210	5418.316	0.355	2	3122.225				
	3838.709	0.223	2	3122.222	6989.530	0.513	−2	3122.215				
					T = 300.000 K							
102.599[a]	2216.654	0.045	3	3099.592	6938.983	0.129	2	3099.603	11602.433	0.241	3	3099.605
	3810.950	0.066	2	3099.598	8495.228	0.160	3	3099.605				
	5379.122	0.092	2	3099.602	10049.420	0.197	3	3099.605				
93.844	2223.181	0.047	3	3108.713	6959.415	0.134	2	3108.723	11636.586	0.254	2	3108.721
	3822.173	0.068	2	3108.720	8520.241	0.167	2	3108.724				
	5394.960	0.096	2	3108.721	10079.004	0.206	2	3108.722				
85.743	2229.145	0.048	3	3117.050	6978.088	0.141	2	3117.062	11667.810	0.271	2	3117.060
	3832.428	0.071	2	3117.057	8543.104	0.181	3	3117.063				
	5409.437	0.100	2	3117.060	10106.047	0.217	2	3117.060				
76.926	2235.582	0.050	3	3126.062	6998.239	0.150	2	3126.072	11701.510	0.292	2	3126.071
	3843.498	0.075	2	3126.071	8567.778	0.194	3	3126.074				
	5425.057	0.105	2	3126.071	10135.235	0.234	2	3126.071				
68.189	2241.894	0.053	3	3134.892	7018.000	0.162	1	3134.903	11734.549	0.320	2	3134.901
	3854.347	0.079	2	3134.899	8591.969	0.209	2	3134.904				
	5440.376	0.113	1	3134.902	10163.852	0.255	2	3134.901				
58.116	2249.105	0.057	3	3144.975	7040.575	0.180	1	3144.985	11772.300	0.360	2	3144.983
	3866.745	0.087	1	3144.981	8619.606	0.233	2	3144.985				
	5457.875	0.125	1	3144.983	10196.546	0.287	2	3144.982				
50.561	2254.458	0.062	3	3152.470	7057.329	0.196	1	3152.477	11800.311	0.400	2	3152.473
	3875.947	0.094	1	3152.474	8640.115	0.254	2	3152.476				
	5470.864	0.137	1	3152.476	10220.810	0.318	1	3152.473				
41.890	2260.552	0.068	3	3160.992	7076.412	0.226	1	3161.000	11832.219	0.469	2	3160.996
	3886.427	0.105	1	3160.999	8663.483	0.290	2	3161.001				
	5485.656	0.155	1	3160.999	10248.448	0.371	1	3160.997				

TABLE 1—*continued*

p/kPa	f_{0n}/Hz	g_{0n}/Hz	δ	(u/a)/s^{-1}	f_{0n}/Hz	g_{0n}/Hz	δ	(u/a)/s^{-1}	f_{0n}/Hz	g_{0n}/Hz	δ	(u/a)/s^{-1}
33.105	2266.671	0.078	3	3169.558	7095.572	0.269	1	3169.565	11864.264	0.571	2	3169.561
	3896.947	0.122	1	3169.562	8686.936	0.348	1	3169.563				
	5500.507	0.183	1	3169.563	10276.195	0.451	2	3169.559				
23.784	2273.102	0.095	4	3178.561	7115.711	0.347	1	3178.565	11897.967	0.755	1	3178.567
	3908.005	0.152	1	3178.563	8711.604	0.456	1	3178.568				
	5516.117	0.234	1	3178.563	10305.379	0.596	1	3178.564				
18.043	2277.027	0.113	5	3184.061	7128.007	0.436	1	3184.063	11918.505	0.973	2	3184.057
	3914.755	0.184	1	3184.060	8726.654	0.573	1	3184.064				
	5525.645	0.288	1	3184.060	10323.175	0.761	2	3184.056				
11.928	2281.182	0.148	7	3189.894	7141.027	0.615	1	3189.890	11940.288	1.417	2	3189.887
	3921.901	0.245	0	3189.890	8742.603	0.837	3	3189.895				
	5535.732	0.400	1	3189.886	10342.039	1.085	1	3189.886				
8.906	2283.220	0.181	9	3192.762	7147.440	0.796	2	3192.764	11951.002	1.871	4	3192.757
	3925.407	0.311	1	3192.756	8750.417	1.062	1	3192.755				
	5540.691	0.506	1	3192.756	10351.293	1.424	1	3192.749				
4.500	2286.157	0.288	13	3196.927	5547.822	0.885	−3	3196.902				
	3930.476	0.540	3	3196.922	7156.675	1.393	−4	3196.915				
					T = 310.000 K							
113.510[a]	2250.546	0.044	3	3147.002	7045.062	0.122	2	3147.007	11779.795	0.228	2	3147.007
	3869.214	0.058	1	3147.004	8625.104	0.153	2	3147.011				
	5461.354	0.086	2	3147.004	10203.040	0.185	2	3147.006				
105.016	2256.352	0.044	3	3155.094	7063.261	0.128	2	3155.111	11810.222	0.233	1	3155.109
	3879.205	0.066	2	3155.105	8647.375	0.156	2	3155.111				
	5475.459	0.090	2	3155.106	10229.394	0.197	2	3155.108				
100.277	2259.553	0.046	3	3159.580	7073.269	0.132	2	3159.590	11826.956	0.248	2	3159.589
	3884.705	0.065	1	3159.588	8659.635	0.160	2	3159.593				
	5483.224	0.089	1	3159.590	10243.895	0.200	2	3159.590				
90.573	2266.072	0.046	2	3168.693	7093.686	0.137	1	3168.707	11861.089	0.260	1	3168.703
	3895.920	0.068	1	3168.706	8684.631	0.170	1	3168.710				
	5499.047	0.103	2	3168.704	10273.460	0.206	1	3168.705				
80.585	2272.726	0.049	2	3177.997	7114.515	0.146	1	3178.009	11895.928	0.283	1	3178.008
	3907.358	0.074	2	3178.007	8710.126	0.185	1	3178.009				
	5515.197	0.105	1	3178.008	10303.632	0.228	1	3178.008				
70.426	2279.421	0.053	3	3187.364	7135.474	0.161	1	3187.375	11930.991	0.312	1	3187.378
	3918.869	0.079	1	3187.374	8735.794	0.206	2	3187.378				
	5531.442	0.112	1	3187.373	10333.989	0.257	1	3187.375				
60.829	2285.695	0.056	2	3196.142	7155.120	0.179	1	3196.154	11963.794	0.363	2	3196.144
	3929.653	0.086	1	3196.149	8759.829	0.230	2	3196.151				
	5546.673	0.123	1	3196.154	10362.426	0.287	1	3196.149				
50.053	2292.674	0.063	3	3205.902	7176.963	0.208	1	3205.911	12000.343	0.428	2	3205.907
	3941.650	0.096	1	3205.908	8786.581	0.270	2	3205.911				
	5563.605	0.142	1	3205.910	10394.081	0.330	1	3205.911				
39.781	2299.258	0.072	3	3215.113	7197.599	0.245	1	3215.130	12034.836	0.511	1	3215.122
	3952.972	0.111	1	3215.119	8811.833	0.318	2	3215.125				
	5579.584	0.168	1	3215.120	10423.943	0.406	1	3215.122				
29.546	2305.758	0.083	3	3224.211	7217.922	0.305	0	3224.212	12068.846	0.664	1	3224.209
	3964.143	0.135	1	3224.211	8836.730	0.404	1	3224.213				
	5595.354	0.205	1	3224.211	10453.399	0.519	1	3224.210				

TABLE I—*continued*

p/kPa	f_{0n}/Hz	g_{0n}/Hz	δ	(u/a)/s^{-1}	f_{0n}/Hz	g_{0n}/Hz	δ	(u/a)/s^{-1}	f_{0n}/Hz	g_{0n}/Hz	δ	(u/a)/s^{-1}
19 752	2311.915	0.111	5	3232.841	7237.211	0.419	0	3232.842	12101.108	0.940	1	3232.839
	3974.735	0.179	1	3232.842	8860.347	0.558	1	3232.842				
	5610.302	0.281	1	3232.839	10481.315	0.737	1	3232.831				
8.754	2318.756	0.190	9	3242.456	5626.934	0.540	0	3242.454	10512.431	1.629	9	3242.451
	3986.501	0.322	−1	3242.449	7258.703	0.888	6	3242.467				
					T = 323.150 K							
100.088	2311.606	0.042	1	3232.352	5609.540	0.092	1	3232.362	8859.117	0.177	3	3232.362
	3974.195	0.069	2	3232.358	7236.212	0.131	1	3232.361				
89.294	2318.042	0.047	2	3241.355	5625.160	0.099	1	3241.365	8883.782	0.187	2	3241.363
	3985.262	0.071	1	3241.362	7256.366	0.143	1	3241.366				
80.092	2323.470	0.051	3	3248.948	5638.331	0.106	1	3248.957	8904.591	0.199	2	3248.958
	3994.598	0.075	1	3248.958	7273.356	0.152	1	3248.957				
69.309	2329.779	0.054	3	3257.779	5653.635	0.119	1	3257.784	8928.772	0.219	1	3257.789
	4005.439	0.080	1	3257.785	7293.098	0.165	0	3257.784				
59.986	2335.193	0.060	3	3265.350	5666.795	0.134	2	3265.367	8949.489	0.249	2	3265.346
	4014.750	0.088	1	3265.357	7310.042	0.183	0	3265.352				
49.946	2340.987	0.065	3	3273.459	5680.829	0.146	1	3273.457	8971.728	0.279	1	3273.464
	4024.705	0.100	1	3273.459	7328.175	0.209	0	3273.456				
40.038	2346.647	0.074	3	3281.383	5694.579	0.172	1	3281.388	8993.421	0.333	1	3281.385
	4034.442	0.114	1	3281.386	7345.918	0.257	1	3281.388				
30.019	2352.332	0.087	4	3289.344	5708.369	0.216	1	3289.341	9015.226	0.426	1	3289.347
	4044.213	0.139	1	3289.343	7363.714	0.321	1	3289.345				
20.040	2357.964	0.114	6	3297.234	5722.043	0.294	1	3297.229	9036.836	0.599	1	3297.238
	4053.899	0.186	1	3297.231	7381.359	0.449	1	3297.233				
10.063	2363.546	0.180	9	3305.073	5735.630	0.508	−1	3305.078	9058.233	1.108	2	3305.060
	4063.506	0.309	0	3305.069	7398.905	0.807	1	3305.086				

[a] Pressure omitted from the final analysis.

excess half width

$$\Delta g = g_{\text{expt}} - g_{\text{th}} - g_{\text{o}} - g_{\text{b}}, \tag{32}$$

would be zero. In general the bulk viscosity is not known for a polyatomic gas, but the differing frequency and density dependences of the various contributions to g may be used to estimate the bulk viscosity η_{b} and to isolate unknown loss mechanisms by analysis in terms of the equation:

$$\Delta g = b_{\text{th}}(f/\rho)^{1/2} + \{(b_{\text{b}}/\rho) + b'_{\text{b}}\}(f/u)^2 + b_{\text{r}} f + \Sigma b_n f_{0n}. \tag{33}$$

From equations (14) and (25), b_{th}^2 is proportional to any error in the thermal conductivity, $b_{\text{b}} = \pi\eta_{\text{b}}$ with b'_{b} representing any apparent density dependence in η_{b}, and b_{r} denotes a constant $(\Delta g/f)$ for the resonator; the b_n are constants, similar to b_{r}, for a particular mode that might arise, for example, from inadequate modelling of the openings in the resonator's wall. As expected, the term in b_{b} always dominated but one additional term in either b'_{b} or b_{r} was also significant. The bulk

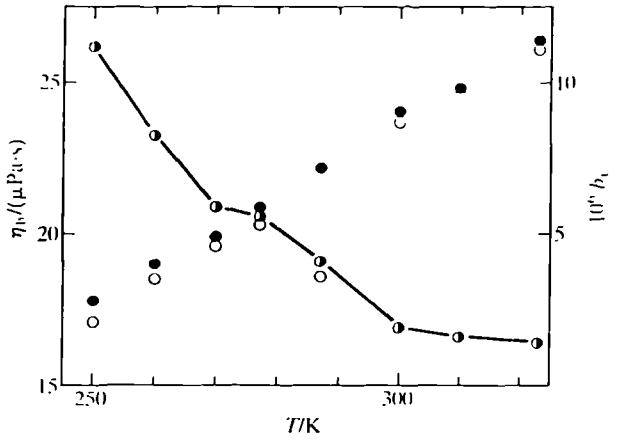

FIGURE 1. Bulk viscosities η_b (left-hand axis) for dimethylpropane and constants b_r (right-hand axis) for the resonator obtained from the excess half widths using equation (33) with two terms. ●, Terms in b_b and b'_b; ○, terms in b_b and b_r; ◑——◑, b_r.

viscosities estimated from these two-term regressions are in good agreement, as shown in figure 1, and may be represented by

$$\eta_b/(\mu Pa \cdot s) = -12.9 + 0.122(T/K), \tag{34}$$

to 0.3 μPa·s, which is similar to the precision of an individual value, except at 287 K where the isotherm has only five pressures. Difficulties arose at lower temperatures as indicated by the discrepancies between the two estimates of the bulk viscosities, or more clearly, by the increase in b_r which is also shown in figure 1; for comparison, b_r is about 3×10^{-6} for a typical isotherm in argon where the bulk viscosity is negligible. The term in b_{th} was not significant for any isotherm (confirming that equation 29 gave κ with sufficient accuracy for our purposes) and, although there was evidence that the first mode behaved somewhat differently, this was not considered further because g_{01} was always small and the value of η_b obtained from three-term fits involving b_1 differed by less than 0.3 μPa·s from those given by equation (34). No particular interpretation is suggested by the behaviour at low temperatures since the precision in Δg is not sufficient to distinguish, for example, between a frequency dependence of f or f^2 once the bulk viscosity has been determined.

At a point on an isotherm, the fractional standard deviation of the mean $\langle u/a \rangle$ is typically 2×10^{-6} and never more than 6×10^{-6}. Since the important perturbations are all proportional to $(\gamma - 1)$, the corrections for dimethylpropane are about a factor of 10 smaller than for argon under similar conditions; g_{th}/f ranged between 6×10^{-6} for the seventh mode at 100 kPa and 65×10^{-6} for the first mode at 4 kPa. Consequently, an error of 3 per cent in κ would contribute less than 10^{-6} to u and there was no serious deterioration in precision even at the low pressures used for some of the isotherms. However, at pressures close to the vapour pressure, the acoustic admittance at the gas-wall interface increases and this precondensation

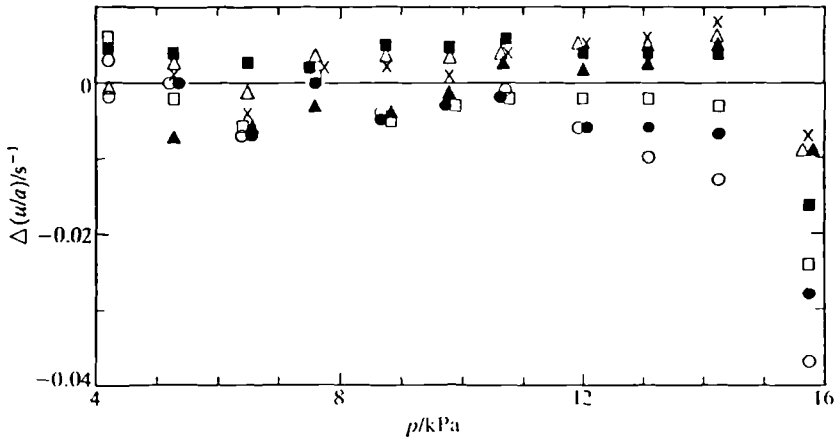

FIGURE 2. Deviations $\Delta(u/a) = [(u/a) - \{u(\text{calc.})/a\}]$, for individual modes in dimethylpropane at 250 K, from equation (1) with coefficients adjusted to fit the results below 15 kPa. ○, Mode 1; ●, mode 2; □, mode 3; ■, mode 4; △, mode 5; ▲, mode 6; ×, mode 7.

phenomenon[13] is observed experimentally as an increased loss and a decrease in resonance frequency; the effect is greatest at low frequencies. Figure 2 shows, for the isotherm at 250 K where the vapour pressure is about 26 kPa, the values of (u/a) as determined from each mode as deviations from the smoothing equation that was finally adopted. At the highest pressure (u/a) increases by 0.03 s^{-1} between the first and seventh mode and the results are clearly affected by precondensation. At lower pressures the results adopt a pattern similar to that observed with argon, and below 9 kPa the standard deviation of $\langle u/a \rangle$ is only 0.003 s^{-1} (fractionally 10^{-6}). In a later paper we shall consider the effect of precondensation on these and other results in more detail but note here merely that some of the higher pressures, greater than about 0.6 of the vapour pressure, were omitted from the final analysis.

The experimental quantity is (u/a) so the coefficients determined in regressions with equation (1) are (A_i/a^2). At the lower temperatures, the results could be adequately represented by equation (1) with three terms but at higher temperatures, where results had been obtained over a wider pressure range, four terms were required. Since there will be significant differences between the estimates of A_2 (and to a lesser, and decreasing, extent between the A_1 and A_0) given by three- and four-term fits, in the analysis of the isotherms at higher temperatures the pressure range was progressivly truncated so as to produce a "best" three-term equation. The pressures omitted (either to produce the three-term equation or to avoid the effects of precondensation) from the final analyses are indicated in table 1.

The possibility of faster convergence with a volume-explicit form of equation (1), with coefficients $A_{V,i}$, was investigated using densities based on the virial coefficients described in section 5. The volume-explicit expansion gave superior two-term equations and $A_{V,2}$ passed through zero near 300 K. However, $A_{V,2}$ varies rapidly with temperature and, away from 300 K, three terms were always required; the three-term pressure-explicit and volume-explicit equations were equivalent, giving

values of $C_{p,m}^{pg}$ that agreed to $0.002R$ and of β_a that agreed to within their combined standard deviations. The following discussion is confined to the pressure-explicit equations because: (a), pressure was the experimental quantity; (b), the density must depend to some extent on the method of solution adopted for equations (7) to (9); and (c), the results will not generally include the temperature at which $A_{V,2}$ is zero. Our observations should not be used to predict the relative virtues of equation (6) and its volume-explicit analogue for representing other results because the acoustic and (p, V_m, T) virial coefficients are related by second-order differential equations.

5. Discussion

Since the construction of the apparatus, the speed of sound in argon has been measured many times. The results are too numerous to report here but they are summarized briefly because they characterize the interferometer and, in particular, give the radius of the resonator since A_0 for argon is known with sufficient accuracy. Twelve isotherms between 250 and 320 K were analysed with three terms in equation (1) and the values of the radius so determined are given by

$$10^6[\{a(T)/(60.1446\ \text{mm})\}-1] = 22.2\{(T/\text{K})-273.16\} + 0.011\{(T/\text{K})-273.16\}^2, \quad (35)$$

with a standard deviation of 0.2 μm; the linear expansivity obtained from these results agrees to 1 per cent with the precise measurements of Kroeger and Swensen[14] on pure aluminium. The experimental second acoustic virial coefficients are compared with a smoothing equation in figure 3 which also shows curves

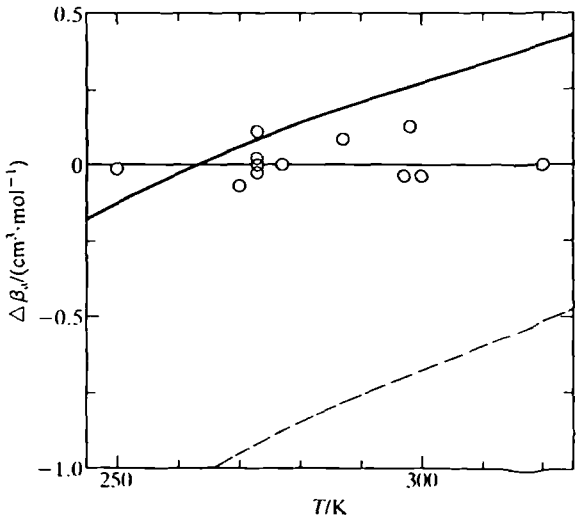

FIGURE 3. Deviations $\Delta\beta_a/(\text{cm}^3\cdot\text{mol}^{-1}) = \beta_a/(\text{cm}^3\cdot\text{mol}^{-1}) - 108.02 + 0.05494(T/\text{K}) + (23970\ \text{K}/T)$, for the second acoustic virial coefficient of Ar. O, This work; ——, HFD-C[15] function; – –, BBMS[16] function.

representing values of β_a obtained by integration of the HFD-C[15] and BBMS[16] pair-potential-energy functions. The deviations of the experimental results are small especially compared with the difference of about 1 $cm^3 \cdot mol^{-1}$ between the values obtained from the HFD-C and BBMS functions near these temperatures. The high level of repeatability of the experiment is demonstrated by the results at 273.16 K. Four sets of measurements over a period of two years give values of β_a that span 0.13 $cm^3 \cdot mol^{-1}$ (the standard deviation of the mean is only 0.06 $cm^3 \cdot mol^{-1}$) while the corresponding values of the radius span 0.3 μm; there appear to be no difficulties with the long-term stability of the interferometer.

The results of the analysis for dimethylpropane are given in table 2 together with the number N of resonance frequencies in the final regression and the standard deviations. The similarity of the fractional standard deviations, of the mean $\langle u/a \rangle^2$ at each pressure, and of u^2 for an isotherm, shows that equation (1) gives a good representation of the results. The coefficients, which were all significant at a probability of 0.999 and were insensitive to further truncation of the pressure range, have been expressed as perfect-gas heat capacities and acoustic virial coefficients using equations (2) to (5) and (35). Uncertainties in (A_0/a^2), T, and a contribute about $0.001R$ to the total error in $C^{pg}_{p,m}$ but the effect of impurities is more difficult to assess. G.l.c. analysis[1] showed a single impurity with mole fraction 0.0005 and if this impurity were another pentane then the molar heat capacity derived from the measurements would change by only $0.002R$ but a butane would be more serious producing a change of about $0.015R$. Although the dimethylpropane was degassed and dried between isotherms,[1] variations of 0.0001 in the mole fraction of air or water would correspond to $0.012R$ or $0.016R$, respectively, in the derived molar heat capacity. Despite these possible difficulties, the values of $C^{pg}_{p,m}$ given in table 2 are in excellent agreement with the flow-calorimetric measurements of Hossenlopp and Scott.[12] Figure 4 shows the two sets of results as deviations from

$$C^{pg}_{p,m}/R = -11.69 + 85.13 \times 10^{-3}(T/\mathrm{K}) - 45.2 \times 10^{-6}(T/\mathrm{K})^2 + 1450(\mathrm{K}/T). \quad (36)$$

The systematic errors in acoustics and flow calorimetry are very different and yet the standard deviation of the combined results is only $0.015R$ (about 0.08 per cent); the maximum discrepancy in the overlapping temperature range is also $0.015R$. The calorimetric results show a systematic undulation from equation (36), which implies

TABLE 2. Perfect-gas molar heat capacities $C^{pg}_{p,m}$ at constant pressure, second β_a and third γ_a acoustic virial coefficients, and standard deviation s obtained by analysis of N modes for dimethylpropane

T/K	N	$C^{pg}_{p,m}/R$	β_a/($cm^3 \cdot mol^{-1}$)	γ_a/($cm^3 \cdot kPa^{-1} \cdot mol^{-1}$)	$10^6 s(u^2)/u^2$
250.000	65	12.567	−2137.6 ± 1.7	2.564 ± 0.089	3.1
260.000	51	12.962	−1966.6 ± 2.0	−1.672 ± 0.063	4.7
270.000	59	13.376	−1815.1 ± 0.6	−1.225 ± 0.013	3.8
277.000	32	13.683	−1722.8 ± 0.7	−0.982 ± 0.011	8.0
287.000	21	14.104	−1601.2 ± 0.6	−0.741 ± 0.007	5.1
300.000	85	14.599	−1460.6 ± 0.2	−0.553 ± 0.002	4.1
310.000	72	15.014	−1365.8 ± 0.2	−0.443 ± 0.002	4.0
323.150	47	15.586	−1256.5 ± 0.5	−0.322 ± 0.004	7.8

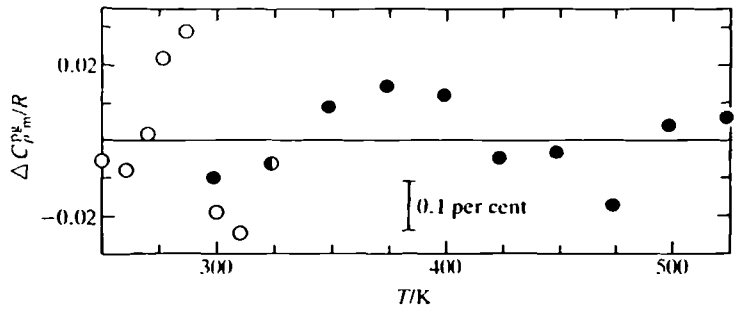

FIGURE 4. Deviations $\Delta C^{ps}_{p,m} = \{C^{ps}_{p,m} - C^{ps}_{p,m}(\text{calc.})\}$, of experimental perfect-gas molar heat capacities of constant pressure for $C(CH_3)_4$ from equation (36). ○, This work; ●, reference 12. The measurements are coincident at 323.15 K.

that the functional form is not entirely suitable, while the acoustic results show random scatter and suggest the possibility that the isotherms at 277 and 287 K were adversely affected by impurities. Nevertheless, the agreement between the results of two such different techniques is exceptional and indicates that perfect-gas heat capacities can be obtained to better than 0.1 per cent from the speed of sound. More recent measurements with other alkanes,[17] where great care was taken with sample purity, are free from many of the problems discussed above.

While it appears that gas purity was the limiting factor in determining $C^{ps}_{p,m}$, the accuracy of the acoustic virial coefficients was determined by the errors in u^2 and p. However, calculation of the (p, V_m, T) virial coefficient B from values of β_s is not straightforward in this case. Formal solution of equation (7) by means of numerical integration with specified boundary or initial conditions was demonstrated by Bruch[33,34] for ^{4}He and by Mehl and Moldover using their precise results for ethene;[35] for the latter the accuracy of the method was confirmed by comparison with high-quality (p, V_m, T) results. Unfortunately this method is sensitive to the constants of integration and it is easy to show that conditions of numerical stability strongly favour the use of at least one initial value near the lowest temperature at which β_s is known.[18] However, it is at low (reduced) temperatures that direct measurements of B are least reliable and in the present case the method is rendered impracticable for just this reason. A complete algorithm by which β_s may be inverted to yield both B and the intermolecular pair energy U is demonstrated elsewhere;[18] this method is independent of non-acoustic results and assumes only that U has spherical symmetry, but results over a wide temperature range are required. Semi-empirical methods involving explict assumptions about the functional form of B were advocated by Boyd and Mountain[36] as a favourable alternative to the formal solution since they place no reliance on (p, V_m, T) measurements; it is to such a method that we now turn. The expression derived from the square-well function is suitable for fitting accurate values of B over a limited temperature range and, once this or another suitable functional form has been chosen for B, it is a simple matter to determine the adjustable parameters by

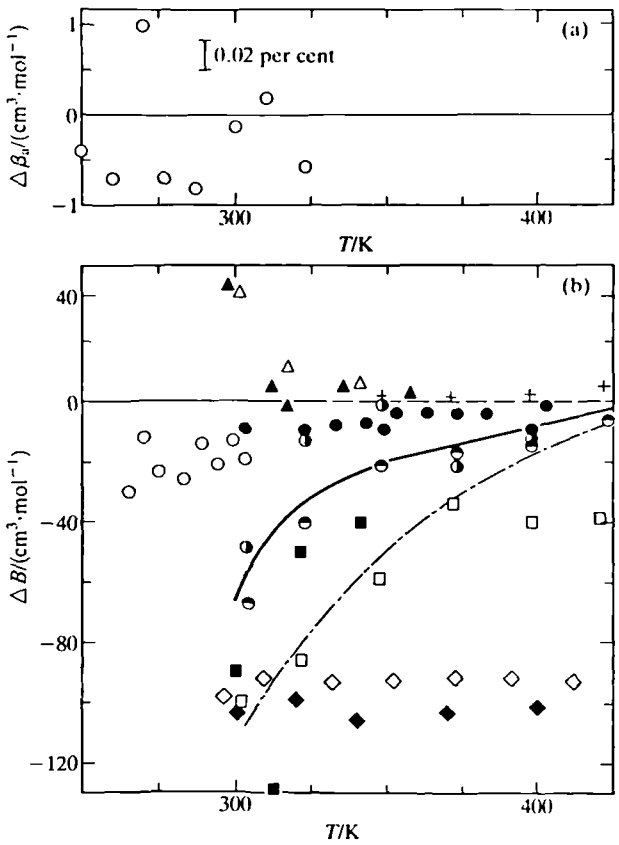

FIGURE 5. (a), Deviations $\Delta\beta_a = \{\beta_a - \beta_a(\text{calc.})\}$, of experimental second acoustic virial coefficients of $C(CH_3)_4$ from equation (7) with (37). (b), Deviations $\Delta B = \{B - B(\text{calc.})\}$, of second ($p$, V_m, T) virial coefficients from equation (37). ○, Reference 12; ●, references 21 and 22; ■, reference 23; □, reference 24; ◑, reference 25; ◓, reference 26; ◇, reference 27; ◆, reference 28; +, reference 29; △, reference 31; ▲, reference 32; ——, reference 19; – – –, reference 30

regression analysis with the experimental β_a and equation (7). Weighted non-linear regression using the results of table 2 gave

$$B/(\text{cm}^3 \cdot \text{mol}^{-1}) = 407.0 - 281.03 \exp(450\ \text{K}/T), \qquad (37)$$

with a standard deviation of $0.47\ \text{cm}^3 \cdot \text{mol}^{-1}$ (about 0.03 per cent) in β_a. Figure 5(a) shows the deviations of β_a from equations (7) and (37) and, although the value of 270 K appears to be against the trend, the maximum deviation is less than 0.06 per cent. The second virial coefficients reported by other workers are plotted, as deviations from equation (37), in figure 5(b) where the ordinate scale has been compressed by a factor of 30 compared with 5(a). Any uncertainties associated with the selection of a functional form for B must be small compared with the scatter in figure 5(b). Although equation (37) is based on measurements below 325 K, it extrapolates to join smoothly with the recommendations of Dymond and Smith[19]

and the work of Beattie *et al.*[20] above 425 K. The results of Hamann and co-workers[21,22] and the most recent work of McKetta *et al.*[29] are in good agreement with equation (37) as are the differential Burnett measurements from this laboratory[31,32] except near 300 K. At low temperatures, the discrepancies between equation (37) and the values derived by Hossenlopp and Scott[12] from their enthalpies of evaporation are less than the estimated errors in the latter. By contrast, the correlation of Das *et al.*[30] is much too low and the measurements of Schäfer, Schramm, and co-workers[27,28] appear to contain a serious systematic error.

A similar approach may be used to assess the internal consistency of γ_a and to estimate the third (p, V_m, T) virial coefficients although the use of three-term fits implies that only apparent third virial coefficients have been obtained. With the

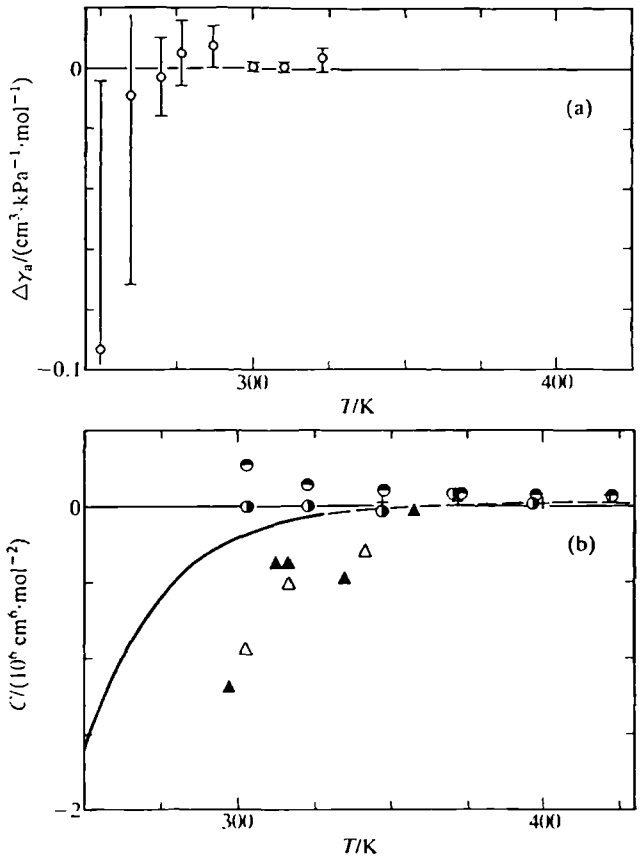

FIGURE 6. (a), Deviations $\Delta\gamma_a = \{\gamma_a - \gamma_a(\text{calc.})\}$, of experimental third acoustic virial coefficients for $C(CH_3)_4$ from equations (8) and (9) with (37) and (38). The error bars are one standard deviation. (b), Third (p, V_m, T) virial coefficients. ◑, Reference 25; ◓, reference 26; +, reference 29; △, reference 31; ▲, reference 32; ——, equation (39) with (37) and (38).

function G of equation (9) calculated using equation (37) for B and its temperature derivatives, the experimental γ_a were used with equation (8) to obtain

$$C'/(\mathrm{cm^3 \cdot kPa^{-1} \cdot mol^{-1}}) = -2.606 \times 10^{-4} \exp(2160\ \mathrm{K}/T), \quad (38)$$

with a weighted standard deviation of 0.0087 $\mathrm{cm^3 \cdot kPa^{-1} \cdot mol^{-1}}$ in γ_a. The uncertainty in the third acoustic virial coefficient depends strongly on the pressure range covered by an isotherm so the results were weighted using the standard deviations given in table 2. The deviations of the experimental γ_a from those calculated using equations (8), (9), (37), and (38) are shown in figure 6(a). The agreement is within the standard deviations given in table 2 and shown as error bars on the diagram, except at 250 K where γ_a(250 K) is based on measurements below 15 kPa. The curve in figure 6(b) is the third virial coefficient:

$$C = B^2 + RTC', \quad (39)$$

calculated using equations (37) and (38). There are few (p, V_m, T) measurements of C but, as with the second virial coefficient, there is good agreement with the recent work of McKetta *et al.*[29] and both studies show a maximum in C at about 400 K. At lower temperatures our (p, V_m, T) results show the correct temperature dependence and, although the discrepancies are quite large, they are not unreasonable in view of the experimental difficulties in the (p, V_m, T) measurements.

In the above, no allowance has been made for the effect of vibrational relaxation on the speed of sound. The fractional shift $\Delta u_{rel}/u$ in u is the real part of equation (27) and depends on both Δ and t. Relaxation times may be calculated from the experimental bulk viscosities using equation (28) once a value has been assigned to Δ. If only the lowest vibrational level of dimethylpropane undergoes relaxation then at 300 K, $\Delta = 0.11$, $t\rho = 78\ \mathrm{ns \cdot kg \cdot m^{-3}}$ and $\Delta u_{rel}/u$ reaches 1×10^{-6} at the lowest pressure and highest frequency. However, it is likely that the vibrational states are strongly coupled in which case $\Delta = 0.73$, $t\rho = 11.6\ \mathrm{ns \cdot kg \cdot m^{-3}}$, and $\Delta u_{rel}/u$ is always less than 10^{-6}. The bulk viscosities at other temperatures give relaxation times that increase, contrary to theoretical predictions,[6] with temperature from $t\rho/(\mathrm{ns \cdot kg \cdot m^{-3}}) = 9.4$ at 250 K to 13.0 at 323 K. However, the energy of the lowest vibrational interval is comparable to the depth of the intermolecular potential-energy well, and at the experimental temperatures the interactions during a collision are not purely repulsive as assumed by the theory.

A.R.H.G. gratefully acknowledges the award of a Research Scholarship by British Gas plc.

REFERENCES

1. Ewing, M. B.; McGlashan, M. L.; Trusler, J. P. M. *J. Chem. Thermodynamics* **1986**, 18, 511.
2. Ewing, M. B.; McGlashan, M. L.; Trusler, J. P. M. *Metrologia* **1986**, 22, 93.
3. Moldover, M. R.; Mehl, J. B.; Greenspan, M. *J. Acoust. Soc. Am.* **1986**, 79, 253.
4. Mehl, J. B.; Moldover, M. R. *J. Chem. Phys.* **1981**, 74, 4062.
5. Mehl, J. B. *J. Acous. Soc. Am.* **1985**, 78, 782; **1986**, 79, 278.
6. Lambert, J. D. *Vibrational and rotational relaxation in gases*. Clarendon Press: Oxford. **1977**, pp. 12, 84–93.

7. Trusler, J. P. M. Ph.D. thesis, University of London. **1984.**
8. Parkinson, C.; Gray, P. *J. Chem. Soc. Faraday Trans. I* **1972,** 68, 1065.
9. Owens, E. J.; Thodos, G. *Am. Inst. Chem. Eng.* **1960,** 6, 676.
10. Prausnitz, J. M.; Reid, R. C.; Sherwood, T. K. *The properties of gases and liquids.* McGraw-Hill: New York. **1977,** p. 473.
11. Diaz Peña, M.; Esteban, F. *An. R. Soc. Espan. Fis. Quim.* **1966,** 62A, 347.
12. Hosenlopp, I. A.; Scott, D. W. *J. Chem. Thermodynamics* **1981,** 13, 415.
13. Mehl, J. B.; Moldover, M. R. *J. Chem. Phys.* **1982,** 77, 455.
14. Kroeger, F. R.; Swenson, C. A. *J. Appl. Phys.* **1977,** 48, 853.
15. Aziz, R. A.; Chen, H. H. *J. Chem. Phys.* **1977,** 67, 5719.
16. Maitland, G. C.; Smith, E. B. *Mol. Phys.* **1971,** 22, 861.
17. Ewing, M. B.; Goodwin, A. R. H.; McGlashan, M. L.; Trusler, J. P. M. to be published.
18. Ewing, M. B.; McGlashan, M. L.; Trusler, J. P. M. *Mol. Phys.* **1987,** 60, 681.
19. Dymond, J. H.; Smith, E. B. *The virial coefficients of pure gases and mixtures.* Clarendon Press: Oxford. **1980,** p. 139.
20. Beattie, J. A.; Douslin, D. R.; Levine, S. W. *J. Chem. Phys.* **1980,** 20, 1619.
21. Hamann, S. D.; Lambert, J. A. *Aust. J. Chem.* **1954,** 7, 1.
22. Hamann, S. D.; Lambert, J. A. *Aust. J. Chem.* **1955,** 8, 149.
23. Ashton, H. M.; Halberstadt, E. S. *Proc. Roy. Soc. A.* **1958,** 245, 373.
24. Hiechelheim, H. R.; McKetta, J. J. *Chem. Eng. Prog. Symp. Ser. (Thermodynamics)* **1963,** 59, 23.
25. Perez Masià, A.; Diaz Peña, M.; Burriel Lluna, J. A. *An. R. Soc. Espan. Fis. Quim.* **1964,** 60B, 229.
26. Silbergberg, I. H.; Lin, D. C. K.; McKetta, J. J. *J. Chem. Eng. Data* **1967,** 12, 226.
27. Strein, K.; Lichtenthaler, R. N.; Schramm, B.; Schäfer, K. *Ber. (Bunsenges. phys. Chem.* **1971,** 75, 1308.
28. Bellm, J.; Reincke, W.; Schäfer, K.; Schramm, B. *Ber. Bunsenges. phys. Chem.* **1974,** 78, 282.
29. Dawson, P. P.; Silbergberg, I. H.; McKetta, J. J. *J. Chem. Eng. Data* **1973,** 18, 7.
30. Das, T. R.; Reed, C. O.; Eubank, P. T. *J. Chem. Eng. Data* **1977,** 22, 16.
31. Ewing, M. B.; Marsh, K. N. *J. Chem. Thermodynamics* **1979,** 11, 793.
32. Toczylkin, L. S. Ph.D. thesis, University of London. **1984.**
33. Bruch, L. W. *Phys. Rev.* **1969,** 178, 303.
34. Bruch, L. W. *Phys. Rev. A* **1970,** 2, 2167.
35. Mehl, J. B.; Moldover, M. R. *Proc. Eighth Symp. on Thermophysical Prop.* Sengers, J. V.: editor. *Am. Soc. Mech. Eng.*: New York. **1982,** p. 134.
36. Boyd, M. E.; Mountain, R. D. *Phys. Rev. A* **1970,** 2, 2164.
37. Mehl, J. B. *J. Acoust. Soc. Am.* **1978,** 64, 1532.